

ALJOSCHA LEONHARDT

CIRCUITS AND ALGORITHMS
UNDERLYING *DROSOPHILA*
MOTION VISION IN NATURAL
ENVIRONMENTS



Dissertation der
Graduate School of Systemic Neurosciences der
Ludwig-Maximilians-Universität
München

29th May 2017

Aljoscha Leonhardt

Circuits and algorithms underlying Drosophila motion vision in natural environments

This dissertation was submitted to LMU Munich in fulfillment of the requirements for a PhD at the Graduate School for Systemic Neurosciences.

CONTACT

✉ leonhardt@neuro.mpg.de

First reviewer and supervisor
Prof. Dr. Alexander Borst

Second reviewer
Dr. Ruben Portugues

Date of submission
29th May 2017

Date of oral defense
21st September 2017

SUMMARY

For organisms navigating in a complex world in constant flux, visual motion is a fundamental cue. Any movement of a physical object results in a specific pattern of spatiotemporal correlation in reflected light. By reliably extracting such regularities from optic signals impinging on appropriate sensory organs, an animal gains the ability to locate and identify objects, segregate foreground from background, determine depth, anticipate collisions, and estimate the motion of its own body in three-dimensional space. It is this multifaceted utility of motion cues that makes their representations particularly prevalent in a wide range of sensory apparatuses, ranging from the small, highly specialized nervous systems of insects up to the comparatively vast brains of primates. Wherever present, motion vision supports a multitude of intricate and critical behaviors, including locomotion, foraging, and mating.

The computation of motion is a non-trivial but well defined task which over many decades has generated considerable interest within the field of sensory neuroscience. As a consequence, direction selectivity has become a canonical example of neural processing and offers a powerful test case for emerging tools of circuit analysis.

During my doctoral studies, I investigated motion vision in the model system *Drosophila melanogaster*. Fruit flies are ubiquitous animals that exhibit a varied but conveniently stereotypical repertoire of behaviors. Among them is the ability to effectively move through their surroundings by walking or flight. *Drosophila* utilize visual motion to stabilize and control these maneuvers. Through the computation of global optic flow fields, flies estimate current ego-motion and calibrate their motor instructions accordingly. An example for this type of motion-guided compensatory mechanism is the so-called optomotor response. When faced with global motion toward one side, flies tend to walk or fly in the same direction. This simple reflex efficiently counteracts the perturbations that may result from, for instance, air turbulence. Early behavioral studies have yielded a compact algorithmic model of how direction selectivity is achieved in the insect visual system. This detector is based on the cross-correlation of spatially separated, asymmetrically delayed luminance signals and closely recapitulates both insect behavior and response properties of global motion-sensitive cells in the fly brain.

Due primarily to its history within the field of genetics, *Drosophila* provides a rich set of genetic tools that allow activation, silencing, visualization, and functional imaging of targeted neuron types. In combination with classical behavioral and physiological techniques as well as high-throughput connectomics, this permits unprecedented access to the visual circuits computing motion.

I focused on two core research questions. First, novel techniques have put a cell-level map of the circuits implementing aforementioned detector model within reach. What are the first direction-selective stages in the fly visual sys-

tem, what are their direct inputs, and what is the correspondence between neural elements and algorithm? Second, flies traverse cluttered and complicated visual surrounds. Realistic stimuli pose severe challenges. How then are the particular properties of natural scenes reflected in the algorithms and neural circuits that underlie motion detection in the fly visual system?

The findings of this work were published in four peer-reviewed articles that together form the cumulative thesis at hand.

In a first study, we identified a set of locally motion-sensitive cells in the *Drosophila* optic lobe. Previous studies had shown that motion is processed twice in the fly visual system: once for positive contrast (ON) and once for negative contrast (OFF). Using calcium imaging from targeted neuron types, we demonstrated that four sub-types of T4 cells respond to localized ON motion in one of the four cardinal directions. Conversely, sub-types of T5 were sensitive to OFF motion in these particular directions. When we genetically silenced T4 or T5, motion responses to either ON or OFF stimuli were selectively abolished in downstream motion-selective cells of the lobula plate that receive input from T4 and T5. Finally, T4- and T5-silenced flies showed polarity-specific deficiencies in walking behavior when stimulated with competitive ON-OFF optomotor stimuli. This work further constrained the locus of motion computation and isolated the critical local direction-selective elements in the fly visual system.

Next, we investigated potential input elements to motion-sensitive T4 cells. Connectivity analysis based on electron microscope imaging of the medulla had suggested cell types Mi1 and Tm3 as likely inputs to the ON motion detector. In this scheme, one neuron would represent the direct and the other the delayed arm of a cross-correlation detector as described above. By genetically silencing either Mi1 or Tm3, we were able to show that this circuit layout is incomplete. In line with model predictions, blocking Mi1 resulted in an ON-specific loss of motion sensitivity in cells downstream from T4 as well as a behavioral optomotor assay. However, when we silenced Tm3, only high-velocity stimuli were affected. At lower speeds, responses remained direction selective. These findings strongly suggested that the underlying circuit scheme is more complex; in all likelihood, additional cell types are involved.

In a subsequent study, we characterized a comprehensive set of T5 input elements. Via calcium imaging, we established the spatial and temporal filter properties of cell types Tm1, Tm2, Tm4, and Tm9, which connectomic reconstructions had identified as the cells providing a vast majority of synapses to the OFF-selective motion detector. None of them were themselves selective for direction. This demonstrated conclusively that motion is computed within the dendrites of T5. Interestingly, temporal signatures were diverse and covered the full range from fast high-pass cells like Tm2 or Tm4 to pure low-pass characteristics in Tm9 via the intermediate Tm1. Such a filter bank is ideally suited to generating direction selectivity. Additionally, we were able to show that silencing single cell types or pairs of cell types noticeably affected motion sensitivity as measured through electrophysiology or behavioral assays, ruling out the redundancy of any element.

Finally, having probed the neural underpinnings of *Drosophila* ON and OFF motion vision, we related tuning properties of the pathways to their

natural context. We evaluated the ability of flies to behaviorally match the velocity of rigidly translating natural images. While silencing T₄ and T₅ in conjunction abolished responses completely, individual blocks had no discernible effect on performance, indicating that both pathways were well adapted to the task of estimating scene velocity. Surprisingly, using electrophysiology and behavioral assays we could show that the ON pathway has starkly different tuning properties when compared to its OFF counterpart. The latter is tuned to much higher edge velocities. When we trained an *in silico* model on the same estimation task, we recovered similar tuning asymmetries. From this, we concluded that neural circuitry in the *Drosophila* visual system is precisely adapted to the statistics of natural scenes.

CONTENTS

1	INTRODUCTION	1
1.1	Normative views of sensory neuroscience	1
1.1.1	Statistics of natural visual scenes	2
1.1.2	Information theory	5
1.1.3	Efficient coding	7
1.1.4	Task-centric approaches	9
1.2	Visually guided behaviors in the fly	10
1.2.1	Optomotor response	11
1.2.2	Landing and escape response	13
1.2.3	Beyond optic flow	14
1.3	Stimulus design	15
1.3.1	System identification techniques	16
1.3.2	Visual illusions	17
1.3.3	Naturalistic stimuli	18
1.4	Tools for circuit neuroscience	18
1.4.1	Neurogenetics	19
1.4.2	Physiological techniques	23
1.4.3	Structural analysis	24
1.5	Neural substrates of fly motion vision	25
1.5.1	Retina	26
1.5.2	Lamina	28
1.5.3	Medulla	30
1.5.4	Lobula complex	32
1.6	Algorithmic models of motion detection	34
1.6.1	Fundamental requirements	35
1.6.2	Gradient detectors	36
1.6.3	Correlation detectors	36
1.7	Concluding remarks	43
2	PUBLICATIONS	45
2.1	A directional tuning map of <i>Drosophila</i> elementary motion detectors	45
2.2	Functional Specialization of Neural Input Elements to the <i>Drosophila</i> ON Motion Detector	57
2.3	Comprehensive Characterization of the Major Presynaptic Elements to the <i>Drosophila</i> OFF Motion Detector	81
2.4	Asymmetry of <i>Drosophila</i> ON and OFF motion detectors enhances real-world velocity estimation	109
3	DISCUSSION	139
3.1	A neural model for motion detection	140
3.1.1	Input lines	140
3.1.2	Nature of the non-linearity	146
3.1.3	Integration of signals	150

3.1.4	Emergence of polarity selectivity	151
3.1.5	Sources of asymmetry	154
3.1.6	Further elaborations	155
3.2	Comparative views	156
3.2.1	Parallels to other visual systems	156
3.2.2	ON and OFF processing	158
3.3	Behavioral investigation of neural circuits	160
3.3.1	Visuomotor transformation	160
3.3.2	State dependencies	161
3.3.3	Motion detectors as feedback sensors	163
3.3.4	Post-hoc approaches	165
3.4	Outlook	165

BIBLIOGRAPHY	167
--------------	-----

LIST OF FIGURES

Figure 1	Natural and artificial images	2
Figure 2	Fundamental statistics of natural images	3
Figure 3	Histogram equalization	8
Figure 4	Behavioral set-ups for sensory neuroscience	11
Figure 5	Anatomy of the fly visual system	26
Figure 6	Correlation-type models for motion detection	38
Figure 7	Response properties of the Reichardt detector	39
Figure 8	Map of ON and OFF pathways	142
Figure 9	Combining Reichardt and Barlow-Levick detectors	148
Figure 10	Peripheral processing of ON and OFF	152

To survive in adverse and dynamic environments, a behaving agent—animal or robot alike—needs to transform sensory signals into adaptive motor output. It is a core goal of systems neuroscience to determine how biological systems accomplish this task using the substrate of neural matter. Motion vision represents a particularly appealing test case for such inquiries. From optic flow, we can infer information about our own movement, track the movement of other organisms, and derive many other ecologically relevant facts about the state of the world.

Investigations of neural circuits are performed at various levels of description. Following the tradition of cybernetics, we can study organisms as black boxes that take input and produce output according to particular rules. At the neural level, we can attempt to unravel the networks that implement these rules. At a teleological level, we can try to understand *why* these networks are designed the way they are. Throughout my thesis, I tackle these questions using motion-guided responses of the fruit fly *Drosophila melanogaster* as a model system. At all aforementioned levels, it exhibits compelling features: a rich set of stereotyped behaviors that support behavioral exploration, small brains that contain orders of magnitude fewer neurons than the mammalian nervous system, and an ecological pervasiveness that implies well-adapted circuitry. In this introduction, I lay some of the groundwork for the articles that represent the main part of the cumulative thesis at hand.

1.1 NORMATIVE VIEWS OF SENSORY NEUROSCIENCE

A core tenet of evolutionary theory is the idea that animals are adapted to their particular niche (Darwin, 1859). This notion naturally extends to brains and specifically sensory systems. Ecological environments are not arbitrary; they exhibit statistical structure. The laws of physics, for instance, impose a level of regularity onto the set of possible sensory stimuli. Some stimuli are then more probable than others while certain configurations are outright incompatible with the rules that govern any given organism's surroundings.

It is a reasonable supposition that nervous systems strive to determine the veridical state of the world based on noisy sensory data, at least insofar as it supports a given behavioral program. *A priori* assumptions about the way the world tends to be should then make the process more efficient and reliable. This approach to sensory systems enjoys a rich history, going back to von Helmholtz who framed perception as the probabilistic problem of "unconscious inference" (von Helmholtz, 1867). It is closely connected to Bayesian theories of sensing but operates on much longer, possibly evolutionary time scales (Doya et al., 2007).

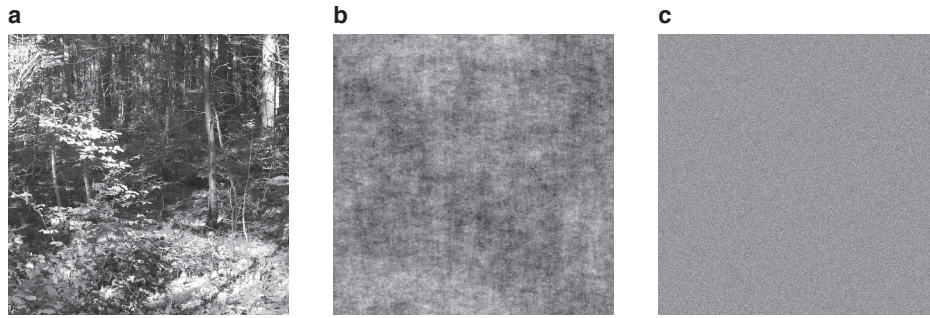


Figure 1: Comparison of natural and artificial images. **a** Natural image patch taken from the in-house library used in [Leonhardt et al. \(2016\)](#). **b** Same image after randomization of phase. **c** Same image after additional flattening of the characteristic amplitude spectrum.

The evolutionary or teleological perspective is inherently normative. From a combination of purpose and environment, one can derive predictions about what properties the system ought to have if it is to fulfill its function effectively and efficiently. These predictions can then be tested experimentally. As such, it complements the purely descriptivist perspective on neural perceptual machinery which heavily relies on simplified, tractable inputs. A central theme of my dissertation is the question to what extent natural visual statistics are reflected in the properties of neural circuitry, using fly motion vision as a model system. The following section provides some relevant background.

1.1.1 Statistics of natural visual scenes

Understanding the natural stimulus distribution is fundamental to normative approaches in sensory neuroscience. Given the topic at hand, this part focuses on natural visual stimuli. Whether captured by eye or camera, natural images exhibit clear regularities that set them apart from uniformly distributed noise. Realistic images thus represent only a small subset of all possible pixel configurations.

This is easily visualized by manipulating pictures in Fourier space ([Hyvriinen et al., 2009](#)). Unaltered images exhibit edges, gradients, homogeneous textures, and segregated objects (Figure 1a). These typical features also extend to natural video sequences. Randomizing the phase structure of images scrambles their higher-order structure and yields phenomenologically atypical textures, even though the manipulation conserves second-order statistics as a consequence of the natural amplitude spectrum (Figure 1b). Nonetheless, local patches may still resemble real image features. Finally, when one flattens the image's amplitude spectrum, only unambiguously artificial noise remains (Figure 1c). Critically, at each stage we can clearly distinguish between images that fall within or outside of the distribution of natural visual scenes.

Large corpora of calibrated natural images like the ones generated by [van Hateren and van der Schaaf \(1998\)](#) or [Tkačik et al. \(2011\)](#) contain thousands

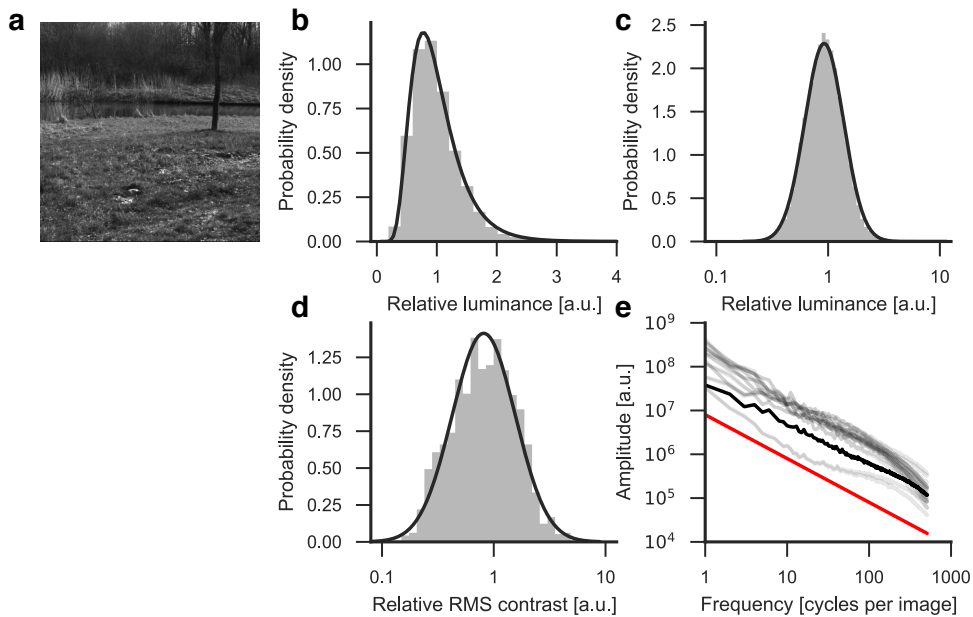


Figure 2: Fundamental statistics of natural images. **a** Calibrated natural image from the database by [van Hateren and van der Schaaf \(1998\)](#). **b** Distribution of per-pixel luminance values for the image in *a*, normalized to a mean luminance of 1. The black curve depicts a log-normal fit to the empirical values. **c** Same distribution replotted on a logarithmic luminance scale. The black curve depicts a corresponding normal distribution fit to the rescaled values. **d** Distribution of log-scaled local contrast for the image from *a*. Root-mean-square (RMS) values were calculated as the ratio of standard deviation to mean in patches of 30×30 pixels and normalized such that the average contrast is 1. The black curve shows a log-scaled Gaussian fit to the empirical distribution. **e** Log-transformed amplitude spectrum of natural images. The image from *a* is depicted by the black line; grey lines correspond to 20 other images from the same database. The red line shows an arbitrarily scaled function $1/f$ for reference, indicating the typical spatial frequency distribution of natural images.

of scenes and make it possible to characterize fundamental statistical properties. Below, I describe a subset of relevant features, ranging from first-order parameters to more complex traits.

Luminance

As a first step, one can measure the distribution of pixel luminance (Figure 2a,b). After per-image normalization, linearly scaled luminance values in natural images are typically positively skewed ([Laughlin, 1981](#); [Brady and Field, 2000](#); [Geisler, 2008](#)). That is, pixels that are dark relative to average luminance numerically outweigh bright ones. When put on a logarithmic scale, this results in a symmetric distribution (Figure 2c). The finding applies universally to image sets across a multitude of environments. Presumably, the asymmetry follows from the basic physical principles that govern scattering of light in nature.

Contrast

Another fundamental statistic is local contrast. Its quantification is less straightforward than in the case of luminance as it requires assumptions about the sensory system and the stimulus under investigation. Common definitions are the difference between feature and background luminance divided by the latter (Weber contrast), the normalized standard deviation of luminance in a small image patch (root-mean-square contrast; see Figure 2d), or the difference of luminance extrema normalized by their sum (Michelson contrast, often applied to periodic stimuli like sine gratings). Alternatively, in analogy to processing in retinal ganglion cells, contrast can be modeled as the response of divisively normalized center-surround receptive fields.

Here, similar skewness as for luminance emerges; only on a logarithmic scale is contrast symmetrically distributed (see Figure 2d for an example). At all spatial scales, natural images thus contain more dark (OFF) than light (ON) contrast (Ratliff et al., 2010; Cooper and Norcia, 2015). This is a direct consequence of the long-tailed luminance distribution. Moreover, luminance and contrast are not fully independent. Their correlation is small but clearly negative (Geisler, 2008).

Spatial patterns

Spatial structure is one of the most informative aspects of any scene. A hallmark of natural images is the shape of their Fourier amplitude spectra (Geisler, 2008). The average contribution of components falls with increasing frequency and is well modelled by the function $1/f^n$ with $n \approx 1.0$ (Field, 1987; Ruderman and Bialek, 1994; Dyakova et al., 2015). This is demonstrated for a range of scenes in Figure 2e. As a consequence, natural images are approximately scale-invariant. Zooming in or out does not substantially affect the shape of the Fourier spectrum. Interestingly, the pink noise model also reproduces spatial properties of local patches in naturalistic video sequences (Dong and Atick, 1995) even though the complex statistics of animal movement make the task of gathering ecologically relevant stimuli difficult.

As discussed above, $1/f$ noise serves as a reasonable local approximation to realistic images but falls short in several ways. One of them is the linearly symmetric luminance distribution which does not reproduce natural skew (Geisler, 2008). Moreover, it fails to model the heavy-tailed response distribution of arbitrary receptive fields scanning natural scenes (Field, 1987). Clearly, the Fourier spectrum does not provide an exhaustive description of real-world spatial features. Natural images show pronounced co-linearity, parallel contours, sharp transitions, and many other forms of spatial regularity that go beyond simple lower-order features.

Other properties

In addition to the most salient subset of features outlined above, researchers have mapped the natural statistics of many additional properties of visual scenes. These efforts include measurements of depth (Huang et al., 2000), color (Ruderman et al., 1998; Wachtler et al., 2001), and optic flow (Roth and Black, 2005, 2007), but are often limited in throughput by available sensors.

Reliable estimation of natural statistics in high-dimensional spaces requires sufficient volumes of data. For this reason, large but static image databases have been an important foundation for research in this space (van Hateren and van der Schaaf, 1998).

Visual ecology

To relate any visual system to naturally occurring stimuli, a reasonable approximation of the neuro-ecologically relevant image distribution is required. Available natural scene libraries are biased toward human visual surrounds when it comes to choice of environment, perspective, focal length, resolution, and other parameters (Tkačik et al., 2011). Many of these qualities are at odds with the experience of a typical fruit fly. For instance, the *Drosophila* eye processes scenes at the comparatively low resolution of approximately 25×25 facets or "pixels", covering close to 180° of azimuth at a separation of $\approx 5^\circ$ (Borst, 2009). The resolution of the fly eye as well as its spatial acuity are orders of magnitude below that of its human counterpart. Moreover, not much is known about the ground-truth visual statistics of the environment in which *Drosophila* and its precursors evolved.

Spatial discrepancies, however, are attenuated by the aforementioned invariance of realistic image amplitude spectra. Generally, fruit flies are extremely widespread and resilient organisms. Their brains possess comparatively few neurons, resulting in limited degrees of freedom. As a consequence, visual adaptation is unlikely to be deeply environment-specific (Dickinson, 2014). Finally, many of the lower-order statistics discussed above appear to be due to fundamental properties of the world and thus generalize to visual environments across the board (Geisler, 2008; Simoncelli and Olshausen, 2001). van Hateren (1997), for instance, studied fly retinal processing and gathered reasonably natural luminance time series simply by walking through a forest while recording the output of an optical system attached at human eye level.

1.1.2 Information theory

Information theory, a branch of probability theory initially developed in the context of electrical communication channels (Shannon, 1948), provides powerful techniques for studying neural and particularly sensory processing (Borst and Theunissen, 1999).

The activity of visual sensory neurons is generally related to some parameter of a given stimulus. In the case of motion-selective units, this could include direction, velocity, acceleration, or contrast. Classically, experiments probe possible relationships by systematically varying parameters and recording stimulus-response curves to determine what feature of the visual input is encoded. When considering the function of neural circuits, however, precision of encoding also matters: we want to quantify rigorously not just what but also how much stimulus-related information a sensory cell carries. Information theory offers a principled way of studying relationships of this type by measuring the reduction in uncertainty about the stimulus any given neural signal provides.

Formally, this is achieved by determining the entropy H of appropriate distributions and closely related to ideal-observer models of decoding. Consider a simple experiment in which the responses of direction-selective neurons are measured as a function of a specific stimulus feature like pattern velocity. Such measurements are stochastic, so we take stimulus and response to be random variables S and R with associated probability distributions. We can quantify our uncertainty about a variable by calculating the Shannon entropy

$$H(X) = - \sum_i p(x_i) \log_2 p(x_i) \geq 0 \quad (1)$$

in which i indexes all possible discrete outcomes x of X and $p(x)$ denotes the probability of x occurring (Cover and Thomas, 2006). For the logarithm with base two, entropy is measured in bits.

Intuitively, information rigorously measures how much an ideal observer learns about the stimulus from the neuron's response. This intuition can be made precise by expressing the quantity as a difference between full stimulus entropy and residual entropy after observing the response

$$I(R; S) = H(S) - H(S|R). \quad (2)$$

This quantity is called mutual information between R and S (Cover and Thomas, 2006). From its definition, we can readily see that the measure is either positive if we learn something about the stimulus or exactly zero if knowing the response does not reduce our uncertainty at all (in which case $H(S) = H(S|R)$ holds). The latter occurs whenever R and S are statistically independent, and thus lines up with experimental intuition.

By expanding the expression above, we can calculate the information about a certain stimulus condition s_x provided by the neuron's response R as

$$I(R; s_x) = \sum_i p(r_i|s_x) \log_2 \frac{p(r_i|s_x)}{p(r_i)} \quad (3)$$

where i indexes the set of enumerated responses, $p(r_i)$ denotes the marginal probability of a specific response across all stimulus conditions, and $p(r_i|s_x)$ denotes the response probability conditioned on a specific stimulus (Borst and Theunissen, 1999). Average information for the full stimulus set is then computed as the probability-weighted sum of specific per-stimulus information

$$I(R; S) = \sum_j p(s_j) I(R, s_j) \quad (4)$$

where j indexes stimuli. This comes out as the mean if stimuli are equally probable (as is the case in balanced experimental designs). Note that information as defined here critically depends on decisions like response binning and the choice of stimulus conditions. In a sense, values hinge on the choice of alphabet used to represent the experiment.

For some designs, one can derive theoretical bounds on the transmission capacity of neural channels and estimate normative qualities like the efficiency of a neural code by weighing transmitted information against maximally possible response entropy. It also extends naturally to the encoding of dynamic stimuli. Note that information theory is a universal method.

It works in the absence of a specific response model and without making strong assumptions about the function of a sensory system or the constraints under which it operates.

The technique has been used to quantify information rates, coding efficiency, and transmission bounds for several model systems including motion-sensitive neurons in flies (Bialek et al., 1991; de Ruyter van Steveninck et al., 1997; Haag and Borst, 1998; Weber et al., 2012), electroreceptors in fish (Wessel et al., 1996), and retinal ganglion cells in the salamander (Warland et al., 1997). Remarkably, measured information rates depend on the choice of stimulus ensemble. In frog auditory neurons, for instance, Rieke et al. (1995) found efficiency values close to 90 % when they tested naturalistic input.

1.1.3 Efficient coding

Sensory systems evolve under a multitude of constraints (Sterling and Laughlin, 2015). One of them is the need to detect stimuli that are survival-critical. Another is the need to perform this task using a minimum of metabolic energy. A third comes from the natural distribution of environmental features. The efficient coding hypothesis, going back to Attneave (1954), Barlow (1961), and others, formalizes this approach to understanding biological sensors. Their theory was of course heavily influenced by the development of information theory which made a rigorous quantification of notions like channel capacity and redundancy feasible.

Efficient coding assumes that the goal of a sensory system is to represent as much relevant information as possible using the smallest feasible amount of resources. Selecting appropriate objective functions is, of course, fraught with difficulty. Ground truth constraints are generally not available and sensory organs often support a broad range of behavioral functions, each of which may necessitate a different definition of relevance. Nonetheless, the theory has successfully predicted features of real systems by assuming basic, tractable goals. In the sensory periphery, this usually takes the form of general preservation of information, thus maximizing the number of possible downstream use cases.

The main target of early vision then becomes reduction of redundancy. Ideally, signals carried by peripheral sensory neurons should be statistically independent in order to minimize wasteful duplication of information. Natural images exhibit regular statistics such as characteristically shaped power spectra that give rise to specific correlation structures. By removing such correlations and emphasizing deviations from expected natural statistics, an operation commonly termed whitening, early vision minimizes energy expenditure while conserving features of the stimulus that are presumed to be behaviorally relevant.

Work on the fly visual system provides seminal demonstrations of this principle at work. Laughlin (1981) measured naturally occurring luminance distributions and compared the resulting histograms to corresponding response functions of lamina monopolar cells, which form the first processing stage after the light-sensitive photoreceptor. In line with predictions from efficient coding, these response functions effectively equalized the input his-

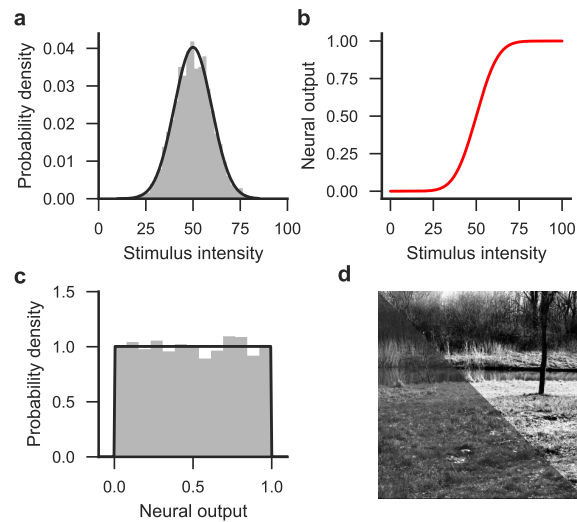


Figure 3: Histogram equalization as a demonstration for efficient coding of sensory stimuli. **a** Sensory samples drawn from a hypothetical Gaussian stimulus distribution (black line; $\mu = 50, \sigma = 10$). **b** Neural transfer function. If this approximates the cumulative distribution function of the stimulus-generating process, as is the case here, the resulting output histogram is effectively equalized. **c** Distribution of samples in **a** transformed by the function depicted in **b**. The black line is a uniform distribution fit to the empirical values. **d** Histogram equalization as a contrast-enhancing image processing technique. The lower triangle shows a picture as taken from the database by [van Hateren and van der Schaaf \(1998\)](#); the upper triangle shows the result of applying the transformation.

tograms, making all outputs equally likely under the assumption of a natural stimulus distribution. An example for this type of transformation is given in Figure 3. For any input histogram (Figure 3a), there is a transfer function that results in a uniformly distributed output histogram and thus maximizes response entropy (Figure 3b,c). In digital image processing, an equivalent technique is used to enhance picture contrast (Figure 3d). A related study ([Srinivasan et al., 1982](#)) could show that lateral inhibition in the fly retina reliably removes the long-range correlations typical for natural images, effectively suppressing background, retaining sensitivity to small fluctuations, and implementing a type of predictive coding.

Constraint triples of this type—minimization of resources, maximization of transmitted information, and assumption of some naturalistic stimulus distribution—have also been applied fruitfully to early processing in mammalian systems. Center-surround receptive fields in both retina and lateral geniculate nucleus (LGN) of the cat have been suggested to implement spatial filters that are well suited to whitening the typical power spectra of natural images ([van Hateren, 1992](#); [Atick and Redlich, 1992](#); [van Hateren, 1993](#)). [Dan et al. \(1996\)](#) confirmed this prediction experimentally by recording LGN responses to natural movies, finding them to be largely statistically independent. [Ratliff et al. \(2010\)](#) argue that the asymmetry between ON and OFF contrast mentioned above explains the difference in numbers between ON and OFF retinal ganglion cells in the vertebrate retina. Interestingly, evidence from primary sensory neurons in V1 of awake mice indicates

that adaptation to natural scene statistics partially depends on experience; if the animals are raised in stimulus-deprived environments, predictive coding specifically of real images is abolished (Pecka et al., 2014).

A closely related normative doctrine is that of sparse and distributed coding: the idea that sensory systems like visual cortex aim to represent natural stimuli using a minimum of active neurons (Simoncelli and Olshausen, 2001). Olshausen and Field (1996), for instance, optimized a linear generative model to reconstruct natural images under the constraint of activation sparseness. The resulting filters bear a striking resemblance to localized oriented bandpass receptive fields in area V₁, indicating that early visual cortex is adapted to the task of efficiently representing real-world stimulus distributions (for a related method based on independent component analysis, see van Hateren and van der Schaaf, 1998; Bell and Sejnowski, 1997).

1.1.4 Task-centric approaches

Efficient coding theory sidesteps the question of task relevance and presupposes that peripheral sensory systems perform lossless compression while maximizing efficiency. This has been a frequent source of criticism (Simoncelli, 2003). After all, brains solve particular problems, so not all information is equal. Relevance may well depend on the exact nature of downstream processing or even behavioral state. For this reason alone, efficient coding is unlikely to scale to higher-level computation.

Instead of choosing a generic normative aim like information preservation, one may be able to do better by picking a specific, task-bound objective function. Encouraging examples come from recent advances in artificial pattern recognition (Bishop, 2006) and specifically the hierarchical models used in so-called deep learning (Goodfellow et al., 2016). Response properties along the visual cortical pathway go from simple local receptive fields in V₁ to object-specific and invariant representations in higher areas (Felleman and Van Essen, 1991; Yamins and DiCarlo, 2016). Such neurons are sensitive to, for instance, images of cars regardless of perspective or brand. Hierarchical neural networks that mimic aspects of this organization (Fukushima, 1980) have reached human-like performance on large object recognition data sets, made possible by advances in optimization techniques (LeCun et al., 1989) and raw processing power (LeCun et al., 2015). Yamins et al. (2014) modeled an artificial deep network after the primate object recognition cascade consisting of areas V₁, V₂, V₄, and IT. After training this system to recognize classes of objects in natural images, they compared learned weights with representations in the biological system and found striking similarities, at least in higher layers (Cadieu et al., 2014). More generally, early stages of visually trained deep networks often exhibit receptive fields that resemble those found in the vertebrate retina or V₁ (Yamins and DiCarlo, 2016).

In psychophysics, studies have successfully predicted texture salience from statistical properties of natural images (Tkačik et al., 2010; Hermundstad et al., 2014). By determining maximally informative features in real stimuli, it was possible to predict behavioral performance for a given synthetic texture.

Task-driven approaches have also been applied to the visual system of the fly. Clark et al. (2014) optimized a motion detector to maximize the linear correlation between time-averaged model output and true velocity of rigidly translating natural images. While functionally plausible, this makes strong assumptions about the true goal of motion-sensing elements and evolutionary pressures at work. Other studies put the fly optomotor response in its functional context by evaluating course stabilization in closed-loop, which is the supposed functional target for wide-field motion responses (Warzecha and Egelhaaf, 1996, 1998). However, this work did not take the natural stimulus distribution into account but used artificial stimuli instead.

Combining behaviorally relevant targets with biologically plausible models appears to be a promising tool for understanding neural computation beyond the sensory periphery. Of course, for complex and highly multiplexed information processing systems like the brain, ascribing goals remains challenging: one may well be wrong about what any given circuit is in fact trying to achieve. Additionally, the approach critically depends on the choice of model—say, a feedforward network for cortical processing as opposed to a more plausible recurrent design—and the techniques used for post-hoc comparisons between model and neural circuit (Yamins and DiCarlo, 2016).

1.2 VISUALLY GUIDED BEHAVIORS IN THE FLY

Flies and specifically *D. melanogaster* exhibit a largely stereotyped, well characterized repertoire of visually driven behaviors (Borst, 2014). This has greatly contributed to their ongoing popularity in the field of motion vision. Reflexive responses facilitate the precise measurement of sensory input-output relationships in large volumes. Systems neuroscience derives predictions about neural processing from quantitative descriptions of behavior which drive physiological work. In turn, behavioral tasks provide powerful high-throughput test beds for hypotheses generated from physiological mapping of neural circuits.

A vast majority of behaviors is not explored in the ecological context of freely moving animals but under strictly controlled conditions instead. Deviations from naturalness include head-fixation, tethering, artificial visual stimulation, and synthetic stimulus statistics. Experimental abstraction allows for full control of sensory input and exact observation of fly movements. However, it also runs the risk of mapping artificial behavioral motifs that do not generalize to ecological settings (Krakauer et al., 2017). A controlled approach and in particular the reliable optomotor response have nonetheless shed significant light on the inner workings of motion detection circuitry in flies.

Behavioral assays were a critical component of my contribution to the studies that comprise this thesis. In the following section, I survey the range of visual reflexes with a clear focus on *Drosophila*, referring to other commonly employed dipteran species (like *Musca domestica* or *Calliphora vicina*) where instructive.

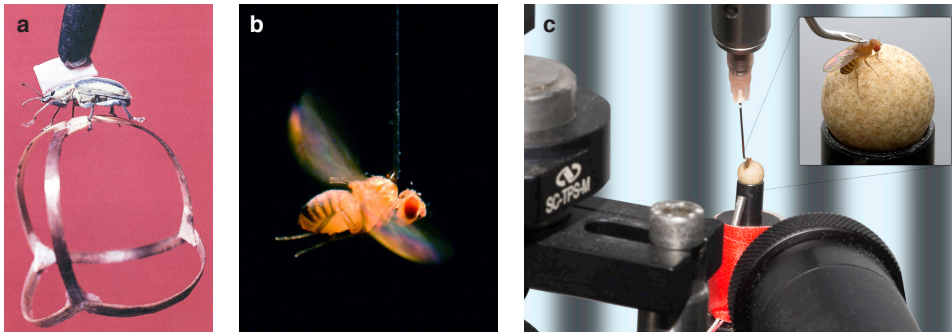


Figure 4: Quantitative behavioral assays. **a** The beetle *Chlorophanus* walking on a Y-maze globe in groundbreaking experiments on the insect optomotor response. Image modified from Hassenstein (1991). **b** A tethered flying *Drosophila* whose wingbeats are monitored optically. Photo courtesy of the National Science Foundation. **c** Fruit fly walking on one of the closed-loop treadmill set-ups used throughout this thesis. Surrounding screens project stimuli. Photo by R. Schorner.

1.2.1 Optomotor response

Flies follow the visual motion of their surround. When for instance tethered to the center of a rotating textured drum, they reflexively attempt to steer in the same direction. This behavioral pattern is termed optomotor response and was a popular model behavior even in early sensory *Drosophila* ethology (Hecht and Wald, 1934; Kalmus, 1943).

A seminal quantitative investigation of the response was conducted by Hassenstein and Reichardt (1956). They placed *Chlorophanus viridis* on a spherical Y-maze that was light enough to be held and moved by the beetle (Figure 4a). This simulated walking while keeping the animal fixed in relation to the visual stimulus. Then, by counting leftward versus rightward choices as a function of various parameters of a rotating drum, they were able to estimate turning tendency in a graded fashion. Their quantitative findings formed the foundation of the algorithmic Hassenstein-Reichardt model for insect optomotor behavior (Reichardt, 1961) which is discussed in more detail below.

The optomotor response is not exclusive to one mode of fly locomotion (Fermi and Reichardt, 1963; Götz, 1964; Götz and Wenking, 1973; Buchner, 1976; Götz, 1987). It can be demonstrated in tethered flying *Drosophila* using a torque meter or the difference between wing beat frequencies as a read-out of turning tendency (Figure 4b). Moreover, it is studied in flies walking on treadmill systems that mimic moving ground while keeping the animal in place (see for instance Figure 4c). While commonly elicited by yaw motion revolving around the vertical body axis of the fly, it generalizes to pitch and roll (Blondeau and Heisenberg, 1982). When the fly's head is left unrestrained, its movements also track stimulus direction (Hengstenberg, 1988).

A multitude of studies has mapped stimulus dependencies of the optomotor response (see Borst et al., 2010). Critically, the behavior is not driven by the true rotational velocity of the visual pattern. Instead, many other stimu-

lus features influence response magnitude. The most salient properties can be summarized as follows:

1. Flies turn in the same direction as the pattern.
2. Stimulus geometry has a strong effect on the velocity tuning. For sine gratings, increasing the pattern wavelength λ shifts the curve towards larger velocities v . Critically, the fly optomotor response is tuned not to stimulus velocity but to contrast frequency instead, which for periodic patterns is given by $f = \frac{v}{\lambda}$.
3. Responses are ambiguous with regard to frequency and only proportional in a limited range. They initially grow with temporal frequency but show a clear optimum after which turning decreases again. In *Drosophila*, measurements of this peak frequency exhibit significant variability but are in the range of 3 Hz to 10 Hz (Götz and Wenking, 1973; Duistermars et al., 2007).
4. Optomotor responses are subject to spatial aliasing. If λ drops below the Nyquist limit of twice the receptor distance, the response inverts due to undersampling of the sine grating. From this, one can estimate the *Drosophila* sampling base as $\approx 4.6^\circ$ of visual space, which matches average inter-ommatidial distance well (Götz, 1964).
5. The magnitude of the response increases with stimulus contrast.

Functionally, the reflex is usually interpreted as a compensatory steering mechanism (Götz, 1968; Heisenberg and Wolf, 1984). Flies are capable of long-duration flight in adverse surroundings (Götz, 1987; Dickinson, 2014). They also perform acrobatic maneuvers whose instantaneous rotational velocity may well exceed $2000^\circ \text{ s}^{-1}$ during unrestrained flight, all at forward speeds that can reach 1.0 m s^{-1} (Land and Collett, 1974; Mronz and Lehmann, 2008; Censi et al., 2013). At the same time, the weight of an individual fruit fly is on the order of 0.2 mg (Seiger, 1966). This makes them preciously vulnerable to external perturbations like sudden gusts of wind. Internal sources of noise, like small asymmetries in wing morphology, add to the problem.

In concert with proprioceptive mechanisms, the optomotor response confers some protection against unintended path deviations. Any turning response that is syndirectional with global optic flow will eventually return the fly to straight heading, assuming that the estimated optic flow provides an accurate read-out of ego-motion. The optomotor response thus implements a simple, reflexive feedback system that keeps the fly on course¹ (Borst, 2014). In this vein, some authors have argued that the non-monotonous velocity tuning of the motion sensor keeps the system from falling into irrecoverable oscillations (Warzecha and Egelhaaf, 1996). Comparable locomotor reflexes are found in other insects or fish (Arnold, 1974; Portugues and Engert, 2009),

¹ Note that some studies have suggested that *Drosophila* is capable of modulating the strength and even sign of optomotor orientation behavior through stochastic adjustment and subsequent evaluation of visual feedback (Wolf and Heisenberg, 1986; Wolf et al., 1992).

and optomotor responses closely resemble the optokinetic nystagmus that stabilizes the eye during movement (Büttner and Kremmyda, 2007).

Traditionally, optomotor responses have been studied in tethered animals. If the functional logic outlined above holds, then it should also be possible to observe a visually induced following reflex in unrestrained behavior. Counter-intuitively, Götz (1970) found that groups of unrestrained fruit flies placed in a rotating drum moved against the direction of the wall pattern. This was later successfully explained as a consequence of complex superpositions of external stimulus and self-induced translating optic flow (Götz, 1975). Strauss et al. (1997) used on-line tracking and live generation of appropriate stimuli to suppress self-generated feedback and confirmed tethered turning behavior in free walking. While tracking flying flies in a large arena, Mronz and Lehmann (2008) could elicit prolonged curved trajectories and largely suppress the body saccades typical for *Drosophila* flight by rotating the cylinder's texture.

1.2.2 Landing and escape response

Flies are notoriously competent at evading fast-moving objects and rarely collide with static landmarks. Motion sensors signal imminent collisions through particular patterns of translational optic flow. Approaching a textured surface results in visual expansion whose magnitude correlates with distance and thus, critically, time to impact (Koenderink, 1986). By selectively extracting looming flow fields, flies can trigger an appropriate response. When at rest, they initiate a fast and largely stereotyped escape maneuver. When flying, they either evade or perform the wing and leg adjustments required for safe landing (Borst, 2014).

Several studies have investigated the latter condition in tethered experimental settings. When stimulated with laterally expanding square-wave gratings, *Drosophila* robustly steer away from the focus of expansion (Tammero and Dickinson, 2002). Centered expansion, on the other hand, activates a landing sequence. Duistermars et al. (2007) systematically compared the tuning properties of expansion-triggered evasion and rotation-triggered optomotor response. The two pathways differed in pooling and contrast sensitivity. Yet, aspects like temporal and spatial sensitivity were preserved. This indicates that both behaviors draw from the same set of motion-sensitive units which are then processed differently.

Centrally positioned expansion of sine or square-wave gratings prompts the landing response which consists of a fixed sequence of postural and steering-related adjustments (Goodman, 1960; Braitenberg and Ferretti, 1966; Borst, 1986). Critically, the delay leading up to initiation of this program depends on spatial and temporal aspects of the expanding stimulus. By manipulating these parameters, Borst and Bahde (1986) demonstrated that a single set of motion detecting units could feasibly underlie both optomotor and landing response in the housefly *M. domestica*. Their model simply integrates motion signals up to a certain threshold after which the landing sequence is started. This system was capable of reliably predicting response latencies.

When at rest, flies respond to fast expansion by rapidly initiating a controlled jump. This happens within ≈ 200 ms of stimulus onset and is not completely stereotyped. In a majority of cases, flies manage to coordinate their take-off such that they escape away from the looming stimulus, which hints at a surprisingly elaborate transformation from visual input to motor output (Card and Dickinson, 2008). Recent high-resolution tracking of escape responses revealed a subtly bimodal distribution of time courses, indicating two distinct, stimulus-dependent escape programs and thus even more complex behavioral phenomenology (von Reyn et al., 2014). Intriguingly, Muijres et al. (2014) tracked the flight kinematics of looming-triggered escape responses in freely flying *D. melanogaster* and observed extremely rapid banked turns consisting of carefully calibrated directional shifts and counter-shifts. This survival-critical sequence is completed within a small number of wing beats and testament to the impressive maneuverability of fruit flies.

1.2.3 Beyond optic flow

All behaviors discussed so far were derived from global optic flow. Of course, the visual environment of the fruit fly provides cues beyond wide-field motion.

A prominent example among behaviors driven by other stimuli is fixation. Ego-motion results in largely coherent flow that spans the complete visual field and drives the optomotor response. Superimposed onto this motion background are the relative movements of nearby objects. Flies need to track such entities in order to find conspecifics or navigate between landmarks.

This can be studied experimentally. Depending on the separation of two bars projected onto the wall of an arena, for instance, walking flies either track the area between the two stripes or choose one of two as they become more distant (Horn and Wehner, 1975). Maimon et al. (2008) studied fixation behavior in freely flying *Drosophila* and discovered a remarkable trade-off between approach and avoidance by varying the height of a rod placed in the flight arena. When this bar was long, flies approached and circled it. When it was shortened, the bar became aversive; flies now tended to steer clear of the object. The pattern is reminiscent of a famous behavioral setting, Buridan's paradigm² (Bülthoff et al., 1982). In a behavioral chamber with two vertical rods, flies will ceaselessly walk from one to the other, entering a seemingly inescapable loop of fixation and anti-fixation.

Experiments in tethered flies have illuminated some functional aspects of the fixation response. Reichardt and Wenking (1969) coupled the output of a torque meter to the position of a vertically elongated bar which enabled the fly to control its visual input in a semi-realistic closed-loop setting. Interestingly, *M. domestica* kept the target in an on average frontal position. Reichardt (1973) ascribed this behavior to asymmetric motion responses. In an open-loop setting, a black stripe moving from front to back results in a

² The set-up is named after a thought experiment attributed to the French priest and philosopher Jean Buridan. In it, an equally hungry and thirsty donkey is trapped between food and water and eventually starves to death (Knowles, 2005).

stronger optomotor response than its back-to-front counterpart. In closed-loop, this imbalance would eventually push the stripe toward the front. In later theoretical treatments of fixation and orienting behavior, the imbalance was analyzed as the superposition of an optomotor-like response and the response of a position system that determines the position of a salient cue and orients the fly towards it (Poggio and Reichardt, 1973). Similarly, Pick (1974) argued that flies simply orient towards flicker. Recent work used neurogenetic silencing techniques to isolate motion- from position-driven responses and found evidence for a position system of the predicted type in *D. melanogaster* (Bahl et al., 2013). Interestingly, the visually guided orientation behavior of fruit flies goes well beyond reflexes. Ofstad et al. (2011), for example, reported robust associative learning based on visual landmarks.

Fruit flies exhibit various other visual behaviors. Bahl et al. (2015) have recently provided evidence that *Drosophila* respond robustly to temporally modulated spatial contrast. The functional significance of this sensitivity, however, remains unclear. In an early piece of sensory ethology, Carpenter (1905) described the tendency to approach light in a fruit fly species. This is an example of phototaxis, one of the most simplistic visual reflexes in the animal kingdom.

On the more sophisticated end of the spectrum, studies have shown that fruit flies utilize the polarization of light to orient their course (Weir and Dickinson, 2012). Polarized light results from atmospheric scattering as well as certain reflecting surfaces and provides critical navigational cues. The information is mediated by two physiological pathways, one sensitive to dorsal polarization emanating from the sky and the other to ventral reflectance-derived stimuli (Wernet et al., 2012). The system may explain the reported long-term migration feats of certain *Drosophila* species that have been reported to travel up to 10 km in the desert (Dickinson, 2014).

Finally, fruit flies possess a narrow repertoire of color-mediated behaviors (Menne and Spatz, 1977). However, this is limited to spatially coarse types of visual sensing. For instance, flies learn to differentiate green and blue in an aversive association task (Schnaitmann et al., 2013). The optomotor response, on the other hand, operates with luminance information only. If a square-wave grating consists of differently colored but brightness-matched stripes, no turning is elicited (Yamaguchi et al., 2008).

1.3 STIMULUS DESIGN

A key step toward understanding sensory systems is the measurement of input-output relationships. In the case of the visual apparatus, this takes the form of displaying controlled, parameterized visual patterns and then quantifying responses at various levels of the processing cascade. Typically, the relevant outputs are neural or behavioral activity. As with any system, the choice of stimulus determines what we can learn about the transformations accomplished. Below, I review common classes of motion stimuli used in the investigation of the fly optomotor response.

1.3.1 System identification techniques

As discussed above, the statistics of natural optic flow are complex and hard to control in experimental contexts. Instead of reverse-engineering the function of a visual system from the top down, it appears preferable to use simplified stimuli and explore relevant computations from the bottom up. The engineering sub-field of signal processing offers a multitude of principled tools that support the rigorous identification of systems based on such input-output measurements.

Oriented moving sine gratings are the workhorse of motion vision research. They can be fully specified using a small number of parameters: spatial wavelength λ , velocity v , mean luminance I , contrast ΔI , and if required the angle of orientation in two-dimensional space. Conveniently, when sampled at a single location, the resulting temporal signal is again a sinusoid with contrast frequency $f = \frac{v}{\lambda}$. Neighboring signals are modulated at the same frequency but differ in relative phase. This means that the brightness input to the photoreceptors has clearly defined mathematical properties, rendering them amenable to the rigorous tools of Fourier analysis and filter theory. Examples of this approach include [Götz \(1964\)](#), who estimated the sampling base of local motion detectors in the fruit fly via quantification of spatial aliasing, or [Egelhaaf et al. \(1989\)](#), who employed spectral analysis to characterize the non-linearity underlying motion computation in the blowfly *C. erythrocephala*. In practice, true sinusoidal stimuli are often replaced by periodic square-wave gratings whose Fourier expansion consists of all odd-integer harmonics of some fundamental spatial frequency λ^{-1} . Such stripe patterns are easier to construct in experimental settings and result in similar temporal photoreceptor signals if substantial spatial blurring is assumed. Moving sinusoidal gratings can be stacked and blended to produce stimuli of higher complexity. A famous example are so-called plaids which consist of two angled moving gratings and may produce ambiguous motion percepts ([Adelson and Movshon, 1982](#)). As a special case, counterphase flicker can be constructed from identically oriented gratings drifting in exactly opposite directions and has been used fruitfully in fly vision research ([Bahl et al., 2015](#)).

Filter theory provides another high-throughput tool for system identification in the form of white-noise techniques and their close relatives ([Dayan and Abbott, 2001](#)). Instead of mapping the relationship between parameters of, say, a sinusoidal motion stimulus and associated responses one by one, we can feed dynamic input into the system, record the output, and recover the transfer function by means of reverse-correlation. This works efficiently if the distribution of the relevant parameter is as decorrelated as possible; in case of a motion stimulus, for instance, the spectrum of velocities ought to be close to flat. The properties of the resulting kernel may then offer insight into the inner workings of the motion detection system. This class of stimuli has been successfully applied to walking behavior in fruit flies ([Theobald et al., 2010](#); [Aptekar and Frye, 2013](#)) as well as response properties of motion-sensitive cells in the fly visual system ([Borst et al., 2005](#); [Weber et al., 2010](#)).

Finally, traveling edges offer yet another tool for motion research. They combine relatively simple stimulus statistics with polarity-specificity; that is, they are defined purely by one direction of luminance change (ON or OFF). This pattern class has had substantial impact on the field of motion vision, particularly in the fruit fly (Joesch et al., 2010; Eichner et al., 2011; Clark et al., 2011).

1.3.2 Visual illusions

The use of visual illusions can be traced back to the earliest roots of psychophysics, with a vague description of motion aftereffects appearing in Aristotle's *Parva Naturalia*. Illusory stimuli elicit naturalistic impressions of motion in the absence of actual physical movement. The fundamental logic then runs as follows: While multiple algorithms may be able to explain the standard phenomenology of motion vision, studying edge cases and deviations from intended function could feasibly narrow down the set of compatible mechanisms.

A classical illustration of this psychophysical principle is the apparent motion percept elicited by two adjacent light spots flashing in quick temporal succession, so-called phi motion (Wertheimer, 1912). The immediacy of the percept critically depends on both spatial and temporal separation; if both are chosen correctly, the two events combine to produce the vivid impression of movement. This stimulus has been extended to whole patterns (Anstis, 1970) and is closely related to the beta motion illusion that underlies the perceptual fluidity of discretized video sequences. In the study of insect motion vision, there is a rich history of using apparent motion to elucidate sensory mechanisms as it allows the isolation of a minimal localized event with clearly defined spatiotemporal parameters. The reverse-phi phenomenon in particular has substantially influenced the design of detector models. If apparent motion is accompanied by contrast reversal of the pattern, perceived direction tends to invert (Anstis and Rogers, 1975; Chubb and Sperling, 1989). This effect is not limited to human perception. Many visual systems across the animal kingdom are subject to the illusion, including the fly (Egelhaaf and Borst, 1992; Orger et al., 2000; Krekelberg and Albright, 2005; Tuthill et al., 2011; Eichner et al., 2011; Clark et al., 2011). The observation was a critical factor in the development of correlation-based motion detectors (Hassenstein and Reichardt, 1956).

Most research on insect vision is concerned with first-order or Fourier motion which is defined by pairwise spatiotemporal correlation of luminance. In this scheme, both phi and reverse-phi stimuli find a convenient explanation as positive and negative correlation, respectively. Physical motion induced by displacement of objects or ego-motion generally produces such dependencies. Psychophysical experiments, however, provide ample evidence for sensitivity to higher-order correlations in humans (Lu and Sperling, 2001). Using an optomotor stimulus in which motion was defined by local contrast reversal within a random stripe pattern, Theobald et al. (2008) elicited optomotor responses to second-order motion in tethered flying *Drosophila*. Hu and Victor (2010) developed a novel class of stimulus to

probe higher-order motion, so-called glider patterns. Here, a deterministic set of update rules seeded with random black and white pixels produces stochastic displays whose average correlation structure is limited to one particular spatiotemporal order. Phi and reverse-phi are recovered as the edge case of two-point correlation, but the algorithm naturally extends to three- and four-point stimuli. Using this scheme, [Clark et al. \(2014\)](#) could demonstrate that walking fruit flies robustly respond to correlations defined by three points in space and time.

1.3.3 Naturalistic stimuli

As discussed in previous sections, naturalistic stimuli represent a double-edged sword. Sensory systems are evolved in particular environments and for particular tasks, so using ecologically plausible stimuli may help illuminate the function of a visual system. This advantage comes at the cost of not being able to clearly relate stimulus features to particular aspects of the response.

Several investigations of fly motion vision have attempted to strike a compromise between the two extremes. [Wertz et al. \(2009\)](#), for instance, studied binocular integration of optic flow using simulated rotations around various body axes in a virtual three-dimensional room whose walls were lined with checkerboard textures. The visual statistics of this stimulus are simpler than they would be in nature, but the motion pattern resembles reality more than a traveling grating would. In a complementary approach, several studies have used natural textures such as panoramic images of real environments to examine response properties of motion-sensitive units in the fly visual system ([Straw et al., 2008](#); [O'Carroll et al., 2011](#)). Here, synthetic motion kinetics were traded off against a more reasonable approximation of natural image statistics. [Lewen et al. \(2001\)](#) took this approach one step further by mounting *Calliphora* on a mobile platform that allowed electrophysiological recordings from motion-sensitive cells while the fly rotated in a wooden area. This way, they were able to guarantee that dynamic range and general statistics of the stimulus are truly natural.

1.4 TOOLS FOR CIRCUIT NEUROSCIENCE

Progress in neuroscience is often driven by advancement of the technologies we use to study circuits. Some of the earliest breakthroughs in neural physiology heavily depended on the development of novel measurement devices. For instance, it was the Lippmann electrometer that allowed Edgar Adrian to measure minuscule currents in the toad optic nerve. His observations lead to the Nobel Prize-winning discovery that cells in the retina respond electrically to visual changes ([Adrian, 1928](#)).

Due to its long-standing history in the field of genetics, *D. melanogaster* offers the arguably richest toolkit for monitoring and manipulating neurons among the dominant model organisms in neuroscience, fruit fly, mouse, *C. elegans*, and zebrafish ([Venken et al., 2011](#)). In the subsequent sections, I

review some of the most prevalent techniques in the field of fruit fly neuroscience.

1.4.1 Neurogenetics

An overarching goal of sensory neuroscience is to relate particular functions to particular neurons or groups thereof. Often, this is achieved by altering or disrupting neural function and then assaying neural and behavioral defects.

Mutagenesis

Classically, such dependencies have been established via gene-centric approaches. This often involves mutagenic disruption of stochastically selected genes and subsequent screens for specific phenotypes, the so-called forward direction from phenotypes of interest to involved genes. Reverse screens start from specific genes and then map phenotypic outcomes. Groundwork for this approach was laid by Thomas Hunt Morgan whose serendipitous discovery of the *white* mutation and its consequence, a distinct lack of eye pigmentation, critically illuminated hereditary mechanisms in the fruit fly (Morgan, 1910). Within visual neuroscience, one may be able to assign function to certain brain areas by carefully correlating mutation-induced changes in neural structure with behavioral effects.

A paradigmatic and germane example comes from Benzer (1967) who screened fruit flies in a phototaxis task while efficiently creating mutations through application of ethylmethane sulfonate. The principle behind his behavioral set-up was modeled after the chemistry technique of countercurrent distribution, which allowed for high-throughput fractionation of visual phenotypes. Götz (1964) investigated the optomotor behavior of *white* mutants and found specific deviations from wild-type behavior which could be explained from a lack of shielding pigment. The population fractionation approach was later successfully extended to optomotor behavior (Götz, 1970). Importantly, post-hoc evaluations of neural aberrations in the optic lobe later allowed some limited inference about causal relationships between neural substrate and visual function (Pak et al., 1970; Heisenberg and Götz, 1975; Heisenberg et al., 1978; Fischbach and Heisenberg, 1981).

Binary expression systems

Disruption of gene activity is likely to affect brain function widely and indiscriminately which puts inherent limits on the usefulness of mutagenic approaches in circuit neuroscience. To draw clear and causal conclusions about neural function, one needs to be able to flexibly manipulate groups of cells with high precision in space and time. This is generally accomplished through the use of binary expression systems like GAL4-UAS (Venken et al., 2011).

Such systems consist of two components: a driver or transactivator that determines *where* expression occurs and a responder that determines *what* is expressed. GAL4 is a yeast-derived transcriptional activator protein that binds specifically to a class of regulatory sites called upstream activating

sequences (UAS). Upon binding, the transcription of a chosen responder is initiated. Rubin and Spradling (1982) pioneered the use of transposable P-elements to stochastically and stably insert DNA sequences into the fly genome. Using this technique, Brand and Perrimon (1993) could place the transgene coding for GAL4 under the control of random endogenous enhancers. Depending on the specific locus, GAL4 is expressed in different subsets of cells. This provides the desired specificity. Analogously, one can insert a combination of UAS and desired effector gene into the genome of another fly line. Assuming that no critical locus is affected, both driver and responder strains are healthy. In isolation, neither GAL4 nor the activating sequence have adverse effects. Critically, the effector gene is not transcribed in the absence of binding GAL4.

If a driver strain shows a relevant expression pattern, it is easily crossed to a chosen effector line. In the resulting progeny, the effector is then transcribed ectopically only in GAL4-labeled cells. This powerful technique thus makes it possible to express virtually arbitrary transgenes in selected groups of neurons. Concerted research effort has since greatly enhanced the technique, improving expression levels as well as rendering the method more reliable (Pfeiffer et al., 2010, 2012), and has produced massive libraries of GAL4 lines with anatomically well-characterized expression patterns (Pfeiffer et al., 2008; Jenett et al., 2012; Kvon et al., 2014).

Standard GAL4 lines are not always sufficiently specific to one neuronal type or even group of types. Intersectional strategies offer a simple algebra for refining expression patterns. Yet another yeast-derived protein, GAL80, can act as a repressor of GAL4; GAL80-expressing cells are thus subtracted from the original GAL4 pattern (Lee and Luo, 1999). Variants of GAL80 whose efficacy depends on temperature offer temporal control over this process, which has proven useful in pausing GAL4-driven expression during critical developmental periods (McGuire et al., 2003).

A particularly powerful operation is provided by the split-GAL4 system (Luan et al., 2006). GAL4 can be divided into two constituents, the activation domain GAL4-AD and the DNA binding domain GAL4-DBD. By putting the two hemidrivers under the control of separate regulators, their simultaneous expression is restricted to the intersection of the two. Only where both are present do the two parts then combine and become effective at binding to UAS. This adds logical conjunction to the set of available operations. split-GAL4 lines have proven especially useful in targeting effector expression to isolated cell types. Finally, when working with stereotyped cell types, it is often desirable to limit expression of the effector to only single, stochastic instantiations. The "flip-out" approach based on a combination of GAL4 and Flp recombinase may be used to generate such mosaic patterns at various levels of labeling frequency (Golic and Lindquist, 1989; Struhl and Basler, 1993; Bohm et al., 2010).

Other binary expression systems exist, derived from transactivators like LexA (Lai and Lee, 2006) or QF (Potter et al., 2010). While these tools are not as highly-engineered as GAL4-based ones, they can be used fruitfully in combination and then allow for simultaneous expression of distinct effectors in distinct neuronal populations.

Effectors

Expression systems afford immense flexibility when it comes to the choice of effector transgenes. The most common use cases are visualization, functional read-out, activation, and silencing. I survey them one by one.

VISUALIZATION To characterize expression patterns, the tool of choice is jellyfish-derived green fluorescent protein (GFP; [Chalfie et al., 1994](#)) whose usefulness has been improved greatly through continuous genetic engineering since its first introduction (see for instance [Heim et al., 1995](#)). Modern iterations like UAS-CD8-GFP are membrane-bound and have been boosted in expression strength by placing many copies under the control of the activation sequence ([Pfeiffer et al., 2010](#)). This allows for high-resolution imaging of neural structures using the full spectrum of fluorescence microscopy techniques.

FUNCTIONAL READ-OUT Instead of just statically tagging neural structures, GFP can be engineered to change its fluorescence as a function of calcium concentration. Given the physiology of neural signal transmission, this can then act as a reasonable proxy for neural activity. Expression of such genetically encoded calcium indicators via GAL4-UAS makes it possible to simultaneously monitor the signaling of large groups of neurons in a minimally invasive and cell type-specific manner, thus providing a significant improvement over chemical indicators like OGB-1 ([Hendel et al., 2008](#)) and enabling access to cells whose size or position prohibits the use of electrophysiological methods.

Genetic engineering has produced a broad range of such proteins, all based on slightly different underlying mechanisms for binding calcium and modulating fluorescence ([Knöpfel, 2012](#)). TN-XXL, for instance, is based on fluorescence resonance energy transfer signalling and has been used successfully in the *Drosophila* visual system ([Mank et al., 2008](#); [Reiff et al., 2010](#)). GCaMP has recently emerged as the dominant class of *in vivo* calcium indicators. It is built from mutated GFP, calmodulin, and a peptide sequence derived from myosin light-chain kinase ([Nakai et al., 2001](#)). At this point, the sensor has gone through many iterations and offers critically improved brightness, signal-to-noise ratio, and temporal resolution ([Chen et al., 2013](#)). Certain issues do of course persist as even the most sophisticated indicators introduce significant delays and non-linearities. Moreover, the relationship between calcium concentration and voltage is complex and masks potentially crucial effects like hyperpolarization of the membrane or sub-threshold deflections. The development of equally well-engineered voltage indicators may help to alleviate these problems in the future ([Looger and Griesbeck, 2012](#)).

In addition, more specialized genetically encoded indicators have been developed for tasks like the cell-specific measurement of glutamate release ([Marvin et al., 2013](#)).

ACTIVATION When manipulating neurons, we have the choice between increasing and decreasing activity. Activating specific groups of neurons may

help in establishing the sufficiency of circuit elements for particular functions. This is sometimes achieved by integrating appropriate ion channels into neural membranes through GAL4-UAS. A pervasive example is the heat-sensitive cation channel UAS-dTrpA1 (Rosenzweig et al., 2005; Parisky et al., 2008) which strongly depolarizes the cell at moderately increased temperatures. This is advantageous as the experimenter can reversibly activate neurons with modest temporal resolution. Alternatives include the bacterial sodium channel NaCh-Bac which renders membranes hyper-excitable but does not permit such on-line control (Nitabach et al., 2006).

A downside of temperature-controlled effectors is that they can only be regulated on comparatively slow timescales. With the advent of optogenetics, however, ultra-precise millisecond-scale control of acute neural excitation has become feasible (Deisseroth, 2011). Lima and Miesenböck (2005), for instance, activated neurons through expression of the channel UAS-P2X₂ which was gated by light-released ATP. Modern techniques tend to focus on intrinsically light-sensitive effectors. Channelrhodopsin-2 is a genetically encodable light-gated cation channel that was initially isolated in green algae (Harz and Hegemann, 1991; Nagel et al., 2003). Upon illumination, it effectively depolarizes neurons (Boyden et al., 2005; Nagel et al., 2005). Its activation spectrum peaks at ≈ 470 nm, but red-shifted versions like UAS-CsChrimson have been engineered which allow for deeper tissue penetration and even activation through the cuticle of the fly head while minimizing visual interference (Klapoetke et al., 2014; Bath et al., 2014).

SILENCING To causally establish the functional necessity of any given neuron, conditional silencing of its activity while monitoring some appropriate read-out of the computation represents a principled and powerful approach. Various genetically targeted tools have been developed for this purpose. At the most extreme end of the spectrum, ectopic expression of apoptosis-related genes like *reaper* or *hid* can be used to irreversibly ablate specific cell types (Zhou et al., 1997). For the investigation of lesion effects in adult animals, this usually requires delayed expression of GAL4 and even then runs the risk of incurring off-target damage.

Thankfully, more subtle techniques for silencing are available. Tetanus toxin-derived UAS-TNT is a popular effector that interferes with the synaptic apparatus by cleaving neural synaptobrevin and thus blocking vesicle release (Sweeney et al., 1995). From the perspective of postsynaptic units, this renders the targeted neuron silent but does not disrupt internal electrophysiology. In contrast, ectopic expression of the mammalian inward-rectifying potassium channel Kir2.1 continuously hyperpolarizes the neuron in question. This disrupts the transmission of electrical signals to downstream cells (Baines et al., 2001). It should be emphasized that the choice of silencing mechanism can greatly influence the interpretation of phenotypes. UAS-TNT suppresses neurotransmitter release but leaves the electrophysiology of the cell largely unaffected. Inward-rectifying channels disrupt regular electric activity, which may result in a different outcome if the silenced cell is electrically coupled to other units in the network under investigation (for a relevant example, see Joesch et al., 2010).

As with activation, only conditional control of the effector cleanly distinguishes between specific and off-target or developmental effects. UAS-Shibire^{ts1} is a dominant-negative temperature-sensitive allele of dynamin, a GTPase that plays a critical role in the synaptic machinery recycling vesicles (Kitamoto, 2001; Pfeiffer et al., 2012). At permissive temperatures below $\approx 29^\circ\text{C}$, it functions normally. At restrictive temperatures, however, UAS-Shibire^{ts1} becomes ineffective; eventually, vesicles deplete and chemical transmission is disrupted. This effect is reversible and enables researchers to acutely silence specified neuron types. Finally, there are optogenetic tools that mediate inhibition at high temporal precision. Halorhodopsins, for instance, are chloride pumps that can be used to inhibit cell activity in a light-controlled, temporally exact way (Gradinaru et al., 2008).

1.4.2 Physiological techniques

Electrophysiology

Internally, neurons use electric potentials to transmit and transform information. The tools of electrophysiology grant a direct look into these processing mechanisms by measuring voltage or current changes in response to experimental manipulations.

Critically, such recordings can be performed at immense temporal resolution and *in vivo*. In bigger flies like *C. erythrocephala*, wide-field motion-processing neurons in the optic lobe have cell bodies and neurites that are sufficiently large to be accessible to sharp electrodes. In addition, the activity of certain spiking neurons can be monitored simply by placing an electrode in close vicinity. Through a combination of such intra- and extra-cellular approaches, the visual response properties of these units were established in great detail (Bishop and Keehn, 1967; Hausen, 1976; Eckert, 1980; Hausen, 1982a,b; Hengstenberg, 1982). Later research extended these techniques to paired recordings which made it possible to map connectivity within networks of motion-sensitive cells (Haag and Borst, 2004).

The comparatively small size of neurons in the *Drosophila* visual system usually prohibits the use of sharp microelectrodes and extracellular recordings. At least for a subset of cells, this limitation can be circumvented through so-called whole-cell patch clamp recordings which are a variation on the classic technique for ion channel characterization developed by Sakmann and Neher (1984). The approach has successfully been applied to various fruit fly brain areas, including the olfactory (Wilson et al., 2004; Murthy et al., 2008) and visual systems (Joesch et al., 2008; Behnia et al., 2014). Tagging neurons of interest using GAL4-driven GFP can assist during targeting of cell bodies. Remarkably, the technique may also be combined with simultaneous high-resolution read-out of locomotor behavior (Maimon et al., 2010).

Imaging

For many neurons, particularly in the visual periphery of *Drosophila*, patch clamp techniques either have small yield or are outright impossible. In the

absence of direct electrophysiological access, functional imaging of neural activity using genetically encoded, GAL4-guided indicators can serve as a powerful stand-in. Traditional microscopy techniques have been employed for this task, but out-of-plane emission, scattering of excitation light, and phototoxicity pose severe challenges when imaging deep layers of neural tissue using linear one-photon techniques.

Two-photon laser-scanning fluorescence microscopy avoids many of these issues and has become the de-facto standard for optical interrogation of neural activity (Denk et al., 1990; Helmchen and Denk, 2005). It exploits the two-photon absorption effect first predicted by Göppert-Mayer (1931). When the arrival of two photons coincides at some fluorescent molecule, energies may combine to lift the molecule into its excited state. Critically, for GFP or GCaMP this can be accomplished using laser-generated infrared light in the region of 1000 nm, modulated at high frequency and an extremely small pulse width on the order of 100 fs. Single photons then produce virtually no excitation. Only in the narrow focus range afforded by an objective with high numerical aperture are photons sufficiently numerous to stochastically interact, thus initiating the fluorescence-emission cascade. This results in high z-resolution as excitation out of plane is minimized. The focused laser beam scans the sample in a raster, so all reflected light collected by high-efficiency photo-multiplier tubes is associated with particular points in space. Light that is not in focus does not stimulate other fluorophore-tagged cells and the excitation wavelength is well out of the fly photoreceptor range. Additionally, infrared light incurs much less tissue damage than is typical for one-photon illumination.

Together with genetically encoded calcium indicators, the technique has been used to characterize neural response properties in the *Drosophila* visual system (Reiff et al., 2010; Clark et al., 2011). As in the case of electrophysiology, it has also been paired with behavioral measurements (Seelig et al., 2010; Chiappe et al., 2010; Seelig and Jayaraman, 2013).

1.4.3 Structural analysis

The project of mapping neural underpinnings of motion vision critically depends on knowledge of anatomy, morphology, and connectivity in vision-related circuits. After all, tools for manipulation and recording are only as valuable as our ability to target them to identified neurons of interest. Groundbreaking work was performed by Ramón y Cajal and Sánchez (1915) who applied Golgi's stochastic labeling method and light microscopy to the optic lobe of *Calliphora*. They assembled exquisitely detailed drawings of gross anatomy as well as individual neurons. Much later, this painstaking work was continued and resulted in neural atlases detailing the *Calliphora* brain (Strausfeld, 1976) as well as the optic lobes of *Drosophila* (Fischbach and Dittrich, 1989; Bausenwein et al., 1992). These maps remain a heavily consulted resource in the study of fly visual circuits (see also recent efforts regarding nomenclature by Ito et al., 2014).

The genetic techniques outlined above offer novel opportunities for the cartography of neural architecture. It is likely that modern GAL4 libraries cover

virtually all cell types in the *Drosophila* brain. Fluorescent reporters like GFP in combination with variations of the flip-out technique discussed in previous sections allow neuroanatomists to visualize isolated, identified neurons with high-resolution microscopy methods like confocal imaging (Minsky, 1988; Venken et al., 2011). In contrast to most other methods, this makes it possible to gather substantial amounts of data in a high-throughput regime. State-of-the-art stochastic and multicolor labeling techniques accelerate the process even more (Hampel et al., 2011; Hadjieconomou et al., 2011; Raghu and Borst, 2011; Nern et al., 2015; Mauss et al., 2015).

One regard in which all the techniques above fall short is proof of connectivity. The fly optic lobe is densely packed, particularly within processing-critical structures like the medulla. So while sufficient distance may rule out connections, mere proximity does not in itself prove chemical or electric synapses between two neurons. Connection matrices are powerful tools for generating hypotheses about functional circuits and excluding others. There are some light microscopy-based technologies that offer more stringent evidence of connectivity, such as GFP reconstitution across synaptic partners (GRASP; Feinberg et al., 2008).

The only anatomical technique that can resolve synaptic ultrastructure and therefore prove connections, however, is electron microscopy (Knoll and Ruska, 1932). The process of densely reconstructing neural tissue from such images is rather involved. Even in semi-automated pipelines, it requires fixation, possibly staining, extremely precise sectioning, scanning, subsequent alignment, two-dimensional segmentation, linkage in three dimensions, synapse annotation, and labor-intensive proofreading by trained researchers (Takemura, 2015). Several techniques have been developed to automate substantial parts of this sequence (Denk and Horstmann, 2004; Jain et al., 2010). The final output then allows exact counting of chemical synapses between identified neuron types. This approach has made great strides in mapping connectivity in the mammalian retina (Briggman et al., 2011; Helmstaedter et al., 2013; Kim et al., 2014). Building on pioneering work in the fly lamina (Meinertzhagen and O'Neil, 1991), motion vision-relevant portions of downstream structures have recently been reconstructed using serial-section transmission electron microscopy (ssTEM; Takemura et al., 2008, 2011, 2013; Rivera-Alba et al., 2011; Shinomiya et al., 2014). Resulting plans of anatomy and connectivity have been crucial guides in subsequent circuit mapping efforts.

1.5 NEURAL SUBSTRATES OF FLY MOTION VISION

In concert, the techniques of circuit neuroscience have painted a detailed picture of how motion is computed in the visual system of flies. At the level of gross anatomy the fruit fly brain consists of two parts, a thoracic ganglion and a central brain located in the head (Figure 5a). Estimates put the overall number of neurons on the order of 10^5 cells³ (Morante and Desplan, 2004).

³ Benzer (1967) remarks that scaled logarithmically, the fly nervous system resides halfway between a single neuron and the human brain.

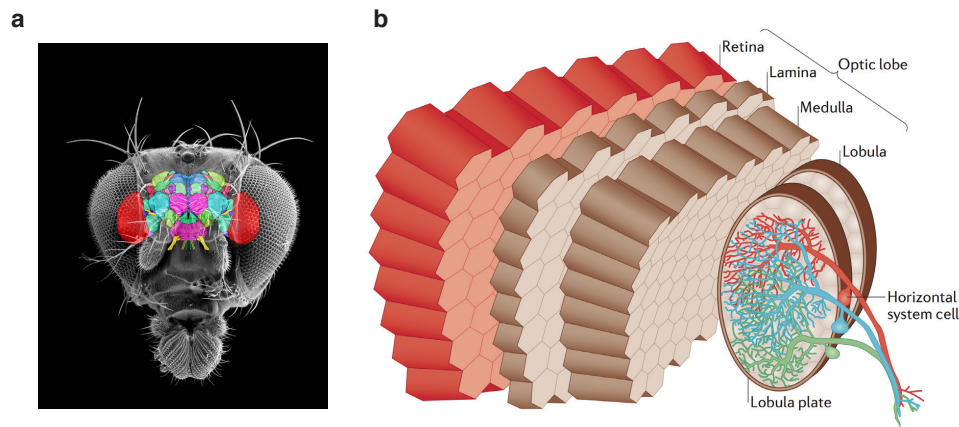


Figure 5: Anatomy of the fruit fly nervous system. **a** Schematic of the fly brain overlaid onto a picture of the *Drosophila* head. Illustration from Ito et al. (2014). **b** Gross anatomy of the fly optic lobe, divided into retina, lamina, medulla, and the lobula complex consisting of lobula and lobula plate. Neuron schematics depict three tangential cells of the horizontal system (HS). Illustration from Borst (2014).

A significant portion of these units, possibly more than half, is devoted to the processing of visual information. This occurs primarily in the optic lobes located behind prominent compound eyes (Figure 5b). The subunits of this ganglion—lamina, medulla, and a lobula complex consisting of lobula plate and lobula—exhibit an interesting combination of stereotypy and cellular diversity, with clearly repetitive columns dominating high-level structure but the number of distinct neural types exceeding a hundred (Fischbach and Dittrich, 1989).

The following sections introduce the neural structure of the *Drosophila* optic lobe, seen through the lenses of function and specifically motion vision. Where suitable, I reference the rich history of inquiry into motion detection in larger flies given that many mechanisms are thought to be preserved among dipteran species.

1.5.1 Retina

All sensory systems start at transduction, the process of transforming physical signals of interest into activity of sensory neurons. For insect vision, this is achieved by photoreceptors in the retina that convert impinging light into electrical signals. The operation yields time- and space-resolved signals from which visual cues like color, motion, or object position can be computed downstream. Critically, incoming optical signals are projected into a sensor-centric, two-dimensional coordinate system where each "pixel" corresponds to some location in retinotopic space.

The compound eye of the fruit fly comprises ≈ 800 hexagonally laid-out ommatidia or facets whose average axial separation is slightly below 5° (for a detailed map of the somewhat inhomogeneous fruit fly eye, as compiled by Erich Buchner, see Heisenberg and Wolf, 1984). Each ommatidium has an acceptance angle of $\approx 5^\circ$ in half-width (Götz, 1965). Resolution and visual

acuity of *Drosophila* are thus comparatively low (Land, 1997). In contrast to single-lens configurations like the mammalian eye, each facet has its own optical system that focuses incoming light onto a set of eight photoreceptors per ommatidium. The sensory neurons separate into six outer (R1 through R6) and two inner units (R7 and R8). These receptors are highly sensitive as well as incredibly fast due to an amplifying and adaptive transduction cascade that scales from single photon incidences to day-light conditions, separated in flux by many orders of magnitude (Hardie and Raghu, 2001; Hardie and Juusola, 2015).

To maximize interaction surface, the inside of the photoreceptor is lined with $\approx 30\,000$ microvilli, each containing the machinery for transduction. Together, they form the wave-guiding rhabdomere. The transduction cascade is initiated when photons are absorbed by rhodopsin which induces the metarhodopsin state via photoisomerization. Interestingly, while the vertebrate cascade requires time-consuming reconstitution of rhodopsin through enzymatic pathways, re-isomerization in flies is simply achieved by exposure to longer-wavelength light. Shielding pigments in the *Drosophila* eye are transparent to these wavelengths, giving them their characteristic red color. Scattering light can therefore continuously and efficiently reset the cascade. Following isomerization, rhodopsin induces the dissolution of the G-protein Gq whose α -subunit in turn binds to a phospholipase C (PLC) isoform encoded by *norpA*. As expected, flies with mutations in this locus are blind (Bloomquist et al., 1988). Via some still partially unmapped mechanism, PLC activation gates transient receptor potential channels, the calcium-conductive TRP and TRPL, which finally depolarize the cell. There is intriguing evidence that the PLC-controlled opening of TRP channels involves a mechanical step, contraction of the cell membrane (Hardie and Franze, 2012). In *Drosophila* this cascade can operate incredibly quickly: single-photon responses are $10\times$ to $100\times$ faster than those in mammalian rod photoreceptors, explaining flicker fusion frequencies in excess of 200 Hz (Heisenberg and Wolf, 1984; Hardie and Juusola, 2015).

Wavelength sensitivity is largely determined by the absorption profile of the rhodopsin. R1-6 express the *ninaE*-encoded wide-spectrum opsin Rh1 with sensitivity that peaks twice, once in the ultraviolet range and once at $\approx 480\text{ nm}$. They provide high-resolution input to achromatic visual behaviors like motion vision. Mutations that affect R1-6 or Rh1 as well as genetic silencing of R1-6 through specific expression of UAS-Shibire^{ts1} drastically impair both optomotor and fixation response (Heisenberg and Buchner, 1977; O'Tousa et al., 1985; Rister et al., 2007). R7 and R8, on the other hand, contain stochastic combinations of more sharply tuned single-peak rhodopsins (Franceschini et al., 1981) and mediate spectral behaviors like color discrimination at low spatial resolution (Schnaitmann et al., 2013). Their inactivation does not substantially affect motion-guided behavior (Yamaguchi et al., 2008), but some have argued that R7 and R8 activity shapes R1-6 responses through gap junctions (Wardill et al., 2012).

An interesting complication arises from the fact that the outer photoreceptors have slightly offset optical axes due to the geometry of the ommatidium that houses them; R1 through R6 thus point in slightly different directions in visual space. If the mapping from ommatidia to downstream cartridges,

each processing signals from a point in the visual field, was one-to-one, summation of the photoreceptors would significantly lower spatial acuity. Instead, *Drosophila* makes use of neural superposition. Photoreceptors with parallel optical axes from neighboring ommatidia are routed into the same cartridge downstream, forming a neuro-cartridge whose inputs are properly aligned (Trujillo-Cenóz and Melamed, 1966; Braitenberg, 1967). This sophisticated wiring scheme preserves acuity while maximizing sensitivity through pooling of multiple receptors and often outperforms the apposition or optical superposition eyes of other arthropods (Kirschfeld, 1967).

1.5.2 Lamina

Structure

Axons of retina photoreceptors R1-6 project into the first neuropil of the optic lobe, the lamina. It consists of eight strictly repeated cell types that are arranged in retinotopic columns corresponding to the neuro-cartridges outlined above. That is, visual information from adjacent points in visual space is processed in anatomically adjacent modules of the lamina (Fischbach and Dittrich, 1989). Lamina monopolar cells L1-5 are the most prominent instances of these periodic neurons, providing feedforward signals to various layers of the subsequent neuropil, the medulla. Centrifugal neurons C2 and C3 as well as T1, on the other hand, receive dendritic input in the medulla and send what is generally presumed to be feedback to the lamina. In addition to this set, there are four infra-periodic cell types whose arbors span multiple columns: lamina wide-field neurons Lawf1 and Lawf2 which receive input from the medulla, the lamina-tangential neuron Lat which connects central brain and lamina, and the lamina-intrinsic neuron Lai.

Electron microscopy studies have shed significant light on lamina connectivity (Meinertzhagen and O'Neil, 1991; Rivera-Alba et al., 2011). Only L1-3 receive direct input from photoreceptors R1-6 although there is evidence that L4 is postsynaptic to at least R6. L1 and L2 are known to be electrically coupled (Joesch et al., 2010), and L2 forms a reciprocal sub-network with L4 cells in its own as well as neighboring columns. Far from being neatly segregated, column-intrinsic lamina networks therefore exhibit substantial complexity. While C2 and C3 synapse onto multiple lamina targets, nothing is known about within-lamina connectivity of T1. The connectivity of multicolumnar feedback neurons is somewhat diffuse, with Lawf1 and Lawf2 for instance connecting to multiple cells. While the neurotransmitter identity of many lamina cells remains unclear, Takemura et al. (2011) could establish L1 as glutamatergic and both L2 and L4 as cholinergic using transcript profiling in single cells.

Function

Monopolar cells L1-3 express an *hcla*-encoded, *ort*-dependent chloride channel that is gated by photoreceptor-released histamine (Hardie, 1989; Gengs et al., 2002). Physiological response properties of lamina monopolar cells were first described in larger fly species where comparatively large cell bod-

ies permit electrophysiological recordings with sharp electrodes (Laughlin and Hardie, 1978; Laughlin, 1981; Laughlin and Osorio, 1989). Photoreceptors depolarize in response to light. Lamina monopolar cells, on the other hand, hyperpolarize transiently in response to step-like illumination, followed by weaker sustained polarization. When the stimulus is switched off, rebound depolarization occurs. All signalling occurs via graded potentials. Lamina processing is therefore well approximated by inverting and high-pass filtering the photoreceptor voltage response. Critically, lamina cells are not selective for direction.

More recently, genetically encoded calcium indicators have made it possible to directly record response properties of identified lamina cells in the fruit fly. L1 and L2 respond identically and in line with blowfly findings to luminance changes (Reiff et al., 2010; Clark et al., 2011) while L4 and particularly L3 exhibit less transient response dynamics (Silies et al., 2013; Meier et al., 2014). Moreover, L2 receptive fields display a noticeable inhibitory surround that contributes to their size selectivity and differentially shapes temporal response characteristics (Freifeld et al., 2013). In contrast, L4 responses appear to pool from large parts of the visual field, suggesting an intriguing role for electric coupling within this lamina network (Meier et al., 2014). Patch-clamp recordings from lamina wide-field neurons revealed sensitivity to slow oscillations in luminance, hinting that these neurons provide feedback about lighting conditions to lamina circuits (Tuthill et al., 2014).

The combination of direct lines L1-3 and indirect relays L4-5 provides heavily multiplexed visual information to downstream medulla circuits. This suggests a form of division of labor when it comes to computations and behaviors mediated by their input. Genetic silencing via GAL4-UAS has allowed multiple studies to examine such functional differences, particularly between the large monopolar cells L1 and L2. Rister et al. (2007) could show in behavioral tasks that blocking both cells in conjunction renders flies optomotor-blind, emphasizing the critical contribution of L1 and L2 to the detection of motion. Moreover, their experiments tentatively suggested that the L1 and L2 pathways mediate the extraction of particular directions of retinal optic flow (back-to-front versus front-to-back, respectively). Other studies implicated L2 specifically in looming detection or the regulation of translational velocity (de Vries and Clandinin, 2012; Katsov and Clandinin, 2008). A critical insight came from the use of contrast-specific stimuli. When stimulating with bright (ON) or dark (OFF) traveling edges, electrophysiological recordings in motion-sensitive tangential cells of the lobula plate revealed a strong divergence between L1 and L2 block phenotypes (Joesch et al., 2010). When L1 was silenced, ON responses were strongly reduced while leaving the other polarity unaffected. Conversely, when L2 was silenced, only OFF responses were abolished. This indicated that similarly to the vertebrate retina, the fly visual system computes motion separately for stimuli defined by positive and negative contrast. L1 then provides the input to an ON pathway and L2 to an OFF pathway. Behavioral experiments later found comparable phenotypes in walking and flying *Drosophila* (Clark et al., 2011; Tuthill et al., 2013). Moreover, Reiff et al. (2010) found evidence of appropriately signed half-wave rectification in flash responses of L2 axon

terminals in the medulla (which may differ in dynamic stimulus regimes, see [Clark et al., 2011](#); [Strother et al., 2014](#)).

There is still considerable uncertainty about the particular functional roles that lamina pathways other than L1 and L2 play. L3 has been associated with chromatic processing ([Gao et al., 2008](#)), but [Silies et al. \(2013\)](#) propose that the monopolar cell is also involved in OFF motion processing. Recording from tangential cells in the lobula plate, [Meier et al. \(2014\)](#) observed abolished OFF motion responses after silencing L4 which again points towards interesting interactions within the local sub-network of L2 and L4. Finally, a large-scale behavioral screen in which all twelve lamina cells were silenced individually could not reveal clear-cut phenotypes for lamina units outside of L1 and L2 ([Tuthill et al., 2013, 2014](#)).

1.5.3 Medulla

Structure

The major target of lamina monopolar cell axons is the medulla, a secondary structure of the optic lobe. It is characteristically stratified and consists of ten layers (M1 through M10), clearly separable by determining projection patterns and arborization ([Fischbach and Dittrich, 1989](#)). Processing in the medulla remains retinotopic but crosses along the antero-posterior axis within the neuropil-separating chiasm. Here, representations fan out drastically. More than 60 columnar cell types can be distinguished based on morphology and ramifications, presumably providing a large number of specialized visual channels to downstream circuits. Medulla neurons send parallel projections into both neuropils of the lobula complex and fall into at least three categories:

- Medulla-intrinsic (Mi) cells that connect upper (distal) to lower (proximal) layers of the medulla
- Trans-medulla (Tm) cells whose projections go beyond the medulla, predominantly into the lobula
- Trans-medulla Y cells (TmY) whose projections bifurcate, reaching both lobula and lobula plate

In addition, so-called "bushy" T cells (T2-5) appear multiple times per column. While T2-4 receive input within the confines of the medulla, T5 connects lobula and lobula plate. T4 and T5 share a particular projection pattern with individual units targeting specific strata of the four-layered lobula plate. For this reason as well as due to functional considerations, I discuss T5 in the section at hand⁴. T4 and T5 can be classified into four sub-types, T4a-d and T5a-d, which target distinct downstream layers. The two types are therefore classified as hypercolumnar ([Bausenwein et al., 1992](#)). Crucially, along with TmY cells, they project retinotopically from medulla and lobula

⁴ Indeed, some studies hold that the lobula and particularly the lobula layers in which T5 cells ramify originated from proximal strata of the medulla that were displaced in the course of evolution ([Douglass and Strausfeld, 1996](#); [Shinomiya et al., 2015](#)).

into the lobula plate where wide-field motion-sensitive tangential cells are located (Fischbach and Dittrich, 1989; Douglass and Strausfeld, 1996).

Through electron microscopy studies, projections of lamina monopolar cells in the upper layers of the medulla have been mapped in great detail (Takemura et al., 2008). L1 and L5 arborize in layers M1 and M5, L2 in layer M2, L3 in layer M3, and L4 in layers M2 and M4. Interestingly, R7 and R8 extend axons that bypass the lamina and directly target distal layers of the medulla. Such patterns have guided hypotheses about connectivity between lamina and medulla cells. The arborization pattern of trans-medulla cell Tm2, for instance, suggested that it receives input from L2. This could later be confirmed by further reconstruction efforts (Takemura et al., 2011).

Bausenwein et al. (1992) analyzed Golgi stainings of medulla cells and proposed at least two major pathways connecting lamina to lobula plate via medulla and lobula. One consists of the sequence L1, Mi1, and T4 and the other involves L2, Tm1, and T5. Recent connectomic efforts within the medulla have started to complete this picture. Takemura et al. (2013) could confirm the L1-Mi1-T4 chain and put forward Tm3 as another critical input to T4. Similarly, Takemura et al. (2011) implicated Tm2 in the pathway downstream of L2, with further projections arising from connections within the L2-L4-Tm2 circuit. Subsequent reconstructions traced connections from Tm1 and Tm2 onto T5 and found that medulla neurons Tm4 and Tm9 also synapse onto T5 dendrites in the lobula (Shinomiya et al., 2014). Interestingly, Tm9 receives dominant lamina input from L3. In light of the functional division between ON and OFF pathways shown through silencing experiments involving L1 and L2, these medulla circuits emerged as likely candidates for the neural implementation of motion detection. Critically, however, any such anatomical model requires confirmation through functional studies.

Function

Neural processes in the medulla are numerous, densely packed, and heavily intertwined. In combination with the small size of associated cell bodies, this has greatly hindered characterization of their visual response properties. Even for larger flies like *C. vicina* only sparse electrophysiological data exist, collected predominantly from unidentified units (Mimura, 1972; DeVoe, 1980; Douglass and Strausfeld, 1995, 1996). An interesting approach for identifying motion-relevant medulla pathways based on 2-deoxyglucose activity labeling under visual stimulation was pursued by Bausenwein and Fischbach (1992). They used a comprehensive set of patterns that included rotating and expanding square-wave gratings as well as isolated traveling stripes. Post-hoc analysis of staining distributions within the fruit fly medulla corroborated the two motion-related pathways anatomy had suggested, again indicating that T4 and T5 may be critical motion-relevant projections to the lobula plate.

Optical interrogation methods like GAL4-targeted two-photon calcium imaging have now made headway toward understanding signal processing that occurs in the medulla. Meier et al. (2014), for instance, used this technique to record visual response properties of Tm2 terminals in the first layer

of the lobula. Tm2 cells respond preferentially to OFF edges and are themselves not selective for direction. Taking a different approach, Behnia et al. (2014) characterized a subset of candidate motion circuit cells using GFP-guided patch clamp. Their work demonstrated that presumed ON pathway cells Mi1 and Tm3 depolarize in response to brightening stimuli; OFF pathway cells Tm1 and Tm2, on the other hand, depolarize in response to darkening stimuli. None of the cells were themselves direction selective. Quantification of their output kinetics revealed exceedingly small differences between time constants of each pair, which were proposed to underlie motion selectivity following non-linear combination downstream. In a first approximation, this agreed with the division into two pathways originating from L1 and L2, respectively, that genetic silencing approaches and anatomy had supported (Joesch et al., 2010; Takemura et al., 2013).

Electrophysiological evidence from the blowfly had indicated that T4 cells are not selective for direction, but these studies were unable to reliably establish cell identity and suffered from low yield (Douglass and Strausfeld, 1996). Two key findings in *Drosophila*, however, made T4 and T5 promising candidates for the task of relaying motion information to the lobula plate. First, when they were genetically silenced in combination using either UAS-Kir2.1 or UAS-Shibire^{ts1}, motion responses in lobula plate tangential cells downstream of the medulla were fully abolished (Schnell et al., 2012). Second, the same block flies could be shown to be completely optomotor-blind when tested on a treadmill set-up (Bahl et al., 2013). Yet, the exact role of T4 and T5 in computing motion as well as potential functional differences still awaited clarification.

1.5.4 Lobula complex

Structure

Two separate neuropils, lobula and lobula plate, together form the lobula complex. As mentioned above, medulla projections bifurcate and target the two downstream structures in parallel. Additionally, lobula processes connect to the lobula plate, most saliently among them the four sub-classes of T5 (Fischbach and Dittrich, 1989). Both structures are stratified; based on arborization patterns and morphology, the lobula can be subdivided into at least six layers and the lobula plate into four.

The lobula complex is the major source of projections from the optic lobe to other areas of the fly brain. Comparatively little is known about lobula projection neurons, both functionally and structurally, but anatomical characterizations have revealed LC neurons as a numerous and heavily subdivided class that collectively spans the retinotopic representation of visual space in the lobula (Otsuna and Ito, 2006).

In contrast and due to its role in motion processing, the lobula plate particularly of larger dipteran species has received a great deal of anatomical and functional attention over the past decades (for thorough reviews, see Borst and Haag, 2002; Borst et al., 2010). Large tangential cells represent the most striking group of neurons in the lobula plate. Based on anatomy and response characteristics, over 60 so-called lobula plate tangential cells

(LPTCs) have been described in *C. vicina*. The tremendous dendritic trees of individual LPTCs sample input from hundreds of columns and thus large portions of visual space. Individual processes can reach diameters close to 10 μm . The ramifications of LPTCs are often highly specific. Cells of the horizontal system (HS), for instance, receive major input from frontal layers of the lobula plate while vertical system (VS) cells arborize primarily in the posterior part. The mapping of the *Drosophila* lobula plate is less complete. However, several studies have been able to identify corresponding LPTCs that closely match their counterparts in larger flies (Fischbach and Dittrich, 1989; Scott et al., 2002; Joesch et al., 2008; Schnell et al., 2010).

From the lobula complex, projections take three major routes. Lobula neurons primarily target optic glomeruli in the lateral protocerebrum (Mu et al., 2012). Axons of LPTCs either go to motor areas of the thoracic ganglion via descending neurons or directly to neck motor neurons that govern head movement (Strausfeld and Bassemir, 1985; Borst, 2014).

Function

Due to their size and accessibility, LPTCs have been prime targets for electrophysiological studies in "big" flies (Hausen, 1976, 1982a,b; Hengstenberg, 1982; Borst et al., 2010) and even *Drosophila* (Joesch et al., 2008; Schnell et al., 2010). They respond to motion in a direction-selectively opponent fashion and have receptive fields that extend over substantial parts of the visual field. HS cells, for example, depolarize when stimulated with front-to-back motion and hyperpolarize in response to the opposite direction. For VS cells, the preferred direction is downward. In the fruit fly, at least three HS cells (HSN, HSE, and HSS) and six VS cells (VS1-6) have been identified (Joesch et al., 2008; Schnell et al., 2010). A significant fraction of LPTCs signals via graded potentials; others, like H1 in *Calliphora*, spike. Interestingly, the cells recapitulate many of the properties of the optomotor reflex. Under sinusoidal stimulation, the response magnitude has an optimum and depends on wavelength and contrast of the pattern. Indeed, similarly to the optomotor response, LPTCs are tuned to the contrast frequency $\frac{\nu}{\lambda}$ of a drifting grating. Sensitivity peaks in the range of 0.5 Hz to 1 Hz.

Multiple lines of evidence have linked these cells to visually guided locomotion. When motion receptive fields of LPTCs are measured at high spatial resolution, they resemble filters that are matched to the optic flow generated by particular maneuvers. VS cells in *Calliphora*, for instance, are tuned such that they are maximally activated by input that would result from rotation around specific horizontal body axes (Krapp and Hengstenberg, 1996). Similar logic holds for other LPTCs like HS and corresponding units in the fruit fly (Krapp et al., 1998; Schnell et al., 2010). This suggests that tangential cells act as ego-motion sensors, allowing the fly to monitor and correct its head orientation and trajectory based on visual input. Intrinsic connections as well as contralateral projections appear to play critical roles in tuning this optic flow-processing network (Borst and Weber, 2011; Weber et al., 2012). For instance, there is evidence that electric coupling within sub-networks like VS further refines flow field selectivity (Haag and Borst, 2004). Finally, micro-surgical ablations of LPTCs as well as mutations that affect the lobula

plate produce specific impairments of associated head or body movements (Heisenberg et al., 1978; Geiger and Nässel, 1981; Hausen and Wehrhahn, 1983).

The layer-specificity of LPTC dendrites has critical functional relevance. Using deoxyglucose-based activity mapping while stimulating fruit flies with moving gratings, Buchner et al. (1984) could show that the four layers of the lobula plate respond to motion along four cardinal directions in visual space: front-to-back (layer 1), back-to-front (layer 2), upward (layer 3), and downward (layer 4). This is compatible with the observation that LPTCs ramify in layers matching their preferred direction (Heisenberg et al., 1978; Schnell et al., 2010). The identity of the relevant projection cells as well as the locus of motion detection, however, have proven elusive.

Little is known about visual response properties of lobula projection neurons. Nonetheless, studies on various fly species have suggested a wide range of stimulus selectivity in the lobula complex, including cells that respond preferentially to looming patterns (de Vries and Clandinin, 2012), figure-ground motion (Egelhaaf, 1985), or movement of small objects (Barnett et al., 2007).

1.6 ALGORITHMIC MODELS OF MOTION DETECTION

What is required before one can reasonably claim to understand any given system? A popular answer—particularly in the tradition of cybernetics—comes in the form of modeling, the process of building artificial mechanisms that emulate the computations and behaviors accomplished by real brains. If we can replicate what any given neural circuit is doing, and ideally do so quantitatively, substantial progress toward understanding has been made. Models then allow us to isolate minimally required elements, explain existing variance, and predict new results, thus driving subsequent experimental work. They come in many forms, ranging from the simplified and abstract (such as regression or filters) to the complex and concrete (such as biophysical cell models or recurrent neural networks).

Yamins and DiCarlo (2016) identify three qualities that models of sensory systems should possess:

- Stimulus-computability (the ability to accept arbitrary stimuli within the relevant domain)
- Mappability (an internal structure that can be compared to neural circuitry)
- Predictivity (the ability to compute output for individual stimuli, particularly ones not seen during model fitting)

While formulated in the context of visual cortical processing, I argue that these demands apply to sensory models in general. Of course, an additional constraint comes from simplicity. If possible, models ought to be as intricate as necessary but no more. With increasing numbers of parameters and general unwieldiness, models run the risk of over-fitting particular data sets

and lose their ability to pinpoint critical computational principles (for an example of a large-scale model of presumably limited explanatory value, see [Markram et al., 2015](#)).

Motion vision offers a noteworthy example for the productive interplay between experiment and modeling. Early attempts at explaining the psychophysics of motion perception in a connectivist model can be traced back to [Exner \(1894\)](#). However, his circuit scheme was quantitative only in the vaguest sense. [Hassenstein and Reichardt \(1956\)](#) then made the crucial step toward an algorithmic description of motion processing, one that related motion stimulus to graded behavioral responses using the rigorous tools of signal processing theory. Decades of subsequent research have shown that this detector beautifully fulfills the criteria outlined above. In the following section, I review major models for motion detection in the specific context of fly vision.

1.6.1 Fundamental requirements

Motion of objects has a simple physical definition, displacement over time. Velocity is then given by the elementary difference

$$v = \frac{dx}{dt} \quad (5)$$

where x denotes position and t time. Direction is easily extracted by identifying the sign of v . If a motion algorithm had access to high-level features like object position, then motion estimation would be a simple task. However, there is strong evidence that animals from fly to primate extract directional signals directly from simple luminance signals ([Borst and Euler, 2011](#); [Adelson and Bergen, 1985](#)).

The geometry of motion dictates some basic requirements that any such detector must satisfy ([Borst and Egelhaaf, 1989](#)):

1. Signals have to be sampled at a minimum of two spatial locations. Any input from one location (which [Reichardt \(1987\)](#) calls a 1-input graph) is inherently ambiguous with regard to direction.
2. The two signals have to be processed asymmetrically. If the detector is mirror-symmetrical, flipping the stimulus along the axis of motion has no effect on the output even though the direction reverses.
3. Input signals have to be combined in a non-linear fashion. Linear motion filters can be constructed and signal direction under certain constraints (see for instance [Watson and Ahumada, 1985](#)). In general, however, they fail to model empirical direction selectivity as their time-averaged output is equivalent to the time-averaged input signals, thereby discarding critical information about stimulus sequence.

In the next part, I discuss the two major classes of motion algorithms that fit the outlined criteria.

1.6.2 Gradient detectors

If one has access to a local gradient of the luminance pattern $I(x, t)$ across space x and time t , then stimulus velocity is readily obtained from the relation

$$\frac{\partial I}{\partial t} = \frac{\partial I}{\partial x} v \quad (6)$$

through division of the temporal gradient by the spatial gradient. The scheme was first described in the context of computer vision (Limb and Murphy, 1975; Fennema and Thompson, 1979) and has several appealing properties. For instance, its output is proportional to local and instantaneous velocity and does not depend on geometrical properties of the stimulus like pattern wavelength or contrast. Moreover, for a fixed-velocity stimulus the estimate is constant in time. Several studies have successfully applied this detector model to the study of biological motion vision (Hildreth and Koch, 1987; Johnston and Clifford, 1995; Borst, 2007).

It is of course unlikely that biological realizations of the gradient detector compute fully localized derivatives. Neurally plausible models commonly estimate the spatial derivative as a finite difference between two luminance-sensitive receptors sampling spatially displaced image locations. They then approximate temporal differentiation through mean adaptation as realized by, say, a basic high-pass filter (Srinivasan, 1990; Borst and Euler, 2011).

To operate effectively, the detector clearly requires robust approximations of the luminance gradient. A divisive non-linearity confers several advantages, such as invariance to stimulus contrast, but fails under challenging stimulus conditions. For instance, if pattern contrast is low, spatial derivatives may approach zero and cause the velocity estimate to either amplify random fluctuations of the temporal gradient or become undefined. For vision, the problem is exacerbated by the Poisson statistics of photon incidence. Such "shot noise" makes photoreceptor output unreliable under low-light conditions (Laughlin, 1996). Simulations indicate that for input conditions dominated by noise, the information rate of gradient detectors drops dramatically (Borst, 2007).

Some formulations circumvent the issue through non-linearities that are less dependent on stable estimates of the gradient, like the logical veto gate put forward by Marr and Ullman (1981). Potters and Bialek (1994) suggested that motion vision should only be mediated by gradient detectors in the regime of large signal-to-noise ratios. If stimuli are noisy, more robust algorithms like the correlation detector described below ought to be preferred. Counter to this dual-mechanism postulate, Haag et al. (2004) could show that blowfly motion vision exhibits the hallmarks of correlation-based schemes across a wide range of pattern luminances. The proposed trade-off between mechanisms was not observed.

1.6.3 Correlation detectors

Correlation detectors represent the predominant class of motion extraction models used in sensory neuroscience. They have successfully been employed to explain properties of motion vision across a wide spectrum rang-

ing from psychophysics and animal behavior down to physiological responses of direction-selective cells.

Fundamentally, the algorithm is based on the asymmetrically delayed comparison of two spatially separated visual inputs. This lines up well with physical intuitions about motion. When an object moves from one location to the next, we observe a visual match across time and space. A bright dot moving from left to right, for instance, produces first a positive deflection in the output of the leftmost photoreceptor and then, after a time determined by the object's velocity, a positive deflection in the adjacent rightward location. In a sense, motion detection then reduces to the task of determining the temporal sequence of these two visual events. The logic conveniently extends to continuous luminance signals. By isolating slanted spatiotemporal correlations, one can compute the direction and magnitude of motion from locally sampled brightness inputs. The operation then closely resembles cross-correlation of two spatially separated inputs (Reichardt, 1987).

Reichardt detector

The first quantitative description of a correlation-type motion detector was derived from optomotor behavior in *Chlorophanus viridis* walking on a Y-maze (Hassenstein, 1951). Their textured rotating drum was only observed through a pair of separated slits, so the stimulus consisted of two spatially and temporally isolated brightness changes resembling apparent motion (Wertheimer, 1912). Hassenstein showed that the beetle would robustly turn with pattern motion if the events had the same contrast polarity. That is, combinations of either two bright (ON) or two dark (OFF) events elicited syndirectional turning. However, for mixed-polarity sequences (ON-OFF or OFF-ON) turning was inverted. This response is closely related to the psychophysical phenomenon of reverse-phi (Anstis, 1970; Anstis and Rogers, 1975). When Hassenstein and Reichardt (1956) varied spatial and temporal separation of the flashes, they found clear optima. Critically, the ideal spatial separation was approximately equivalent to beetle's inter-ommatidial distance.

A critical insight for model building came from analogy to the rules of sign-correct multiplication. Equally signed products are positive, mixed products negative. This led to the development of what is interchangeably called Hassenstein-Reichardt correlator, Reichardt detector, or elementary motion detector (Reichardt, 1961). It computes local motion and can operate directly on continuous luminance signals, thus processing arbitrary visual inputs.

In its basic form, the detector consists of two mirror-symmetrical subunits (Figure 6a). Each receives visual input from two distinct points in visual space separated by the sampling distance $\Delta\phi$, one of which is then delayed with respect to the other. This processing step can take many forms, including a true delay that leaves the signal otherwise unchanged, but is often implemented as a first- or second-order linear temporal filter. Such low-pass filters incur a phase shift that effectively delays arbitrary time-varying signals. Subsequently, the two signals are multiplied.

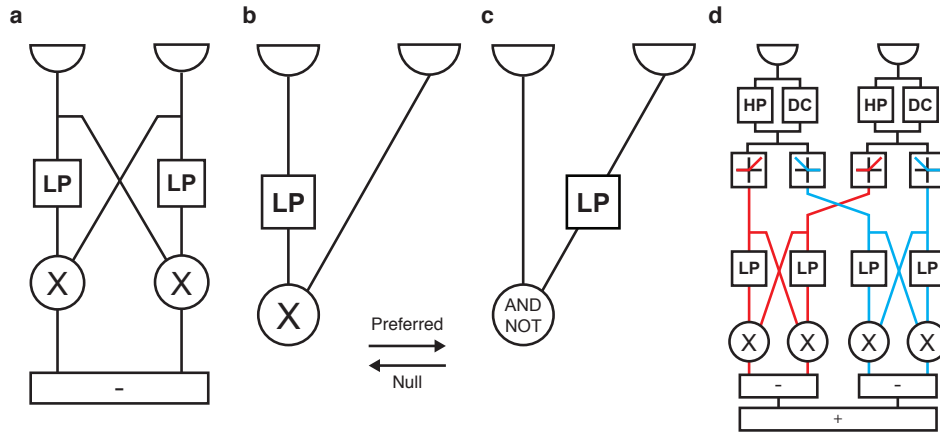


Figure 6: Architecture of basic and elaborated correlation detectors. **a** Fully opponent Reichardt detector based on multiplication of spatially separated, asymmetrically filtered inputs. It responds positively to preferred rightward and negatively to null leftward motion. **b** Reichardt-type half-detector using facilitation of preferred motion. **c** Barlow-Levick detector. Note that here, the non-linearity is a veto gate and the delay has switched sides to maintain preferred direction. **d** Elaborated Reichardt detector derived from findings on polarity specialization in the *Drosophila* visual system (Eichner et al., 2011).

This combination of filtering and multiplication implements the delay-and-compare algorithm described above: if $\Delta\phi$ and the time constant of the delay filter are matched to the direction and velocity of the traveling object, two signal deflections will coincide at the multiplier and give rise to a large signal. This happens only when the object first passes the delayed line, therefore moving along the preferred direction of the subunit. Conversely, if the object moves in the opposite (or null) direction, excitations are mistimed and produce small or no output. Finally, the output signals of the two oppositely tuned subunits are subtracted. This results in a fully opponent direction-selective detector that responds positively for its preferred and negatively for its null direction. Additionally, the subtraction stage suppresses signals produced by motion-unrelated visual cues like static illumination or full-field flicker. Under the assumption that each ommatidium provides one such input signal, the algorithm parsimoniously explains the aforementioned findings on optomotor responses in the beetle. In particular, it predicts the inversion that occurs when negative and positive contrast are combined in appropriately spaced spatial and temporal succession. Its architecture also adheres to the three criteria listed in the previous section, with multiplication supplying the non-linearity (Borst and Egelhaaf, 1989).

Any elementary motion detector is only sensitive to motion within the small part of the visual field defined by nearest-neighbor interactions of inputs. To generate the behavioral optomotor response, Hassenstein and Reichardt (1956) proposed that a large array of detectors is spatially integrated. When stimulated with periodic sine gratings traveling at a fixed velocity, individual detectors produce sinusoidally modulated output. Direction is encoded in the offset or temporal mean of the response. After summation, responses still show some initial oscillations. However, the steady-state re-

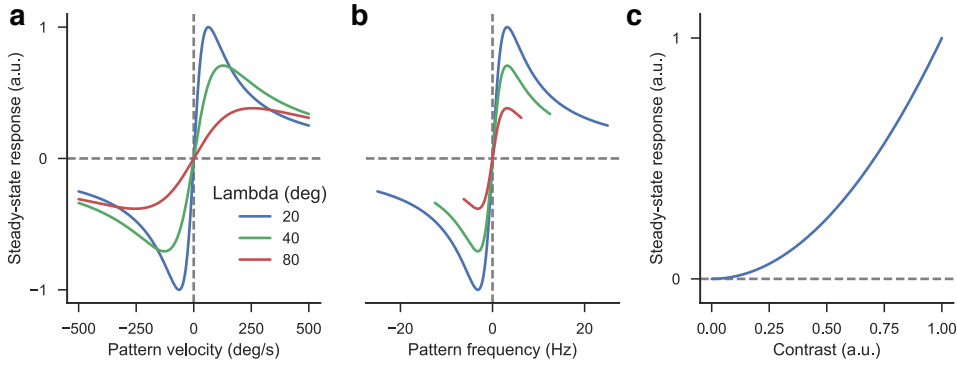


Figure 7: Response properties of a Reichardt detector array. **a** Velocity tuning for simple sinusoidal gratings. The value of the response optimum depends on pattern wavelength λ . **b** Data from **a** replotted on a frequency scale. Peaks now align, indicating that the detector is tuned to contrast frequency. **c** Responses depend quadratically on contrast. The simulated detector array consisted of 50 units; each had a first-order low-pass filter with a 50 ms time constant in the delay arm. Receptor distance was 5° .

sponse does not vary with time. The length of this modulated period is determined by the filter time constants of the input lines (Egelhaaf et al., 1989; Egelhaaf and Borst, 1989).

Depending on the particular model in question, different filter configurations may be used. Some instantiations have a peripheral high-pass filter in both arms, some only in the non-delayed line; others use a single low-pass filter in the delayed line. Qualitatively, response properties of these variations are similar (Borst et al., 2003).

For specific forms of the Reichardt detector, the steady-state frequency optimum can be calculated analytically. Consider a simple model that has a first-order linear low-pass filter with time constant τ in the delayed arm and passes the signal unfiltered in the direct line. The time- and space-averaged steady-state response of the array is then given by

$$R = \Delta I^2 \sin\left(2\pi \frac{\Delta\phi}{\lambda}\right) \frac{\tau\omega}{1 + \tau^2\omega^2} \quad (7)$$

where ΔI denotes grating contrast, λ the spatial wavelength of the pattern, and ω the circular contrast frequency $2\pi f$ (Borst et al., 2003).

From this, we can see that Reichardt detector arrays neatly recapitulate the fundamental tuning properties of the grating-induced *Drosophila* optomotor response (Götz, 1964) as well as functional properties of tangential cells (Joesch et al., 2008):

1. The sign of the response depends on the direction of the moving pattern (Figure 7a).
2. The velocity tuning hinges critically on the spatial wavelength of the pattern and the detector is tuned to temporal frequency $\frac{v}{\lambda}$ (Figure 7a,b).
3. The frequency tuning has an optimum (Figure 7b).
4. When the stimulus is under-sampled, responses invert (as evident from the $\Delta\phi$ -dependent geometric interference term). Setting the sampling

base to the inter-ommatidial angle reproduces empirically measured aliasing, supporting the notion that the fly visual system extracts motion from local interactions.

5. Responses increase quadratically with contrast due to the multiplication stage (Figure 7c).

The close match between a model initially derived from beetle behavior and fly vision data suggests that insects share the basic algorithms underlying motion detection. Correlation-based algorithms appear to be a fundamental solution for the problem of determining spatiotemporal sequence.

In contrast to gradient detection strategies and due to the properties of multiplication, Reichardt correlators are rather robust to spatial gradients that approach zero as well as tolerant of degraded input. The detector's output carries substantial information about motion direction and magnitude even in the presence of strong Poisson noise (Lei and Borst, 2006; Borst, 2007). This comes at the cost of output that strongly depends on unrelated properties of the pattern and is approximately proportional to velocity only within a limited range. Note, however, that for naturalistic image sets, the output of the Reichardt detector becomes a more reliable read-out of image velocity (Dror et al., 2000, 2001).

Motion energy detectors

Research on vertebrate vision, including psychophysics in humans, has given rise to the so-called motion energy model of direction selectivity (van Santen and Sperling, 1984; Adelson and Bergen, 1985). It involves the construction of spatiotemporally oriented filters that operate on luminance signals. When viewed across space and time, moving images exhibit a characteristic tilt whose angle of course depends on direction and velocity. An appropriately tilted filter is then sensitive to image motion that matches its receptive field.

In practice, the approach makes use of an elegant trick to create such filters from non-tilted receptive fields. By combining appropriate one-dimensional filters in space and time, one can create odd and even receptive fields that are linearly separable. Summing them in various combinations yields inseparable, spatiotemporally oriented linear filters. Input sequences are convolved with this set of kernels, squared, and finally summed. The resulting output is selective for direction and explains significant aspects of motion phenomenology.

Interestingly, with mild assumptions about the peripheral filters, the motion energy model can be proven equivalent to the Reichardt detector (van Santen and Sperling, 1985). The product of differentially delayed signals, as it is calculated in the Hassenstein-Reichardt scheme, reappears in the output of the algorithm proposed by Adelson and Bergen (1985). Response properties derived for one therefore generally apply to the other. Both are examples of the more general delay-and-compare strategy. Note, however, that internal structure and intermediate representations differ between the two.

Barlow-Levick detector

Following physiological investigations in the rabbit retina, [Barlow and Levick \(1965\)](#) proposed a cognate algorithm for motion sensitivity that has been particularly influential in studies on the vertebrate visual system ([Borst and Helmstaedter, 2015](#)). Their model is structured like an isolated Reichardt detector subunit (Figure 6b); again, two spatially displaced inputs are compared after one of them is delayed. Instead of multiplication, however, the detector uses a veto gate (Figure 6c). If two signals reach the non-linear stage at the same time, no output is produced. Otherwise, signals pass through. While subunits in a Reichardt detector amplify responses to motion in their preferred direction, Barlow-Levick detectors suppress signals elicited by motion in their null direction.

Reichardt and Barlow-Levick detectors with identical preferred direction thus differ in the type of non-linearity they employ (amplifying versus inhibitory) as well as the placement of the temporal delay (on the arm passed first by a preferred stimulus versus the second). From a functional perspective, however, their characteristics are strikingly similar.

Elaborated architectures

Most models described so far were initially designed as black-box approximations of stimulus-response relationships. Circuit neuroscience is of course interested in the correspondence of algorithm and implementation—which neural elements perform the individual computations that make up the detector model? To advance mappability, we may be interested in neurons that act as direct and delayed line or the biophysics that govern the non-linearity of a Reichardt detector. Of further interest are discrepancies between model layout and implementation. In this section, I give some examples of elaborated detector architectures that provide closer fits with either empirical data or biological substrate.

A typical complication, for instance, concerns peripheral receptor elements. At their most basic, these are samples from a single point in the image plane. This model of their optic properties is of course insufficient. Real ommatidia have acceptance angles that in the case of *D. melanogaster* are well approximated by a Gaussian with a half-width at maximum of $\approx 5^\circ$ ([Götz, 1965](#)). Real-world simulations thus often apply appropriate spatial blurring at the input stage.

More complex modifications were put forward based on experimental findings that responses of direction-selective fly tangential cells are subject to velocity-specific motion adaptation ([Harris et al., 1999](#)). Moreover, in a dynamic regime, horizontally-sensitive H1 in *C. vicina* adjusts its coding range depending on the velocity distribution of the motion stimulus ([Brenner et al., 2000](#); [Fairhall et al., 2001](#)). Some models postulated adaptation of the Reichardt detector time constant in order to account for these effects. Intriguingly, however, even the unmodified model with fixed τ provides gain control and expands or contracts its coding range in accord with the stimulus distribution ([Borst et al., 2005](#)).

A breakthrough in understanding of peripheral motion processing in the fruit fly came with the discovery that direction selectivity is computed in

parallel bright- and dark-processing channels (Joesch et al., 2010), similarly to the mammalian retina (Borst and Helmstaedter, 2015). Silencing the L1 or L2 pathway led to a loss of motion-sensitivity in tangential cells that was specific to ON or OFF edges, respectively. Moreover, calcium imaging from L2 terminals had revealed approximately half-wave rectified responses to luminance steps (Reiff et al., 2010).

The internal structure of a classical Reichardt detector does not take the ON-OFF distinction into account. Input signals are free to vary between positive and negative and the non-linear stage is a simple mathematical operation. Interestingly, half-wave rectification had previously been suggested in the context of biophysically plausible sign-correct multiplication (see Egelhaaf and Borst, 1992). By splitting the incoming signal into its positive and negative components, multiplying the four quadrants (ON-ON, OFF-OFF, ON-OFF, and OFF-ON) individually, and summing them with appropriate signs, multiplication is realized without having to postulate synaptic machinery capable of performing the operation in one step.

Physiological findings had hinted that the fly motion detection system consists of only two same-sign quadrants. However, it is well established that both optomotor response and tangential cells exhibit inverted sensitivity to apparent motion sequences that consist of mixed ON and OFF steps, closely related to reverse-phi stimuli (Hassenstein and Reichardt, 1956; Egelhaaf and Borst, 1992; Clark et al., 2011). Eichner et al. (2011) constructed an elaborated Reichardt detector that was able to reconcile these findings (Figure 6d). It consists of two Reichardt-type sub-detectors, each of which processes either positive or negative luminance changes. Pre-processing is modeled as a differentiation-approximating high-pass filter whose output is half-wave rectified to generate either an ON or an OFF signal. Critically, this high-pass signal is summed with a small tonic luminance contribution (DC) before rectification. The DC signal simulates lamina processing (see Kern and Egelhaaf, 2000) and accounts for the extreme temporal latencies between apparent motion steps that still produce a measurable response in tangential cells. Additionally, tonic sensitivity leads to incomplete separation between ON and OFF. Resulting signals are then fed into regular Reichardt detectors. At the end, ON and OFF units are added to yield a final output.

The resulting model faithfully reproduces the hallmarks of similarly tuned classical correlation models despite not directly computing mixed ON-OFF or OFF-ON quadrants. Critically, due to the DC component and resulting border effects it also produces inverted output for apparent motion steps that involve oppositely signed polarities. Moreover, the elaborated model could successfully predict that for temporally non-overlapping apparent motion flashes, only same-sign combinations would elicit responses in tangential cells of both *D. melanogaster* and *C. vicina* (see also Franceschini et al., 1989). By aiming for biological plausibility in its internal structure, the model thus gained in explanatory power.

A related study used genetic silencing of L1 and L2 to study similar reverse-phi responses in walking fruit flies (Clark et al., 2011). To explain their findings, they proposed an alternative model that computes six combinations of positive or negative signal contrast and sums them with differential weights. A subsequent investigation of reverse-phi responses in

tangential cells combined measurements with genetic silencing of L1 or L2. For all stimulus configurations, the two-quadrant detector predicted blocking results more accurately than the six-quadrant alternative (Joesch et al., 2013).

1.7 CONCLUDING REMARKS

When I began my doctoral work, starting and end points of motion computation in the *Drosophila* brain had been characterized in great detail. Direction selectivity is computed in two channels, one specializing in ON (starting from L1) and the other one in OFF stimuli (starting from L2). Tangential cells in the lobula plate exhibit finely tuned flow field sensitivity. Two questions were then central to this dissertation. First, what is the neural substrate mediating between lamina and lobula plate and how does it map onto operations in an algorithmic model of motion detection? Second, how do the functional properties of the polarity-split architecture relate to motion vision in its naturalistic context? Through behavioral methods, computational modeling, and intense collaboration with physiologists, I set out to attack these questions. The findings were published in four peer-reviewed articles that comprise the main part of this thesis. They are presented in chronological order.

2 | PUBLICATIONS

2.1 A DIRECTIONAL TUNING MAP OF DROSOPHILA ELEMENTARY MOTION DETECTORS

This article characterized the response properties of T4 and T5 cells and quantified their particular contribution to downstream networks and behavior. It was published in *Nature* in August 2013 (Maisak et al., 2013) and highlighted in several journals (Masland, 2013; Gilbert, 2013; Yonehara and Roska, 2013; Flight, 2013).

SUMMARY Previous work had shown that combined silencing of bushy T4 and T5 cells renders downstream lobula plate tangential cells insensitive to motion stimuli. Using two-photon imaging, we recorded calcium activity in GAL4-targeted T4 or T5 cells. T4 cells that projected to a specific layer of the lobula plate were sensitive to localized ON motion in one of the four cardinal directions (front-to-back, back-to-front, upward, and downward). The four subtypes of T5 cells, in turn, responded to corresponding OFF motion stimuli. Overall, the two cell arrays could be shown to form a retinotopic, polarity-specific, direction-selective map of visual space. Critically, chiasmatic neurites of T4 and T5 already exhibited strong selectivity. Finally, when blocking T4 or T5 individually, downstream tangential cells lost their sensitivity to ON or OFF motion, respectively, while remaining sensitive to the other polarity. A competitive motion assay confirmed these results in walking behavior, strongly suggesting that only T4 and T5 relay ON and OFF motion signals.

AUTHORS Matthew S. Maisak, Juergen Haag (co-first author), Georg Ammer, Etienne Serbe, Matthias Meier, **Aljoscha Leonhardt**, Tabea Schilling, Armin Bahl, Gerald M. Rubin, Aljoscha Nern, Barry J. Dickson, Dierk F. Reiff, Elisabeth Hopp, and Alexander Borst.

CONTRIBUTIONS M.S.M. and J.H. jointly performed and, together with A.Bo., evaluated all calcium imaging experiments. G.A., E.S. and M.M. recorded from tangential cells. **A.L.**, T.S. and A.Ba. performed the behavioural experiments. G.R., B.D. and A.N. generated the driver lines and characterized their expression pattern. D.F.R. performed preliminary imaging experiments. E.H. helped with programming and developed the PMT shielding for the two-photon microscope. A.Bo. designed the study and wrote the manuscript with the help of all authors.

A directional tuning map of *Drosophila* elementary motion detectors

Matthew S. Maisak^{1*}, Juergen Haag^{1*}, Georg Ammer¹, Etienne Serbe¹, Matthias Meier¹, Aljoscha Leonhardt¹, Tabea Schilling¹, Armin Bahl¹, Gerald M. Rubin², Aljoscha Nern², Barry J. Dickson³, Dierk F. Reiff[†], Elisabeth Hopp¹ & Alexander Borst¹

The extraction of directional motion information from changing retinal images is one of the earliest and most important processing steps in any visual system. In the fly optic lobe, two parallel processing streams have been anatomically described, leading from two first-order interneurons, L1 and L2, via T4 and T5 cells onto large, wide-field motion-sensitive interneurons of the lobula plate¹. Therefore, T4 and T5 cells are thought to have a pivotal role in motion processing; however, owing to their small size, it is difficult to obtain electrical recordings of T4 and T5 cells, leaving their visual response properties largely unknown. We circumvent this problem by means of optical recording from these cells in *Drosophila*, using the genetically encoded calcium indicator GCaMP5 (ref. 2). Here we find that specific subpopulations of T4 and T5 cells are directionally tuned to one of the four cardinal directions; that is, front-to-back, back-to-front, upwards and downwards. Depending on their preferred direction, T4 and T5 cells terminate in specific sublayers of the lobula plate. T4 and T5 functionally segregate with respect to contrast polarity: whereas T4 cells selectively respond to moving brightness increments (ON edges), T5 cells only respond to moving brightness decrements (OFF edges). When the output from T4 or T5 cells is blocked, the responses of postsynaptic lobula plate neurons to moving ON (T4 block) or OFF edges (T5 block) are selectively compromised. The same effects are seen in turning responses of tethered walking flies. Thus, starting with L1 and L2, the visual input is split into separate ON and OFF pathways, and motion along all four cardinal directions is computed separately within each pathway. The output of these eight different motion detectors is then sorted such that ON (T4) and OFF (T5) motion detectors with the same directional tuning converge in the same layer of the lobula plate, jointly providing the input to downstream circuits and motion-driven behaviours.

Most of the neurons in the fly brain are dedicated to image processing. The respective part of the head ganglion, called the optic lobe, consists of several layers of neuropile called lamina, medulla, lobula and lobula plate, all built from repetitive columns arranged in a retinotopic way (Fig. 1a). Each column houses a set of identified neurons that, on the basis of Golgi staining, have been described anatomically in great detail^{3–5}. Owing to their small size, however, most of these columnar neurons have never been recorded from electrophysiologically. Therefore, their specific functional role in visual processing is still largely unknown. This fact is contrasted by rather detailed functional models about visual processing inferred from behavioural studies and recordings from the large, electrophysiologically accessible output neurons of the fly lobula plate (tangential cells). As the most prominent example of such models, the Reichardt detector derives directional motion information from primary sensory signals by multiplying the output from adjacent photoreceptors after asymmetric temporal filtering⁶. This model makes a number of rather counter-intuitive predictions all of which have been confirmed experimentally (for review, see ref. 7). Yet, the neurons corresponding to most

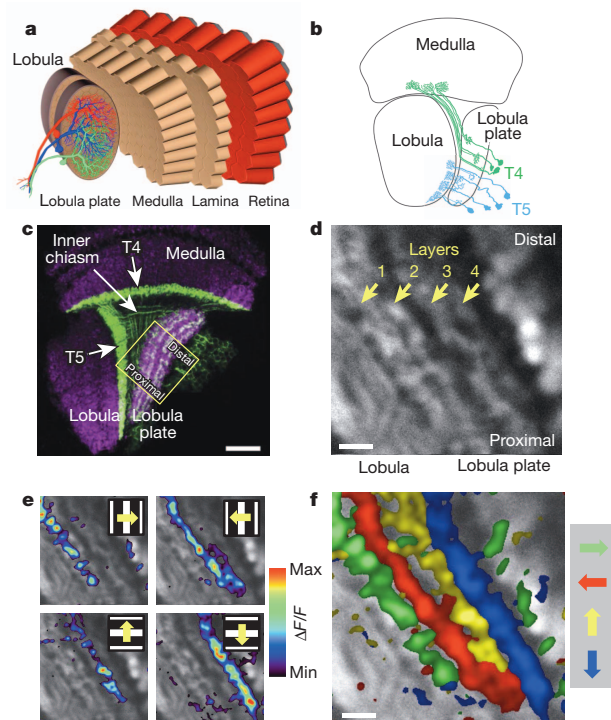


Figure 1 | Directional tuning and layer-specific projection of T4 and T5 cells. **a**, Schematic diagram of the fly optic lobe. In the lobula plate, motion-sensitive tangential cells extend their large dendrites over many hundreds of columns. Shown are the reconstructions of the three cells of the horizontal system²². **b**, Anatomy of T4 and T5 cells, as drawn from Golgi-impregnated material (from ref. 5). **c**, Confocal image of the Gal4-driver line R42F06, shown in a horizontal cross-section (from ref. 10). Neurons are marked in green (Kir2.1-EGFP labelled), whereas the neuropile is stained in purple by an antibody against the postsynaptic protein Dlg. Scale bar, 20 μm . **d**, Two-photon image of the lobula plate of a fly expressing GCaMP5 under the control of the same driver line R42F06. Scale bar, 5 μm . The size and orientation of the image approximately corresponds to the yellow square in **c**. **e**, Relative fluorescence changes ($\Delta F/F$) obtained during 4-s grating motion along the four cardinal directions, overlaid on the greyscale image. Each motion direction leads to activity in a different layer. Minimum and maximum $\Delta F/F$ values were 0.3 and 1.0 (horizontal motion), and 0.15 and 0.6 (vertical motion). **f**, Compound representation of the results obtained from the same set of experiments. Scale bar, 5 μm . Results in **e** and **f** represent the data obtained from a single fly averaged over four stimulus repetitions. Similar results were obtained from six other flies.

¹Max Planck Institute of Neurobiology, 82152 Martinsried, Germany. ²Janelia Farm Research Campus, Ashburn, Virginia 20147, USA. ³Institute of Molecular Pathology, 1030 Vienna, Austria. [†]Present address: Institute Biology 1, Albert-Ludwigs University, 79085 Freiburg, Germany.

*These authors contributed equally to this work.

of the circuit elements of the Reichardt detector have not been identified so far. Here, we focus on a set of neurons called T4 and T5 cells (Fig. 1b) which, on the basis of circumstantial evidence, have long been speculated to be involved in motion detection^{1,8–10}. However, it is unclear to what extent T4 and T5 cells are directionally selective or whether direction selectivity is computed or enhanced within the dendrites of the tangential cells. Another important question concerns the functional separation between T4 and T5 cells; that is, whether they carry equivalent signals, maybe one being excitatory and the other inhibitory on the tangential cells, or whether they segregate into directional- and non-directional pathways¹¹ or into separate ON- and OFF-motion channels^{12,13}.

To answer these questions, we combined Gal4-driver lines specific for T4 and T5 cells¹⁴ with GCaMP5 (ref. 2) and optically recorded the visual response properties using two-photon fluorescence microscopy¹⁵. In a first series of experiments, we used a driver line labelling both T4 and T5 cells. A confocal image (Fig. 1c, modified from ref. 10) revealed clear labelling (in green) in the medulla (T4 cell dendrites), in the lobula (T5 cell dendrites), as well as in four distinct layers of the lobula plate, representing the terminal arborizations of the four subpopulations of both T4 and T5 cells. These four layers of the lobula plate can also be seen in the two-photon microscope when the calcium indicator GCaMP5 is expressed (Fig. 1d). After stimulation of the fly with grating motion along four cardinal directions (front-to-back, back-to-front, upwards and downwards), activity is confined to mostly one of the four layers, depending on the direction in which the grating is moving (Fig. 1e). The outcome of all four stimulus conditions can be combined into a single image by assigning a particular colour to each pixel depending on the stimulus direction to which it responded most strongly (Fig. 1f). From these experiments it is clear that the four subpopulations of T4 and T5 cells produce selective calcium signals depending on the stimulus direction, in agreement with previous deoxyglucose labelling⁸. Sudden changes of the overall luminance evokes no responses in any of the layers (field flicker; $n = 4$ experiments, data not shown). However, gratings flickering in counter-phase lead to layer-specific responses, depending on the orientation of the grating (Supplementary Fig. 1).

The retinotopic arrangement of this input to the lobula plate is demonstrated by experiments where a dark edge was moved within a small area of the visual field only. Depending on the position of this area, activity of T4 and T5 cells is confined to different positions within the lobula plate (Fig. 2a). Consequently, when moving a bright vertical edge horizontally from back to front, activity of T4 and T5 cells is elicited sequentially in layer 2 of the lobula plate (Fig. 2b). These two experiments also demonstrate that T4 and T5 cells indeed signal motion locally. We next investigated the question of where direction selectivity of T4 and T5 cells arises; that is, whether it is already present in the dendrite, or whether it is generated by synaptic interactions within the lobula plate. This question is hard to answer, as the dendrites of both T4 and T5 cells form a dense mesh within the proximal layer of the medulla (T4) and the lobula (T5), respectively. However, signals within the inner chiasm where individual processes of T4 and T5 cells can be resolved in some preparations show a clear selectivity for motion in one over the other directions (Fig. 2c). Such signals are as directionally selective as the ones measured within the lobula plate, demonstrating that the signals delivered from the dendrites of T4 and T5 cells are already directionally selective.

To assess the particular contribution of T4 and T5 cells to the signals observed in the above experiments, we used driver lines specific for T4 and T5 cells, respectively. Applying the same stimulus protocol and data evaluation as in Fig. 1, identical results were obtained as before for both the T4- as well as the T5-specific driver line (Fig. 3a, b). We conclude that T4 and T5 cells each provide directionally selective signals to the lobula plate, in contrast to previous reports¹¹. Thus, both T4 and T5 cells can be grouped, according to their preferred direction, into four subclasses covering all four cardinal directions, reminiscent of ON-OFF ganglion cells of the rabbit retina¹⁶.

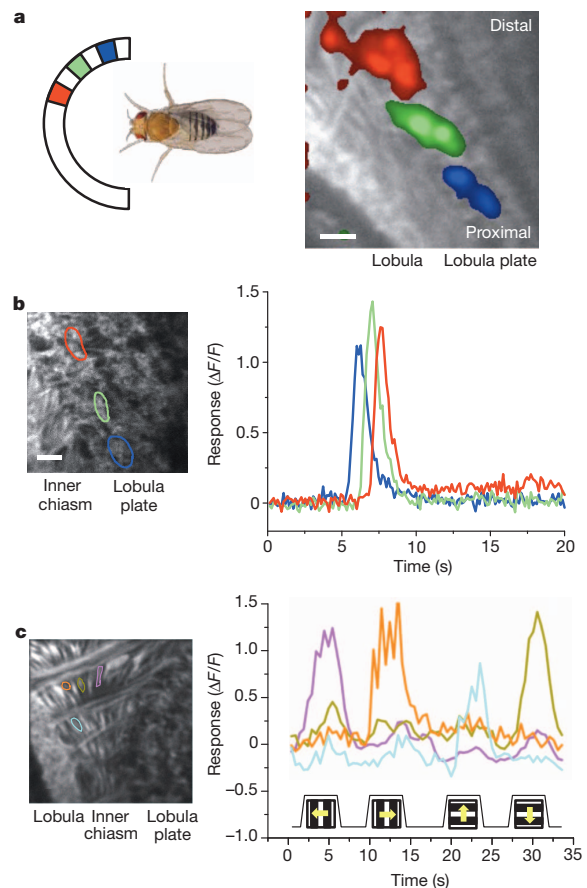


Figure 2 | Local signals of T4 and T5 cells. **a**, Retinotopic arrangement of T4 and T5 cells. A dark edge was moving repeatedly from front-to-back within a 15° wide area at different azimuthal positions (left). This leads to relative fluorescence changes at different positions along the proximal–distal axis within layer 1 of the lobula plate (right). Scale bar, $5 \mu\text{m}$. Similar results have been obtained in four other flies. **b**, Sequential activation of T4 and T5 cells. A bright edge was moving from back-to-front at 15° s^{-1} . Scale bar, $5 \mu\text{m}$. Similar results have been obtained in six other flies. **c**, Signals recorded from individual fibres within the inner chiasm (left) reveal a high degree of direction selectivity (right). Scale bar, $5 \mu\text{m}$. Similar results were obtained from four other flies, including both lines specific for T4 and T5 cells. Response traces in **b** and **c** are derived from the region of interest encircled in the image with the same colour.

We next addressed whether T4 cells respond differently to T5 cells. To answer this question, we used, instead of gratings, moving edges with either positive (ON edge, brightness increment) or negative (OFF edge, brightness decrement) contrast polarity as visual stimuli. We found that T4 cells strongly responded to moving ON edges, but showed little or no response to moving OFF edges (Fig. 3c). This is true for T4 cells terminating in each of the four layers. We found the opposite for T5 cells. T5 cells selectively responded to moving OFF edges and mostly failed to respond to moving ON edges (Fig. 3d). Again, we found this for T5 cells in each of the four layers. We next addressed whether there are any other differences in the response properties between T4 and T5 cells by testing the velocity tuning of both cell populations by means of stimulating flies with grating motion along the horizontal axis from the front to the back at various velocities covering two orders of magnitude. T4 cells revealed a maximum response at a stimulus velocity of 30° s^{-1} , corresponding to a temporal frequency of 1 Hz (Fig. 3e). T5 cell responses showed a similar dependency on stimulus velocity, again with a peak at a temporal frequency of

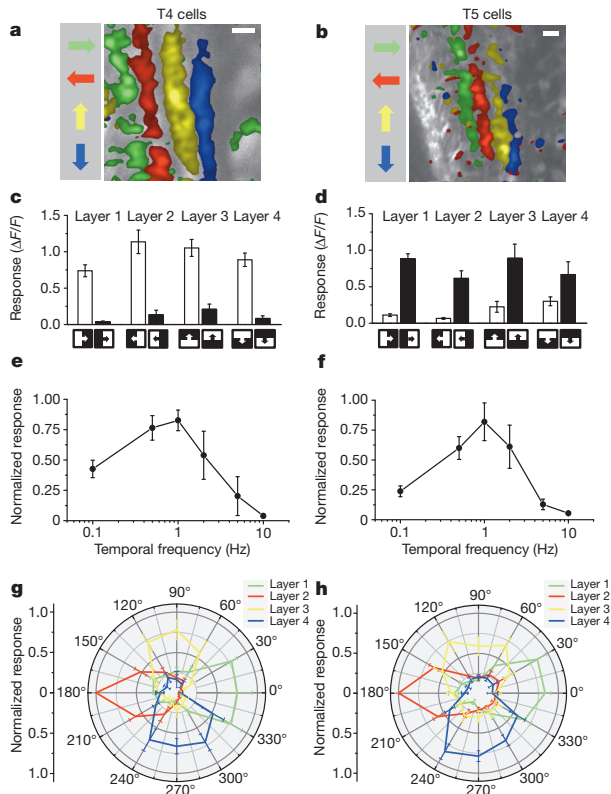


Figure 3 | Comparison of visual response properties between T4 and T5 cells. **a, b**, Relative fluorescence changes ($\Delta F/F$) of the lobula plate terminals of T4 (**a**) and T5 (**b**) cells obtained during grating motion along the four cardinal directions. Results represent the data obtained from a single fly each, averaged over two stimulus repetitions. Scale bars, 5 μm . Similar results have been obtained in ten other flies. **c, d**, Responses of T4 (**c**) and T5 (**d**) cells to ON and OFF edges moving along all four cardinal directions. ON (white) and OFF (black) responses within each layer are significantly different from each other, with $P < 0.005$ except for layers 3 and 4 in T5 cells, where $P < 0.05$. **e, f**, Responses of T4 (**e**) and T5 (**f**) cells to gratings moving horizontally at different temporal frequencies. Relative fluorescence changes were evaluated from layer 1 of the lobula plate and normalized to the maximum response before averaging. **g, h**, Responses of T4 (**g**) and T5 (**h**) cells to gratings moving in 12 different directions. Relative fluorescence changes were evaluated from all four layers of the lobula plate normalized to the maximum response before averaging. Data represent the mean \pm s.e.m. of the results obtained in $n = 8$ (**c**), $n = 7$ (**d**), $n = 6$ (**e**), $n = 7$ (**f**), $n = 6$ (**g**) and $n = 5$ (**h**) different flies. Significances indicated are based on two-sample *t*-test.

1 Hz (Fig. 3f). Thus, there is no obvious difference in the velocity tuning between T4 and T5 cells. As another possibility, T4 cells might functionally differ from T5 cells with respect to their directional tuning width. To test this, we stimulated flies with gratings moving into 12 different directions and evaluated the relative change of fluorescence in all four layers of the lobula plate. Using the T4-specific driver line, we found an approximate half width of $60\text{--}90^\circ$ of the tuning curve, with the peak responses in each layer shifted by 90° (Fig. 3g). No decrease of calcium was detectable for grating motion opposite to the preferred direction of the respective layer. When we repeated the experiments using the T5-specific driver line, we found a similar dependence of the relative change of fluorescence on the stimulus direction (Fig. 3h). We conclude that T4 cells have the same velocity and orientation tuning as T5 cells. The only functional difference we were able to detect remains their selectivity for contrast polarity.

Our finding about the different preference of T4 and T5 cells for the polarity of a moving contrast makes the strong prediction that selective

blockade of T4 or T5 cells should selectively compromise the responses of downstream lobula plate tangential cells to either ON or OFF edges. To test this prediction, we blocked the output of either T4 or T5 cells via expression of the light chain of tetanus toxin¹⁷ and recorded the responses of tangential cells via somatic whole-cell patch to moving ON and OFF edges. In response to moving ON edges, control flies, strong and reliable directional responses were observed in all control flies (Fig. 4a). However, T4-block flies showed a strongly reduced response to ON edges, whereas the responses of T5-block flies were at the level of control flies (Fig. 4b, c). When we used moving OFF edges, control flies again responded with a large amplitude (Fig. 4d). However, the responses of T4-block flies were at the level of control flies, whereas the responses of T5-block flies were strongly reduced (Fig. 4e, f). These findings are reminiscent of the phenotypes obtained from blocking lamina cells L1 and L2 (ref. 13) and demonstrate that T4 and T5 cells are indeed the motion-coding intermediaries for these contrast polarities on their way to the tangential cells of the lobula plate. Whether the residual responses to ON edges in T4-block flies and to OFF edges in T5-block flies are due to an incomplete signal separation between the two pathways or due to an incomplete genetic block in both fly lines is currently unclear.

To address the question of whether T4 and T5 cells are the only motion detectors of the fly visual system, or whether they represent one cell class, in parallel to other motion-sensitive elements, we used tethered flies walking on an air-suspended sphere¹⁸ and stimulated them by ON and OFF edges moving in opposite directions¹⁹. As in the previous experiments, we blocked T4 and T5 cells specifically by selective expression of the light chain of tetanus toxin. During balanced motion, control flies did not show significant turning responses to either side (Fig. 4g). T4-block flies, however, strongly followed the direction of the moving OFF edges, whereas T5-block flies followed the direction of the moving ON edges (Fig. 4h, i). In summary, the selective preference of T4-block flies for OFF edges and of T5-block flies for ON edges not only corroborates our findings about the selective preference of T4 and T5 cells for different contrast polarities, but also demonstrates that the signals of T4 and T5 cells are indeed the major, if not exclusive, inputs to downstream circuits and motion-driven behaviours.

Almost a hundred years after T4 and T5 cells have been anatomically described³, this study reports their functional properties in a systematic way. Using calcium as a proxy for membrane voltage²⁰, we found that both T4 and T5 cells respond to visual motion in a directionally selective manner and provide these signals to each of the four layers of the lobula plate, depending on their preferred direction. Both cell types show identical velocity and orientation tuning which matches the one of the tangential cells^{21,22}. The strong direction selectivity of both T4 and T5 cells is unexpected, as previous studies had concluded that the high degree of direction selectivity of tangential cells is due to a push-pull configuration of weakly directional input with opposite preferred direction^{23,24}. Furthermore, as the preferred direction of T4 and T5 cells matches the preferred direction of the tangential cells branching within corresponding layers, it is currently unclear which neurons are responsible for the null-direction response of the tangential cells. As for the functional separation between T4 and T5 cells, we found that T4 cells selectively respond to brightness increments, whereas T5 cells exclusively respond to moving brightness decrements. Interestingly, parallel ON and OFF motion pathways had been previously postulated on the basis of selective silencing of lamina neurons L1 and L2 (ref. 13). Studies using apparent motion stimuli to probe the underlying computational structure arrived at controversial conclusions: whereas some studies concluded that there was a separate handling of ON and OFF events by motion detectors^{12,25,26}, others did not favour such a strict separation^{19,27}. The present study directly demonstrates the existence of separate ON and OFF motion detectors, as represented by T4 and T5 cells, respectively. Furthermore, our results anatomically confine the essential processing steps of elementary

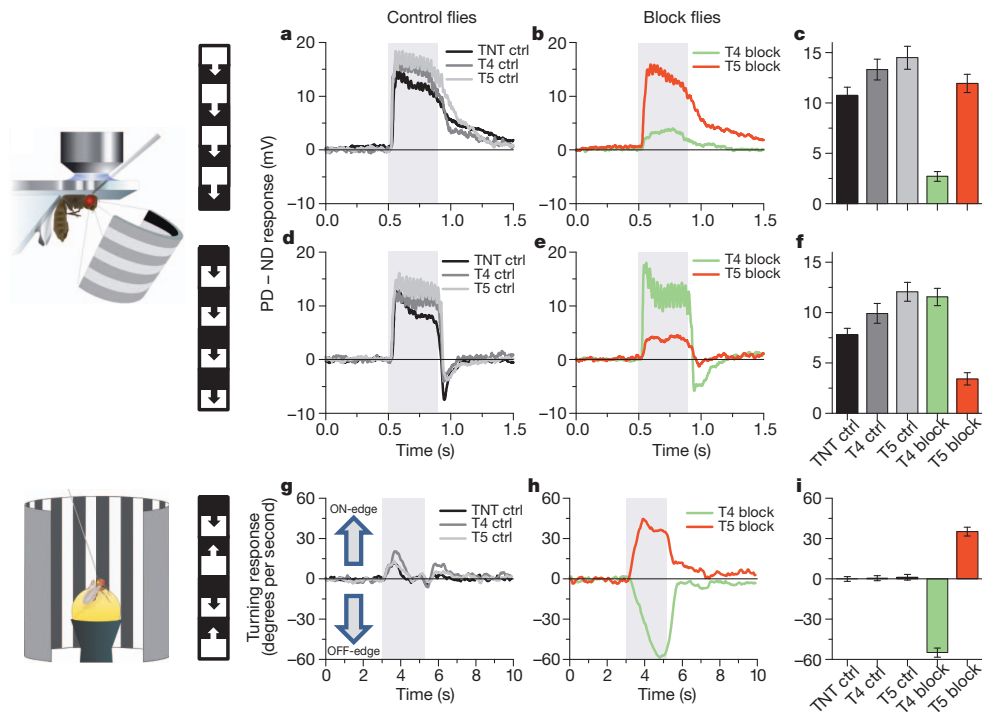


Figure 4 | Voltage responses of lobula plate tangential cells and turning responses of walking flies to moving ON and OFF edges. **a, d,** Average time course of the membrane potential in response to preferred direction motion minus the response to null direction motion (PD – ND response) as recorded in three types of control flies (stimulation period indicated by shaded area). **b, e,** Same as in **a, d,** but recorded in T4-block flies (green) and T5-block flies (red). The stimulus pattern, shown to the left, consisted of multiple ON- (a) or OFF-edges (d). **c, f,** Mean voltage responses (PD – ND) of tangential cells in the five groups of flies. Recordings were done from cells of the vertical²¹ and the horizontal²² system. Because no difference was detected between them, data were pooled. Data comprise recordings from $n = 20$ (TNT control), $n = 12$ (T4 control), $n = 16$ (T5 control), $n = 17$ (T4 block) and $n = 18$ (T5 block) cells. In both T4 and T5-block flies, ON and OFF responses are significantly different

from each other with $P < 0.001$. In T4-block flies, ON responses are significantly reduced compared to all three types of control flies, whereas in T5-block flies, OFF responses are significantly reduced, both with $P < 0.001$. **g,** Average time course of the turning response of three types of control flies to ON and OFF edges moving simultaneously to opposite directions (stimulation period indicated by shaded area). **h,** Same as in **g,** but recorded from T4-block flies (green) and T5-block flies (red). **i,** Mean turning tendency (\pm s.e.m.) during the last second of the stimulation period averaged across all flies within each group. Data comprise average values obtained in $n = 12$ (TNT controls), $n = 11$ (T4 controls), $n = 11$ (T5 controls), $n = 13$ (T4 block) and $n = 12$ (T5 block) flies. Values of T4 and T5-block flies are highly significantly different from zero with $P < 0.001$. Significances indicated are based on two-sample t -test.

motion detection—that is, asymmetric temporal filtering and non-linear interaction—to the neuropile between the axon terminals of lamina neurons L1 and L2 (ref. 28) and the dendrites of directionally selective T4 and T5 cells (Supplementary Fig. 2). The dendrites of T4 and T5 cells might well be the place where signals from neighbouring columns interact in a nonlinear way, similar to the dendrites of starburst amacrine cells of the vertebrate retina²⁹.

METHODS SUMMARY

Flies. Flies used in calcium imaging experiments (Figs 1–3) had the following genotypes: T4/T5 line ($w^-/+;$ $UAS-GCaMP5, R42F06-GAL4/UAS-GCaMP5, R42F06-GAL4$), T4 line ($w^-/+;$ $UAS-GCaMP5, R54A03-GAL4/UAS-GCaMP5, R54A03-GAL4$), T5 line ($w^-/+;$ $UAS-GCaMP5, R42H07-GAL4/UAS-GCaMP5, R42H07-GAL4$). Flies used in electrophysiological and behavioural experiments (Fig. 4) had identical genotypes of the following kind: TNT control flies ($w^+/w^+;$ $UAS-TNT-E/UAS-TNT-E/+;$), T4 control flies ($w^+/w^-;$ $+/+;$ $VT37588-GAL4/+;$), T5 control flies ($w^+/w^-;$ $+/+;$ $R42H07-GAL4/+;$), T4-block flies ($w^+/w^-;$ $UAS-TNT-E/+;$ $VT37588-GAL4/+;$), T5-block flies ($w^+/w^-;$ $UAS-TNT-E/+;$ $R42H07-GAL4/+;$).

Two-photon microscopy. We used a custom-built two-photon laser scanning microscope²⁹ equipped with a $\times 40$ water immersion objective and a mode locked Ti:sapphire laser. To shield the photomultipliers from the stimulus light, two separate barriers were used: the first was placed directly over the LEDs, the second extended from the fly holder over the arena. Images were acquired at a resolution of 256×256 pixels and a frame rate of 1.87 Hz, except where indicated, using ScanImage software³⁰.

Electrophysiology. Recordings were established under visual control using a Zeiss Microscope and a $\times 40$ water immersion objective.

Behavioural analysis. The locomotion recorder was custom-designed according to ref. 18. It consisted of an air-suspended sphere floating in a bowl-shaped sphere holder. Motion of the sphere was recorded by two optical tracking sensors.

Visual stimulation. For calcium imaging and electrophysiological experiments, we used a custom-built LED arena covering 180° and 90° of the visual field along the horizontal and the vertical axis, respectively, at 1.5° resolution. For the behavioural experiments, three 120-Hz LCD screens formed a U-shaped visual arena with the fly in the centre, covering 270° and 114° of the visual field along the horizontal and the vertical axes, respectively, at 0.1° resolution.

Data evaluation. Data were evaluated off-line using custom-written software (Matlab and IDL).

Full Methods and any associated references are available in the online version of the paper.

Received 16 April; accepted 20 May 2013.

- Bausenwein, B., Dittrich, A. P. M. & Fischbach, K. F. The optic lobe of *Drosophila melanogaster* II. Sorting of retinotopic pathways in the medulla. *Cell Tissue Res.* **267**, 17–28 (1992).
- Akerboom, J. *et al.* Optimization of a GCaMP calcium indicator for neural activity imaging. *J. Neurosci.* **32**, 13819–13840 (2012).
- Cajal, S. R. & Sanchez, D. *Contribucion al conocimiento de los centros nerviosos de los insectos* (Imprenta de Hijos de Nicholas Moja, 1915).
- Strausfeld, N. J. *Atlas of an Insect Brain* (Springer, 1976).
- Fischbach, K. F. & Dittrich, A. P. M. The optic lobe of *Drosophila melanogaster*. I. A Golgi analysis of wild-type structure. *Cell Tissue Res.* **258**, 441–475 (1989).

6. Reichardt, W. Autocorrelation, a principle for the evaluation of sensory information by the central nervous system. In *Sensory Communication* (ed. Rosenblith, W. A.) 303–317 (MIT Press and John Wiley & Sons, 1961).
7. Borst, A., Haag, J. & Reiff, D. F. Fly motion vision. *Annu. Rev. Neurosci.* **33**, 49–70 (2010).
8. Buchner, E., Buchner, S. & Buelthoff, I. Deoxyglucose mapping of nervous activity induced in *Drosophila* brain by visual movement. 1. Wildtype. *J. Comp. Physiol. A* **155**, 471–483 (1984).
9. Strausfeld, N. J. & Lee, J. K. Neuronal basis for parallel visual processing in the fly. *Vis. Neurosci.* **7**, 13–33 (1991).
10. Schnell, B., Raghu, V. S., Nern, A. & Borst, A. Columnar cells necessary for motion responses of wide-field visual interneurons in *Drosophila*. *J. Comp. Physiol. A* **198**, 389–395 (2012).
11. Douglass, J. K. & Strausfeld, N. J. Visual motion-detection circuits in flies: Parallel direction- and non-direction-sensitive pathways between the medulla and lobula plate. *J. Neurosci.* **16**, 4551–4562 (1996).
12. Franceschini, N., Riehle, A. & Le Nestour, A. Directionally selective motion detection by insect neurons. In *Facets of Vision* (ed. Stavenha, H.) 360–390 (Springer, 1989).
13. Joesch, M., Schnell, B., Raghu, S. V., Reiff, D. F. & Borst, A. ON and OFF pathways in *Drosophila* motion vision. *Nature* **468**, 300–304 (2010).
14. Pfeiffer, B. D. *et al.* Tools for neuroanatomy and neurogenetics in *Drosophila*. *Proc. Natl Acad. Sci. USA* **105**, 9715–9720 (2008).
15. Denk, W., Strickler, J. H. & Webb, W. W. Two-photon laser scanning fluorescence microscopy. *Science* **248**, 73–76 (1990).
16. Oyster, C. W. & Barlow, H. B. Direction-selective units in rabbit retina: distribution of preferred directions. *Science* **155**, 841–842 (1967).
17. Sweeney, S. T., Broadie, K., Keane, J., Niemann, H. & O’Kane, C. J. Targeted expression of tetanus toxin light chain in *Drosophila* specifically eliminates synaptic transmission and causes behavioral defects. *Neuron* **14**, 341–351 (1995).
18. Seelig, J. D. *et al.* Two-photon calcium imaging from head-fixed *Drosophila* during optomotor walking behavior. *Nature Methods* **7**, 535–540 (2010).
19. Clark, D. A., Bursztyn, L., Horowitz, M. A., Schnitzer, M. J. & Clandinin, T. R. Defining the computational structure of the motion detector in *Drosophila*. *Neuron* **70**, 1165–1177 (2011).
20. Egelhaaf, M. & Borst, A. Calcium accumulation in visual interneurons of the fly: Stimulus dependence and relationship to membrane potential. *J. Neurophysiol.* **73**, 2540–2552 (1995).
21. Joesch, M., Plett, J., Borst, A. & Reiff, D. F. Response properties of motion-sensitive visual interneurons in the lobula plate of *Drosophila melanogaster*. *Curr. Biol.* **18**, 368–374 (2008).
22. Schnell, B. *et al.* Processing of horizontal optic flow in three visual interneurons of the *Drosophila* brain. *J. Neurophysiol.* **103**, 1646–1657 (2010).
23. Borst, A. & Egelhaaf, M. Direction selectivity of fly motion-sensitive neurons is computed in a two-stage process. *Proc. Natl Acad. Sci. USA* **87**, 9363–9367 (1990).
24. Single, S., Haag, J. & Borst, A. Dendritic computation of direction selectivity and gain control in visual interneurons. *J. Neurosci.* **17**, 6023–6030 (1997).
25. Eichner, H., Joesch, M., Schnell, B., Reiff, D. F. & Borst, A. Internal structure of the fly elementary motion detector. *Neuron* **70**, 1155–1164 (2011).
26. Joesch, M., Weber, F., Eichner, H. & Borst, A. Functional specialization of parallel motion detection circuits in the fly. *J. Neurosci.* **33**, 902–905 (2013).
27. Egelhaaf, M. & Borst, A. Are there separate ON and OFF channels in fly motion vision? *Vis. Neurosci.* **8**, 151–164 (1992).
28. Takemura, S. Y., Lu, Z. & Meinertzhagen, I. A. Synaptic circuits of the *Drosophila* optic lobe: the input terminals to the medulla. *J. Comp. Neurol.* **509**, 493–513 (2008).
29. Euler, T., Detwiler, P. B. & Denk, W. Directionally selective calcium signals in dendrites of starburst amacrine cells. *Nature* **418**, 845–852 (2002).
30. Pologruto, T. A., Sabatini, B. L. & Svoboda, K. ScanImage: Flexible software for operating laser scanning microscopes. *Biomed. Eng. Online* **2**, 13 (2003).

Supplementary Information is available in the online version of the paper.

Acknowledgements We thank L. Looger, J. Simpson, V. Jayaraman and the Janelia GECI team for making and providing us with the GCaMP5 flies before publication; J. Plett for designing and engineering the LED arena; C. Theile, W. Essbauer and M. Sauter for fly work; and A. Mauss, F. Gabbiani and T. Bonhoeffer for critically reading the manuscript. This work was in part supported by the Deutsche Forschungsgemeinschaft (SFB 870). M.S.M., G.A., E.S., M.M., A.L., A.Ba and A.Bo are members of the Graduate School of Systemic Neurosciences.

Author Contributions M.S.M. and J.H. jointly performed and, together with A.Bo., evaluated all calcium imaging experiments. G.A., E.S. and M.M. recorded from tangential cells. A.L., T.S. and A.Ba. performed the behavioural experiments. G.R., B.D. and A.N. generated the driver lines and characterized their expression pattern. D.F.R. performed preliminary imaging experiments. E.H. helped with programming and developed the PMT shielding for the two-photon microscope. A.Bo. designed the study and wrote the manuscript with the help of all authors.

Author Information Reprints and permissions information is available at www.nature.com/reprints. The authors declare no competing financial interests. Readers are welcome to comment on the online version of the paper. Correspondence and requests for materials should be addressed to A.Bo. (borst@neuro.mpg.de).

METHODS

Flies. Flies were raised on standard cornmeal-agar medium at 25 °C and 60% humidity throughout development on a 12 h light/12 h dark cycle. For calcium imaging, we used the genetically encoded single-wavelength indicator GCaMP5, variant G, with the following mutations: T302L, R303P and D380Y (ref. 2). Expression of GCaMP5 was directed by three different Gal4 lines, all from the Janelia Farm collection¹⁴. Flies used in calcium imaging experiments (Figs 1–3) had the following genotypes: T4/T5 line ($w^-/+;$ $UAS-GCaMP5,R42F06-GAL4/UAS-GCaMP5,R42F06-GAL4$), T4 line ($w^-/+;$ $UAS-GCaMP5,R54A03-GAL4/UAS-GCaMP5,R54A03-GAL4$), T5 line ($w^-/+;$ $UAS-GCaMP5,R42H07-GAL4/UAS-GCaMP5,R42H07-GAL4$). All driver lines were generated by the methods described in ref. 14 and were identified by screening a database of imaged lines, followed by reimaging of selected lines³¹. As homozygous for both the Gal4-driver and the UAS-GCaMP5 genes, T4 flies also showed some residual expression in T5 cells, and T5 flies also in T4 cells. This unspecific expression, however, was in general less than 25% of the expression in the specific cells. Flies used in electrophysiological and behavioural experiments (Fig. 4) had identical genotypes of the following kind: TNT control flies ($w^+/w^+;$ $UAS-TNT-E/UAS-TNT-E/+;$), T4 control flies ($w^+/w^-;$ $+/+;$ $VT37588-GAL4/+;$), T5 control flies ($w^+/w^-;$ $+/+;$ $R42H07-GAL4/+;$), T4-block flies ($w^+/w^-;$ $UAS-TNT-E/+;$ $VT37588-GAL4/+;$), T5-block flies ($w^+/w^-;$ $UAS-TNT-E/+;$ $R42H07-GAL4/+;$). UAS-TNT-E flies were derived from the Bloomington Stock Center (stock no. 28837) and VT37588-Gal4 flies were derived from the VDRC (stock no. 205893). Before electrophysiological experiments, flies were anaesthetized on ice and waxed on a Plexiglas holder using bees wax. The dissection of the fly cuticle and exposure of the lobula plate were performed as described previously (for imaging experiments, see ref. 32; for electrophysiology, see ref. 21). Flies used in behavioural experiments were taken from 18 °C just before the experiment and immediately cold-anaesthetized. The head, the thorax and the wings were glued to a needle using near-ultraviolet bonding glue (Sinfony Opaque Dentin) and strong blue LED light (440 nm, dental curing-light, New Woodpecker).

Two-photon microscopy. We used a custom-built two-photon laser scanning microscope³³ equipped with a $\times 40$ water immersion objective (0.80 NA, IR-Achroplan; Zeiss). Fluorescence was excited by a mode locked Ti:sapphire laser (<100 fs, 80 MHz, 700–1,020 nm; pumped by a 10 W CW laser; both Mai Tai; Spectraphysics) with a DeepSee accessory module attached for dispersion compensation control resulting in better pulse compression and fluorescence at the target sample. Laser power was adjusted to 10–20 mW at the sample, and an excitation wavelength of 910 nm was used. The photomultiplier tube (H10770PB-40, Hamamatsu) was equipped with a dichroic band-pass mirror (520/35, Brightline). Images were acquired at a resolution of 256×256 pixels and a frame rate of 1.87 Hz, except in Fig. 2 (7.5 Hz), using the ScanImage software³⁰.

Electrophysiology. Recordings were established under visual control using a $\times 40$ water immersion objective (LumplanF, Olympus), a Zeiss microscope (Axiotech vario 100, Zeiss), and illumination (100 W fluorescence lamp, hot mirror, neutral density filter OD 0.3; all from Zeiss). To enhance tissue contrast, we used two polarization filters, one located as an excitation filter and the other as an emission filter, with slight deviation on their polarization plane. For eye protection, we additionally used a 420-nm LP filter on the light path.

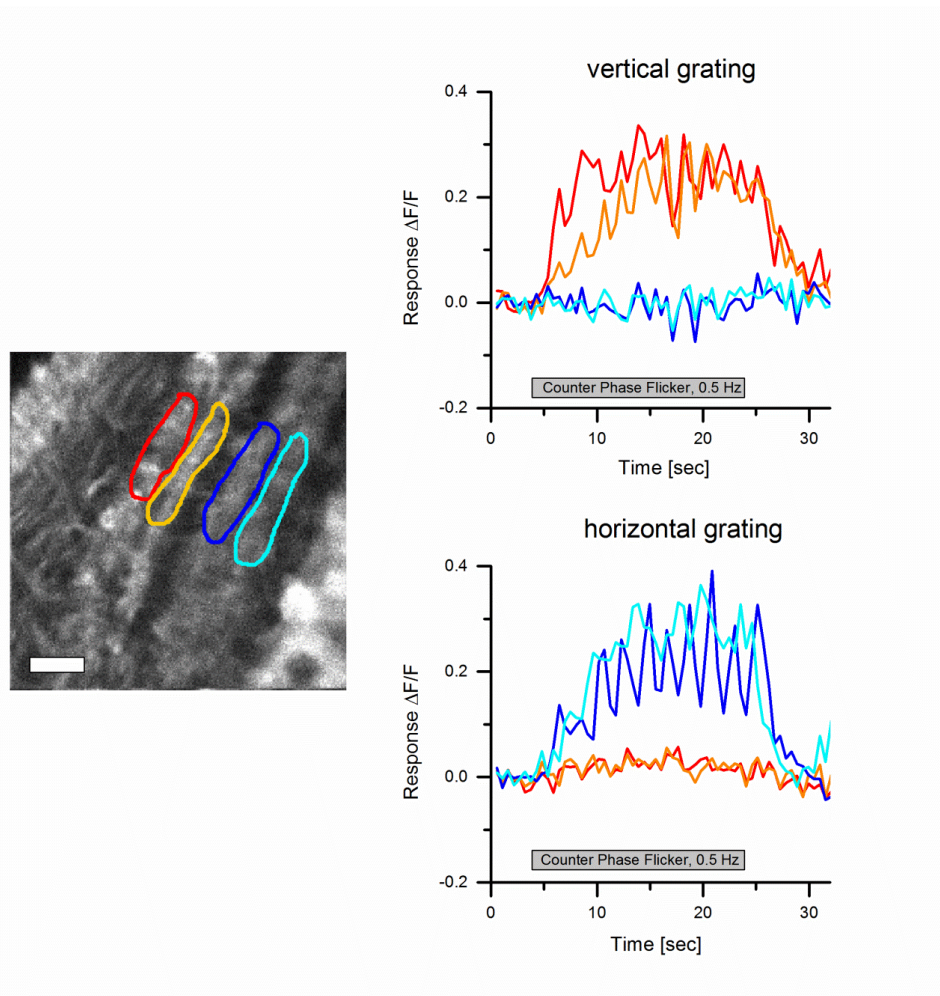
Behavioural analysis. The locomotion recorder was custom-designed according to ref. 18. Briefly, it consists of an air-suspended sphere floating in a bowl-shaped sphere holder. A high-power infrared LED (800 nm, JET series, 90 mW, Roithner Electronics) is located in the back to illuminate the fly and the sphere surface. Two optical tracking sensors are equipped with lens and aperture systems to focus on the sphere behind the fly. The tracking data are processed at 4 kHz internally, read out via a USB interface and processed by a computer at ≈ 200 Hz. This allows real-time calculation of the instantaneous rotation axis of the sphere. A third camera (GRAS-20S4M-C, Point Grey Research) is located in the back which is essential for proper positioning of the fly and allows real-time observation and video recording of the fly during experiments.

Visual stimulation. For calcium imaging and electrophysiological experiments, we used a custom-built LED arena that allowed refresh rates of up to 550 Hz and 16 intensity levels. It covered 180° (1.5° resolution) and 90° (1.5° resolution) of the visual field along the horizontal and the vertical axis, respectively. The LED arena was engineered and modified based upon ref. 34. The LED array consists of 7×4 individual TA08-81GWA dot-matrix displays (Kingbright), each harbouring 8×8 individual green (568 nm) LEDs. Each dot-matrix display is controlled by an ATmega168 microcontroller (Atmel) combined with a ULN2804 line driver (Toshiba America) acting as a current sink. All panels are in turn controlled via an I2C interface by an ATmega128 (Atmel)-based main controller board, which reads in pattern information from a compact flash (CF) memory card. Matlab was used for programming and generation of the patterns as well as for sending the serial command sequences via RS-232 to the main controller board. The

luminance range of the stimuli was $0.5\text{--}33\text{ cd m}^{-2}$. For the calcium imaging experiments, two separate barriers were used to shield the photomultipliers from the stimulus light coming from the LED arena. The first was a spectral filter with transparency to wavelengths >540 nm placed directly over the LEDs (ASF SFG 10, Microchemicals). The second was a layer of black PVC extending from the fly holder over the arena. Square wave gratings had a spatial wavelength of 30° of visual angle and a contrast of 88%. Unless otherwise stated, they were moving at 30° s^{-1} . Edges had the same contrast and were also moving at 30° s^{-1} . For the experiments shown in Figs 1, 2b and 3, each grating or edge motion was shown twice within a single sweep, resulting in a total of eight stimulation periods. Each stimulus period lasted 4 s, and subsequent stimuli were preceded by a 3-s pause. In the experiment shown in Fig. 2a, a dark edge of 88% contrast was moved for 1 s at 15° s^{-1} from the front to the back at three different positions (22° , 44° , 66° , from frontal to lateral). At each position, edge motion was repeated 15 times. For the experiment shown in Fig. 2b, a bright edge of 88% contrast was moving at 15° s^{-1} from the back to the front, and images were acquired at a frame rate of 7.5 Hz. For the experiments shown in Figs 3e, f, all six stimulus velocities were presented once within one sweep, with the stimulus lasting 4 s, and different stimuli being separated by 2 s. In the experiments shown in Figs 3g, h, a single sweep contained all 12 grating orientations with the same stimulus and pause length as above. For the electrophysiology experiments (Fig. 4a–f), multiple edges were used as stimuli moving simultaneously at 50° s^{-1} . To stimulate cells of horizontal system (HS cells), a vertical, stationary square-wave grating with 45° spatial wavelength was presented. For ON-edge motion, the right (preferred direction, PD) or the left edge (null direction, ND) of each light bar started moving until it merged with the neighbouring bar. For OFF-edge motion, the right or the left edge of each dark bar was moving. To stimulate cells of the vertical system (VS cells), the pattern was rotated by 90° clockwise. For the behavioural experiments (Fig. 4g–i), three 120-Hz LCD screens (Samsung 2233 RZ) were vertically arranged to form a U-shaped visual arena ($w = 31\text{ cm} \times d = 31\text{ cm} \times h = 47\text{ cm}$) with the fly in the centre. The luminance ranged from 0 to 131 cd m^{-2} and covered large parts of the flies' visual field (horizontal, $\pm 135^\circ$; vertical, $\pm 57^\circ$; resolution, $<0.1^\circ$). The three LCD screens were controlled via NVIDIA 3D Vision Surround Technology on Windows 7 64-bit allowing a synchronized update of the screens at 120 frames per second. Visual stimuli were created using Panda3D, an open-source gaming engine, and Python 2.7, which simultaneously controlled the frame rendering in Panda3D, read out the tracking data and temperature and streamed data to the hard disk. The balanced motion stimulus consisted of a square-wave grating with 45° spatial wavelength and a contrast of 63%. Upon stimulation onset, dark and bright edges moved into opposite directions at 10° s^{-1} for 2.25 s. This stimulation was performed for both possible edge directions and two initial grating positions shifted by half a wavelength, yielding a total of four stimulus conditions.

Data evaluation. Data were evaluated off-line using custom-written software (Matlab and IDL). For the images shown in Figs 1e, f, 2a and 3a, b, the raw image series was converted into four images representing the relative fluorescence change during each direction of grating motion: $(\Delta F/F)_{\text{stim}} = (F_{\text{stim}} - F_{\text{ref}})/F_{\text{ref}}$. The image representing the stimulus fluorescence (F_{stim}) was obtained by averaging all images during stimulation; the image representing the reference fluorescence (F_{ref}) was obtained by averaging three images before stimulation. Both images were smoothed using a Gaussian filter of 10 pixel half-width. For the images shown in Figs 1f and 3a, b, $\Delta F/F$ images were normalized by their maximum value. Then, a particular colour was assigned to each pixel according to the stimulus direction during which it reached maximum value, provided it passed a threshold of 25%. Otherwise, it was assigned to background. The response strength of each pixel was coded as the saturation of that particular colour. For the data shown in Figs 2b, c and 3c–h, the raw image series was first converted into a $\Delta F/F$ series by using the first three images as reference. Then, a region was defined within a raw image, and average $\Delta F/F$ values were determined within that region for each image, resulting in a $\Delta F/F$ signal over time. Responses were defined as the maximum $\Delta F/F$ value reached during each stimulus presentation minus the average $\Delta F/F$ value during the two images preceding the stimulus. For the bar graphs shown in Fig. 4c, f, the average voltage responses during edge motion (0.45 s) along the cell's preferred (PD) and null direction (ND) were calculated. For each recorded tangential cell, the difference between the PD and the ND response was determined, and these values were averaged across all recorded cells. The data shown in Fig. 4g, h were obtained from the four stimulus conditions by averaging the turning responses for the two starting positions of the grating and calculating the mean difference between the turning responses for the two edge directions. For the bar graph shown in Fig. 4i, the average turning response of each fly during the last second of balanced motion stimulation was calculated. These values were averaged across all recorded flies within each genotype.

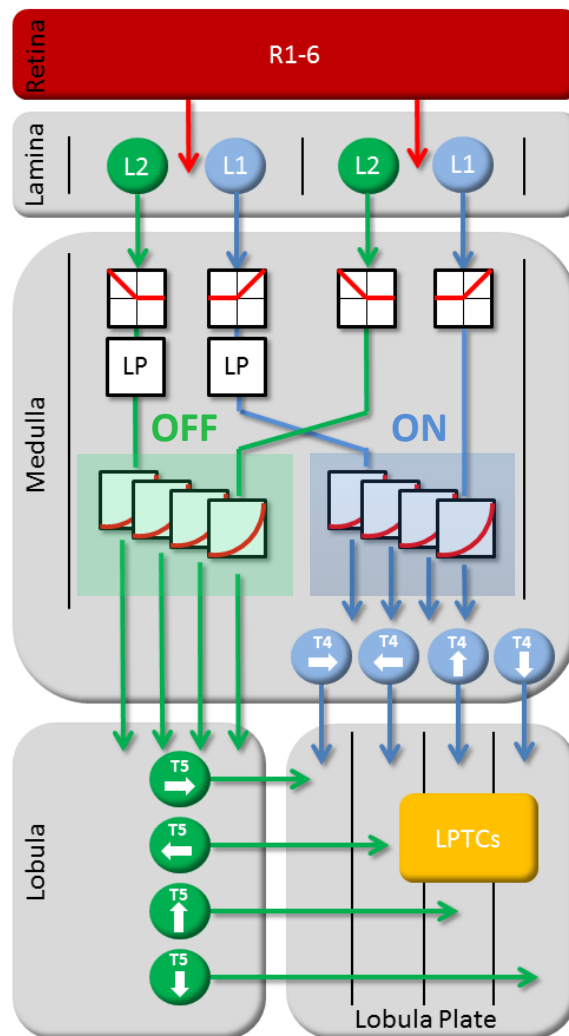
31. Jenett, A. *et al.* A Gal4-driver line resource for *Drosophila* neurobiology. *Cell Rep.* **2**, 991–1001 (2012).
32. Reiff, D. F., Plett, J., Mank, M., Griesbeck, O. & Borst, A. Visualizing retinotopic half-wave rectified input to the motion detection circuitry of *Drosophila*. *Nature Neurosci.* **13**, 973–978 (2010).
33. Euler, T. *et al.* Eyecup scope—optical recording of light stimulus-evoked fluorescence signals in the retina. *Pflüger Arch.* **457**, 1393–1414 (2009).
34. Reiser, M. B. & Dickinson, M. H. A modular display system for insect behavioral neuroscience. *J. Neurosci. Methods* **167**, 127–139 (2008).



Supplemental Fig.1 Responses of T4 and T5 cells to counter-phase flicker. Square-wave gratings (15 deg spatial wavelength and 88% contrast) with vertical (top) and horizontal (bottom) orientation were phase-shifted every second by 180 deg for 20 seconds. Response traces are derived from the region of interest encircled in the image to the left with the same color from a single stimulation period. T4 and T5 cells in layers 1 and 2 only respond to the vertical grating, cells in layers 3 and 4 selectively respond to the horizontal grating. Similar results were obtained in n=4 flies. Scale bar = 5 μ m. Together with the missing response of T4 and T5 cells to full-field flicker, these findings suggest that T4 and T5 cells receive input signals from neurons with different orientation tuning, depending on whether they respond to motion along the horizontal (layers 1 and 2) or the vertical (layers 3 and 4) axis^{1,2}.

1 Pick, B. & Buchner, E. Visual movement detection under light- and dark-adaptation in the fly, *Musca domestica*. *J. Comp. Physiol.* **134**, 45-54 (1979).

2 Srinivasan, M.V. & Dvorak, D.R. Spatial processing of visual information in the movement-detecting pathway of the fly. *J. Comp. Physiol.* **140**, 1-23 (1980).



Supplemental Fig.2 Circuit diagram of the fly elementary motion detector. Visual input from photoreceptors R1-6 is split into parallel pathways, L1 and L2, at the level of the lamina. Two neighboring columns are shown. The outputs from both L1 and L2 are half-wave rectified, such that downstream elements carry information about ON (L1-pathway) and OFF (L2-pathway) signals separately. After temporal low-pass filtering ('LP') the signals from one column, they interact in a supra-linear way with the instantaneous signals derived from the other column. This interaction takes place, separately in both pathways, along all four cardinal directions. Directionally selective signals are carried via T4 and T5 cells to the four layers of the lobula plate where T4 and T5 cells with the same preferred direction converge again on the dendrites of the tangential cells ('LPTCs').

2.2 FUNCTIONAL SPECIALIZATION OF NEURAL INPUT ELEMENTS TO THE DROSOPHILA ON MOTION DETECTOR

In this study, we investigated the functional significance of two major input elements to T₄ cells, Mi₁ and Tm₃. The paper was published in *Current Biology* in July 2015 (Ammer et al., 2015).

SUMMARY An electron microscope-based analysis of presynaptic T₄ connectivity had previously revealed two numerically dominant inputs: columnar medulla cells Mi₁ and Tm₃. A marginal spatial offset between the two projection fields supported a model in which Mi₁ and Tm₃ implement the two arms of a Reichardt-type motion detector, one transmitting fast visual signals from one retinal location and the other relaying delayed input from a slightly offset position. We tested this hypothesis by silencing Mi₁ or Tm₃ and assaying motion sensitivity in either lobula plate tangential cells or flies walking on an air-suspended ball. Interestingly, while the loss of Mi₁ activity selectively abolished responses to ON motion, as had been predicted from the aforementioned model, the phenotype of Tm₃ silencing was limited to ON stimuli traveling at high velocities. These findings were in disagreement with the suggested model and strongly hinted at further complexity and functional specialization in the T₄ input structure.

AUTHORS Georg Ammer, Aljoscha Leonhardt, Armin Bahl, Barry J. Dickson, and Alexander Borst.

CONTRIBUTIONS G.A. and A. Borst designed the study. G.A. performed electrophysiological experiments and anatomical characterization of expression patterns, analyzed the data, and wrote the manuscript with the help of A. Borst, A.L., and A. Bahl. A.L. and A. Bahl performed behavioral experiments and analyzed data. B.J.D. generated SplitGal4 fly lines and hosted G.A. for characterization of Gal4 lines. A. Borst performed computational modeling.

Functional Specialization of Neural Input Elements to the *Drosophila* ON Motion Detector

Georg Ammer,^{1,*} Aljoscha Leonhardt,¹ Armin Bahl,^{1,3} Barry J. Dickson,² and Alexander Borst^{1,*}

¹Max Planck Institute of Neurobiology, Am Klopferspitz 18, 82152 Martinsried, Germany

²Janelia Research Campus, Howard Hughes Medical Institute, 19700 Helix Drive, Ashburn, VA 20147, USA

³Present address: Department of Molecular and Cell Biology, Harvard University, 16 Divinity Avenue, Cambridge, MA 02138, USA

*Correspondence: gammer@neuro.mpg.de (G.A.), aborst@neuro.mpg.de (A.B.)

<http://dx.doi.org/10.1016/j.cub.2015.07.014>

SUMMARY

Detecting the direction of visual movement is fundamental for every sighted animal in order to navigate, avoid predators, or detect conspecifics. Algorithmic models of correlation-type motion detectors describe the underlying computation remarkably well [1–3]. They consist of two spatially separated input lines that are asymmetrically filtered in time and then interact in a nonlinear way. However, the cellular implementation of this computation remains elusive. Recent connectomic data of the *Drosophila* optic lobe has suggested a neural circuit for the detection of moving bright edges (ON motion) with medulla cells Mi1 and Tm3 providing spatially offset input to direction-selective T4 cells, thereby forming the two input lines of a motion detector [4]. Electrophysiological characterization of Mi1 and Tm3 revealed different temporal filtering properties and proposed them to correspond to the delayed and direct input, respectively [5]. Here, we test this hypothesis by silencing either Mi1 or Tm3 cells and using electrophysiological recordings and behavioral responses of flies as a readout. We show that Mi1 is a necessary element of the ON pathway under all stimulus conditions. In contrast, Tm3 is specifically required only for the detection of fast ON motion in the preferred direction. We thereby provide first functional evidence that Mi1 and Tm3 are key elements of the ON pathway and uncover an unexpected functional specialization of these two cell types. Our results thus require an elaboration of the currently prevailing model for ON motion detection [6, 7] and highlight the importance of functional studies for neural circuit breaking.

RESULTS

A large number of studies provide strong evidence that motion vision in flies is based on correlation-type motion detectors (Figure 1A) [8–12]. In recent years, great progress has been made in revealing the internal structure and identifying some of the cellular elements constituting the *Drosophila* motion-detection

circuit [13, 14]. In particular, it was shown that motion detection occurs in two parallel pathways that differ with respect to their preference for moving brightness increments (ON pathway) and brightness decrements (OFF pathway) [15, 16]. Genetic approaches to specifically silence neuronal cell types combined with electrophysiological and behavioral measurements have mainly focused on lamina circuits and identified cells that feed into the ON or OFF pathway, or both [15, 17–19]. T4 and T5 cells were discovered as the first cells in the *Drosophila* visual system that are direction selective and represent the output stages of ON and OFF elementary motion detectors, respectively [20]. Medulla cells that relay information from the lamina to the dendrites of T4 and T5 have been characterized anatomically [4, 21, 22] and, in part, electrophysiologically [5] or by calcium imaging [23, 24]. However, the functional role of medulla cells in generating direction-selective responses in postsynaptic T4 or T5 cells is still unknown. In this study, we focus on two medulla cell types of the ON pathway: Mi1 and Tm3. These two cell types form the great majority of synaptic inputs to T4 cells (Figure 1B) [4] and exhibit different temporal filtering properties [5]. Thus, it has been proposed that Mi1 and Tm3 constitute the delayed and direct input lines of the *Drosophila* ON motion detector, respectively (Figure 1C) [4, 5]. Here, we test this hypothesis experimentally.

A Candidate Circuit for ON Motion Detection

We first generated a simple computational model for a fully opponent correlation-type motion detector that computes ON and OFF motion in separate channels [25]. To test the functional role of the individual input elements, we simulated their removal from the circuit by setting their output gain to zero and computed the response of the detector. As expected, when we blocked either of the two input arms of the ON channel, the detector lost its direction selectivity for ON motion completely (Figure 1D). This model thus generates a clear prediction for our subsequent physiological and behavioral investigations: if Mi1 and Tm3 indeed constitute the two input lines of the ON motion detector, then functionally silencing either of them should lead to a complete loss of direction-selective responses to moving ON stimuli in downstream circuits and behavior under all stimulus conditions.

Mi1 Is an Essential Element of the ON Motion Vision Pathway

In order to measure the output of the motion-detection circuit, we performed *in vivo* patch-clamp recordings from direction-selective lobula plate tangential cells, which receive input from



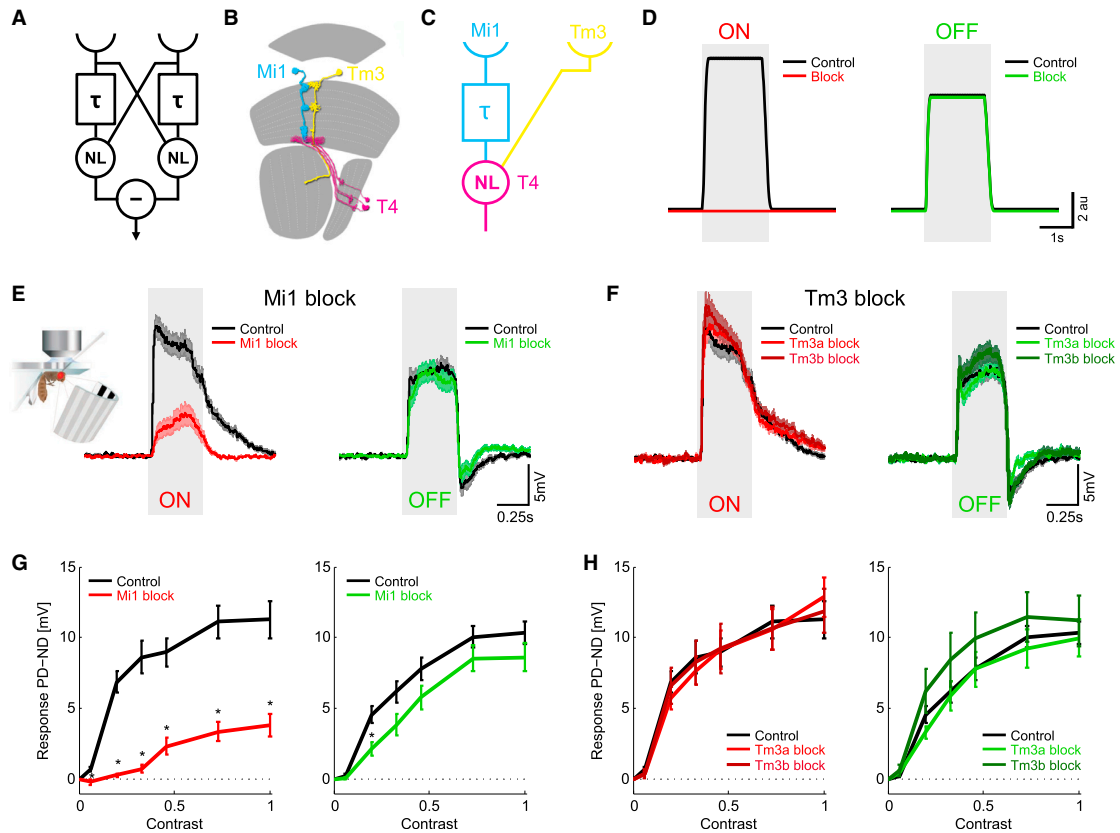


Figure 1. Voltage Responses of Lobula Plate Tangential Cells in Mi1 and Tm3 Block Flies

(A) Correlation-type motion detector. Two spatially separated input lines interact in a nonlinear way after one of them has been temporally delayed. Two mirror-symmetrical subunits are subtracted to yield a fully opponent direction-selective response.

(B) Anatomy of the neural input elements to T4 cells. Mi1 (cyan) and Tm3 (yellow) are the cells with the strongest input to direction-selective T4 cells (magenta).

(C) Schematic model suggesting that Mi1 and Tm3 form the delayed and non-delayed arm of a motion detector. The nonlinearity occurs in T4 cells.

(D) Response of a computational simulation of correlation-type motion detectors when removing either the delayed or the direct line. With both input lines intact, the detector produces direction-selective responses to both moving ON and OFF edges (black). Blocking either of the two input lines of the ON channel abolishes responses to ON motion (red) while leaving OFF motion (green) responses intact.

(E and F) Voltage responses of lobula plate tangential cells (calculated by subtracting the response for null direction [ND] stimulation from the response to preferred direction [PD] stimulation) to moving ON or OFF edges when Mi1 cells (E) or Tm3 cells (F) are silenced. Responses of control flies are depicted in black and of Mi1 or Tm3 block flies in red for ON motion and green for OFF motion (control, $n = 16$; Mi1 block, $n = 21$; Tm3a block, $n = 23$; Tm3b block, $n = 20$).

(G and H) Contrast dependence of lobula plate tangential cells to moving ON or OFF edges of Mi1 (G) and Tm3 (H) block flies. Control flies are depicted in black and block flies in red for ON and green for OFF motion stimuli. Null direction responses were subtracted from preferred direction responses (PD – ND) (control, $n = 12$; Mi1 block, $n = 14$; Tm3a block, $n = 9$; Tm3b block, $n = 10$).

Data are presented as mean \pm SEM. n indicates the number of recorded cells. Significant differences between control and block flies are indicated by asterisks (two-sided Student's t test, Benjamini-Hochberg corrected, $*p < 0.05$). Detailed statistics are provided in Table S2. Recordings from vertical system (VS) and horizontal system (HS) cells were pooled. See also Figures S1 and S2 and Table S1.

a large number of T4 and T5 cells [26, 27], and stimulated flies with visual motion on an LED arena [9]. To silence the neuronal activity of Mi1 or Tm3 cells, we used the Gal4/UAS system [28] to specifically express the EGFP-tagged inward-rectifying potassium channel Kir2.1 [29]. We generated a specific SplitGal4 line [30] to target Mi1 cells and used two independent Gal4 lines for manipulation of Tm3 cells [31]. All transgenic lines showed clear expression of the Kir2.1 channel in the respective cell types when stained with antibodies against the EGFP tag (Figure S1). We selectively stimulated the ON and OFF motion vision path-

ways with either multiple ON or OFF edges moving in the same direction at a velocity of 50° s^{-1} . Control flies responded with strong direction-selective responses to both moving ON and OFF edges (Figures 1E and 1F). In contrast, Mi1 block flies showed a strong reduction in response to ON motion but were unaffected for OFF motion (Figure 1E). Thus, in accordance with the predictions from the proposed model [4, 5], Mi1 is an essential element of the ON motion pathway. Surprisingly however, when we blocked Tm3 cells, responses to both ON and OFF stimuli were indistinguishable from those of control flies

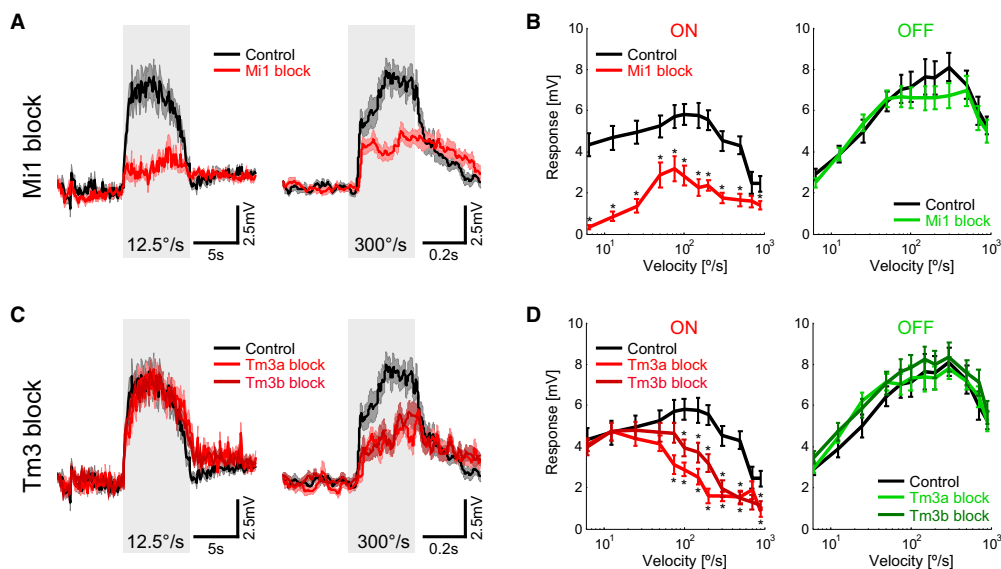


Figure 2. Differential Velocity Tuning of Mi1 and Tm3 Block Flies

(A) Average voltage responses of lobula plate tangential cells of control (black) and Mi1 block flies (red) to slow ($12.5^\circ \text{ s}^{-1}$) and fast (300° s^{-1}) ON edges moving in the preferred direction.

(B) Velocity tuning curves of lobula plate tangential cells of control (black) and Mi1 block flies to ON edges (red) and OFF edges (green) moving in the preferred direction (control, $n = 13$; Mi1 block, $n = 11$).

(C) Average voltage responses of lobula plate tangential cells of control (black) and Tm3 block (red) flies to slow ($12.5^\circ \text{ s}^{-1}$) and fast (300° s^{-1}) ON edges moving in the preferred direction.

(D) Velocity tuning curves of lobula plate tangential cells of control (black) and Tm3 block flies to ON edges (red) and OFF edges (green) moving in the preferred direction (control, $n = 13$; Tm3a block, $n = 15$; Tm3b block, $n = 17$).

Data are presented as mean \pm SEM. n indicates the number of recorded cells. Significant differences between control and block flies are indicated by asterisks (two-sided Student's t test, Benjamini-Hochberg corrected, $*p < 0.05$). Detailed statistics are provided in Table S2. Recordings from VS and HS cells were pooled. See also Figures S1 and S3 and Table S1.

(Figure 1F). To rule out that the strong stimulus drives the system to saturation and that possible residual Tm3 activity was sufficient to generate the observed responses, we varied the stimulus strength by reducing the contrast. Compared to control flies, Mi1 block flies showed a strong reduction to ON stimuli for all contrasts and a minor reduction to OFF stimuli in the low-contrast range (Figure 1G). However, responses of Tm3 block flies were again unaffected, even for very low contrasts (Figure 1H). Thus, we conclude, in disagreement with the proposed model [4, 5], that Tm3 cells are not necessary in general for the detection of ON motion.

Differential Velocity Dependence of Mi1 and Tm3 Block Flies

The finding that Tm3 is a dispensable circuit element under the tested stimulus conditions does not completely rule out its involvement in ON motion detection. It is possible that Tm3 plays an essential part under certain other stimulus conditions. In addition to the contrast tuning curve of a motion detector, another important characteristic is its dependence on velocity. We determined the velocity tuning curves by presenting single ON or OFF edges moving in the preferred direction at velocities that spanned two orders of magnitude. When blocking Mi1 cells, we found a strong response reduction for all velocities tested

(Figures 2A and 2B). The peak of the residual response was similar to that of control flies (Figure 2B). Flies in which Tm3 cells were silenced showed a drastically different phenotype: For slow velocities, responses were at control level, whereas responses to fast-moving ON edges were severely reduced (Figures 2C and 2D). The maxima of the ON tuning curves of Tm3 block flies were shifted to $12.5^\circ \text{ s}^{-1}$ and 25° s^{-1} , respectively, as compared to 100° s^{-1} for control flies. For both Mi1 and Tm3 block flies, the responses to OFF motion remained at control levels. In conclusion, these experiments demonstrate that Tm3 cells are dispensable for the detection of slow ON edges but play a pivotal role in detecting fast ON motion.

Directionally Asymmetric Effect of Blocking Tm3 Cells

In addition to presenting edges moving in the preferred direction, we tested responses of Mi1 and Tm3 block flies to null direction stimulation. Control flies responded with a brief transient depolarization followed by a sustained hyperpolarization (Figure 3). For Mi1 block flies, we found a strong response reduction to moving ON edges over all tested velocities (Figures 3A and 3B). For high velocities, Mi1 block flies even showed a slight tonic depolarization, revealing an excitatory input that is largely masked in control flies. The source of this input is currently unknown but may be related to a T4/T5-independent

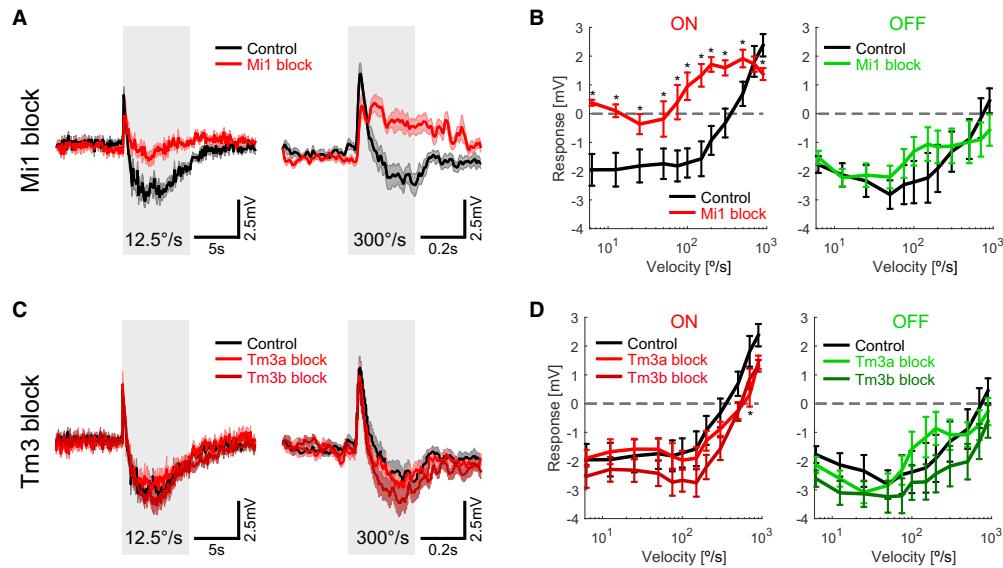


Figure 3. Voltage Responses of Lobula Plate Tangential Cells in Mi1 and Tm3 Block Flies to Edges Moving in the Null Direction

(A) Average voltage responses of lobula plate tangential cells of control (black) and Mi1 block flies (red) to slow ($12.5^\circ \text{ s}^{-1}$) and fast (300° s^{-1}) ON edges moving in the null direction.

(B) Velocity tuning curves of lobula plate tangential cells of control (black) and Mi1 block flies (red) to ON edges (red) and OFF edges (green) moving in the null direction (control, $n = 13$; Mi1 block, $n = 11$).

(C) Average voltage responses of lobula plate tangential cells of control (black) and Tm3 block (red) flies to slow ($12.5^\circ \text{ s}^{-1}$) and fast (300° s^{-1}) ON edges moving in the null direction.

(D) Velocity tuning curves of lobula plate tangential cells of control (black) and Tm3 block flies to ON edges (red) and OFF edges (green) moving in the null direction (control, $n = 13$; Tm3a block, $n = 15$; Tm3b block, $n = 17$).

Data are presented as mean \pm SEM. n indicates the number of recorded cells. Significant differences between control and block flies are indicated by asterisks (two-sided Student's t test, Benjamini-Hochberg corrected, $*p < 0.05$). Detailed statistics are provided in Table S2. Recordings from VS and HS cells were pooled. See also Figures S1 and S3 and Table S1.

flicker-sensitive pathway [27]. Responses to OFF motion were unaffected. Surprisingly, we did not find any effect of blocking Tm3 cells on responses to null direction motion (Figures 3C and 3D). Thus, the effect of blocking Tm3 cells is not only velocity dependent but is also dependent on the direction of stimulus motion.

Furthermore, we compared resting membrane potentials of control and Mi1 or Tm3 block flies (Table S1) and did not find significant differences. This suggests that a possible tonic synaptic transmission from Mi1 or Tm3 cells does not contribute significantly to the resting membrane potential of VS and HS cells, which otherwise might have influenced the amplitude of visual responses. Additionally, we did not observe any effect on magnitude, velocity tuning, or directional tuning of OFF motion responses for both Mi1 and Tm3 block flies (Figures 2 and 3), arguing for a strict separation of ON and OFF pathways at the level of Mi1 and Tm3.

Effects of Blocking Mi1 and Tm3 on Motion-Driven Behavior

In addition to the electrophysiological recordings from lobula plate tangential cells, we tested the functional contribution of Mi1 and Tm3 cells to motion-driven behaviors by blocking their synaptic output and measuring the turning responses of tethered

flies walking on an air-suspended ball [32, 33]. We used the temperature-sensitive silencing tool *shibire^{ts}* [34], which allowed us to block synaptic transmission conditionally by precisely controlling the ambient temperature in our behavioral setup. Thereby, we could rule out developmental effects that may have been caused by silencing Mi1 and Tm3 with Kir2.1 [29]. In order to test the differential impairment of ON and OFF motion channels, we used a balanced motion stimulus [19] and determined velocity tuning curves. This stimulus consists of multiple bright and dark edges moving simultaneously in opposite directions. Flies turn with the direction of moving edges [19]. Thus, wild-type flies with intact ON and OFF motion pathways are expected to show little or no turning responses, whereas flies with an impairment of the ON pathway turn with the direction of moving OFF edges and vice versa [19, 20]. Indeed, control flies showed only small turning responses for all velocities (Figures 4A–4D, black traces). Flies with silenced Mi1 cells, however, turned strongly with the direction of moving OFF edges, reflecting an impairment of the ON motion pathway in accordance with the electrophysiological experiments (Figure 4A). This was true for the whole range of tested velocities (Figure 4B). In contrast, Tm3 block flies showed only small turning responses to slowly moving edges but similarly strong responses as Mi1 block flies at high stimulus velocities (Figures 4C and 4D). The differential effect of silencing Mi1

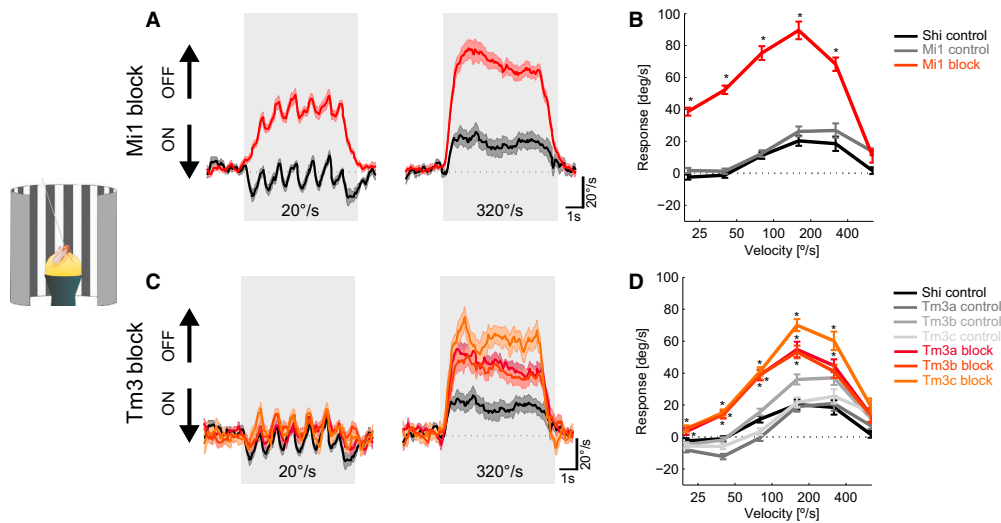


Figure 4. Behavioral Responses of Mi1 and Tm3 Block Flies

(A) Average turning speed of shibire control (black) and Mi1 block flies (red) to slow-moving ($20^{\circ} \text{ s}^{-1}$) and fast-moving ($320^{\circ} \text{ s}^{-1}$) opposing ON and OFF edges. Arrows at the left indicate the direction of moving ON and OFF edges.

(B) Velocity tuning curves for control (black and gray) and Mi1 block flies (red) to moving opposing edges (shibire control, $n = 14$; Mi1 control, $n = 12$; Mi1 block, $n = 16$).

(C) Average turning speed of shibire control (black) and Tm3 block flies (red) to slow-moving ($20^{\circ} \text{ s}^{-1}$) and fast-moving ($320^{\circ} \text{ s}^{-1}$) opposing ON and OFF edges. Arrows at the left indicate the direction of moving ON and OFF edges.

(D) Velocity tuning curves for control (black and gray) and Tm3 block flies (red) to moving opposing edges (shibire control, $n = 14$; Tm3a control, $n = 12$; Tm3b control, $n = 12$; Tm3c control, $n = 13$; Tm3a block, $n = 12$; Tm3b block, $n = 15$; Tm3c block, $n = 12$).

In (A) and (C), response traces of Gal4 controls were omitted for clarity. Data are presented as mean \pm SEM. n indicates the number of measured flies. Significant differences between both genotype controls and block flies are indicated by asterisks (two-sided Student's t test, Benjamini-Hochberg corrected, $*p < 0.05$). Detailed statistics are provided in Table S2. See also Figures S1 and S4.

and Tm3 was again strongest for low velocities and decayed for high velocities, as was seen before in the recordings from lobula plate tangential cells. The velocity range in which Mi1 and Tm3 block flies responded in a similar manner, however, was shifted to higher values compared to the electrophysiological measurements. This discrepancy is reminiscent of the difference in the temporal frequency optimum between lobula plate tangential cells and the optomotor response of walking flies [35] and is therefore likely to be due to the same mechanisms [36, 37]. The behavioral phenotype of Tm3 block flies resembles the preferred direction-specific effect that we observed in the electrophysiological experiments. It is currently unclear whether the hyperpolarization in tangential cells that is caused by null direction stimulation has a direct effect on the turning behavior of walking flies. Our results suggest that the depolarization that is induced by movement in the preferred direction is the dominant, if not the only force that drives turning behavior. Taken together, the findings from behavioral experiments are in agreement with the electrophysiological measurements and suggest a functional specialization of Mi1 and Tm3 cells with respect to their velocity-dependent input to T4 cells.

DISCUSSION

Direction-selective responses to moving bright edges first arise in T4 cells, but it is still unclear how these responses are shaped by T4's presynaptic inputs. Our results provide insight into this

question and demonstrate that Mi1 is an essential element for the detection of ON motion over all contrasts, velocity ranges, and directions of motion. This is consistent with Mi1 being one of the two input lines of an elementary motion detector. In contrast, Tm3 is dispensable under slow-motion stimulus conditions but necessary for the detection of fast movement in the preferred direction. Consequently, a Tm3-independent mechanism must exist that computes the direction of motion for slowly moving ON edges. Thus, ON motion is detected by at least two functionally specialized, complementary mechanisms: one detector for slow and another for fast motion, both sharing Mi1 cells as a common component. The combined action of these mechanisms allows the fly to detect visual motion over a larger range of velocities and more robustly. Additionally, modulatory or adaptive mechanisms would then be able to affect fast- and slow-motion-detection mechanisms independently.

Mechanistically, our findings give rise to two alternative hypotheses. First, Mi1 alone may be sufficient for generating direction-selective responses in T4 cells at slow velocities. In this scenario, the delay could be implemented by differential temporal filtering of Mi1 inputs that arrive at distal versus proximal locations of T4 cell dendrites. The asymmetric filtering may be due to the passive electrical properties of T4 cell dendrites which would impose a larger delay on signals arriving more distally, possibly in interaction with active dendritic conductances [38, 39]. This would offer a functional explanation for the finding that the anatomical orientation of T4 dendrites correlates with their

directional preference [4]. Indeed, such a role for dendritic morphology in conferring direction selectivity has been found in the Hb9⁺ subtype of retinal ganglion cells [40]. For these cells, compatible with our findings, dendritically mediated direction selectivity is only apparent at slow velocities, with inhibition-mediated direction selectivity dominating at high velocities. Alternatively, the delay may be implemented by Mi1 cells that have spatially offset receptive fields and target the same T4 cell dendrite but synapse onto receptors with different temporal transduction properties. Mi1 is reported to be cholinergic [41] and both fast nicotinic and slow muscarinic acetylcholine receptors are expressed in T4 cells [21]. These two scenarios would allow a single cell type (Mi1) to act as both the direct and delayed line, depending on the postsynaptic transduction mechanisms.

As a second hypothesis, additional inputs to T4 cells, other than Mi1 and Tm3, might be essential for the detection of ON motion at low velocities. Indeed, an ongoing connectomic study encompassing a larger volume of the medulla reports additional cells apart from Mi1 and Tm3 providing input to T4 cells (<http://emanalysis.janelia.org>). The strength of these newly described inputs was severely underestimated in the previous study [4], raising the possibility that they play an essential role in generating direction-selective signals in T4. Interestingly, such a scheme has recently been proposed for the OFF pathway, with Tm2 being the instantaneous input line of a motion detector that receives the delayed input from Tm1 and Tm9 cells, which are hypothesized to possess different temporal filtering characteristics [21]. Notably, for the first hypothesis, the delay needs to be implemented postsynaptically to Mi1, whereas the second hypothesis is compatible with a cell-intrinsic delay mechanism. Clearly, a definite understanding of the underlying cellular and biophysical mechanisms will require identification of the sign and temporal characteristics of all T4 synaptic inputs as well as blocking their synaptic output under different stimulus conditions.

Furthermore, our results revealed that the effect of blocking Tm3 cells is dependent on the direction of stimulus motion, with preferred direction responses being selectively affected. This directionally asymmetric effect is reminiscent of the behavioral phenotype that was observed when blocking certain subtypes of lamina cells [18]. Most interestingly, when blocking lamina cells C3, turning responses of tethered flying flies were selectively impaired only when presenting motion from back to front, but not from front to back. As an additional parallel to our Tm3 results, this effect was only present at high stimulus speeds [18]. C3 cells, as Mi1 and Tm3, receive strong input from lamina cells L1 and L5 and form, albeit few, input synapses to T4 [4]. The direction-dependent effect of blocking C3 cells was linked to wiring asymmetries of this cell type. Such an anatomical asymmetry has not yet been reported for Tm3 cells, as the directionality of wiring was not comprehensively analyzed in the recently published medulla connectome [4]. We hypothesize that such an anatomical asymmetry might exist and that it could account for the direction-dependent effect of blocking Tm3 cells that we observed.

In addition to the specific effects of blocking Mi1 or Tm3 on responses to ON motion, we found only a very mild effect on OFF responses. This suggests that Mi1 and Tm3, in contrast to many

lamina cells [17] and in agreement with an increase of rectification from distal to proximal medulla layers [24], feed almost exclusively into the ON pathway.

In conclusion, our study is the first functional demonstration that Mi1 and Tm3 cells are indeed crucial elements of the *Drosophila* ON motion detector, as previously suggested [4, 5]. However, while Mi1 is a necessary component under all stimulus conditions tested, the functionally segregated requirement of Tm3 with respect to stimulus velocity and direction suggests that additional yet unidentified cells or circuit mechanisms are involved as well.

SUPPLEMENTAL INFORMATION

Supplemental Information includes Supplemental Experimental Procedures, four figures, and two tables and can be found with this article online at <http://dx.doi.org/10.1016/j.cub.2015.07.014>.

AUTHOR CONTRIBUTIONS

G.A. and A. Borst designed the study. G.A. performed electrophysiological experiments and anatomical characterization of expression patterns, analyzed the data, and wrote the manuscript with the help of A. Borst, A.L., and A. Bahl. A.L. and A. Bahl performed behavioral experiments and analyzed data. B.J.D. generated SplitGal4 fly lines and hosted G.A. for characterization of Gal4 lines. A. Borst performed computational modeling.

ACKNOWLEDGMENTS

We thank Alexander Arenz and Jesus Pujol-Marti for critical comments on the manuscript, Etienne Serbe and Matthias Meier for many helpful discussions, Christian Theile and Romina Kutlesa for excellent help with behavioral experiments, and Wolfgang Essbauer and Michael Sauter for fly work. G.A., A.L., A. Bahl, and A. Borst are members of the Graduate School of Systemic Neurosciences (GSN) Munich.

Received: May 22, 2015

Revised: July 1, 2015

Accepted: July 2, 2015

Published: July 30, 2015

REFERENCES

- Hassenstein, B., and Reichardt, W. (1956). Systemtheoretische Analyse der Zeit-, Reihenfolgen- und Vorzeichenbewertung bei der Bewegungspersonen des Rüsselkäfers *Chlorophanus*. *Z. Naturforsch. B 11b*, 513–524.
- Barlow, H.B., and Levick, W.R. (1965). The mechanism of directionally selective units in rabbit's retina. *J. Physiol.* *178*, 477–504.
- Borst, A., and Euler, T. (2011). Seeing things in motion: models, circuits, and mechanisms. *Neuron* *71*, 974–994.
- Takemura, S.Y., Bharioke, A., Lu, Z., Nern, A., Vitaladevuni, S., Rivlin, P.K., Katz, W.T., Olbris, D.J., Plaza, S.M., Winston, P., et al. (2013). A visual motion detection circuit suggested by *Drosophila* connectomics. *Nature* *500*, 175–181.
- Behnia, R., Clark, D.A., Carter, A.G., Clandinin, T.R., and Desplan, C. (2014). Processing properties of ON and OFF pathways for *Drosophila* motion detection. *Nature* *512*, 427–430.
- Plaza, S.M., Scheffer, L.K., and Chklovskii, D.B. (2014). Toward large-scale connectome reconstructions. *Curr. Opin. Neurobiol.* *25*, 201–210.
- Takemura, S.Y. (2015). Connectome of the fly visual circuitry. *Microscopy (Oxf.)* *64*, 37–44.
- Buchner, E. (1976). Elementary movement detectors in an insect visual system. *Biol. Cybern.* *24*, 86–101.

9. Joesch, M., Plett, J., Borst, A., and Reiff, D.F. (2008). Response properties of motion-sensitive visual interneurons in the lobula plate of *Drosophila melanogaster*. *Curr. Biol.* *18*, 368–374.
10. Götz, K.G. (1964). Optomotorische Untersuchung des visuellen Systems einiger Augenmutanten der Fruchtfliege *Drosophila*. *Kybernetik* *2*, 77–92.
11. Götz, K.G. (1965). Die optischen Übertragungseigenschaften der Komplexaugen von *Drosophila*. *Kybernetik* *2*, 215–221.
12. Schnell, B., Joesch, M., Forstner, F., Raghu, S.V., Otsuna, H., Ito, K., Borst, A., and Reiff, D.F. (2010). Processing of horizontal optic flow in three visual interneurons of the *Drosophila* brain. *J. Neurophysiol.* *103*, 1646–1657.
13. Borst, A. (2014). In search of the Holy Grail of fly motion vision. *Eur. J. Neurosci.* *40*, 3285–3293.
14. Silies, M., Gohl, D.M., and Clandinin, T.R. (2014). Motion-detecting circuits in flies: coming into view. *Annu. Rev. Neurosci.* *37*, 307–327.
15. Joesch, M., Schnell, B., Raghu, S.V., Reiff, D.F., and Borst, A. (2010). ON and OFF pathways in *Drosophila* motion vision. *Nature* *468*, 300–304.
16. Joesch, M., Weber, F., Eichner, H., and Borst, A. (2013). Functional specialization of parallel motion detection circuits in the fly. *J. Neurosci.* *33*, 902–905.
17. Silies, M., Gohl, D.M., Fisher, Y.E., Freifeld, L., Clark, D.A., and Clandinin, T.R. (2013). Modular use of peripheral input channels tunes motion-detecting circuitry. *Neuron* *79*, 111–127.
18. Tuthill, J.C., Nern, A., Holtz, S.L., Rubin, G.M., and Reiser, M.B. (2013). Contributions of the 12 neuron classes in the fly lamina to motion vision. *Neuron* *79*, 128–140.
19. Clark, D.A., Bursztyn, L., Horowitz, M.A., Schnitzer, M.J., and Clandinin, T.R. (2011). Defining the computational structure of the motion detector in *Drosophila*. *Neuron* *70*, 1165–1177.
20. Maisak, M.S., Haag, J., Ammer, G., Serbe, E., Meier, M., Leonhardt, A., Schilling, T., Bahl, A., Rubin, G.M., Nern, A., et al. (2013). A directional tuning map of *Drosophila* elementary motion detectors. *Nature* *500*, 212–216.
21. Shinomiya, K., Karuppudurai, T., Lin, T.Y., Lu, Z., Lee, C.H., and Meinertzhagen, I.A. (2014). Candidate neural substrates for off-edge motion detection in *Drosophila*. *Curr. Biol.* *24*, 1062–1070.
22. Takemura, S.Y., Karuppudurai, T., Ting, C.Y., Lu, Z., Lee, C.H., and Meinertzhagen, I.A. (2011). Cholinergic circuits integrate neighboring visual signals in a *Drosophila* motion detection pathway. *Curr. Biol.* *21*, 2077–2084.
23. Meier, M., Serbe, E., Maisak, M.S., Haag, J., Dickson, B.J., and Borst, A. (2014). Neural circuit components of the *Drosophila* OFF motion vision pathway. *Curr. Biol.* *24*, 385–392.
24. Strother, J.A., Nern, A., and Reiser, M.B. (2014). Direct observation of ON and OFF pathways in the *Drosophila* visual system. *Curr. Biol.* *24*, 976–983.
25. Eichner, H., Joesch, M., Schnell, B., Reiff, D.F., and Borst, A. (2011). Internal structure of the fly elementary motion detector. *Neuron* *70*, 1155–1164.
26. Mauss, A.S., Meier, M., Serbe, E., and Borst, A. (2014). Optogenetic and pharmacologic dissection of feedforward inhibition in *Drosophila* motion vision. *J. Neurosci.* *34*, 2254–2263.
27. Schnell, B., Raghu, S.V., Nern, A., and Borst, A. (2012). Columnar cells necessary for motion responses of wide-field visual interneurons in *Drosophila*. *J. Comp. Physiol. A Neuroethol. Sens. Neural Behav. Physiol.* *198*, 389–395.
28. Brand, A.H., and Perrimon, N. (1993). Targeted gene expression as a means of altering cell fates and generating dominant phenotypes. *Development* *118*, 401–415.
29. Baines, R.A., Uhler, J.P., Thompson, A., Sweeney, S.T., and Bate, M. (2001). Altered electrical properties in *Drosophila* neurons developing without synaptic transmission. *J. Neurosci.* *21*, 1523–1531.
30. Luan, H., Peabody, N.C., Vinson, C.R., and White, B.H. (2006). Refined spatial manipulation of neuronal function by combinatorial restriction of transgene expression. *Neuron* *52*, 425–436.
31. Jenett, A., Rubin, G.M., Ngo, T.T., Shepherd, D., Murphy, C., Dionne, H., Pfeiffer, B.D., Cavallaro, A., Hall, D., Jeter, J., et al. (2012). A GAL4-driver line resource for *Drosophila* neurobiology. *Cell Rep.* *2*, 991–1001.
32. Bahl, A., Ammer, G., Schilling, T., and Borst, A. (2013). Object tracking in motion-blind flies. *Nat. Neurosci.* *16*, 730–738.
33. Seelig, J.D., Chiappe, M.E., Lott, G.K., Dutta, A., Osborne, J.E., Reiser, M.B., and Jayaraman, V. (2010). Two-photon calcium imaging from head-fixed *Drosophila* during optomotor walking behavior. *Nat. Methods* *7*, 535–540.
34. Kitamoto, T. (2001). Conditional modification of behavior in *Drosophila* by targeted expression of a temperature-sensitive shibire allele in defined neurons. *J. Neurobiol.* *47*, 81–92.
35. Chiappe, M.E., Seelig, J.D., Reiser, M.B., and Jayaraman, V. (2010). Walking modulates speed sensitivity in *Drosophila* motion vision. *Curr. Biol.* *20*, 1470–1475.
36. Schnell, B., Weir, P.T., Roth, E., Fairhall, A.L., and Dickinson, M.H. (2014). Cellular mechanisms for integral feedback in visually guided behavior. *Proc. Natl. Acad. Sci. USA* *111*, 5700–5705.
37. Suver, M.P., Mamiya, A., and Dickinson, M.H. (2012). Octopamine neurons mediate flight-induced modulation of visual processing in *Drosophila*. *Curr. Biol.* *22*, 2294–2302.
38. Branco, T., Clark, B.A., and Häusser, M. (2010). Dendritic discrimination of temporal input sequences in cortical neurons. *Science* *329*, 1671–1675.
39. Hausselt, S.E., Euler, T., Detwiler, P.B., and Denk, W. (2007). A dendrite-autonomous mechanism for direction selectivity in retinal starburst amacrine cells. *PLoS Biol.* *5*, e185.
40. Trenholm, S., Johnson, K., Li, X., Smith, R.G., and Awatramani, G.B. (2011). Parallel mechanisms encode direction in the retina. *Neuron* *71*, 683–694.
41. Hasegawa, E., Kitada, Y., Kaido, M., Takayama, R., Awasaki, T., Tabata, T., and Sato, M. (2011). Concentric zones, cell migration and neuronal circuits in the *Drosophila* visual center. *Development* *138*, 983–993.

Current Biology

Supplemental Information

**Functional Specialization of Neural Input Elements
to the *Drosophila* ON Motion Detector**

Georg Ammer, Aljoscha Leonhardt, Armin Bahl, Barry J. Dickson, and Alexander Borst

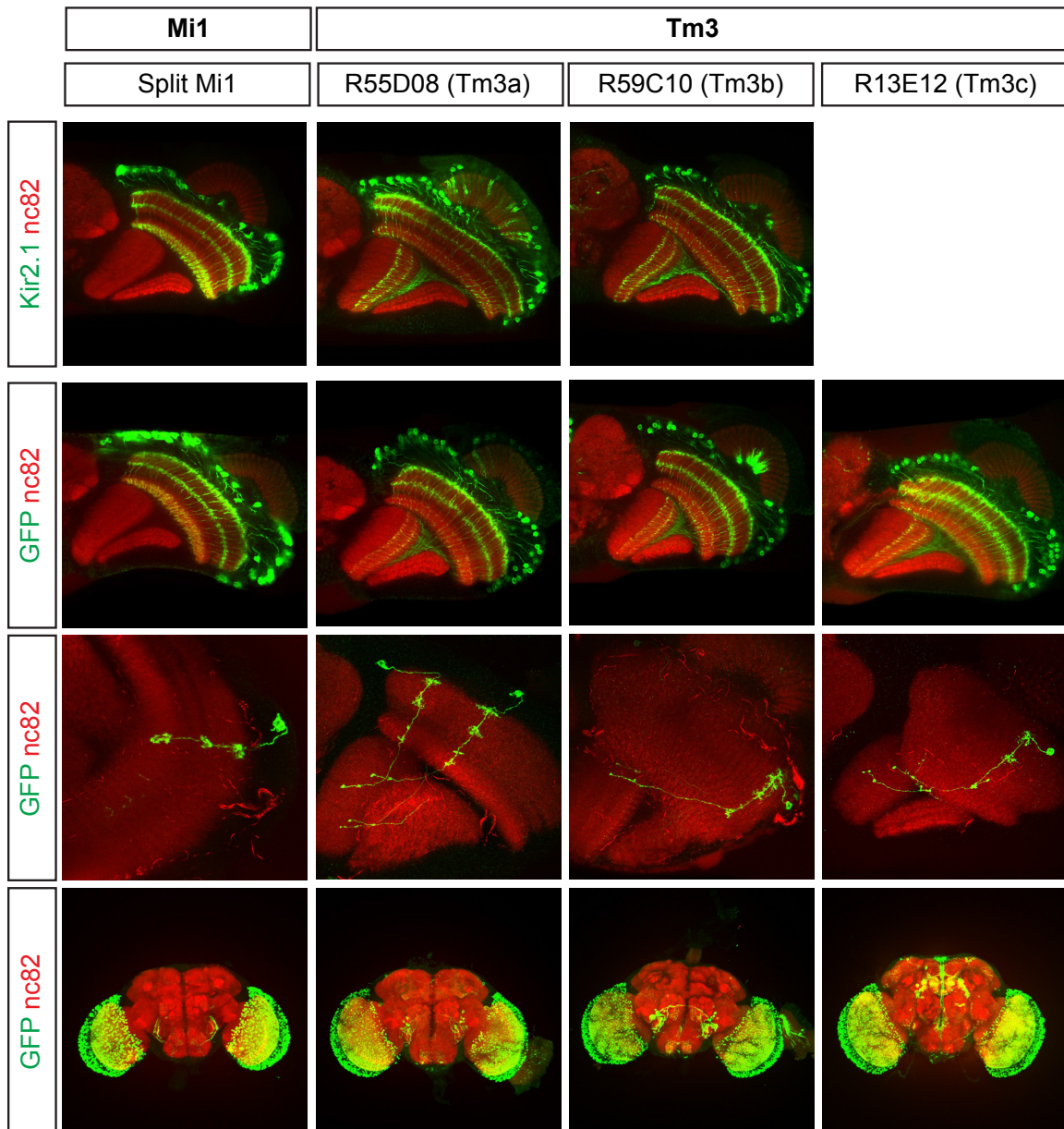


Figure S1 related to Figures 1-4: Expression Patterns of Gal4 Lines

Panels in the upper row show horizontal sections of brains dissected from flies with identical genotypes as in the electrophysiological experiments. Expression of Kir2.1 is visualized by staining for the EGFP tag that is fused to the Kir2.1-channel. Lower three panels show horizontal sections (top), single cell flip-outs (middle) and frontal sections (bottom) of brains of all fly lines used in this study. For characterization of expression patterns, UAS-GFP was driven by the respective Gal4 lines (see [Supplemental Experimental Procedures](#) for details).

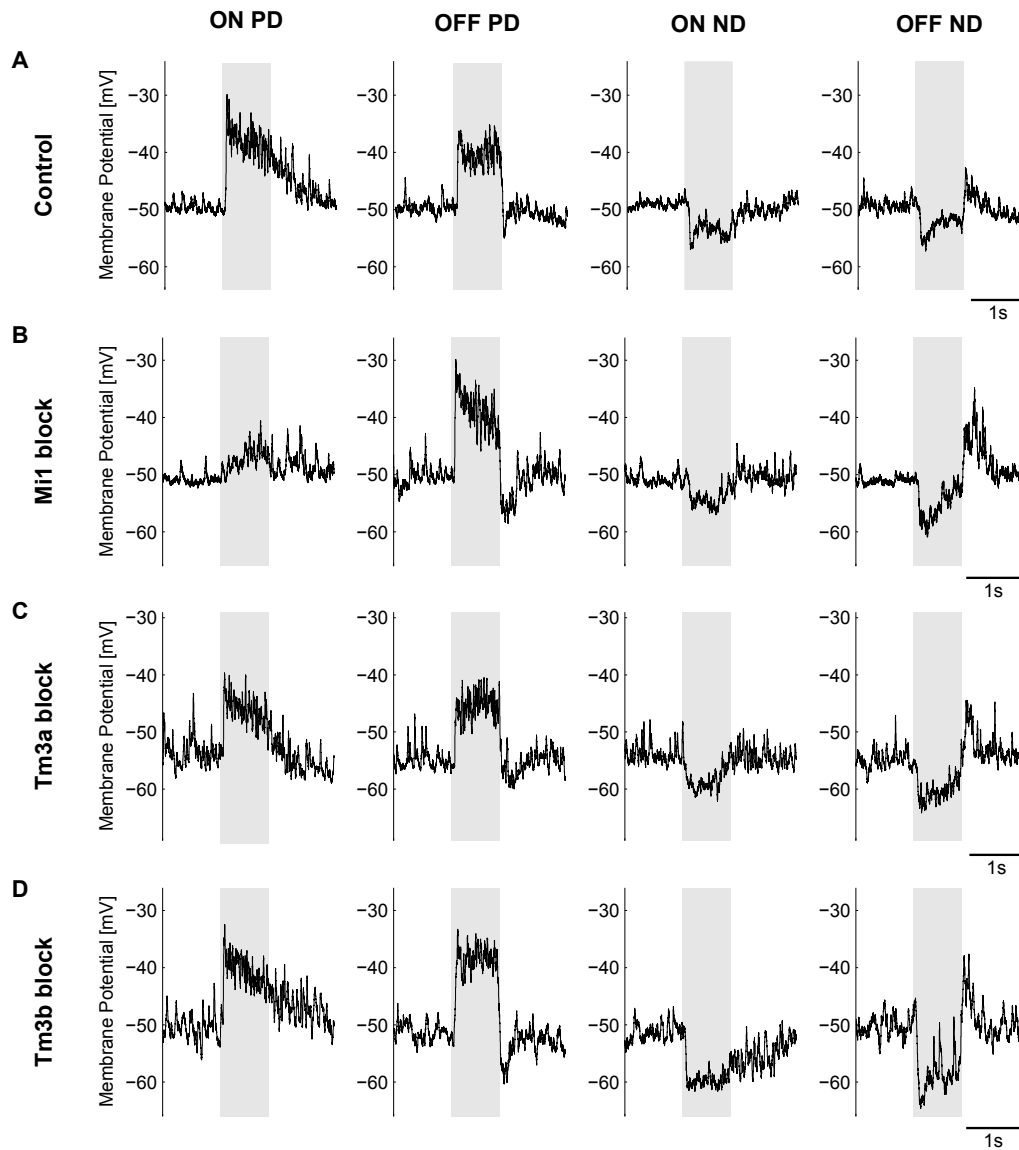


Figure S2 related to Figure 1: Representative Raw Voltage Traces of Control and Block Flies

Voltage responses of single VS or HS cells to multiple edges moving at a velocity of 50 %/s at full contrast. Traces are shown for ON and OFF edges moving in either the preferred direction (PD) or null direction (ND). (A) Single HS cell recording from a control fly. (B) Single HS cell recording from a Mi1 block fly. (C) Single HS cell recording from a Tm3a block fly. (D) Single VS cell recording from a Tm3b block fly. Grey shaded area indicates the stimulation period. Specific genotypes are listed in [Supplemental Experimental Procedures](#).

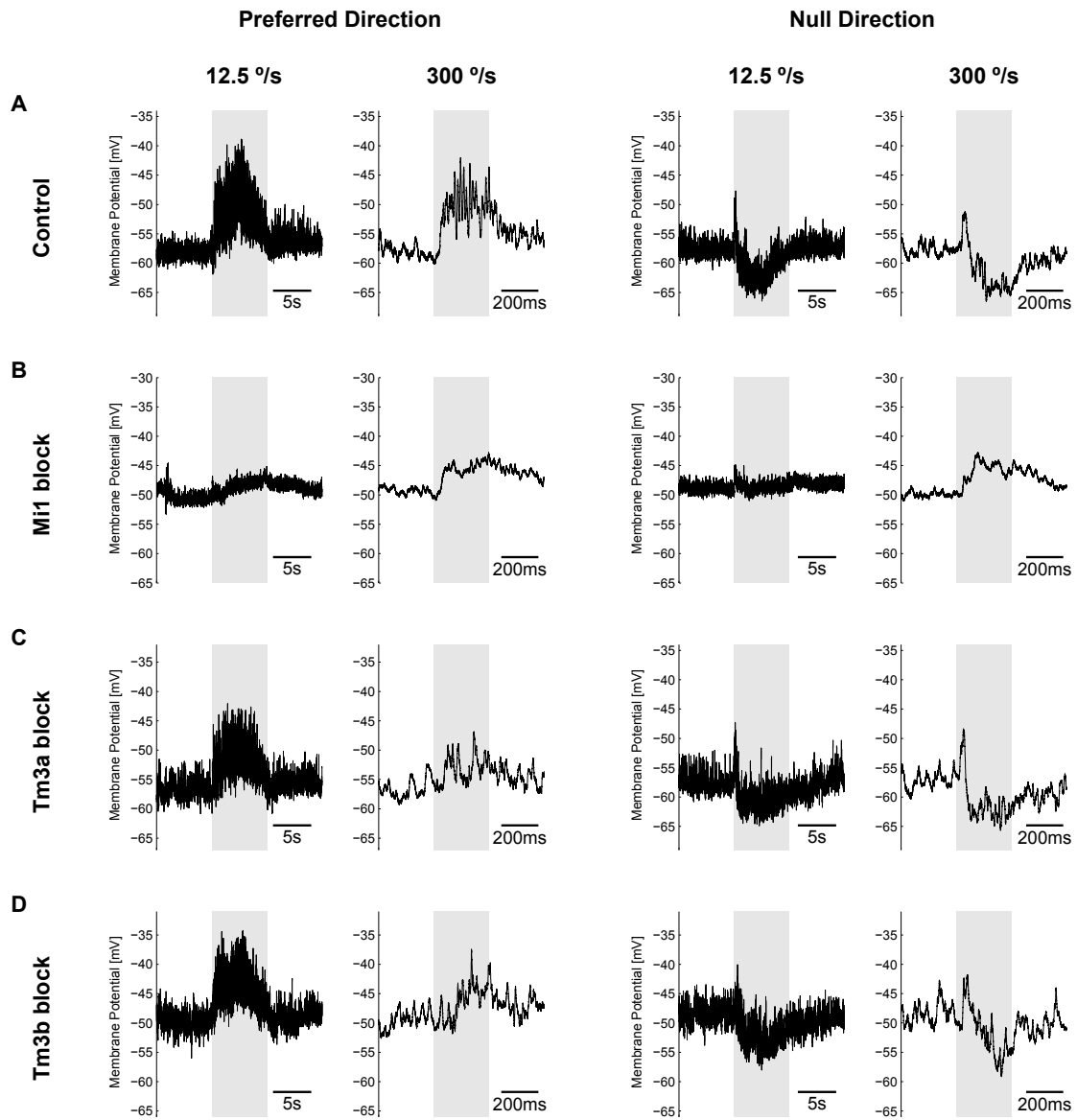


Figure S3 related to Figures 2 and 3: Representative Raw Voltage Traces of Control and Block Flies
Voltage responses of single VS or HS cells to single ON edges moving in the preferred direction (left panels) or null direction (right panels) at velocities of 12.5 °/s or 300 °/s at full contrast. (A) Single VS cell recording from a control fly. (B) Single VS cell recording from a Mi1 block fly. (C) Single VS cell recording from a Tm3a block fly. (D) Single VS cell recording from a Tm3b block fly. Grey shaded area indicates the stimulation period. Specific genotypes are listed in [Supplemental Experimental Procedures](#).

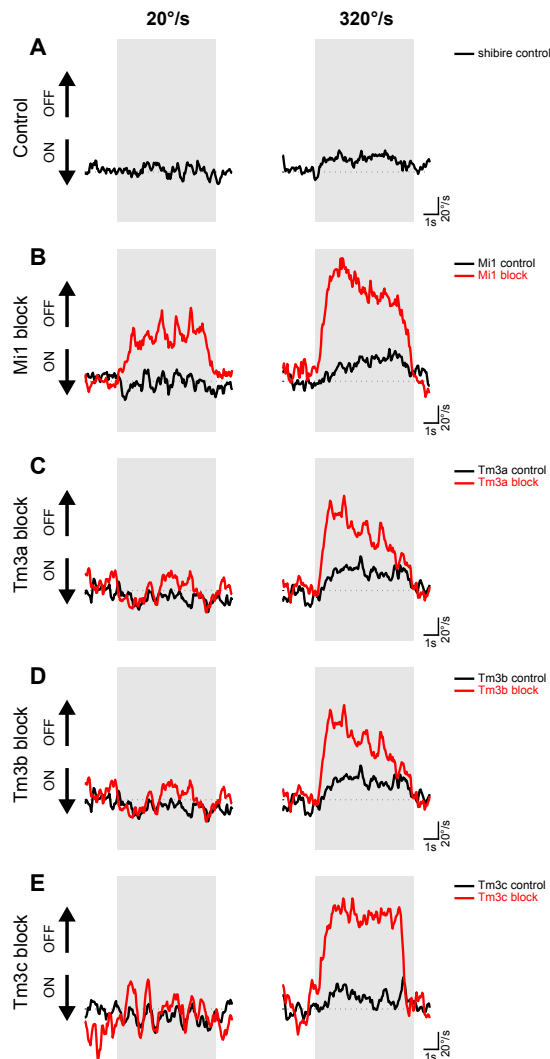


Figure S4 related to Figure 4: Representative Single Fly Responses of Control and Block Flies

Turning responses of single flies to multiple opposing edges moving at a velocity of either 20 °/s or 300 °/s. (A) Turning response of a single shibire control fly. (B) Turning response of a single Mi1 control fly (black) and Mi1 block fly (red). (C) Turning response of a single Tm3a control fly (black) and Tm3a block fly (red). (D) Turning response of a single Tm3b control fly (black) and Tm3b block fly (red). (E) Turning response of a single Tm3c control fly (black) and Tm3c block fly (red). Grey shaded area indicates the stimulation period. Specific genotypes are listed in [Supplemental Experimental Procedures](#).

Figure 1 E, F

Genotype	mean (mV)	s.e.m. (mV)	n (cells)
Control	-51.88	0.61	16
Mi1	-51.67	0.76	21
R55D08 (Tm3a)	-53.00	0.50	23
R59C10 (Tm3b)	-51.89	0.66	20

Figure 1 G, H

Genotype	mean (mV)	s.e.m. (mV)	n (cells)
Control	-51.75	0.65	12
Mi1	-51.64	0.63	14
R55D08 (Tm3a)	-53.44	0.69	9
R59C10 (Tm3b)	-51.75	0.98	10

Figure 2, 3

Genotype	mean (mV)	s.e.m. (mV)	n (cells)
Control	-51.58	0.81	13
Mi1	-51.50	0.70	11
R55D08 (Tm3a)	-52.07	0.52	15
R59C10 (Tm3b)	-52.06	0.71	17

Table S1 related to Figures 1-3: Resting Membrane Potentials of Lobula Plate Tangential Cells

Mean and s.e.m. of the resting membrane potentials of all recorded cells are listed. n denotes the number of recorded cells. Resting membrane potentials were corrected for a liquid junction potential of -12 mV. We did not find any statistically significant difference ($p < 0.05$) between controls and all tested genotypes when applying an unpaired two-sided Student's t-test. Specific genotypes are listed in [Supplemental Experimental Procedures](#).

Table S2 related to Figures 1-4: Detailed Statistics for all Figures

n-numbers, p-values and t-values for all statistical tests applied throughout the study. Statistical significance was tested by using a two-sided Student's t-test followed by a Benjamini-Hochberg correction (* $p < 0.05$). Table S2 is supplied as a separate Excel spreadsheet.

Supplemental Experimental Procedures

Fly Stocks

Flies were reared on cornmeal agar medium under standard conditions (25° C, 60% humidity, 12hr dark/light cycle). For electrophysiology flies were used 5-30 hours post-eclosion. For behavioral experiments flies were aged 1-3 days. Only female flies were used in all experiments.

Genotypes of all fly strains used in the experiments:

Figures 1 - 3

w^+ / w^- ; 10xUAS-Kir2.1-EGFP / + ; + (Control)

w^+ / w^- ; 10xUAS-Kir2.1-EGFP / VT7747AD ; VT49371DBD / + (Mi1 block)

w^+ / w^- ; 10xUAS-Kir2.1-EGFP / + ; R55D08-Gal4 / + (Tm3a block)

w^+ / w^- ; 10xUAS-Kir2.1-EGFP / + ; R59C10-Gal4 / + (Tm3b block)

Figure 4

w^+ / w^- ; 20xUAS-shibire^{ts} / + ; + (Shi control)

w^+ / w^- ; VT7747AD / + ; VT49371DBD / + (Mi1 control)

w^+ / w^- ; + / + ; R55D08-Gal4 / + (Tm3a control)

w^+ / w^- ; + / + ; R59C10-Gal4 / + (Tm3b control)

w^+ / w^- ; + / + ; R13E12-Gal4 / + (Tm3c control)

w^+ / w^- ; 20xUAS-shibire^{ts} / VT7747AD ; VT49371DBD / + (Mi1 block)

w^+ / w^- ; 20xUAS-shibire^{ts} / + ; R55D08-Gal4 / + (Tm3a block)

w^+ / w^- ; 20xUAS-shibire^{TS} / +; R59C10-Gal4 / + (Tm3b block)

w^+ / w^- ; 20xUAS-shibire^{TS} / +; R13E12-Gal4 / + (Tm3c block)

Figure S1

For analysis of expression patterns:

w^+ / w^- ; UAS-mCD8-GFP, UAS-syt-HA / VT7747AD; VT49371DBD / + (Mi1)

w^+ / w^- ; UAS-mCD8-GFP, UAS-syt-HA / +; R55D08-Gal4 / + (Tm3a)

w^+ / w^- ; UAS-mCD8-GFP, UAS-syt-HA / +; R59C10-Gal4 / + (Tm3b)

w^+ / w^- ; UAS-mCD8-GFP, UAS-syt-HA / +; R13E12-Gal4 / + (Tm3c)

For single cell flip-outs:

w^- , pBPhsFlp2::PEST / w^- ; VT7747AD / +; VT49371DBD / UAS-FRT>>FRT-myr::GFP (Mi1)

w^- , pBPhsFlp2::PEST / w^- ; + / +; R55D08-Gal4 / UAS-FRT>>FRT-myr::GFP (Tm3a)

w^- , pBPhsFlp2::PEST / w^- ; + / +; R59C10-Gal4 / UAS-FRT>>FRT-myr::GFP (Tm3b)

w^- , pBPhsFlp2::PEST/ w^- ; + / +; R13E12-Gal4 / UAS-FRT>>FRT-myr::GFP (Tm3c)

Immunohistochemistry and confocal microscopy

Antibody stainings were performed as previously described [S1]. We generated single cell flip-outs using a recently published method [S2]. Briefly, brains were dissected in PBS, fixed in 4% PFA (containing 0.1% Triton-X) for 25 min, washed 3x in PBT (PBS containing 0.3% Triton-X) and blocked with 10% NGS in PBT. Primary antibodies were diluted in PBT containing 5% NGS and incubated for 48 hrs at 4°C. After washing 3x in PBT, brains were incubated in secondary antibody solution for 48-72 hrs at 4°C. After washing 3x in PBT and 1x in PBS, brains were mounted in Vectashield (Vector labs). Following antibodies were used in this study:

Primary antibodies: rabbit anti-GFP (Torri Pines, 1:2000), mouse anti-nc82 (DSHB, 1:25); secondary antibodies: goat anti-rabbit 488 (Invitrogen, 1:500), goat anti-mouse 633 (Invitrogen, 1:500). Imaging was performed on a Leica SP5 confocal microscope with a 63x objective (HCx PL APO, 1.40 NA, Leica) for horizontal sections or a 20x objective (HC PL APO, 0.70 NA, Leica) for vertical sections at a resolution of 1024x1024. Images were processed in ImageJ 1.46f (NIH). Single z-slices are shown for horizontal views and maximum intensity projections for single cell flip-outs and frontal views.

Electrophysiology

Flies were anesthetized on ice, waxed to a plexiglas holder, inserted into an opening cut into aluminum foil and mounted in a recording chamber. A part of the posterior side of the head cuticle and the muscle that covers the cell bodies of LPTCs was removed with a needle and fine forceps. Extracellular saline (103 mM NaCl, 3 mM KCl, 5 mM TES, 10 mM trehalose, 10 mM glucose, 7 mM sucrose, 26 mM NaHCO₃, 1 mM NaH₂PO₄, 1.5 mM CaCl₂ and 4 mM MgCl₂, pH 7.3, 280 mOsm) was bubbled with 95% O₂ and 5% CO₂ and perfused over the preparation. The brain of the fly was visualized with an upright microscope (Axiotech Vario 100, Zeiss) equipped with a 40x water-immersion objective (LumPlanFL, NA 0.8, Olympus), an Hg-light source (HXP-120, Visitron Systems) and polarization filters for contrast enhancement. A glass electrode filled with collagenase (Collagenase IV, Gibco, 0.5 mg/ml in extracellular saline) was used to expose the somata of LPTCs. Somata of VS and HS cells were patched with a glass electrode (5–9 MΩ) filled with internal solution (140 mM potassium aspartate, 10 mM HEPES, 4 mM Mg-ATP, 0.5 mM Na-GTP, 1 mM EGTA, 1 mM KCl and 0.03 mM Alexa 568-hydrazide sodium, pH 7.26, 265 mOsm). Recordings were performed with an NPI BA-1S amplifier (NPI electronics) in

current-clamp bridge mode, low-pass filtered with a cut-off frequency at 3 kHz and digitized at 10 kHz. Data acquisition was performed with Matlab (version R2011a, MathWorks). Cell types were identified on the basis of their typical response profiles to moving gratings. In addition, the majority of recorded cells were dye filled and their identity verified anatomically.

Visual stimulation

Visual stimulation was performed with a custom-built LED arena that had dimensions of 170° in azimuth and 90° in elevation and a spatial resolution of approximately 1.4° per LED. The arena allowed refresh rates of up to 600 Hz and had a maximum luminance of 80 cd m⁻². Data analysis was performed with Matlab (version R2011b, MathWorks) using custom-written scripts. Multiple moving edges were presented as standing square wave gratings with a wavelength of 42°. During stimulation, either all the bright or all the dark edges of the grating moved at a velocity of 50° s⁻¹ for 0.45 s. To measure contrast tuning curves we varied the contrast of the gratings from 6% to 100% while keeping the mean luminance constant. To determine velocity tuning curves we used single edges at full contrast that covered at distance of 90° moving at the following velocities: 6.25, 12.5, 25, 50, 75, 100, 150, 200, 300, 500, 700 and 900 ° s⁻¹. Different velocities were presented in randomized order. Edges moved in the horizontal direction when recording from HS cells and in the vertical direction when recording from VS cells.

Data Analysis

For all stimuli, we averaged voltage traces during the whole stimulation period and calculated the mean and standard errors over cells.

Behavioral experiments

Flies were cold anesthetized before the experiment. Head, thorax, and wings were glued to a needle with near-UV bonding glue (Sinfony Opaque Dentin) and blue LED light (440 nm, dental curing-light, New Woodpecker). Flies were then placed on an air-suspended polyurethane ball in a virtual environment projected onto three monitors spanning approximately 270° (vertical) and 114° (horizontal) of the fly's visual field. This stimulation system offered less than 0.1° of angular pixel size, a value well below *Drosophila's* optical resolution capability. We used six such setups for recording fly locomotion as described previously [S3]. On two setups, stimuli were presented at a screen refresh frequency of 120 Hz; on four setups, the refresh frequency was 144Hz. We never observed qualitative or quantitative differences between these setups in any of the experiments. All monitors were equilibrated in brightness and contrast. Temperature within the immediate surround of the fly was controlled using a custom-built closed-loop thermoregulation system. We employed the following temperature protocol for all experiments and genotypes: Temperature was kept at 25°C for the first 5 minutes and then, within 10 minutes, raised to a restrictive temperature of 34°C.

Visual Stimulation

Our balanced motion stimulus resembled the one used in previous studies [S4, S5]. Briefly, we presented flies with a stationary square wave grating that had an initial spatial wavelength of 45° visual angle and Michelson contrast of 50%. Each individual trial lasted 9s. Between 2s and 7s, bright edges moved in one direction at a fixed velocity while dark edges moved in the other direction at the same velocity. In contrast to previous versions, we reset the stimulus to the initial state after edges had traversed 20° of visual angle. This allowed us to keep the stimulus duration

fixed for varying edge velocities. Additionally, we applied a random phase shift after each reset in order to rule out symmetry effects. This was done for 6 velocities (20, 40, 80, 160, 320, and 640° s^{-1}) and 2 possible edge directions (dark edge leftwards/bright edge rightwards and vice versa), resulting in 12 conditions that were repeated 50 times per fly. The stimulus was rendered in real-time using Panda3D, an open source game engine, and Python 2.7.

Data Analysis

We analyzed the data as described previously [S5]. Briefly, optical tracking sensors were equipped with lens and aperture systems to focus on the sphere behind the fly. The tracking data were processed at 4 kHz internally, read out via a USB interface and processed by a computer at 100 Hz. This allowed real-time calculation of the instantaneous rotation axis of the sphere. We resampled the rotation traces to 20Hz for further processing and applied a first-order low pass filter with a time constant of 100ms to each trace. For all flies, we manually selected 20 consecutive trials out of the 50 available that fulfilled the following criteria: First, the temperature was at a stable 34°C . Second, the average turning tendency of the fly was approximately 0° s^{-1} . Third, the average forward velocity of the fly was at least 5mm s^{-1} , indicating a visually responsive state. Flies were selected without blinding. Application of the criteria excluded, on average, 20% of all measured flies. For further processing, we subtracted responses for the two symmetrical edge directions in order to reduce the impact of walking asymmetries. Trials were then averaged. For statistical purposes, we calculated the turning tendency of each fly for each velocity condition as the mean of the turning response between 3s (walking onset) and 7s (stimulus offset). Other evaluation time frames produced qualitatively equivalent results. All data analysis was performed using Python 2.7 and the NumPy library.

Modeling

Modeling the motion detection pathway followed Eichner et al., 2011 [S6]. Briefly, stimuli were represented as brightness values between 0 and 1 at the level of 40x40 photoreceptors with an angular resolution of 5° at a temporal resolution of 10 ms. Signals of lamina cells L1 and L2 were calculated by high-pass filtering (time-constant 250 ms) the photoreceptor input plus 10% of their DC level. The ON (L1) signal was obtained by half-wave rectifying the signal at a threshold of 0, the OFF (L2) signal was inverted and half-wave rectified at a threshold of 0.05. These signals were then processed by separate ON- and OFF-motion detectors. Within each detector (Figure 1A), the output signal of the lamina cell at one location was low-pass filtered ($\tau = 50$ ms) and subsequently multiplied with the instantaneous signal of the lamina cell from the adjacent location. This was done twice in a mirror-symmetrical way and the results subtracted from each other. Finally, the output signals of all ON- and OFF-motion detectors were added.

Statistics

Throughout the paper we tested for statistical significance by using a two-sided Student's t-test followed by a Benjamini-Hochberg correction (* $p < 0.05$). Detailed statistics are documented in Table S2.

Supplemental References

- S1. Yu, J.Y., Kanai, M.I., Demir, E., Jefferis, G.S., and Dickson, B.J. (2010). Cellular organization of the neural circuit that drives *Drosophila* courtship behavior. *Curr Biol* 20, 1602-1614.
- S2. Nern, A., Pfeiffer, B.D., and Rubin, G.M. (2015). Optimized tools for multicolor stochastic labeling reveal diverse stereotyped cell arrangements in the fly visual system. *PNAS* 112, 2967-2976.

- S3. Bahl, A., Ammer, G., Schilling, T., and Borst, A. (2013). Object tracking in motion-blind flies. *Nat Neurosci* 16, 730-738.
- S4. Clark, D.A., Bursztyn, L., Horowitz, M.A., Schnitzer, M.J., and Clandinin, T.R. (2011). Defining the computational structure of the motion detector in *Drosophila*. *Neuron* 70, 1165-1177.
- S5. Maisak, M.S., Haag, J., Ammer, G., Serbe, E., Meier, M., Leonhardt, A., Schilling, T., Bahl, A., Rubin, G.M., Nern, A., et al. (2013). A directional tuning map of *Drosophila* elementary motion detectors. *Nature* 500, 212-216.
- S6. Eichner, H., Joesch, M., Schnell, B., Reiff, D.F., and Borst, A. (2011). Internal structure of the fly elementary motion detector. *Neuron* 70, 1155-1164.

2.3 COMPREHENSIVE CHARACTERIZATION OF THE MAJOR PRESYNAPTIC ELEMENTS TO THE DROSOPHILA OFF MOTION DETECTOR

This study mapped the response properties and functional roles of a comprehensive set of input elements to OFF-selective, motion-sensitive T5 cells. The work was published in *Neuron* in February 2016 (Serbe et al., 2016) and highlighted in a News & Views (Tuthill and Borghuis, 2016).

SUMMARY Connectomic analysis had identified four major OFF input cells which together make up more than 90% of all synapses onto T5. Transmedullar units Tm1, Tm2, Tm4, and Tm9 relay signals from lamina projection neurons to the lobula where they contact the dendrites of T5. We used two-photon imaging to monitor calcium signals from each of these cells under visual stimulation. Critically, none of the input elements were themselves selective for direction. This confined the origin of motion detection in the OFF pathway to the dendrites of T5. A broad range of spatial and temporal filters emerged: Tm2 and Tm4 exhibited fast, transient responses to negative contrast change; Tm9 was best approximated as a slow, tonic low-pass filter; and Tm1 showed intermediate kinetics. Simulations indicated that this broad filter bank was well suited to extracting motion at relevant time scales. Finally, when blocking cell activity individually or in pairs, we observed a broad range of OFF-specific motion deficits in tangential cells and walking behavior. This strongly suggests that each input cell is involved in detecting OFF motion; none were found to be redundant.

AUTHORS Etienne Serbe, Matthias Meier (co-first author), Aljoscha Leonhardt, and Alexander Borst.

CONTRIBUTIONS E.S. and M.M. jointly performed and evaluated all calcium imaging and electrophysiology experiments. A.L. performed and evaluated the behavioral experiments. A.L. and A.B. performed computer simulations. A.B., E.S., and M.M. designed the study. E.S. and M.M. wrote the manuscript with the help of the other authors.

Comprehensive Characterization of the Major Presynaptic Elements to the *Drosophila* OFF Motion Detector

Etienne Serbe,^{1,2,*} Matthias Meier,^{1,2,*} Aljoscha Leonhardt,¹ and Alexander Borst¹

¹Max-Planck-Institute of Neurobiology, Am Klopferspitz 18, 82152 Martinsried, Germany

²Co-first author

*Correspondence: serbe@neuro.mpg.de (E.S.), mmeier@neuro.mpg.de (M.M.)

<http://dx.doi.org/10.1016/j.neuron.2016.01.006>

SUMMARY

Estimating motion is a fundamental task for the visual system of sighted animals. In *Drosophila*, direction-selective T4 and T5 cells respond to moving brightness increments (ON) and decrements (OFF), respectively. Current algorithmic models of the circuit are based on the interaction of two differentially filtered signals. However, electron microscopy studies have shown that T5 cells receive their major input from four classes of neurons: Tm1, Tm2, Tm4, and Tm9. Using two-photon calcium imaging, we demonstrate that T5 is the first direction-selective stage within the OFF pathway. The four cells provide an array of spatiotemporal filters to T5. Silencing their synaptic output in various combinations, we find that all input elements are involved in OFF motion detection to varying degrees. Our comprehensive survey challenges the simplified view of how neural systems compute the direction of motion and suggests that an intricate interplay of many signals results in direction selectivity.

INTRODUCTION

Extracting the direction of visual motion is an essential operation for most animals to successfully perform tasks like navigation, prey capture, predator avoidance, and mating. Correlation-type motion detectors represent a class of algorithmic models that achieve direction selectivity by multiplying signals from two adjacent photoreceptors after asymmetric temporal filtering (Figure 1A; Hassenstein and Reichardt, 1956). In various vertebrate and invertebrate species, this is realized separately for brightness increments (ON) and decrements (OFF; Werblin and Dowling, 1969; Joesch et al., 2010; Borst and Euler, 2011). In the mouse retina, for example, direction selectivity in OFF-type starburst amacrine cells is proposed to arise from spatially offset bipolar cell input (Kim et al., 2014). These cells exhibit temporally diverse calcium (Baden et al., 2013) and glutamate release signals (Borghuis et al., 2013). In *Drosophila melanogaster*, photoreceptor signals are processed in a retinotopic way within

the four neuropils of the optic lobe, called lamina, medulla, lobula, and lobula plate (Figure 1B). In the lobula plate, wide-field tangential cells respond to motion stimuli in a fully opponent, direction-selective manner: they depolarize to motion along their preferred direction (PD) and hyperpolarize to motion along the opposite or null direction (ND; Joesch et al., 2008; Schnell et al., 2010). Tangential cells receive excitatory cholinergic input from two types of neurons, called T4 and T5 cells (Mauss et al., 2014). They were first described via Golgi stainings (Cajal and Sánchez, 1915) and exist in four subtypes, depending on their projection layer in the lobula plate (Figure 1B; Fischbach and Dittrich, 1989). Genetically silencing both cell types turns tangential cells motion insensitive and walking flies motion blind (Schnell et al., 2012; Bahl et al., 2013). Each of the four subtypes responds only to either brightness increments (ON for T4) or decrements (OFF for T5), moving in one of the four cardinal directions (front to back, back to front, upward, and downward). Blocking either T4 or T5 results in selectively diminished responses of lobula plate tangential cells to ON and OFF stimuli, respectively (Maisak et al., 2013). The splitting of ON and OFF signals starts at the level of lamina monopolar cells, which receive direct input from photoreceptors. L1 signals feed into the ON pathway; L2–L4 signals feed into the OFF pathway (Joesch et al., 2010, 2013; Clark et al., 2011; Eichner et al., 2011; Takemura et al., 2011; Silies et al., 2013; Meier et al., 2014). Electron microscopy reconstructions identified the primary interneurons that connect lamina monopolar cells to the dendrites of T4 and T5 cells. L1 synapses mainly onto the medulla intrinsic neuron Mi1 and onto the transmedulla neuron Tm3, which both contact T4 cells (Takemura et al., 2013). In the OFF pathway, reciprocally connected L2 and L4 cells (Riviera-Alba et al., 2011) connect to Tm1, Tm2, and Tm4 cells while L3 cells synapse onto Tm9 cells (Figure 1B; Takemura et al., 2013). These four Tm cells have been described as cholinergic and collectively account for nearly 90% of T5 input synapses, with Tm2 being the numerically dominant input (~33%), followed by Tm9 (~22%), Tm1 (~20%), and Tm4 (~13%; Takemura et al., 2011; Shinomiya et al., 2014). Calcium imaging and electrophysiological recordings revealed that Tm1 and Tm2 respond to OFF stimuli with transient activation, independent of the direction of motion (Meier et al., 2014; Strother et al., 2014; Behnia et al., 2014). Their dynamic properties, estimated using a white-noise stimulus, revealed an offset in peak response times of 13 ms. This led to the suggestion that Tm1 and Tm2 cells form the

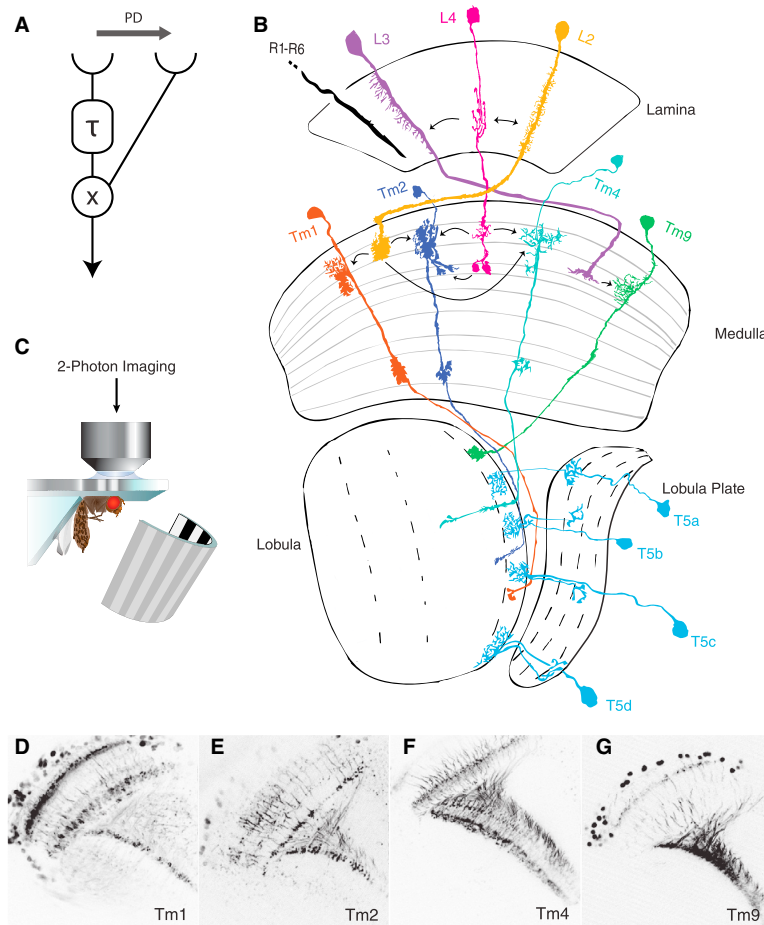


Figure 1. The OFF Pathway of *Drosophila* Motion Vision

(A) Schematic representation of a subunit of a Hassenstein-Reichardt correlator tuned to rightward motion (preferred direction, PD). Signals from two spatially offset inputs are multiplied (\times) after one of them has been temporally delayed by a low-pass filter with the time constant τ .

(B) Wiring diagram of the proposed OFF pathway neurons. Photoreceptors R1–R6 project onto interconnected lamina monopolar cells L2 (yellow), L3 (purple), and L4 (magenta). The L2–L4 sub-pathway consists of transmedullary neurons Tm2 (dark blue) and Tm4 (cyan). L3 contacts Tm9 cells (green). Tm1 (orange) only receives input via L2 (yellow). All four Tm cells project into the lobula, giving input to the four subtypes of T5 (light blue). Arrows indicate synaptic contacts between cell types. (Modified from Fischbach and Dittrich, 1989.)

(C) Experimental setup for two-photon calcium imaging.

(D–G) Contrast-inverted maximum intensity z projections of two-photon image stacks through the optic lobe of flies expressing GCaMP6f in Tm1 (D), Tm2 (E), Tm4 (F), and Tm9 (G) cells.

two input lines of an OFF elementary motion detector (Behnia et al., 2014). Indeed, blocking Tm2 cells strongly reduces the responses of tangential cells to moving dark edges (Meier et al., 2014). Whether Tm1 is equally critical has not been clarified; neither have the roles of the other two input neurons, Tm4 and Tm9. We therefore set out to explore the response properties and necessity of all four major inputs to T5 cells, which constitutes a crucial step toward a mechanistic understanding of how direction selectivity is computed in the OFF pathway of *Drosophila*.

First, we performed two-photon calcium imaging (Figure 1C) to assess the visual response properties of all major T5 inputs, including direction selectivity, response dynamics, and receptive fields. Second, we blocked the synaptic output of single-cell types, as well as combinations of two-cell types, using *shibire^{ts}* (Kitamoto, 2001) and analyzed responses of tangential cells and walking flies to visual motion stimuli. Our results demonstrate that all four Tm cell types are activated by brightness decrements, irrespective of the direction of motion, confirming the notion that T5 cells are the first direction-selective cells within the OFF pathway (Maisak et al., 2013;

Fisher et al., 2015). Their responses revealed substantially different temporal dynamics. Blocking their synaptic output individually and in combination exclusively impaired OFF motion vision, though by different magnitudes. Combinatorial blocking of two Tm cell types resulted in an increased reduction of the OFF motion response. These data do not map easily onto classical models of motion detection involving two input

RESULTS

Response Properties of Tm1, Tm2, Tm4, and Tm9 Cells

To directly examine the response properties of Tm cells, we expressed calcium indicator GCaMP5 (Akerboom et al., 2012) under the control of cell-type-specific Gal4 lines (Brand and Perrimon, 1993). We manually chose regions of interest that corresponded to single axonal terminals in the lobula where T5 dendrites are located (Figures 1D–1G) and determined the fluorescence change during visual stimulation. First, we characterized the calcium responses of T5's presynaptic elements by presenting edges of both polarities (ON and OFF edges) moving in the four cardinal directions. With these visual stimuli, we addressed two questions: First, are neurons upstream of T5 cells direction selective? Second, do they exhibit rectified responses with respect to the contrast polarity of the stimulus? In agreement with previous studies (Meier et al., 2014; Strother et al., 2014; Behnia et al., 2014), we found that Tm1 and Tm2 cells

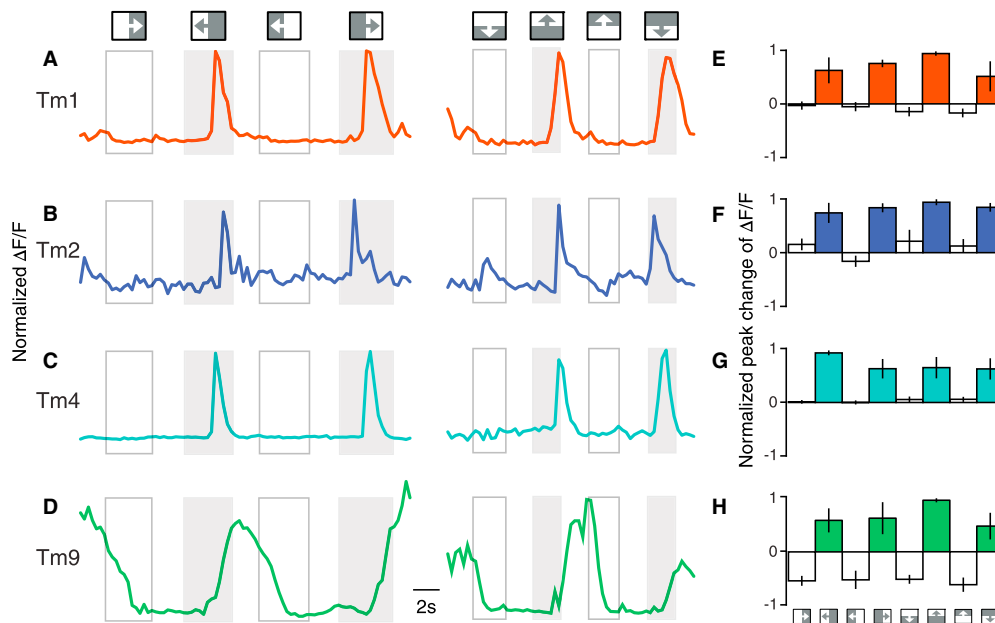


Figure 2. OFF Edges Activate Tm Cells Irrespective of the Direction of Motion

(A–D) Normalized $\Delta F/F$ calcium responses of single Tm1 (A), Tm2 (B), Tm4 (C), and Tm9 (D) cells. Flies were visually stimulated with ON and OFF edges moving horizontally (left panel) and vertically (right panel). Empty boxes indicate stimulation periods of ON edge motion; gray boxes indicate stimulation periods of OFF edge motion. Directions and polarity of edge motion are illustrated by little boxes on top. Between stimulations, luminance levels remain constant; i.e., after presentation of OFF edges, the stimulation device remains dark until the subsequent ON stimulus. After presentation of ON edges, the arena remains bright. (E–H) Average normalized peak changes in calcium signals during edge presentation. Stimuli are represented at the bottom of (H). Tm1 (E; $n = 11$ cells in $N = 11$ flies), Tm2 (F; $n = 8$, $N = 8$), Tm4 (G; $n = 9$, $N = 9$), and Tm9 (H; $n = 8$, $N = 8$). Error bars indicate \pm SEM. See also Figure S7.

respond to moving brightness decrements (OFF edges) with a transient increase in calcium, independent of the direction of motion. In this experiment, neither Tm1 nor Tm2 cells showed any response when stimulated with moving brightness increments (ON edges; Figures 2A and 2B). Tm4 cells exhibited similar characteristics with short increases of activity when stimulated with OFF edges moving along all four cardinal directions (Figure 2C). The calcium levels of Tm9, however, changed more tonically, inversely following the local luminance level: when presented with a moving ON edge, the cell's initial calcium level dropped, and it only increased when a dark edge was moved through the fly's visual field (Figure 2D). Again, this was true for all four directions. To quantify the calcium responses to moving edges—and to detect increases, as well as decreases—we calculated the extremum (maximum or minimum) of the derivative of the fluorescence change for each stimulus (Figures 2E–2H). This demonstrated that all transmedullary neurons, anatomically identified to be presynaptic to T5, are not themselves direction selective and respond with increased activity to visual stimulation with dark edges. The response kinetics of the different Tm cells, however, looked qualitatively different. To more precisely characterize the temporal properties of Tm cells and to investigate whether the four cell types exhibit rectified responses with respect to contrast polarity, we increased the temporal resolution of the scanning microscope from 1.8 to 480 Hz by

acquiring data from a single line through one axonal arbor in the lobula. Moreover, we expressed a faster calcium indicator, GCaMP6f (Chen et al., 2013), in the Tm cells. We used a 4.5° -wide, dark, vertical bar appearing and disappearing on a bright background for seven durations (50, 75, 125, 225, 425, 825, and 1,625 ms). All four Tm cells responded with an increase in calcium levels to local brightness decrements (Figures 3A–3D). Consistent with the edge stimulation results, this set of experiments revealed a broad range of response kinetics for the four Tm cell types. Furthermore, we observed a drop in calcium signaling upon stimulus offset. Based on these observations, we simulated their responses by fitting a three-stage filter model to the mean calcium traces (Figure 3E). Within this model, inputs were first linearly high-pass filtered (τ_{HP}), then rectified by setting negative values to zero, and finally low-pass filtered (τ_{LP}). Using this simple model, we were able to reproduce the measured calcium dynamics and estimate filter time constants for each cell type from the observed responses (Figures 3F–3I). In agreement with the data from the stimulation with moving edges, the four cell types could be classified in three groups: fast, transient Tm2 ($\tau_{HP} = 0.36$ s and $\tau_{LP} = 0.1$ s; Figures 3B and 3G) and Tm4 ($\tau_{HP} = 0.25$ s and $\tau_{LP} = 0.2$ s; Figures 3C and 3H), intermediate Tm1 ($\tau_{HP} = 1.23$ s and $\tau_{LP} = 0.23$ s; Figures 3A and 3F), and tonic Tm9 ($\tau_{LP} = 0.63$ s; Figures 3D and 3I). In contrast to the other cell types, the slow dynamics of Tm9 responses were best predicted

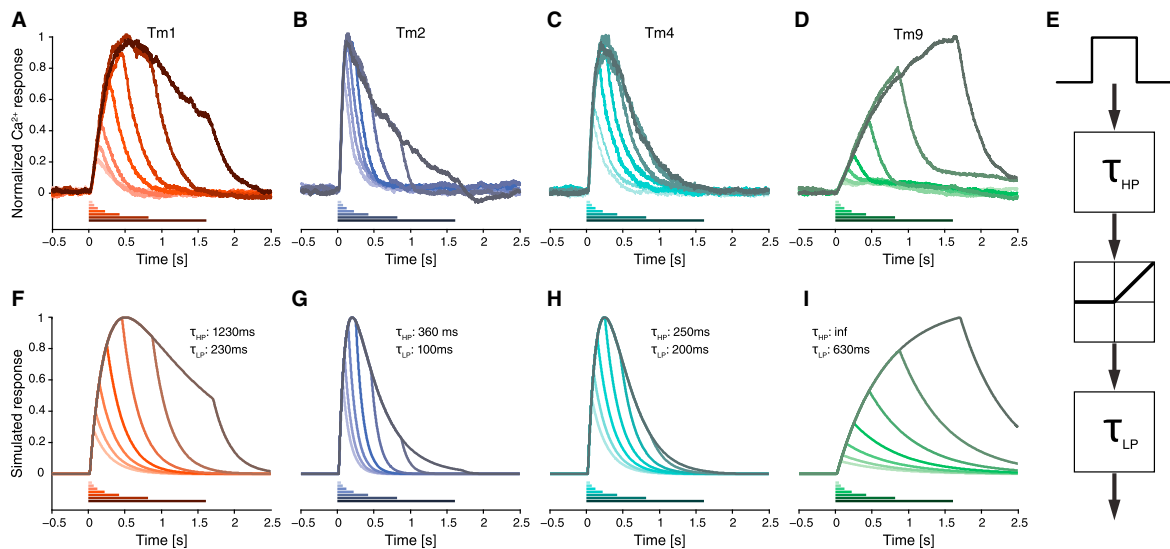


Figure 3. Temporal Tm Cell Response Properties

(A–D) Normalized $\Delta F/F$ calcium responses of Tm1 (A; $n = 32$, $N = 5$), Tm2 (B; $n = 38$, $N = 5$), Tm4 (C; $n = 26$, $N = 3$), and Tm9 (D; $n = 44$, $N = 4$), obtained by line scans through individual axonal arbors. Flies were presented with a 4.5° -wide, dark, vertical bar appearing on a bright background for seven periods: 50, 75, 125, 225, 425, 825, and 1,625 ms. Color-coded bars at the bottom of the graphs indicate the duration of stimulus presentation.

(E) Simulation procedure. The input signals were high-pass filtered (τ_{HP}), rectified, and low-pass filtered (τ_{LP}). Filter time constants are indicated in each panel. (F–I) Simulated responses of Tm1 (F), Tm2 (G), Tm4 (H), and Tm9 (I) obtained by using the indicated time constants for the low-pass and high-pass filtering. For Tm9, no high-pass filtering was applied.

See also [Figures S1](#) and [S7](#).

by a pure low-pass filter. Also, prolonging the period of stimulus presentation to 2 and 4 s supported the finding that Tm9 cells respond tonically to visual stimulation with dark bars ([Figure S1](#)). To exclude that calcium buffering caused the slow dynamics of the Tm9 responses, we repeated the experiments using flies heterozygous for Gal4 and upstream activating sequence (UAS)-GCaMP6f to reduce expression levels of GCaMP. Here, we obtained the same results. In summary, the preceding results demonstrate that Tm1, Tm2, Tm4, and Tm9 are directionally unselective and thus confine the computation of direction selectivity in the OFF pathway to the dendrites of T5 cells. Furthermore, our data indicate that Tm cells provide a variety of temporal filters, ranging from fast, transient Tm2 and Tm4 over intermediate Tm1 to slow and sustained Tm9 cells.

Receptive Field Characteristics of Tm1, Tm2, Tm4, and Tm9

Current models for motion detection are based on the spatio-temporal correlation of input signals. It is thus crucial to characterize receptive field sizes and spatial integration properties of columnar neurons. To probe the receptive fields of the four Tm cells, we recorded changes in fluorescence at a lower temporal resolution of 1.8 Hz. Because our previous experiments ([Figures 2](#) and [3](#)) had revealed that all four cell types respond to changes in local luminance, we stimulated flies with 4.5° -wide, dark, vertical bars flickering on a bright background with 0.5 Hz at different azimuthal positions, each shifted by 1.5° . All

four Tm cells tested with this stimulus exhibited similar receptive field sizes, ranging from 4.2° to 5.5° of half-width ([Figures 4A–4E](#)). We next used horizontal bars and presented them at different elevations. Again, we found comparable receptive field sizes with half-widths between 3.9° and 4.2° ([Figure 4E](#)). From this, we conclude that Tm1, Tm2, Tm4, and Tm9 cells have small isotropic receptive fields. The size of the measured receptive fields approximately corresponded to the visual acceptance angle of one neuro-ommatidium ([Götz, 1964](#); [Land, 1997](#)), which indicates that the main activation of Tm cells is restricted to visual information detected by only one ommatidium. Stimulating the fly's eye in consecutive steps along the azimuth with terminals of several adjacent Tm9 cells in focus nicely revealed the retinotopic organization of columnar elements projecting from the medulla to the lobula ([Movie S1](#)). Next, we investigated spatial integration properties by centering a flickering dark, vertical bar at the position of maximal excitability of individual Tm cells. After each period of stimulation, we increased the width of the bar. All four cell types showed maximum responses when stimulated with bars of a 4.5° to 7.5° width but decreased activity when presented with stimuli spanning larger areas in visual space ([Figures 4F–4I](#)). Hence, all cells seem to be subject to lateral inhibition, preventing them from responding to wide-field flicker. The responses of Tm9 cells diverged from the other cell types for full-field stimulation (180° azimuth): while the calcium response levels elicited by flicker between a 13.5° and a 67.5° width were small, the response to full-field darkening amounted

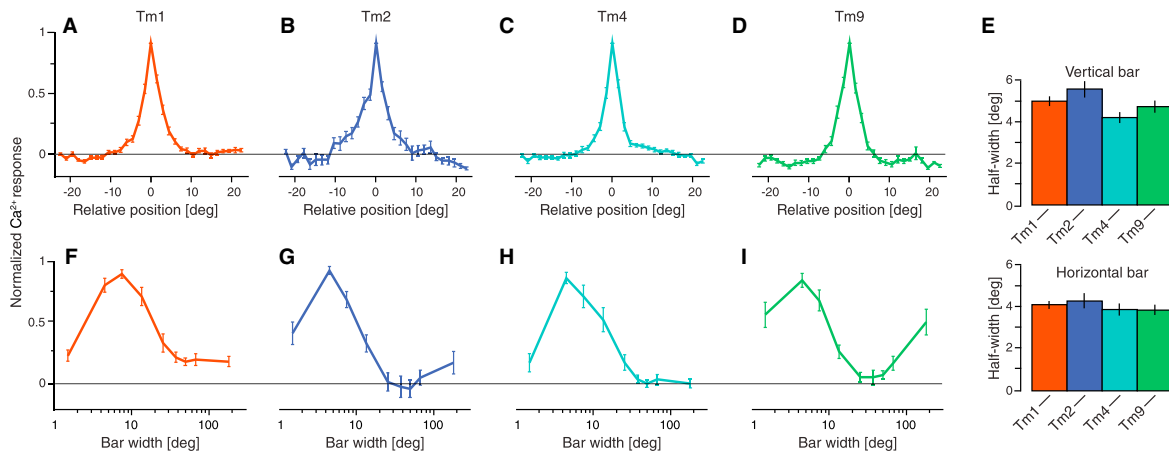


Figure 4. Receptive Field Properties of Tm Cells

(A–D) Spatial receptive fields measured by normalized calcium responses of Tm1 (A; $n = 45$, $N = 10$), Tm2 (B; $n = 29$, $N = 8$), Tm4 (C; $n = 30$, $N = 5$), and Tm9 (D; $n = 31$, $N = 8$) to 4.5° -wide, dark, vertical bars appearing and disappearing at various positions (shifted by 1.5°) on a bright background at a frequency of 0.5 Hz. (E) Quantification of receptive field half-width for vertical bars (top panel) and horizontal bars (bottom panel). Tm1 ($n = 37$, $N = 8$), Tm2 ($n = 26$, $N = 6$), Tm4 ($n = 20$, $N = 3$), and Tm9 ($n = 24$, $N = 3$).

(F–I) Spatial integration properties measured by normalized calcium responses of Tm1 (F; $n = 15$, $N = 9$), Tm2 (G; $n = 16$, $N = 7$), Tm4 (H; $n = 9$, $N = 4$), and Tm9 (I; $n = 9$, $N = 4$) to dark, vertical bars of increasing size (bar widths: 1.5° , 4.5° , 7.5° , 13.5° , 25.5° , 37.5° , 49.5° , 67.5° , and 180°). Error bars indicate \pm SEM. See also Figure S7.

to approximately 50% of the maximum response. Tm9 has been shown to receive its main synaptic inputs through a different set of neurons from those for Tm1, Tm2, and Tm4 (L3 for Tm9, compared to L2 for Tm1, Tm2, and Tm4; Takemura et al., 2013). Together with the particular spatial integration property, the anatomical distinctness of Tm9 suggests that lateral inhibition could be implemented by two different mechanisms in the OFF pathway. Taken together, using calcium levels as a proxy for neuronal activity, we established that Tm1, Tm2, Tm4, and Tm9 are small-field columnar neurons that receive isotropic lateral inhibition.

Blocking OFF Pathway Tm Cells Reduces Responses of Lobula Plate Tangential Cells Specifically to OFF Edges

The response properties of *Drosophila* lobula plate tangential cells have been well characterized using various visual stimuli (Joesch et al., 2008, 2010; Schnell et al., 2010; Mauss et al., 2015). Furthermore, these large-field interneurons have been demonstrated to receive excitatory input from T4 and T5 cells (Schnell et al., 2012; Mauss et al., 2014). Hence, responses of lobula plate tangential cells can be used as a readout to assess the contribution of presynaptic elements within the motion detection circuit (Joesch et al., 2010; Schnell et al., 2012; Maisak et al., 2013; Meier et al., 2014). We performed somatic whole-cell patch clamp recordings from tangential cells of the vertical system (VS) and horizontal system (HS) while blocking the output of different Tm cells. We stimulated flies with either multiple ON or OFF edges (Figure S7). Synaptic transmission was silenced by expressing temperature-sensitive *shibire^{ts}* (Pfeiffer et al., 2012) under the control of specific Gal4 driver lines. We confirmed the identities of cell types in the Gal4 lines by expressing GFP

in a small subset of neurons using a flip-out approach (Figures 5A–5D; Nern et al., 2015). To increase block strength without a loss of expression specificity, we used flies with two copies of *UAS-shibire^{ts}* (*shi^{ts}/shi^{ts}*) and one copy of the Gal4 driver. Tangential cells of control flies responded with approximately equal strength to motion of bright or dark edges (Figures 5E–5H). We could thus use these stimuli to probe contrast-polarity-specific effects of Tm cell blocks. Based on the diversity of temporal response properties observed in our calcium imaging experiments reported earlier, we hypothesized that different Tm cell types may play distinct roles depending on motion velocity, as was recently shown for input elements to the ON direction-selective T4 cells (Ammer et al., 2015). We therefore tested flies using edges moving at nine velocities across two orders of magnitude ($3.125^\circ/\text{s}$ – $800^\circ/\text{s}$; Figure S2). When Tm1 was removed from the circuit, lobula plate tangential cells responded only with about half of the magnitude of control flies to moving dark edges (Figures 5E and 5I). In agreement with a previous study, responses were strongly reduced when Tm2 was blocked (Meier et al., 2014). Both effects were present over all velocities tested (Figures 5F and 5J). Blocking Tm4 produced the weakest phenotype (Figures 5G and 5K). Interrupting Tm9 signaling resulted in the strongest effect of all cells tested and, as with the other cells, did so consistently across all stimulus velocities (Figures 5H and 5L). To our surprise, here, we did not find differential effects of blocking any of the four Tm cell types when using different edge velocities. To compare the overall effects of silencing single Tm cells, we calculated the average response relative to control flies over the whole range of stimulus velocities (Figures 5M–5P). Critically, in all silencing experiments, responses to ON edges were not significantly altered. Blocking

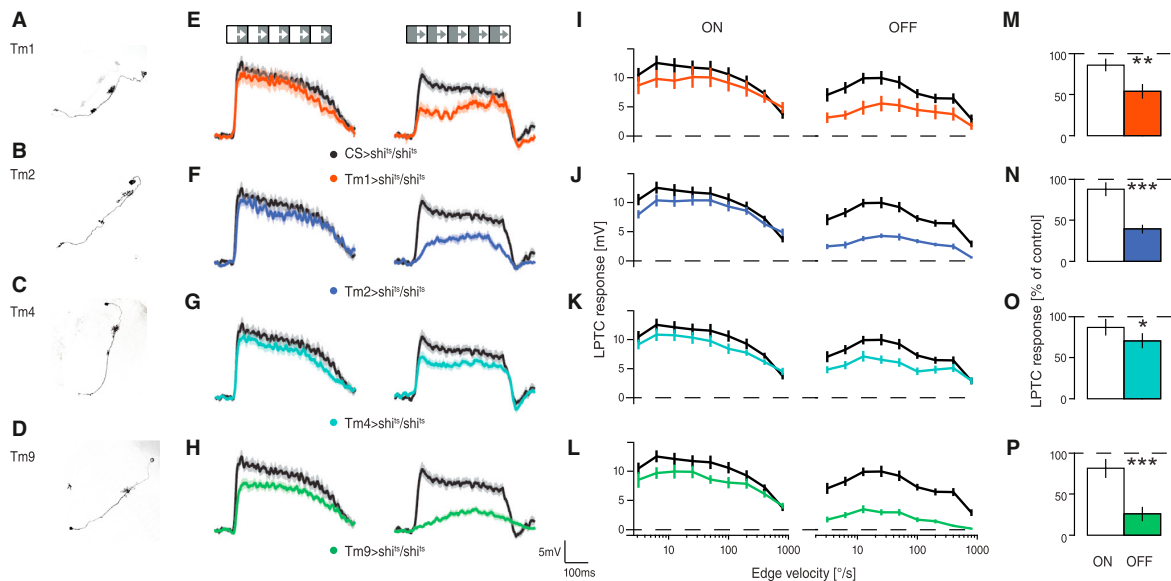


Figure 5. Blocking Tm Cells Impairs OFF Motion Vision

(A–D) Stochastic labeling of single Tm1 (A), Tm2 (B), Tm4 (C), and Tm9 (D) cells, showing the specificity of the Gal4 driver lines. (E–H) Example traces of mean responses to motion along the PD minus the response to motion along the ND of lobula plate tangential cell (LPTC) responses upon stimulation with multiple ON (left) and OFF (right) edges (50°/s) in control CS > *shi^{ts}/shi^{ts}* (black), Tm1 > *shi^{ts}/shi^{ts}* (E), Tm2 > *shi^{ts}/shi^{ts}* (F), Tm4 > *shi^{ts}/shi^{ts}* (G), and Tm9 > *shi^{ts}/shi^{ts}* (H) flies. Stimulus presentation is indicated by the panels on top. (I–L) Mean PD-ND LPTC responses of control (black), Tm1 (I), Tm2 (J), Tm4 (K), and Tm9 (L) block flies upon ON (left panel) and OFF edge (right panel) stimulation for nine velocities (3.125°/s, 6.25°/s, 12.5°/s, 25°/s, 50°/s, 100°/s, 200°/s, 400°/s, and 800°/s). (M–P) Responses averaged over all nine velocities of Tm1 (M), Tm2 (N), Tm4 (O), and Tm9 (P) block flies plotted as percentages of the controls. Responses were obtained from HS and VS cells. Because no difference was detected, data from both cell types were pooled. CS > *shi^{ts}/shi^{ts}* data are from 13 cells (5 HS, 8 VS) in 5 flies, Tm1 block data are from 10 cells (3 HS, 7 VS) in 7 flies, Tm2 block data are from 14 cells (7 HS, 7 VS) in 7 flies, Tm4 block data are from 16 cells (5 HS, 11 VS) in 9 flies, and Tm9 block data are from 15 cells (3 HS, 12 VS) in 8 flies. In all four Tm cell blocks, ON responses are not significantly reduced in comparison to control flies. OFF responses, however, are reduced at different significance levels. * $p < 0.05$, ** $p < 0.01$, *** $p < 0.001$, tested using two-tailed t tests against the controls. Error shades and error bars indicate \pm SEM. See also [Figures S2–S4](#) and [S7](#).

any of the four Tm cell types specifically impaired the responses of lobula plate tangential cells to moving dark edges, irrespective of stimulus velocity. The magnitude of effects, however, covered a wide range, with strong phenotypes for Tm9 (25.69% \pm 6.37% of control, mean \pm SEM, $n = 15$ recordings, $p < 0.001$) and Tm2 (39.22% \pm 4.50%, $n = 14$, $p < 0.001$), intermediate effects for Tm1 block (53.98% \pm 8.33%, $n = 10$, $p < 0.01$), and a weak phenotype for silencing Tm4 (70.59% \pm 8.41%, $n = 16$, $p < 0.05$).

Combinatorial Blocking of Tm Cells Increases OFF Edge Phenotypes

Tm cells could contribute in parallel or modularly to direction selectivity in T5. Combining two cell-specific Gal4 lines, thereby driving the expression of *shibire^{ts}* in two cell populations simultaneously, allowed us to investigate how different Tm cells interact. To detect potential synergistic effects, we decreased individual blocking strength by using flies with only one copy of *shibire^{ts}* (*shi^{ts}/+*). When we repeated the same experiment as described earlier, the tangential cell responses of Tm1 block flies to dark-edge stimulation were only reduced to 76.29% \pm 7.88% (percent of control, $n = 11$, $p = 0.18$; [Figures 6A](#) and [6B](#)) as opposed to 54% for two copies of *shibire^{ts}*. Blocking Tm2 with one copy of

shibire^{ts} resulted in a response reduction to 69.13% \pm 4.25% ($n = 11$, $p = 0.07$; [Figures 6G](#) and [6H](#)), while blocking Tm4 cells did not result in a detectable reduction of tangential cell responses (89.17% \pm 7.95%, $n = 12$, $p = 0.50$; [Figures 6M](#) and [6N](#)). Only responses of Tm9 block flies to dark edges remained significantly different from those of control flies (51.39% \pm 6.02%, $n = 10$, $p < 0.01$; [Figures 6S](#) and [6T](#)), even with only one copy of *shibire^{ts}*. Overall, we found that the effect size was reduced while relative effects remained the same, with blocking Tm9 resulting in the strongest reduction of the OFF response, followed by Tm2, Tm1, and finally Tm4. This offered an opportunity to compare partial single-cell blocks with the combinations of two incompletely blocked classes of neurons. The images in [Figure S3](#) provide an overview of the expression patterns of the six binary combinations of the four Tm cell types. Combining Tm9 with one of the other three cell types resulted in the strongest reductions of tangential cell responses to OFF edges ([Figures 6E](#), [6J](#), and [6O–6R](#)). All three Tm9 combinations decreased responses beyond what we had determined for the single Tm9 block. Furthermore, Tm1/Tm2 and Tm2/Tm4 blocks reduced the responses of lobula plate tangential cells to moving dark stimuli ([Figures 6C](#), [6F](#), [6I](#), and [6L](#)) compared to the isolated

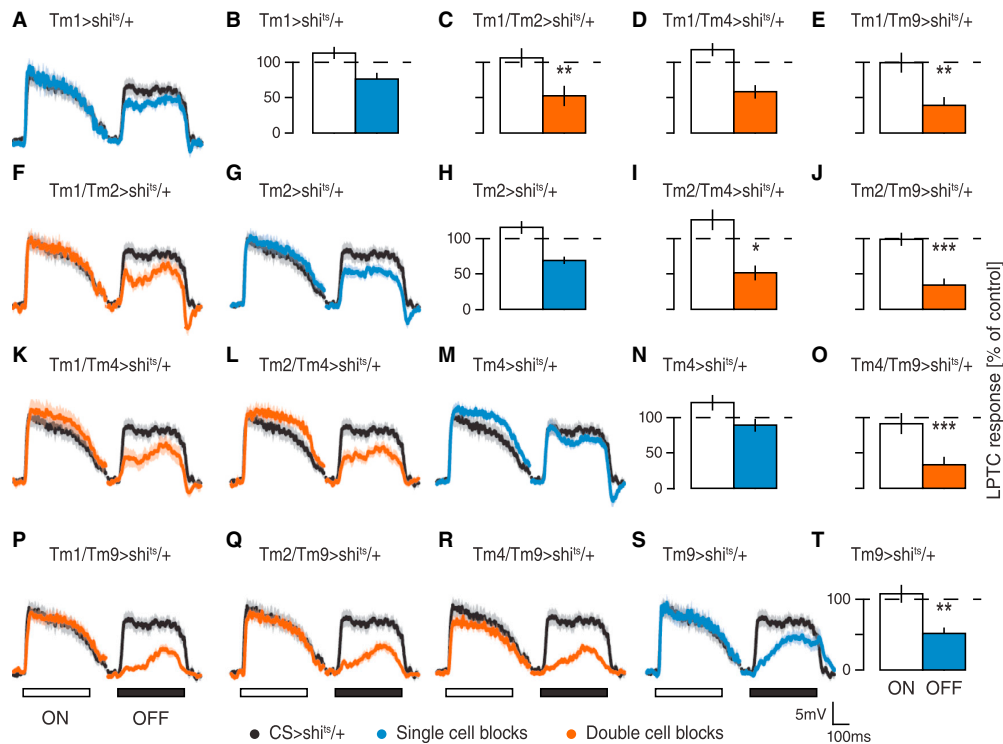


Figure 6. Combinatorial Blocking of Tm Cells

(A, F, G, K–M, and P–S) Mean traces of control (black), single-block (blue), and double-block (orange) flies for ON (left) and OFF (right) edge stimulation at a representative velocity of $50^\circ/\text{s}$.

(B–E, H–J, N, O, and T) Mean ON and OFF lobula plate tangential cell (LPTC) responses of single (blue) and double (orange) Tm cell block flies compared to control flies over nine velocities. Control $CS > shi^{ts}/+$ data are from 13 cells (5 HS, 8 VS) in 5 flies, $Tm1 > shi^{ts}/+$ data are from 11 cells (4 HS, 7 VS) in 6 flies, $Tm2 > shi^{ts}/+$ data are from 13 cells (6 HS, 7 VS) in 9 flies, $Tm4 > shi^{ts}/+$ data are from 12 cells (4 HS, 8 VS) in 6 flies, $Tm9 > shi^{ts}/+$ data are from 10 cells (3 HS, 7 VS) in 7 flies, $Tm1/Tm2 > shi^{ts}/+$ data are from 11 cells (3 HS, 8 VS) in 7 flies, $Tm1/Tm4 > shi^{ts}/+$ data are from 11 cells (4 HS, 7 VS) in 7 flies, $Tm1/Tm9 > shi^{ts}/+$ data are from 10 cells (3 HS, 7 VS) in 7 flies, $Tm2/Tm4 > shi^{ts}/+$ data are from 13 cells (3 HS, 10 VS) in 7 flies, $Tm2/Tm9 > shi^{ts}/+$ data are from 12 cells (4 HS, 8 VS) in 8 flies, and $Tm4/Tm9 > shi^{ts}/+$ data are from 10 cells (3 HS, 7 VS) in 7 flies. In all block flies, ON responses are not significantly reduced in comparison to control flies. OFF responses, however, are reduced at different levels. * $p < 0.05$, ** $p < 0.01$, *** $p < 0.001$, tested using two-tailed t tests against the controls. Error shades and error bars indicate \pm SEM. See also Figures S3–S5 and S7.

Tm2 block. When the output of Tm1 and Tm4 was blocked simultaneously, we observed an intermediate reduction of tangential cell responses to OFF edges (Figures 6D and 6K). For all single- and double-block experiments with one copy of *shibire^{ts}*, responses to ON edges remained unaltered. Effects were consistent across all velocities tested for PD and ND stimulation (Figure S4). These results corroborate the conclusion drawn from single blocks, namely, that all four Tm cell types are involved in the detection of moving brightness decrements. Moreover, all combinatorial restrictions of two Tm cell outputs decreased OFF responses beyond the level of the respective single-cell blocks. To further investigate the effects of blocking T5 input elements on motion responses in tangential cells, we used square wave gratings (Figure S7) moving at eight temporal frequencies (from 0.07 to 8.89 Hz; Figure S5). In contrast to ON or OFF edges, square wave gratings did not allow for a specific stimulation of ON or OFF pathways. However, in contrast to a

moving edge, they led to ongoing, permanent stimulation of local T5 motion-detecting cells, as well as their input neurons. The responses to square wave gratings were only mildly reduced. The reduction pattern, however, was similar to that for OFF edges (Figures S5A–S5N). Compared to controls (Figures S5O–S5X), it is apparent that responses to gratings in almost all blocking conditions decreased as temporal frequency increased. This effect can be explained through differentially tuned responses of lobula plate tangential cells to ON and OFF edges: tangential cells respond maximally to bright edges moving ~ 100 deg/s, whereas their responses to dark edges peak ~ 300 deg/s (Ammer et al., 2015). Hence, the ON channel appears to contribute more strongly to responses at lower frequencies. High frequencies seem to be mostly mediated through the OFF system. This asymmetry could thus account for the increased reductions in high-frequency regimes for the strongest OFF blocks (Figures S5R, S5S, S5U, S5W, and S5X).

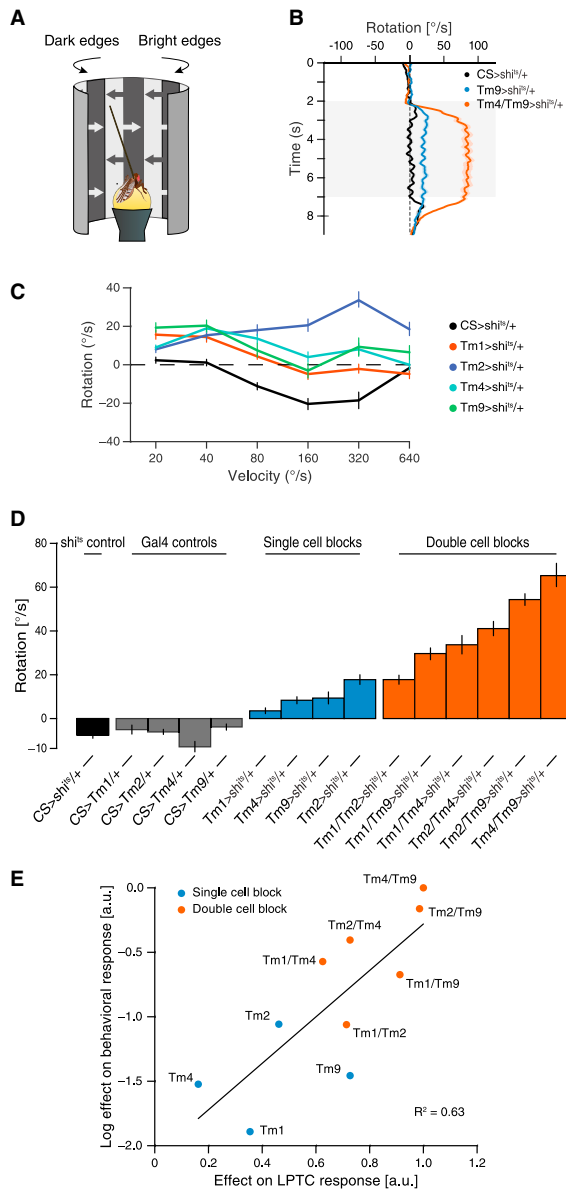


Figure 7. Blocking Tm Cells Affects Turning Behavior in Walking Flies

(A) Schematic illustration of the behavioral setup used in this study. A tethered fruit fly is walking on an air-suspended ball, facing a visual stimulation device. The fly is presented with a balanced motion stimulus (see [Experimental Procedures](#)).

(B) Exemplary optomotor responses of three genotypes to visual stimulation moving at 40°/s. Positive (rightward) rotation follows ON edges; negative (leftward) rotation follows OFF edges. Control flies do not exhibit any turning response for this velocity (black line), Tm9 block flies follow the bright edges with a low turning speed (blue line), and Tm4/Tm9 block flies turn with the direction of ON motion with a high angular velocity (orange line).

Blocking Tm Cells Affects Optomotor Responses in Walking Flies

The detection of visual motion is ultimately used to control behavior. The model proposed by [Hassenstein and Reichardt \(1956\)](#) was derived from quantitative observations of tethered walking beetles. To examine the effects of Tm cell blocks on the flies' turning responses during visual stimulation ([Figure 7A](#)), we monitored tethered *Drosophilae* walking on an air-suspended ball and repeated the blocking experiments as described earlier. We used multiple dark and bright edges, simultaneously moving in opposing directions ([Clark et al., 2011](#)). Compared to the direct measurement of optomotor responses to edge motion of a single polarity, this stimulus allows for a differential measurement of the flies' sensitivity to moving ON and OFF edges. Turning responses in walking and flying *Drosophilae* are not a direct readout of the membrane potential of lobula plate tangential cells ([Schnell et al., 2014](#)). Instead, signals are subject to leaky integration over a time window of multiple seconds. When examining responses, this may lead to robust behavioral responses despite strongly reduced lobula plate tangential cell signals. The opposing edge assay circumvents this issue by having edges of opposite polarities compete before the integration stage, such that small differences are amplified and become detectable at the level of turning responses. Critically, our electrophysiological experiments demonstrate that ON responses are generally not affected by blocking either of the four cells, suggesting that any imbalance we detect in behavior results from a defect specific to OFF motion processing.

At a stimulus velocity of 40°/s, control flies showed no turning response during presentation of opposing edges ([Figure 7B](#)), indicating that ON and OFF responses are intact and in balance. When we disrupted the output of either Tm9 or Tm4 and Tm9 in combination, block flies constantly followed the direction of moving ON edges (positive turning responses) with different amplitudes. This suggests an impairment of OFF motion detection at the behavioral level. When we used opposing edges moving at multiple velocities, control flies exhibited no turning response for slowly moving stimuli (20°/s and 40°/s) and started following dark edges (negative turning) when stimulated with patterns moving at higher speeds (80°/s–320°/s; [Figures 7C and S6](#)).

(C) Mean turning responses of control (black), Tm1 block (orange), Tm2 block (blue), Tm4 block (cyan), and Tm9 block (green) flies for stimulation with six velocities (20°/s, 40°/s, 80°/s, 160°/s, 320°/s, and 640°/s).

(D) Mean turning response of control (black and gray), single-block (blue), and double-block (orange) flies to stimulation with the balanced motion stimulus over all velocities tested. All blocking experiments were performed using one copy of *shibire^{ts}*. shi-control (N = 14), Tm1-control (N = 13), Tm2-control (N = 17), Tm4-control (N = 15), Tm9-control (N = 13), Tm1 (N = 12), Tm2-block (N = 13), Tm4-block (N = 13), Tm9-block (N = 12), Tm1/Tm2-block (N = 16), Tm1/Tm4-block (N = 12), Tm1/Tm9-block (n = 12), Tm2/Tm4-block (n = 16), Tm2/Tm9-block (n = 17), Tm4/Tm9-block (n = 14).

(E) Comparison of block effect strengths in the turning response of walking flies (y axis, log-transformed data) versus the effect of Tm cell blocks on the responses of lobula plate tangential cell (LPTCs; x axis, data not transformed). Single-cell blocks are colored in blue; double-cell blocks are in orange. The black line indicates a linear fit with $R^2 = 0.63$, indicating an exponential relationship between the behavioral effect and the reduction of the motion response as observed in the tangential cells. For details, see [Experimental Procedures](#). Error shades and error bars indicate \pm SEM. See also [Figures S3, S6, and S7](#).

Turning behavior of Tm1, Tm4, and Tm9 block flies differed from control flies in a roughly constant way across all velocities, showing positive responses (following bright edges) for low velocities and no turning response for higher velocities. To our surprise, and in contrast to our electrophysiological data (Figure 5), we could see a velocity-dependent effect in Tm2 block flies, which followed the motion of bright edges more strongly at high velocities (Figure 7C). These data suggest that removing Tm2 from the circuit has comparatively little effect at low velocities but a pronounced effect at high velocities, suggesting a specialized role of Tm2 for processing of fast input signals.

To compare effects from electrophysiological recordings with the behavioral data, we averaged the turning response over all velocities tested (Figure 7D). On average, all control flies exhibit a small negative turning tendency that can be explained by the high-velocity stimuli where OFF signals dominate (Ammer et al., 2015; Figures 7C and S6). Blocking Tm2 with one copy of *shibire^{TS}* resulted in the strongest turning response, whereas flies with blocked Tm1 cells showed only weak turning responses syndirectional with bright edges. Tm4 and Tm9 block flies exhibited intermediate phenotypes. Hence, suppressing synaptic transmission in single Tm cell types resulted in phenotypes that resembled those of T5 block flies (Maisak et al., 2013) and were qualitatively comparable to the results obtained in electrophysiological experiments. Next, we looked at the turning responses of flies with combinations of two Tm cell types silenced. When we combined Tm9 with Tm4- or Tm2-specific driver lines, we observed the strongest effects, in accordance with our electrophysiological data (Figure 7D). For combinatorial blocks of Tm1/Tm9, Tm1/Tm4, and Tm2/Tm4, the behavioral response was increased compared to single blocks (Figure 7D). Only the combined block of Tm1 and Tm2 cells did not elicit a turning response stronger than that for the Tm2 block alone. To investigate the relation between behavioral and tangential cell responses, we plotted effects of single- and double-cell silencing observed in the tangential cell responses versus those observed in walking flies (Figure 7E). To compare positive measures of effect strength in behavior and electrophysiology, we subtracted the electrophysiological phenotypes (in percent of control) from 100 and normalized them via division by the strongest phenotype. We then normalized the behavioral effect in the same way. We found an interesting relationship between the response reduction at the level of lobula plate tangential cells and the behaviorally measured ON-OFF imbalance. This relation is well explained by an exponential fit (black line in Figure 7E), suggesting that the transformation of tangential cell responses into behavioral output is highly nonlinear. A saturating transfer function, for instance, would explain how small and intermediate block effects at the level of the lobula plate produce comparatively weak effects at the level of walking behavior. Only when lobula plate tangential cell activity is heavily suppressed do walking flies show strong deficiencies for dark-edge motion, as indicated by the opposing edge results. Given that lobula plate networks feed into complex post-synaptic cascades before controlling motor output, this is not surprising. Generally, our electrophysiological findings predicted the behavioral phenotypes well, lending further credence to our results and indicating that the reductions we see at the level of lobula plate tangential cells

have direct impact on course control of behaving flies. Considering the combined dataset of tangential cell responses and behavior of walking flies, we conclude that all four Tm cells investigated here contribute to the computation of motion in the OFF pathway.

Reichardt Detector Simulations Using Tm Cells' Temporal Filters

A classical elementary motion detector (Hassenstein and Reichardt, 1956) consists of two spatially offset input lines that are multiplied after temporal filtering (Figure 1A). This is done in a mirror-symmetric fashion, and the outputs of the multiplication stages are subtracted from each other (insets in Figures 8A–8F). We used the calculated temporal filters of the Tm cells from Figures 3F–3I to simulate the responses of elementary motion detectors that are built from the six binary combinations of two Tm cells to grating stimulation (Figures 8A–8F). To obtain velocity tuning curves, we modeled responses to temporal frequencies ranging from 0.1 to 10 Hz (Figure 8). Except for the combination of Tm2 and Tm4, which have almost identical response dynamics, all Tm cell combinations led to direction-selective responses that varied in relative amplitude and tuning (Figures 8A–8F). Tuning curves of the four pairs Tm1/Tm2, Tm1/Tm4, Tm9/Tm2, and Tm9/Tm4 showed similar shapes and response amplitudes, peaking ~0.5 Hz. The Tm1/Tm9 model produced the strongest responses, peaking ~0.2 Hz. We calculated the mean of all detector outputs and normalized the tuning curve to compare the results with the physiological data (from Figure S5). The frequency tuning curves were largely similar, and both peaked ~0.5 Hz (Figure 8G). The shape of the tangential cell tuning curve, however, was wider than that of the simulation curve, which can be explained by saturation effects in tangential cells. From this, we conclude that the measured temporal response properties of all Tm cells are suitable for correlation-type elementary motion detectors.

DISCUSSION

In this study, we characterized the response properties of the four Tm cell types Tm1, Tm2, Tm4, and Tm9 and analyzed their involvement in *Drosophila* OFF motion detection. We demonstrated that none of these cells are direction selective and thus conclude that the computation of direction selectivity in the OFF pathway takes place on the dendrites of T5 cells.

At multiple levels, this circuit arrangement bears a striking resemblance to a network motif found in the mammalian retina (Kim et al., 2014). First, comparable to T5 cells, direction-selective starburst amacrine cells receive synaptic input from several anatomically similar cell types, i.e., the OFF bipolar cells 1, 2, 3a, 3b, and 4 (Masland, 2012). Second, like the Tm cells presynaptic to T5, these OFF bipolar cells have been shown to respond in a directionally unselective manner (Yonehara et al., 2013; Park et al., 2014). Third, the five OFF bipolar cell types show dynamics similar to those of the four Tm cells described here, ranging from sustained over slow decaying to fast transient (Baden et al., 2013; Borghuis et al., 2013). Depending on their temporal response properties, Tm cells receive input from particular groups of lamina monopolar cells. The two fast and transient

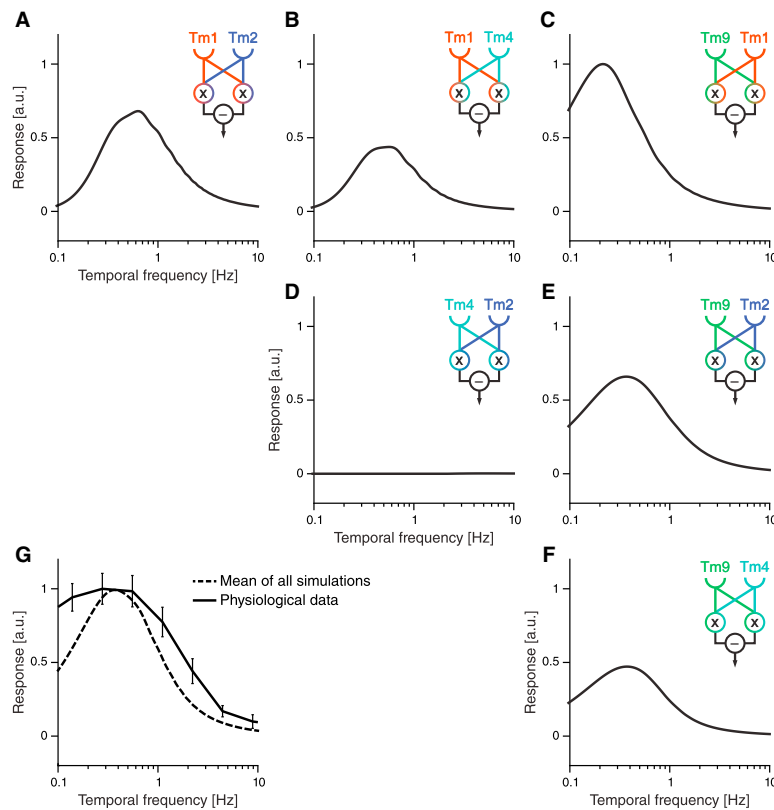


Figure 8. Simulated Frequency Tunings for the Six Combinations of Tm Cells

(A–F) Reichardt detector responses to grating stimulation using the simulated temporal filters (Figure 3) of Tm1/Tm2 (A), Tm1/Tm4 (B), Tm1/Tm9 (C), Tm2/Tm4 (D), Tm2/Tm9 (E), and Tm4/Tm9 (F). The responses were normalized to the maximal response of the Tm1/Tm9 detector (C). (G) Comparison of the normalized mean response of all six simulations with the normalized physiological data of control flies (from Figure S5). Error bars indicate \pm SEM. See also Figure S5.

wave gratings moving at a temporal frequency of about 0.5 Hz (Figures 8G and S5). Except for Tm2/Tm4, whose filter time constants are almost identical, all combinations resulted in frequency optima in a range compatible with tangential cell responses. Furthermore, the mean signal of all simulations matches the tuning curve of electrophysiologically measured responses well. These simulations only represent a simplified view. They do not take into account several important aspects, such as the temporal frequency tuning of the ON channel, the different synaptic weights, or any spatial offsets of Tm cells on the T5 dendrites. Nevertheless, this simple model confirms the functional plausibility of the time constants of the four Tm cells tested.

cells, Tm2 and Tm4, receive their major input from L2 and L4; intermediate Tm1 cells primarily receive input from L2; and tonic Tm9 cells receive input from similarly slow and sustained L3 (Clark et al., 2011; Freifeld et al., 2013; Silies et al., 2013; Takemura et al., 2013; Meier et al., 2014). Finally, the mechanism for the computation of direction selectivity on the dendrites of starburst amacrine cells has been proposed to rely on dendritically offset input from bipolar cells with different temporal filter properties (Kim et al., 2014). For T5, comparable spatial shifts among dendritic target sites of Tm1, Tm2, and Tm9 have been reported (Shinomiya et al., 2014). The aforementioned study, however, was not able to identify the preferred direction of corresponding T5 cells and thus could not correlate it with the particular arrangement of Tm cell input on the dendrite. Nevertheless, the remarkable resemblance of neural circuits between invertebrates and mammals suggests a universality of underlying computational principles (Borst and Helmstaedter, 2015).

Are the measured temporal response properties functionally relevant for the computation of direction-selective signals? We addressed this question by modeling six elementary motion detectors through filtering of the signals in the two neighboring arms with the time constants of all six possible binary combinations of Tm cells (Figure 8). Lobula plate tangential cells exhibit a maximal steady-state response when presented with square

We also demonstrated that the functional importance of each of the four Tm cell types correlates with the number of synaptic contacts to T5 (Shinomiya et al., 2014). Silencing Tm4 cells, which out of the four provide the smallest number of synapses onto T5 cells, resulted in the weakest phenotype, followed by Tm1. Blocking Tm2 and Tm9, numerically the strongest inputs to T5, produced the strongest impairment of the OFF response (Figures 5 and 7). However, silencing L3, which is thought to be the main input to Tm9, does not result in similar, purely OFF-specific effects (Silies et al., 2013; Tuthill et al., 2013). This can be due to two facts. First, L3 also strongly connects to crucial ON pathway element Mi1 (Takemura et al., 2013; Ammer et al., 2015). Second, additional inputs to Tm9 cells may influence their response properties.

Given the increased effects of impairment when blocking pairs of Tm cells, we are able to rule out complete redundancy of individual elements (Figures 6 and 7). How do these four cell types then map onto the elements of correlation-type models? First, the interaction of several Tm cell types may give rise to a nonlinear stage more complex than the simple multiplication in the Hassenstein-Reichardt correlator. It is conceivable that the biophysical implementation of a suitable nonlinearity requires more than two appropriately tuned input lines. Our behavioral data lend some support to this hypothesis, because the

strongest combinatorial blocks display a supra-linear increase in effect strength compared to the sum of the single-cell effects (Figure 7E). Second, standard algorithms generally model the asymmetric processing of direct and delayed lines as single-stage linear filters. For biophysical realizations, this filtering may be more complex. Multiple cells with varying intrinsic membrane properties and different synaptic transmission characteristics could provide many degrees of freedom when implementing filters that are appropriate for motion detection. Thus, temporal processing within one input line of the algorithmic model (Figure 1A) may involve the combination of two or more cells; Tm9 and Tm4, for instance, could both correspond to a module implementing what is the delay line in the Hassenstein-Reichardt model. Third, the four cells may in principle play different roles in different stimulus regimes defined by, for instance, velocity, contrast, luminance, or color. Our results provide some evidence for such a division of labor. In walking flies, the velocity-dependent phenotype of Tm2 block flies, together with the cells' fast response characteristics (Figure 3B), suggests a specific role for Tm2 at high velocities (Figure 7C). Such a design principle may be realized in at least two ways. Functional specialization could be a static property of the system, derived from cell-intrinsic spatiotemporal or chromatic filter properties, or a dynamic property that is subject to regulation depending on stimulus conditions. A recent study showed that changes in the behavior of hawkmoths under dim light conditions can be reproduced by adapting the filter time constants of a Hassenstein-Reichardt correlator (Sponberg et al., 2015). Tm9 could represent a candidate to detect changes in global luminance due to its slow filter properties, which make it sensitive to both brightness increments and decrements at all timescales (Figures 3D and 3I), as well as due to its responsiveness to full-field flicker (Figure 4). Moreover, inputs from the color vision pathway have been demonstrated to improve motion discrimination (Wardill et al., 2012). Histaminergic photoreceptors R7 and R8, known to be involved in color perception (for review, see Behnia and Desplan, 2015), project to the medulla layers where Tm cell dendrites reside. Both Tm2 and Tm9 express a histamine-gated chloride channel (Gao et al., 2008), potentially linking the color and motion detection pathways. Finally, different Tm cells could be of different importance depending on the behavioral state of the animal, e.g., whether it is at rest, walking, or flying. Such behavioral-state dependency has been described at the level of the lobula plate tangential cells (Maimon et al., 2010; Chiappe et al., 2010; Haag et al., 2010; Jung et al., 2011; Schnell et al., 2014) and could be well explained by changes in contribution of synaptic input to T4 and T5 cells. Such a scenario could explain why blocking Tm2, Tm4, and their combinations resulted in stronger phenotypes in walking flies compared to tangential cell responses in a quiescent preparation (Figure 7E).

Taken together, our study sheds light on the circuitry underlying the computation of motion and uncovers striking parallels between vertebrate and invertebrate systems. Unraveling the exact mechanisms awaits further investigation. More naturalistic stimuli and modified algorithmic or biophysically realistic models that reflect the complexity of the neural correlate will play critical roles in this endeavor.

EXPERIMENTAL PROCEDURES

For calcium imaging, we used the genetically encoded indicators GCaMP5 (Akerboom et al., 2012) and GCaMP6f (Chen et al., 2013). Blocking experiments were accomplished using Tm cell-specific Gal4 lines crossed with pJFRC100-20XUAS-TTS-Shibire-ts1 (Pfeiffer et al., 2012) flies. Fly line specificity was tested using stochastic flip-out labeling (Nern et al., 2015) and expression of mCD8-GFP. All genotypes used in this study can be found in Table S1. Flies were prepared as described before: imaging experiments (Reiff et al., 2010), electrophysiology (Joesch et al., 2008), and behavior (Bahl et al., 2013). Two-photon microscopy and visual stimulus presentation was as described in Maisak et al. (2013). The recording protocol for electrophysiological experiments was adapted from Joesch et al. (2008). Under polarized light contrast, the glial sheet was digested locally by applying a stream of 0.5 mg/ml collagenase IV (Gibco) through a cleaning micropipette (~5 μ m opening). Recordings for the blocking electrophysiology experiments were obtained within 2 hr after a 60 min heat-shock application at 37°C. For statistical analysis, we used a two-tailed t test to compare *shibire*^{ts} controls and block flies (* $p < 0.05$, ** $p < 0.01$, *** $p < 0.001$). Behavioral experiments were conducted as previously described (Ammer et al., 2015). For immunostaining procedures, see Schnell et al. (2010). Data were evaluated offline using custom written software (Matlab and Python) and Origin (OriginLab). For modeling the time constants in Figure 3, we fit a three-stage filter model to the mean calcium traces. Within this model, inputs were first high-pass filtered, then rectified by setting negative values to zero, and finally low-pass filtered (Figure 3E). For the modeling results in Figure 8, we simulated grating responses of hypothetical Reichardt detectors whose inputs were band-pass filters as determined in Figure 3E. See Supplemental Experimental Procedures for detailed methods.

SUPPLEMENTAL INFORMATION

Supplemental Information includes Supplemental Experimental Procedures, seven figures, one table, and one movie and can be found with this article online at <http://dx.doi.org/10.1016/j.neuron.2016.01.006>.

AUTHOR CONTRIBUTIONS

E.S. and M.M. jointly performed and evaluated all calcium imaging and electrophysiology experiments. A.L. performed and evaluated the behavioral experiments. A.L. and A.B. performed computer simulations. A.B., E.S., and M.M. designed the study. E.S. and M.M. wrote the manuscript with the help of the other authors.

ACKNOWLEDGMENTS

We thank J. Haag for technical support and help with the two-photon microscope; R. Kutlesa and C. Theile for excellent help with behavior experiments; W. Essbauer, R. Kutlesa, C. Theile, and M. Sauter for fly work and immunostainings; T. Schilling for artwork; and D. Soll for the Dlg antibody. We thank G. Ammer, A. Arenz, J. Pujol-Marti, and A. Mauss for carefully reading the manuscript. All authors are members of the Graduate School for Systemic Neurosciences, Munich. We thank B. Dickson, G. Rubin, and A. Nern for providing us with unpublished fly lines.

Received: June 25, 2015

Revised: November 18, 2015

Accepted: December 18, 2015

Published: February 4, 2016

REFERENCES

Akerboom, J., Chen, T.-W., Wardill, T.J., Tian, L., Marvin, J.S., Mutlu, S., Calderón, N.C., Esposti, F., Borghuis, B.G., Sun, X.R., et al. (2012). Optimization of a GCaMP calcium indicator for neural activity imaging. *J. Neurosci.* 32, 13819–13840.

- Ammer, G., Leonhardt, A., Bahl, A., Dickson, B.J., and Borst, A. (2015). Functional specialization of neural input elements to the *Drosophila* ON motion detector. *Curr. Biol.* *25*, 2247–2253.
- Baden, T., Berens, P., Bethge, M., and Euler, T. (2013). Spikes in mammalian bipolar cells support temporal layering of the inner retina. *Curr. Biol.* *23*, 48–52.
- Bahl, A., Ammer, G., Schilling, T., and Borst, A. (2013). Object tracking in motion-blind flies. *Nat. Neurosci.* *16*, 730–738.
- Behnia, R., and Desplan, C. (2015). Visual circuits in flies: beginning to see the whole picture. *Curr. Opin. Neurobiol.* *34*, 125–132.
- Behnia, R., Clark, D.A., Carter, A.G., Clandinin, T.R., and Desplan, C. (2014). Processing properties of ON and OFF pathways for *Drosophila* motion detection. *Nature* *512*, 427–430.
- Borghuis, B.G., Marvin, J.S., Looger, L.L., and Demb, J.B. (2013). Two-photon imaging of nonlinear glutamate release dynamics at bipolar cell synapses in the mouse retina. *J. Neurosci.* *33*, 10972–10985.
- Borst, A., and Euler, T. (2011). Seeing things in motion: models, circuits, and mechanisms. *Neuron* *71*, 974–994.
- Borst, A., and Helmstaedter, M. (2015). Common circuit design in fly and mammalian motion vision. *Nat. Neurosci.* *18*, 1067–1076.
- Brand, A.H., and Perrimon, N. (1993). Targeted gene expression as a means of altering cell fates and generating dominant phenotypes. *Development* *118*, 401–415.
- Cajal, S.R., and Sánchez, D. (1915). Contribución al conocimiento de los centros nerviosos de los insectos. *Trab. Lab. Inv. Biol.* *13*, 1–168.
- Chen, T.W., Wardill, T.J., Sun, Y., Pulver, S.R., Renninger, S.L., Baohan, A., Schreiter, E.R., Kerr, R.A., Orger, M.B., Jayaraman, V., et al. (2013). Ultrasensitive fluorescent proteins for imaging neuronal activity. *Nature* *499*, 295–300.
- Chiappe, M.E., Seelig, J.D., Reiser, M.B., and Jayaraman, V. (2010). Walking modulates speed sensitivity in *Drosophila* motion vision. *Curr. Biol.* *20*, 1470–1475.
- Clark, D.A., Bursztyn, L., Horowitz, M.A., Schnitzer, M.J., and Clandinin, T.R. (2011). Defining the computational structure of the motion detector in *Drosophila*. *Neuron* *70*, 1165–1177.
- Eichner, H., Joesch, M., Schnell, B., Reiff, D.F., and Borst, A. (2011). Internal structure of the fly elementary motion detector. *Neuron* *70*, 1155–1164.
- Fischbach, K.-F., and Dittrich, A.P.M. (1989). The optic lobe of *Drosophila melanogaster*. I. A Golgi analysis of wild-type structure. *Cell Tissue Res.* *258*, 441–475.
- Fisher, Y.E., Silies, M., and Clandinin, T.R. (2015). Orientation selectivity sharpens motion detection in *Drosophila*. *Neuron* *88*, 390–402.
- Freifeld, L., Clark, D.A., Schnitzer, M.J., Horowitz, M.A., and Clandinin, T.R. (2013). GABAergic lateral interactions tune the early stages of visual processing in *Drosophila*. *Neuron* *78*, 1075–1089.
- Gao, S., Takemura, S.-Y., Ting, C.-Y., Huang, S., Lu, Z., Luan, H., Rister, J., Thum, A.S., Yang, M., Hong, S.-T., et al. (2008). The neural substrate of spectral preference in *Drosophila*. *Neuron* *60*, 328–342.
- Götz, K.G. (1964). Optomotorische Untersuchung des visuellen Systems einiger Augenmutanten der Fruchtfliege *Drosophila*. *Kybernetik* *2*, 77–92.
- Haag, J., Wertz, A., and Borst, A. (2010). Central gating of fly optomotor response. *Proc. Natl. Acad. Sci. USA* *107*, 20104–20109.
- Hassenstein, B., and Reichardt, W. (1956). Systemtheoretische Analyse der Zeit-, Reihenfolgen- und Vorzeichenbewertung bei der Bewegungsperzeption des Rüsselkäfers *Chlorophanus*. *Z. Naturforsch. B* *11*, 513–524.
- Joesch, M., Plett, J., Borst, A., and Reiff, D.F. (2008). Response properties of motion-sensitive visual interneurons in the lobula plate of *Drosophila melanogaster*. *Curr. Biol.* *18*, 368–374.
- Joesch, M., Schnell, B., Raghu, S.V., Reiff, D.F., and Borst, A. (2010). ON and OFF pathways in *Drosophila* motion vision. *Nature* *468*, 300–304.
- Joesch, M., Weber, F., Eichner, H., and Borst, A. (2013). Functional specialization of parallel motion detection circuits in the fly. *J. Neurosci.* *33*, 902–905.
- Jung, S.N., Borst, A., and Haag, J. (2011). Flight activity alters velocity tuning of fly motion-sensitive neurons. *J. Neurosci.* *31*, 9231–9237.
- Kim, J.S., Greene, M.J., Zlateski, A., Lee, K., Richardson, M., Turaga, S.C., Purcaro, M., Balkam, M., Robinson, A., Behabadi, B.F., et al.; EyeWriters (2014). Space-time wiring specificity supports direction selectivity in the retina. *Nature* *509*, 331–336.
- Kitamoto, T. (2001). Conditional modification of behavior in *Drosophila* by targeted expression of a temperature-sensitive *shibire* allele in defined neurons. *J. Neurobiol.* *47*, 81–92.
- Land, M.F. (1997). Visual acuity in insects. *Annu. Rev. Entomol.* *42*, 147–177.
- Maimon, G., Straw, A.D., and Dickinson, M.H. (2010). Active flight increases the gain of visual motion processing in *Drosophila*. *Nat. Neurosci.* *13*, 393–399.
- Maisak, M.S., Haag, J., Ammer, G., Serbe, E., Meier, M., Leonhardt, A., Schilling, T., Bahl, A., Rubin, G.M., Nern, A., et al. (2013). A directional tuning map of *Drosophila* elementary motion detectors. *Nature* *500*, 212–216.
- Masland, R.H. (2012). The neuronal organization of the retina. *Neuron* *76*, 266–280.
- Mauss, A.S., Meier, M., Serbe, E., and Borst, A. (2014). Optogenetic and pharmacologic dissection of feedforward inhibition in *Drosophila* motion vision. *J. Neurosci.* *34*, 2254–2263.
- Mauss, A.S., Pankova, K., Arenz, A., Nern, A., Rubin, G.M., and Borst, A. (2015). Neural circuit to integrate opposing motions in the visual field. *Cell* *162*, 351–362.
- Meier, M., Serbe, E., Maisak, M.S., Haag, J., Dickson, B.J., and Borst, A. (2014). Neural circuit components of the *Drosophila* OFF motion vision pathway. *Curr. Biol.* *24*, 385–392.
- Nern, A., Pfeiffer, B.D., and Rubin, G.M. (2015). Optimized tools for multicolor stochastic labeling reveal diverse stereotyped cell arrangements in the fly visual system. *Proc. Natl. Acad. Sci. USA* *112*, E2967–E2976.
- Park, S.J.H., Kim, I.-J., Looger, L.L., Demb, J.B., and Borghuis, B.G. (2014). Excitatory synaptic inputs to mouse on-off direction-selective retinal ganglion cells lack direction tuning. *J. Neurosci.* *34*, 3976–3981.
- Pfeiffer, B.D., Truman, J.W., and Rubin, G.M. (2012). Using translational enhancers to increase transgene expression in *Drosophila*. *Proc. Natl. Acad. Sci. USA* *109*, 6626–6631.
- Reiff, D.F., Plett, J., Mank, M., Griesbeck, O., and Borst, A. (2010). Visualizing retinotopic half-wave rectified input to the motion detection circuitry of *Drosophila*. *Nat. Neurosci.* *13*, 973–978.
- Rivera-Alba, M., Vitaladevuni, S.N., Mishchenko, Y., Lu, Z., Takemura, S.Y., Scheffer, L., Meinertzhagen, I.A., Chklovskii, D.B., and de Polavieja, G.G. (2011). Wiring economy and volume exclusion determine neuronal placement in the *Drosophila* brain. *Curr. Biol.* *21*, 2000–2005.
- Schnell, B., Joesch, M., Forstner, F., Raghu, S.V., Otsuna, H., Ito, K., Borst, A., and Reiff, D.F. (2010). Processing of horizontal optic flow in three visual interneurons of the *Drosophila* brain. *J. Neurophysiol.* *103*, 1646–1657.
- Schnell, B., Raghu, S.V., Nern, A., and Borst, A. (2012). Columnar cells necessary for motion responses of wide-field visual interneurons in *Drosophila*. *J. Comp. Physiol. A Neuroethol. Sens. Neural Behav. Physiol.* *198*, 389–395.
- Schnell, B., Weir, P.T., Roth, E., Fairhall, A.L., and Dickinson, M.H. (2014). Cellular mechanisms for integral feedback in visually guided behavior. *Proc. Natl. Acad. Sci. USA* *111*, 5700–5705.
- Shinomiya, K., Karupudurai, T., Lin, T.Y., Lu, Z., Lee, C.H., and Meinertzhagen, I.A. (2014). Candidate neural substrates for off-edge motion detection in *Drosophila*. *Curr. Biol.* *24*, 1062–1070.
- Silies, M., Gohl, D.M., Fisher, Y.E., Freifeld, L., Clark, D.A., and Clandinin, T.R. (2013). Modular use of peripheral input channels tunes motion-detecting circuitry. *Neuron* *79*, 111–127.
- Sponberg, S., Dyrh, J.P., Hall, R.W., and Daniel, T.L. (2015). Insect Flight: luminance-dependent visual processing enables moth flight in low light. *Science* *348*, 1245–1248.
- Strother, J.A., Nern, A., and Reiser, M.B. (2014). Direct observation of ON and OFF pathways in the *Drosophila* visual system. *Curr. Biol.* *24*, 976–983.

Takemura, S.Y., Karuppudurai, T., Ting, C.-Y., Lu, Z., Lee, C.-H., and Meinertzhagen, I.A. (2011). Cholinergic circuits integrate neighboring visual signals in a *Drosophila* motion detection pathway. *Curr. Biol.* 21, 2077–2084.

Takemura, S.Y., Bharioke, A., Lu, Z., Nern, A., Vitaladevuni, S., Rivlin, P.K., Katz, W.T., Olbris, D.J., Plaza, S.M., Winston, P., et al. (2013). A visual motion detection circuit suggested by *Drosophila* connectomics. *Nature* 500, 175–181.

Tuthill, J.C., Nern, A., Holtz, S.L., Rubin, G.M., and Reiser, M.B. (2013). Contributions of the 12 neuron classes in the fly lamina to motion vision. *Neuron* 79, 128–140.

Wardill, T.J., List, O., Li, X., Dongre, S., McCulloch, M., Ting, C.-Y., O’Kane, C.J., Tang, S., Lee, C.-H., Hardie, R.C., and Juusola, M. (2012). Multiple spectral inputs improve motion discrimination in the *Drosophila* visual system. *Science* 336, 925–931.

Werblin, F.S., and Dowling, J.E. (1969). Organization of the retina of the mudpuppy, *Necturus maculosus*. II. Intracellular recording. *J. Neurophysiol.* 32, 339–355.

Yonehara, K., Farrow, K., Ghanem, A., Hillier, D., Balint, K., Teixeira, M., Jüttner, J., Noda, M., Neve, R.L., Conzelmann, K.-K., and Roska, B. (2013). The first stage of cardinal direction selectivity is localized to the dendrites of retinal ganglion cells. *Neuron* 79, 1078–1085.

Neuron

Supplemental Information

**Comprehensive Characterization
of the Major Presynaptic Elements
to the *Drosophila* OFF Motion Detector**

Etienne Serbe, Matthias Meier, Aljoscha Leonhardt, and Alexander Borst

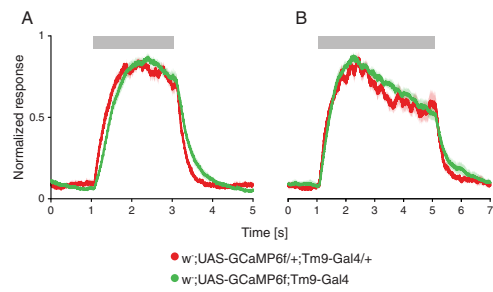


Figure S1. Related to Figure 3. Different expression levels of GCaMP do not affect the response kinetics of Tm9

(A and B) Normalized line scan calcium responses in Tm9 axonal arbors upon stimulation with a 4.5° wide, dark bar appearing for 2s (A) and 4s (B) to investigate long term temporal dynamics of Tm9 responses. To exclude effects of GCaMP6f expression level on the dynamics of the response, two traces were obtained using flies with homozygous (green) and heterozygous (red) expression of the Gal4 and the UAS construct. Error shades indicate \pm SEM.

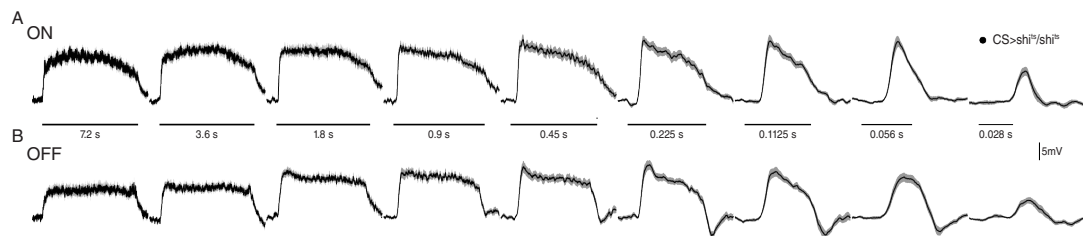


Figure S2. Related to Figure 5. LPTC responses to multiple edges moving at different velocities

Average voltage traces of lobula plate tangential cells in control flies (N=5, n=13), stimulated with multiple moving ON (A) and OFF (B) edges at 9 different velocities (3.125°/s, 6.25°/s, 12.5°/s, 25°/s, 50°/s, 100°/s, 200°/s, 400°/s, and 800°/s). Black bars indicate duration of stimulus presentation. Error shades indicate \pm SEM.

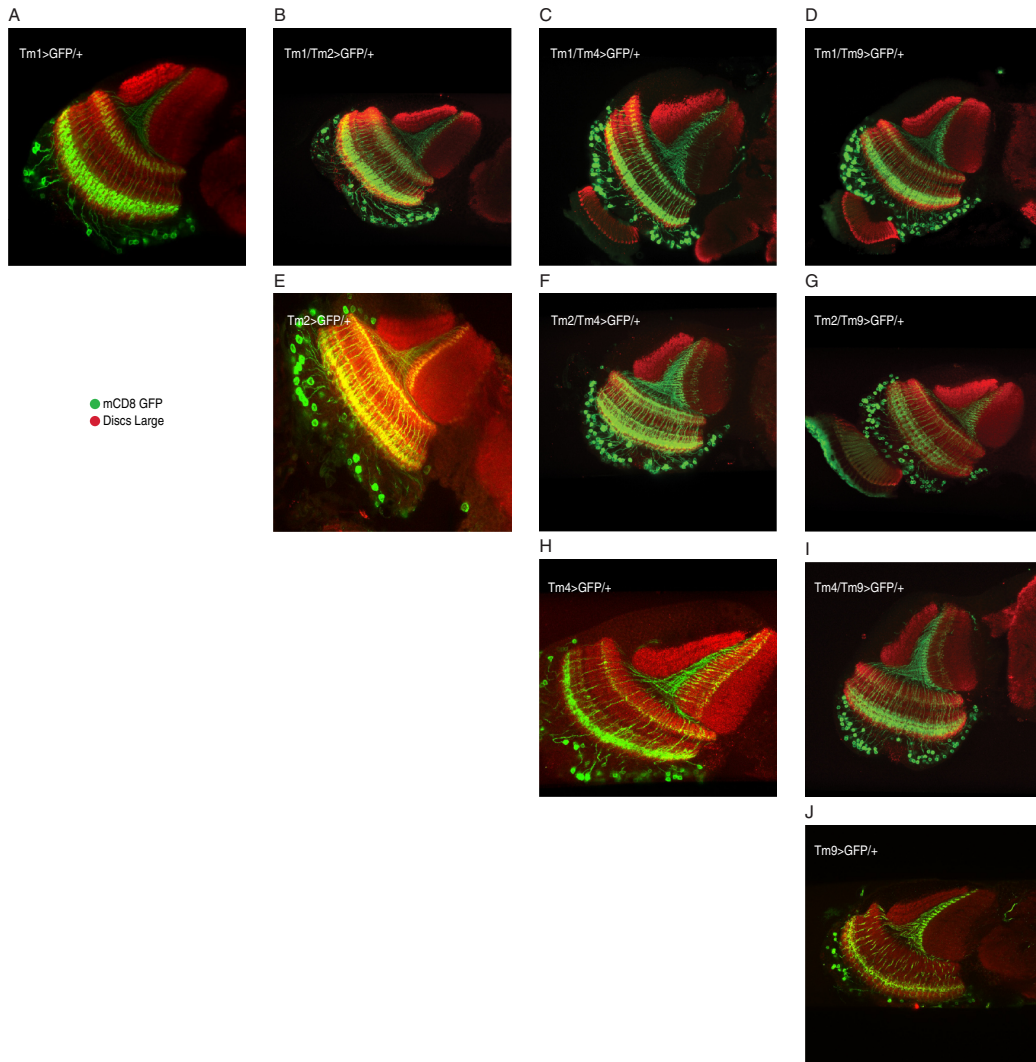


Figure S3. Related to Figures 5-7. Tm cell expression patterns

(A-J) Confocal images of the Gal4 driver cell lines used in the silencing experiments, shown in horizontal cross sections. Tm1 (A), Tm2 (E), Tm4 (H), and Tm9 (J) neurons are labeled in green (mCD8-GFP expression) and neuropils in red (antibody against Discs Large). The six possible binary combinations (B-D, F, G, I) of the Gal4 driver lines exhibit clear expression of two neuron types.

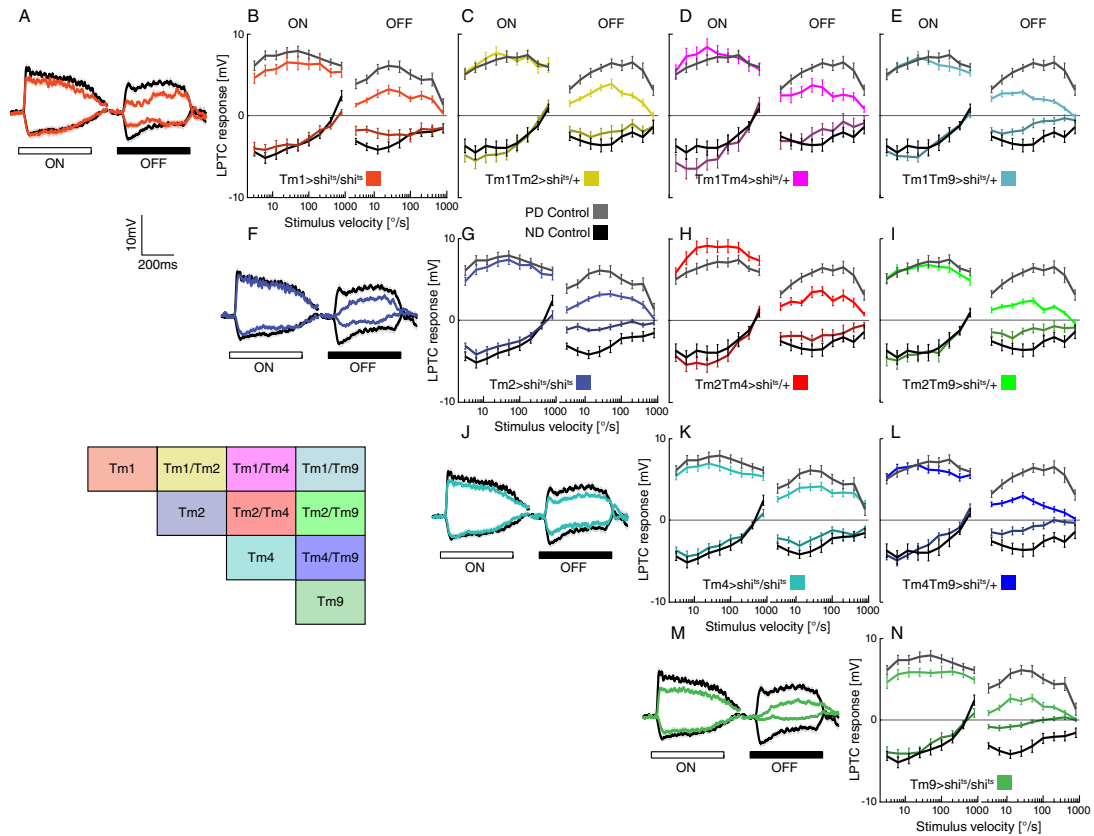
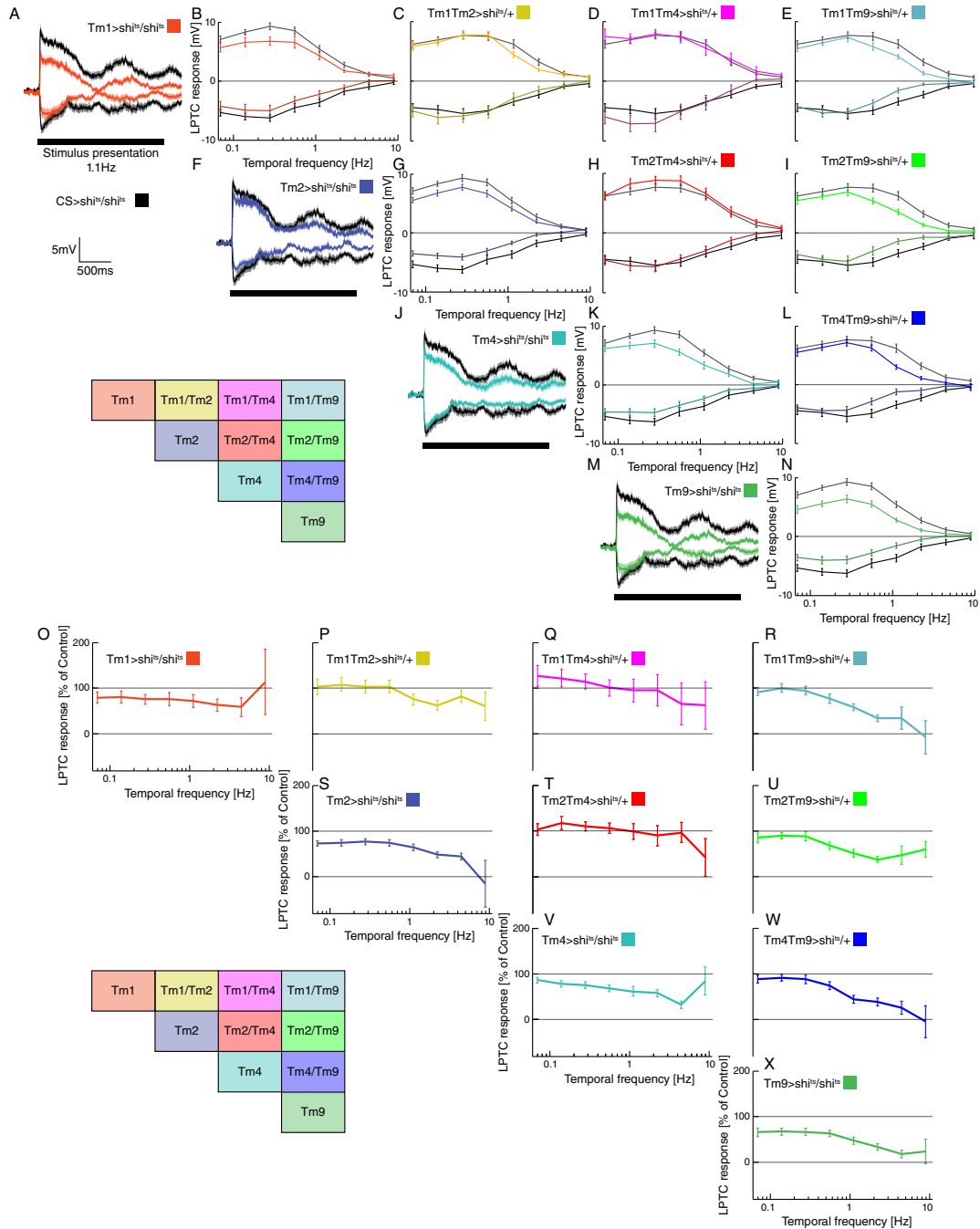


Figure S4. Related to Figures 5 and 6. Preferred and null direction responses of LPTCs to multiple ON and OFF edges (A, F, J, M) Mean voltage traces of lobula plate tangential cells stimulated with multiple ON and OFF edges moving at $50^\circ/\text{s}$ in preferred (PD) and null direction (ND). Black traces depict recordings from control flies. Red traces in (A) represent LPTC responses in Tm1 block flies, blue traces in (F) Tm2 block flies, cyan traces in (J) Tm4 block flies, and green traces in (M) Tm9 block flies. Error shades indicate \pm SEM. (B-E, G-I, K, L, and N) Average responses (errorbars indicate \pm SEM) of all four single block (with two copies of *shibire^{ts}*) and six possible combinations with corresponding controls (black) to multiple ON and OFF edges moving with nine different velocities ($3.125^\circ/\text{s}$, $6.25^\circ/\text{s}$, $12.5^\circ/\text{s}$, $25^\circ/\text{s}$, $50^\circ/\text{s}$, $100^\circ/\text{s}$, $200^\circ/\text{s}$, $400^\circ/\text{s}$, $800^\circ/\text{s}$) in PD (light colors) and ND (dark colors). Colored boxes on the bottom left indicate locations of corresponding panels in the matrix.



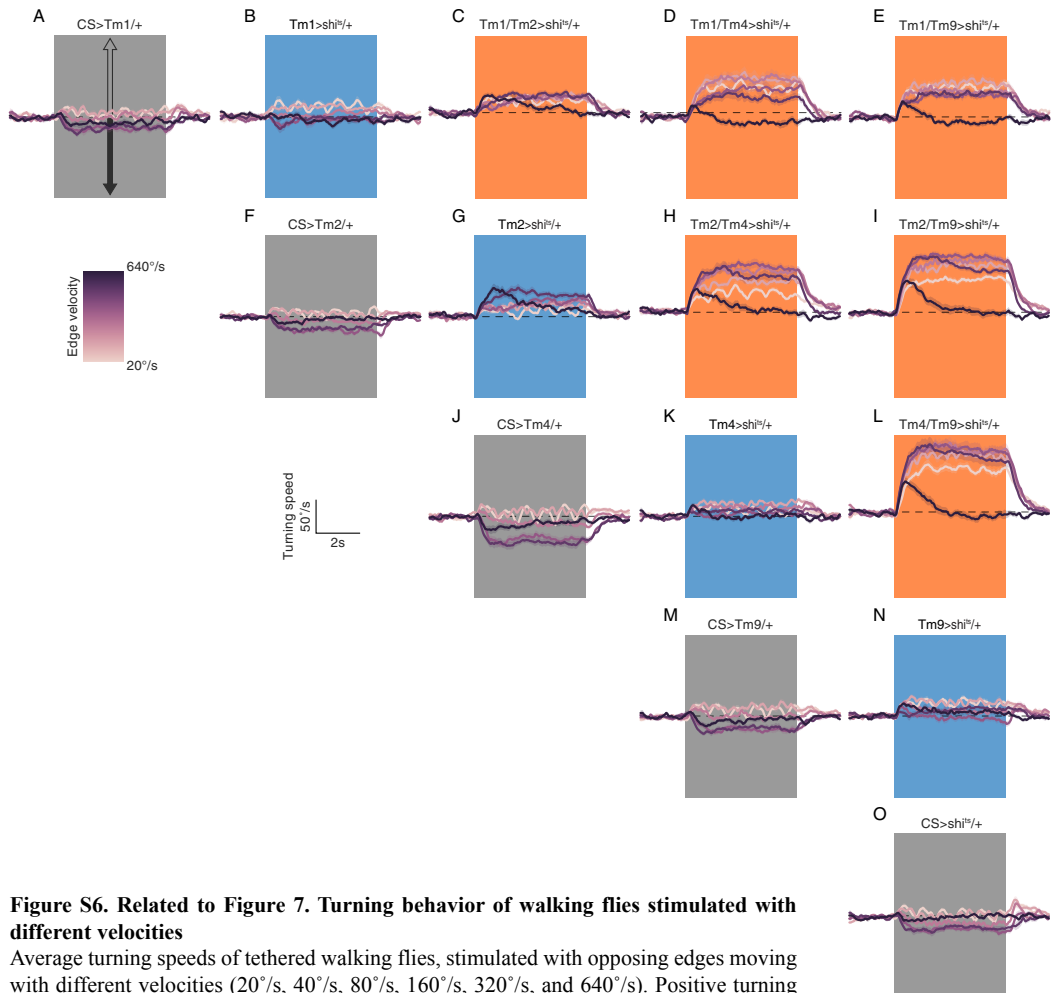


Figure S6. Related to Figure 7. Turning behavior of walking flies stimulated with different velocities

Average turning speeds of tethered walking flies, stimulated with opposing edges moving with different velocities (20°/s, 40°/s, 80°/s, 160°/s, 320°/s, and 640°/s). Positive turning responses correspond to flies turning with ON-edges, negative turning responses indicate turning with OFF-edges (see arrows in A). Stimulus presentation is indicated by shaded boxes. Errorshades indicate \pm SEM. (A, F, J, M, and O) Four Gal4 controls and the *shibire^{ts}* control. (B, G, K, and N) Single cell blocks with one copy of *shibire^{ts}*. (C-E, H, I and L) Double cell blocks with one copy of *shibire^{ts}*.

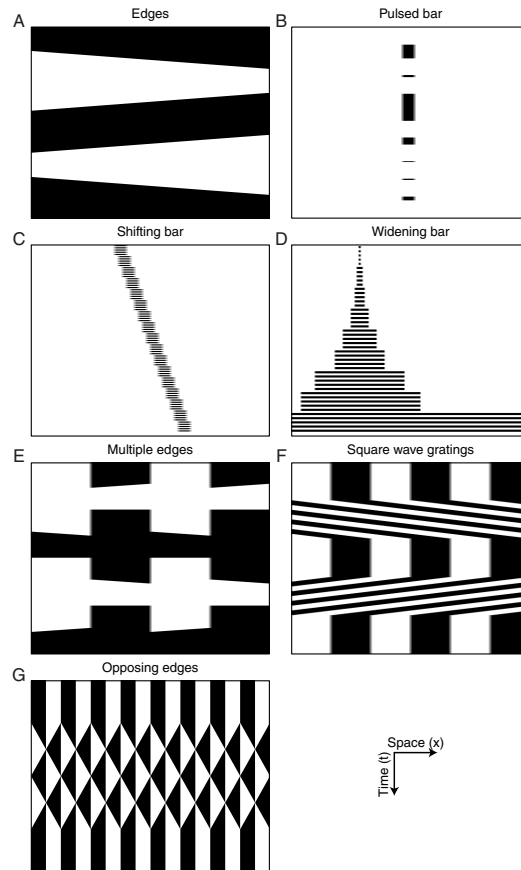


Figure S7. Related to Figures 2-7. Space-time (xt) plots of all visual stimuli used in the study

(A) Single ON and OFF Edges were used for stimulation in Figure 2. (B) Flickering bars with randomly ordered durations were used to test temporal properties in Figure 3. (C and D) Shifting and widening bars were used to test spatial properties in Figure 4. (E) Multiple edges were used in electrophysiological experiments in Figures 5 and 6. (F) Square wave gratings were used in electrophysiological experiments in Figure S5. (G) Opposing edges were used for behavioral experiments in Figure 7.

Movie S1. Related to Figure 4. Retinotopic organization of Tm9 cells

Representative raw two-photon microscope time course of Tm9 cells expressing GCaMP5 (smoothed in ImageJ). The fly is stimulated with a 4.5° wide vertical dark bar that is flickering five times at one position and is subsequently shifted by 1.5° (see Figure 3, Supplemental Experimental Procedures). The movie has been accelerated 8 times (15fps compared to 1.87Hz acquisition). The insert at the top right indicates the stimulus. Tm9 cell activity follows the stimulus in a retinotopic fashion.

Table S1. Related to Figures 1-7. Genotypes used throughout the study.

Supplemental Experimental Procedures

Flies

Flies were raised on standard cornmeal-agar medium with 12hr light/12hr dark cycles, 25°C, and 60% humidity. Female flies were used for all experiments. For calcium imaging, we used the genetically encoded indicators GCaMP5 (Akerboom et al., 2012) and GCaMP6f (Chen et al., 2013). Blocking experiments were accomplished using Tm cell-specific Gal4 lines crossed with pJFRC100-20XUAS-TTS-Shibire-ts1 (Pfeiffer et al., 2012) flies. Fly line specificity was tested using stochastic flip-out labeling (Nern et al., 2015) and expression of mCD8-GFP. We used different driver lines because of different expression strengths and specificities. All genotypes used in this study can be found in Table S1. Flies were prepared as described previously: imaging experiments, Reiff et al., 2010; electrophysiology, Joesch et al., 2008; and behavior, Bahl et al., 2013.

Immunohistochemistry and confocal imaging

For immuno-staining procedures see Schnell et al., 2010. Primary antibodies used were mouse anti-Discs Large (DLG, RRID:MGI_4354991, Developmental Studies Hybridoma Bank) and anti-GFP-Alexa488 conjugate (RRID:AB_221477, Molecular Probes). For visualization we used (1:200 in PBT): goat anti-mouse Alexa 568 (RRID:AB_10562737). Brains were mounted (Vectashield) and optically sectioned in the horizontal plane with a Leica SP5 confocal microscope. For documentation, single sections were processed in ImageJ 1.46r (NIH, Bethesda, Maryland, USA).

Behavioral experiments

Flies were placed on an air-suspended polyurethane ball in a virtual environment projected onto three monitors spanning approximately 270° (horizontal) and 114° (vertical) of the fly's visual field. This stimulation system offered less than 0.1° of angular pixel size, a value well below *Drosophila's* optical resolution capability. We used six such setups for recording fly locomotion as described previously (Bahl et al., 2013). On two setups, stimuli were presented at a screen refresh frequency of 120Hz; on four setups, the refresh frequency was 144Hz. We never observed qualitative or quantitative differences between these setups in any of the experiments. All monitors were equilibrated in brightness and contrast. Temperature within the immediate surround of the fly was controlled using a custom-built closed-loop thermoregulation system. We employed the following temperature protocol for all experiments and genotypes: Temperature was kept at 25°C for the first 5 minutes and then, within 10 minutes, raised to a restrictive 34°C.

Two-photon microscopy and visual stimulation

Two-photon microscopy and visual stimulus presentation was as described in Maisak et al., 2013. Edges had a contrast of 88%, moving at 30°/s. Each edge motion was shown twice within a single sweep, resulting in a total of eight stimulation periods, each lasting 4s. Subsequent stimuli were preceded by a 3s pause. To map the receptive fields, we flickered 4.5° wide vertical and horizontal dark bars on a bright background with 0.5 Hz at 20 different positions shifted by 1.5°. The position with the maximum response was set to 0°. The responses of the surrounding locations were normalized and plotted dependent on their distance to the peak response. The spatial integration experiments were conducted using vertical dark bars, increasing in size. We measured the responses of flickering bars with 9 different widths (1.5°, 4.5°, 7.5°, 13.5°, 25.5°, 37.5°, 49.5°, 67.5°, 180°) at the peak response position. The responses were normalized to their peak response. For the line scan experiments, a 4.5° vertical dark bar was presented on a bright background for 7 different periods: 50ms, 75ms, 125ms, 225ms, 425ms, 825ms, and 1625ms. The duration of bar presentation was varied in a randomized fashion and each stimulus was presented three times. For the electrophysiology experiments, multiple edges were used as stimuli moving simultaneously at nine different velocities (3.125°/s, 6.25°/s, 12.5°/s, 25°/s, 50°/s, 100°/s, 200°/s, 400°/s, 800°/s). To stimulate HS cells, a vertical, stationary square wave grating with 45° spatial wavelength was presented. For ON edge motion, the right (PD) or the left edge (ND) of each light bar started moving until it merged with the neighboring bar. For OFF edge motion, the right or the left edge of each dark bar was moving. To stimulate VS cells, the pattern was rotated by 90°. Consequently, we used the 36 different stimuli for every recording in a randomized fashion for one to three trials. For behavioral experiments, the balanced motion stimulus resembled previous iterations (Clark et al., 2011). Briefly, we presented flies with a stationary square wave grating that had an initial spatial wavelength of 45° visual angle and a constant Michelson contrast of 50%. Each individual trial lasted 9s. Between 2s and 7s, bright edges moved in one

direction at a fixed velocity while dark edges moved in the other direction at the same velocity. In contrast to previous versions, we reset the stimulus to the initial state after edges had traversed 20° of visual angle. This allowed us to keep the stimulus duration fixed for varying edge velocities. Additionally, we applied a random phase shift after each reset in order to rule out symmetry effects. This was done for 6 velocities (20°/s, 40°/s, 80°/s, 160°/s, 320°/s, and 640°/s) and 2 possible edge directions (dark edge leftwards/bright edge rightwards and vice versa), resulting in 12 conditions that were repeated 50 times per fly. The stimulus was rendered in real-time using Panda3D, an open source game engine, and Python 2.7. x-t plots of all stimuli used are illustrated in Figure S7.

Data analysis and simulations

Data were evaluated off-line using custom written software (Matlab and Python) and Origin (OriginLab Corporation, Massachusetts, USA). To evaluate the calcium imaging data, the raw image series were first converted into a relative fluorescence change ($\Delta F/F$) series by using the first five images as reference. Then, a region was defined within a raw image, and average $\Delta F/F$ values were determined within that region for each image, resulting in a $\Delta F/F$ signal over time. Example calcium signal traces to edge stimulation were obtained by calculating the average $\Delta F/F$ signal over trials. For Figures 2E-2H we normalized the derivative of the mean response trace of every cell. Then, we calculated the mean of the extrema over cells. The evaluation time was the stimulation period with additional four frames.

We fit a three-stage filter model to the mean calcium traces. Within this model, inputs were first high-pass filtered, then rectified by setting negative values to zero, and finally low-pass filtered (Figure 3E). The filters were linear RC filters and of first order. We simulated the visual stimuli as one-dimensional time series whose baseline was zero; for the duration of bar presentation, the values were set to one. The fitting procedure minimized the mean squared error between model output and the calcium traces by exhaustively scanning the two-dimensional parameter space spanned by the time constants of the filters. Errors were summed across presentation lengths of the dark bar, yielding a single optimum per cell type across all seven stimuli. We mapped time constants up to 2000ms in steps of 10ms and additionally allowed filtering to be switched off, equivalent to the time constant being either zero (for a low-pass) or infinite (for a high-pass). The time step for the simulations was 1ms.

To obtain the graphs in Figures 4A-4D and 4F-4I we calculated the mean of the $\Delta F/F$ signal of a single axonal arbor of a Tm cell during the time when dark vertical bars were flickering at a certain position for five times and divided that response by the mean of the $\Delta F/F$ signal when no stimulation was present. For electrophysiological experiments we calculated the mean over the stimulation time shifted by 25ms. For behavioral experiments we analyzed the data as described previously (Maisak et al., 2013). Briefly, optical tracking sensors were equipped with lens and aperture systems to focus on the sphere behind the fly. The tracking data were processed at 4 kHz internally, read out via a USB interface and processed by a computer at <200 Hz. This allowed real-time calculation of the instantaneous rotation axis of the sphere. We resampled the rotation traces to 20Hz for further processing and applied a first-order low pass filter with a time constant of 100ms to each trace. For all flies, we manually selected 20 consecutive trials out of the 50 available that fulfilled the following criteria: First, the temperature was at a stable 34°C. Second, the average turning tendency of the fly was approximately 0°/s. Third, the average forward velocity of the fly was at least 5mm/s, indicating a visually responsive state. Flies were selected without blinding. Application of the criteria excluded, on average, 20% of all flies. For further processing, we subtracted responses for the two symmetrical edge directions in order to reduce the impact of walking asymmetries. Trials were then averaged. For statistical purposes, we calculated the turning tendency of each fly for each velocity condition as the mean of the turning response between 3s (walking onset) and 7s (stimulus offset). Other evaluation time frames produced qualitatively equivalent results. The scatter plot in Figure 7E was generated by linearly normalizing values to the average of the respective genotype that showed the largest effect and plotting electrophysiology block effects against the natural logarithm of behavioral block effects. We then fit a linear regression model to the transformed data using the least-squares method. All data analysis was performed using Python 2.7 and the NumPy library.

For the modelling results in Figure 8, we simulated grating responses of hypothetical Reichardt detectors whose inputs were bandpass filters as determined in Figure 8. Sinusoidal grating stimuli moved for 3s, preceded and followed by 1s of stationary presentation. The gratings had a spatial wavelength of 10 degrees; no further spatial filtering was applied. An array of 10 detectors viewed the grating. For each possible combination of cells, we then applied the corresponding filters to the two input signals, multiplied the output, and summed over all detectors. This was done twice with spatially mirrored input lines, and results were subtracted and rectified in order to generate an approximation of lobula plate tangential cell signals. Finally, we averaged across the stimulation period. For each cell type combination, we chose the spatial order of input filters such that the mean grating responses were positive. This simulation was performed for 150 temporal frequencies located on a logarithmic scale. Each output was normalized to the maximum response across all cell type combinations.

2.4 ASYMMETRY OF DROSOPHILA ON AND OFF MOTION DETECTORS ENHANCES REAL-WORLD VELOCITY ESTIMATION

In this article, we studied the link between natural scene statistics and asymmetric tuning properties of ON and OFF pathways in the *Drosophila* visual system. The paper was published in *Nature Neuroscience* in May 2016 (Leonhardt et al., 2016).

SUMMARY To study motion vision, we commonly make use of simplified, easily parameterized stimuli like sine gratings or edges. Animals, however, solve the problem of detecting direction in natural environments which have varied and complex statistical structure. Here, we attempted to connect the two settings. We examined the transfer function between the velocity of translating natural images and the magnitude of the optomotor response performed by walking fruit flies. Interestingly, this yielded high correlation values which were not substantially affected by silencing T4 or T5 individually, suggesting that both pathways are well adapted to the task. When we examined the velocity tuning of the two pathways using polarity-specific edge stimuli, we found strong asymmetries: for OFF edges, responses both in tangential cells and walking behavior were tuned to higher velocities than for ON edges. We optimized the *in silico* velocity estimation performance of an algorithmic motion detector using a large set of natural images and found ON-OFF asymmetries that closely resembled our empirical findings. When we scrambled the higher-order structure of the images, these asymmetries disappeared. Our findings suggest that ON and OFF pathways in fly motion vision are precisely tuned to the particular demands of natural scenes. Finally, the discovered asymmetries could play a critical role in explaining higher-order motion responses in *Drosophila*.

AUTHORS Aljoscha Leonhardt, Georg Ammer (co-first author), Matthias Meier, Etienne Serbe, Armin Bahl, and Alexander Borst.

CONTRIBUTIONS A.L., G.A. and A. Borst designed the study. A.L. performed behavioral experiments, associated data analysis and all modeling work. G.A., M.M. and E.S. performed electrophysiological experiments. G.A. performed calcium imaging. A.L. and G.A. analyzed physiological data. A. Bahl designed the behavioral apparatuses and performed behavioral experiments. A.L. wrote the manuscript with help from all of the authors.

Asymmetry of *Drosophila* ON and OFF motion detectors enhances real-world velocity estimation

Aljoscha Leonhardt^{1,3}, Georg Ammer^{1,3}, Matthias Meier¹, Etienne Serbe¹, Armin Bahl^{1,2} & Alexander Borst¹

The reliable estimation of motion across varied surroundings represents a survival-critical task for sighted animals. How neural circuits have adapted to the particular demands of natural environments, however, is not well understood. We explored this question in the visual system of *Drosophila melanogaster*. Here, as in many mammalian retinas, motion is computed in parallel streams for brightness increments (ON) and decrements (OFF). When genetically isolated, ON and OFF pathways proved equally capable of accurately matching walking responses to realistic motion. To our surprise, detailed characterization of their functional tuning properties through *in vivo* calcium imaging and electrophysiology revealed stark differences in temporal tuning between ON and OFF channels. We trained an *in silico* motion estimation model on natural scenes and discovered that our optimized detector exhibited differences similar to those of the biological system. Thus, functional ON-OFF asymmetries in fly visual circuitry may reflect ON-OFF asymmetries in natural environments.

Motion cues resulting from movement through space constitute an important source of information about the external world, supporting course stabilization, navigation or tracking of landmarks¹. Biological motion detectors have evolved in environments of astounding complexity. Visual landscapes from which animals derive such cues are cluttered and produce rapidly fluctuating signals. Exploiting a priori knowledge about scene features is therefore critical for organisms to reliably extract the spatiotemporal correlations that indicate motion. Basic statistical properties such as the shape of power spectra are known to be conserved between natural scenes^{2–4}. Higher order features such as textures, edges or contrast distributions yield additional cues and exhibit consistent statistics across visual environments. Examples of neural adaptation to natural scene statistics abound, operating at various levels of visual processing hierarchies^{5–7}.

Segregated processing of positive (ON) and negative (OFF) changes in sensory magnitude is a common trait among modalities ranging from olfaction to motion detection in the insect and mammalian visual systems^{1,8,9}. Splitting time-varying signals into two streams, covering opposite directions of change, is thought to confer various advantages to sensory circuits. For instance, ON-OFF systems maximize information transfer when resources are constrained⁸. In the case of motion detection, the ON-OFF split may drastically simplify the biophysical implementation of operations such as sign-correct multiplication^{10,11}.

Luminance distributions in real-world environments are heavily asymmetric with regard to positive and negative contrast^{2,12}. Visual systems take this into account: in the mammalian retina, for example, more ganglion cells are dedicated to processing negative than positive spatial contrast, consistent with naturally encountered skewness¹³. Theoretical studies on motion detection have proposed that, in ON-OFF asymmetric environments, higher order correlations carry valuable

information about scene motion¹⁴. Indeed, flies and humans alike appear to be capable of extracting higher order cues^{12,15}, suggesting that both apply this strategy for motion estimation. However, little is known about the neural mechanism by which either visual system gains access to higher order correlations.

As a result of the availability of powerful genetic tools and extensive connectomic^{16,17} as well as functional^{18–24} characterizations, knowledge about the neural substrate of *Drosophila* motion detectors has grown exponentially in recent years⁹. Briefly, signals impinging on the photoreceptors are split into two polarity-specific channels, with one processing brightness increases (from L1 to T4 via at least Mi1 and Tm3) and the other processing brightness decreases (from L2, L3 and L4 to T5 via Tm1, Tm2, Tm4 and Tm9). Local ON and OFF motion signals are then extracted on the dendrites of T4 and T5, respectively, in a manner that is well explained by the Hassenstein-Reichardt correlation model^{9,11,21}. Large tangential cells in the lobula plate pool these signals and influence behavioral output^{1,9,25,26}.

Given the ON-OFF asymmetries encountered in natural environments, we set out to determine how the specific features of natural scenes have shaped ON and OFF motion detectors in the fly visual system. In contradistinction to previous studies, we were able to directly assess the behavioral performance of neural pathways by isolating them genetically. We found that asymmetries of natural environments had direct correspondence in tuning asymmetries of the fly motion detection system.

RESULTS

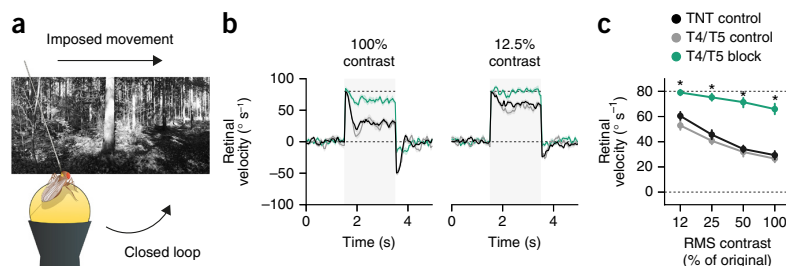
ON and OFF motion detectors reliably estimate velocity

Flies react to visual wide-field motion by turning with the environment^{1,19,27}. During navigation, this optomotor response stabilizes the animal's course in the face of external perturbations or internal noise.

¹Max Planck Institute of Neurobiology, Martinsried, Germany. ²Present address: Department of Molecular and Cell Biology, Harvard University, Cambridge, Massachusetts, USA. ³These authors contributed equally to this work. Correspondence should be addressed to A.L. (leonhardt@neuro.mpg.de).

Received 19 November 2015; accepted 29 January 2016; published online 29 February 2016; corrected online 7 March 2016 (details online); doi:10.1038/nn.4262

Figure 1 Flies stabilize their path in naturalistic environments using a combination of ON and OFF motion detectors. **(a)** Illustration of behavioral setup. Tethered flies walk in a virtual closed-loop environment. During certain time periods, their trajectories are perturbed externally. **(b)** Path stabilization under different contrast conditions. Retinal velocity describes environment rotation relative to the fly's eye. During epochs shaded in gray, a constant rotation bias of 80° s^{-1} was added. Upper dashed line indicates imposed velocity. Control flies (TNT control in black, $N = 19$;



T4/T5 control in gray, $N = 12$) reduced the imposed retinal velocity effectively whereas T4/T5 block flies (in green, $N = 13$) did not. Left, unmodified image contrast. Right, artificial reduction of root-mean-square (RMS) contrast to 12.5% of initial value. Exact genotypes are listed in **Supplementary Table 1**. **(c)** Quantification of stabilization performance across contrasts. Retinal velocity was averaged between 2 and 3 s. Dashed lines correspond to zero and full correction of the perturbation. Shaded areas around traces and vertical bars signify bootstrapped 68% confidence intervals around the mean. Asterisks indicate significant differences of block flies from both genotype controls after Bonferroni-corrected two-tailed t tests ($*P < 0.05$); exact test statistics are reported in **Supplementary Table 2**.

Any deviation from a straight path results in retinal flow that is counteracted by matching direction and, ideally, velocity of perceived drift through locomotion. Responses of behaving fruit flies and wide-field motion-sensitive neurons to simplified motion stimuli such as sinusoidal gratings have been studied extensively^{27,28}. Tethered flying flies placed in such artificial environments do indeed correct for externally applied biases²⁹. However, flies generally solve this problem in vastly more complex environments. So far, nothing is known about the quantitative extent of their ability to perform path stabilization in naturalistic contexts.

We addressed this question by allowing tethered flies to stabilize their walking trajectories in virtual environments. To cover many possible surroundings, we generated a library of panoramic images spanning the entire visual field of the fly. Randomly selected images were projected onto a virtual cylinder whose orientation was controlled in closed loop through the angular trajectory of flies walking on an air-suspended ball (**Fig. 1a**). In addition, we superimposed fixed-velocity rotations and recorded the relative motion between the fly and its environment. Our approach therefore simulated translation-free walking through a distant visual scene in the presence of external course perturbations. As expected, control flies actively reduced retinal slip speed by rotating in the direction of and with similar velocity as their visual environment (**Fig. 1b**). A combination of neural, motor and setup-intrinsic delays resulted in characteristic over- and undershoots on the order of hundreds of milliseconds, trailing both onset and offset of the motion bias. Notably, control flies rarely achieved a retinal velocity of zero, which would indicate full compensation of the involuntary rotation.

Although combined synaptic silencing of cell types T4 and T5 abolishes behavioral and electrophysiological sensitivity to grating motion^{27,30}, it is unclear whether naturalistic stimuli can provide additional cues exploited by secondary circuits. When we used Gal4-controlled³¹ expression of the light chain of tetanus toxin³² (TNT) to genetically disrupt synaptic output of all T4 and T5 cells, which are known to implement local motion detection^{21,27,30}, we discovered a marked impairment of stabilization performance. This was the case across the full range of artificially reduced image contrasts tested (**Fig. 1b,c**). The effect did not stem from gross motor defects; the flies' walking speed was at control level (**Supplementary Fig. 1**). Contrast reductions also negatively affected the stabilization ability of control flies. This replicated a previously described property of motion-sensitive lobula plate tangential cells in a behavioral setting: response gain of these cells is diminished for natural images artificially reduced in contrast³³. In summary, we found that flies actively

stabilized their path in complex visual scenes and that T4 and T5 cells were necessary neural elements for this feedback behavior.

Previous work confirmed that T4 and T5 cells are predominantly sensitive to motion defined by luminance increases and decreases, respectively²¹. Full-field motion of naturalistic scenes, especially at large viewing distances and in cluttered environments, creates a rich gamut of both ON and OFF motion. Arrays of ON or OFF detectors may therefore be equally capable of reporting the direction and velocity of realistic global motion. However, nothing is known about the individual contributions of ON and OFF detectors to velocity estimation in such contexts. Moreover, the transformation from stimulus velocity to response strength for all read-outs of the fly motion system is highly sensitive to geometrical features of the stimulus: the fly motion detector is generally not a pure speedometer^{1,9}. Even though most gain regimes would eventually lead to stabilization, the optomotor response should ideally match true retinal velocity to correct the fly's course quickly and efficiently²⁹. Indeed, tangential cells exhibit a linearized and reliable velocity-response curve when stimulated with natural images as opposed to periodic stimuli such as gratings³³. We sought to test whether this is reflected by optomotor behavior.

To this end, we assessed *Drosophila's* behavioral ability to track scene velocity in open loop (**Fig. 2a**). Velocity-response curves were stochastically probed by presenting randomly chosen images moving at constant velocities drawn from a Gaussian distribution on each individual trial. Estimation performance was then defined as the linear correlation between environment rotation and average turning response of the fly. A correlation coefficient of $r = 1.0$ indicates a perfectly reliable linear mapping of global motion onto behavioral response across all scenes, as would be required of a functional speedometer. Following visual stimulation, flies responded with robust turning responses that increased until stimulus offset and decayed right after (**Supplementary Fig. 2**). To our surprise, control flies performed the velocity estimation task exceedingly well (**Fig. 2b**). For our image set, individual flies reached correlation coefficients above 0.8 across hundreds of trials. Not all behavioral complexity was captured by the linear model: trials with turning responses close to 0° s^{-1} , for instance, were rare (**Fig. 2b**). However, several effects suggested that our simplified measure was indeed valid. First, as anticipated, flies with disrupted T4 and T5 activity exhibited correlation coefficients and response gain close to zero (**Fig. 2c–e**). Second, the correlation coefficients of control flies were heavily decreased by the reduction of image contrast (**Fig. 2d**). This reflected increasing task difficulty at the lower end of the contrast spectrum. Third,

Figure 2 ON and OFF channels are equally capable of estimating the velocity of natural scenes. **(a)** Sketch of experimental approach. Flies were subjected to a set of natural images rotating at random velocities drawn from a Gaussian distribution (s.d. = 50° s^{-1}) in open loop. **(b)** Velocity estimation performance of control flies. Each dot represents the average rotational response for one trial at full contrast. Trials were pooled across flies of all control groups ($n = 1,936$ trials from $N = 13$ TNT control flies, $n = 1,879/N = 12$ for T4/T5 control, $n = 2,070/N = 13$ for T4 control, $n = 1,331/N = 12$ for T5 control); the linear fit is for illustrative purposes only. The shaded curve to the right shows a kernel density estimate of rotational responses. **(c)** Velocity estimation performance of block flies, displayed as in **b** ($n = 1,755/N = 11$ for T4/T5 block, $n = 1,976/N = 12$ for T4 block, $n = 1,778/N = 12$ for T5 block). **(d)** Quantification of velocity estimation performance across artificially modified image contrasts. Performance was measured as the Pearson correlation between environment rotation and integrated response. Although T4/T5 block flies were strongly impaired at all contrasts, silencing T4 or T5 individually had no measurable effect on estimation performance. **(e)** Quantification of response gain across contrast range. Gain was measured as the slope of a linear regression model mapping environmental rotation onto rotational response. Vertical bars signify bootstrapped 68% confidence intervals around the mean. Asterisks indicate significant differences for block flies from both Gal4 and UAS controls after Bonferroni-corrected two-tailed t tests ($*P < 0.05$); exact test statistics are reported in **Supplementary Table 3**.

we once again found a contrast-dependent decrease of response gain as determined by the slope of a linear fit (**Fig. 2e**). It should be noted that these gain values depend on the choice of averaging window. For this reason, and because control systems tend to overcompensate in the absence of feedback, large gain values in open loop do not necessarily entail full compensation in closed loop (**Fig. 1c**).

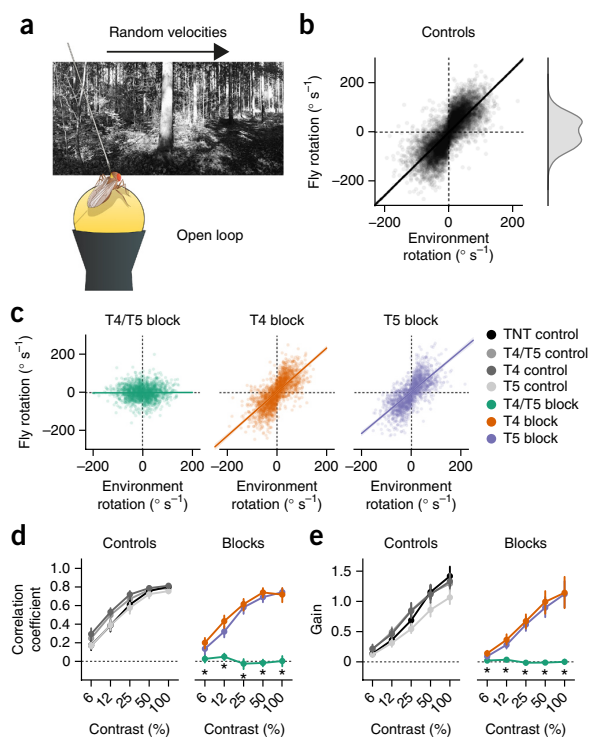
To determine potentially differential contributions of ON and OFF detectors to velocity estimation in naturalistic contexts, we then silenced only T4 or T5 using TNT. In a previous study using the same lines²¹, we found that blocking T4 or T5 led to a strongly reduced ability to detect bright or dark edges, respectively, at both the electrophysiological and behavioral level. In stark contrast to these effects, we found no impairment of velocity estimation for our naturalistic image set. Correlation coefficients for both T4 block and T5 block flies were not substantially different from control groups, even at low contrast levels (**Fig. 2c,d** and **Supplementary Fig. 2**). Finally, we alternatively quantified estimation performance as the root-mean-square error of a Bayesian estimator trained on the behavioral data, the results of which supported similar conclusions (**Supplementary Fig. 3**).

Taken together, we found that combined silencing of T4 and T5 completely abolished flies' ability to track the velocity of global motion in naturalistic scenes. Notably, ON and OFF channels appeared to be redundant for this task. Either was sufficient to recapitulate naturalistic behavior.

Tuning properties of ON and OFF channels are asymmetric

Given that ON and OFF channels seemed equally capable of performing reliable velocity estimation across various visual scenes, it is plausible to assume that they share temporal tuning properties. Previous studies reported comparable temporal frequency optima for sinusoidal gratings²¹. Calcium imaging, however, lacks the temporal resolution required for a precise characterization of pathway kinetics. Moreover, considering the polarity specialization of T4 and T5, we sought to characterize the channels using pure ON or OFF stimuli as opposed to sinusoidal gratings defined equally by brightness increments and decrements.

First, we confirmed that T4 and T5 respond exclusively to bright and dark edges, respectively. The T4 driver line used for imaging

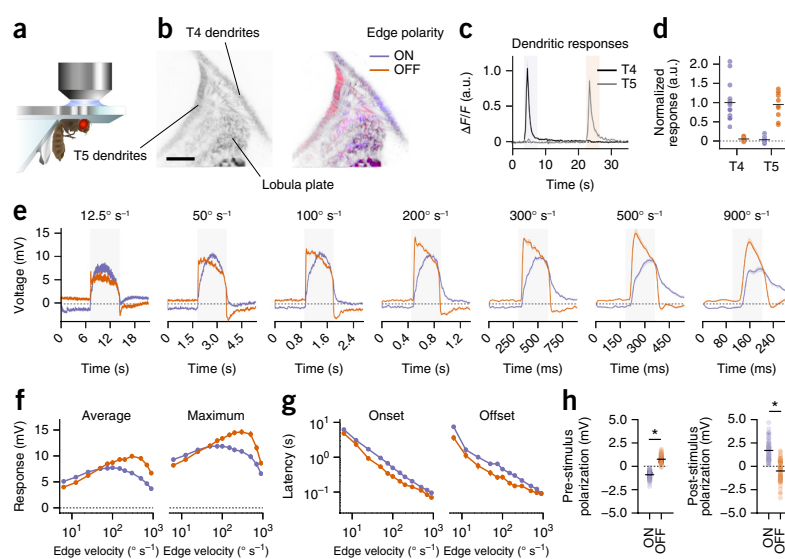


in a previous study²¹ showed marginal coexpression in T5 cells; the converse applied to the T5 driver line. Our earlier work had revealed minor sensitivity for OFF edges in T4 cells as well as small responses for ON edges in T5 cells, measured in the confines of the lobula plate, where both cell types intermingle. We speculated that this was a result of either Gal4 coexpression or actual physiological crosstalk between ON and OFF circuitry. Moreover, a physiological characterization of T4 input elements suggests that T4 should only be mildly selective for ON motion²⁴. To conclusively decide between the alternatives, we performed two-photon calcium imaging using a combined T4 and T5 line in conjunction with the calcium reporter GCaMP6f³⁴ (**Fig. 3a**). Separation of T4 and T5 signals was then achieved by restricting the region of interest to the cells' dendrites in the medulla or lobula, respectively (**Fig. 3b**). Dendrites showed strong calcium increases following visual edge stimulation that were perfectly polarity specific (**Fig. 3c,d**). This allowed us to characterize the temporal tuning properties of T4 and T5 by means of highly time-resolved electrophysiological recordings from downstream cells.

We determined velocity tuning curves for ON and OFF edges moving at speeds spanning two orders of magnitude by recording from the large-field motion-sensitive cells of the horizontal and vertical systems^{9,28} in the lobula plate. These cells are the primary recipients of feedforward ON and OFF signals, receiving direct input from T4 and T5 for stimuli moving in preferred direction and indirect inhibitory input via lobula plate interneurons for null direction motion^{30,35}. Cells depolarized when stimulated with ON or OFF edge motion along their preferred direction. Unexpectedly, tuning curves as well as general kinetics differed substantially between ON and OFF (**Fig. 3e**). Both channels showed increasing response strength up to a certain velocity, after which responses fell off (**Fig. 3f**). For ON edges, however, this peak was located at approximately 100° s^{-1} , whereas OFF responses reached their maximum at edge velocities of $\sim 300^\circ \text{ s}^{-1}$. This held true

Figure 3 Physiological characterization of ON and OFF channels reveals tuning asymmetries.

(a) Schematic of preparation used for two-photon calcium imaging and patch-clamp recordings from lobula plate tangential cells (LPTCs). (b) Left, two-photon image of GCaMP6f expression in T4 and T5 cells. Scale bar represents 10 μm . Right, representative T4 and T5 activity during ON (blue) or OFF (red) edge stimulation overlaid onto left-hand image. Activity was confined to T4 or T5 dendrites, depending on edge polarity. (c) Relative fluorescence ($\Delta F/F$) across time for regions of interest centered on either T4 (black, $N = 14$) or T5 (gray, $N = 10$) dendrites. (d) Quantification of responses as averages over edge presentation period indicated by shaded areas in c. (e) Average responses of LPTCs for ON and OFF edges moving at a range of velocities in preferred direction. Time axes are scaled differently. Shaded area indicates edge presentation and covers visual field traversal (90°) at the specified velocity. Vertical and horizontal system cells from wild-type flies were pooled ($n = 70$ from $N = 43$ flies). (f) Velocity tuning curves for ON and OFF edges based on either average or maximum response during full stimulation period. (g) Response kinetics for ON and OFF edges on logarithmic scale. (h) Static properties averaged across velocities. Dots represent individual observations and black bars indicate group averages. Vertical bars and shaded areas signify bootstrapped 68% confidence intervals around the mean. Asterisks indicate significant differences between ON and OFF after two-tailed t tests ($*P < 0.05$). Exact test statistics are reported in **Supplementary Table 4**.



regardless of whether we quantified average or maximum voltage. Moreover, both onset and offset latencies were larger for ON edges than for OFF edges across the full range of velocities tested (**Fig. 3g**). We also observed a constant polarization that closely reflected surround luminance (**Fig. 3h**); for instance, the field illumination preceding the onset of an OFF edge led to steady-state depolarization of the cell, which gave way to hyperpolarization after the dark edge had traveled through the fly's visual field (**Fig. 3e**). In a second set of experiments, we examined whether such differential pre-stimulus polarization could explain the observed ON-OFF asymmetries. Flies were presented with edges starting from an intermediate background luminance that was equal for both polarities (**Supplementary Fig. 4a**). Notably, edge velocity tuning curves were not affected by this alteration, whereas differences in onset kinetics vanished (**Supplementary Fig. 4b,c**). This suggests that luminance adaptation has a strong effect on the dynamics of tangential cell responses, but does not influence temporal tuning.

In summary, we observed strongly differential velocity tuning for ON and OFF pathways, with the former responding maximally to slower velocities than the latter. To determine whether the observed tuning differences are behaviorally relevant, we performed balanced motion experiments on walking flies. Multiple resetting ON and OFF edges distributed across the visual field moved simultaneously in opposite directions over several seconds^{19,21,23} (**Fig. 4a**). This was done for a large velocity range and offered a behavioral read-out of the weighting between ON and OFF pathways. Here, a turning tendency of zero implies equal ON and OFF responses. Consistent with electrophysiological results, we found that the balance between ON and OFF responses was clearly modulated by edge velocity (**Fig. 4b**). At low speeds, ON responses dominated the overall turning behavior and control flies continuously rotated in the direction of bright edges (**Fig. 4c**). At higher velocities, this turning tendency was reversed, indicating dominant OFF responses. ON and OFF were only completely in balance at an edge velocity of around 80° s^{-1} . To test whether these imbalances also occur at the transient time scales dominating walking behavior,

we then shortened the stimulus duration to 500, 250 or 100 ms. These opposing edge pulses produced robust responses whose amplitude diminished with decreasing stimulus length. Notably, all tuning curves had shapes that were comparable to the steady-state condition (**Supplementary Fig. 5**).

We also performed blocking experiments using this assay (**Fig. 4c**). Removing T4 and T5 from the circuit resulted in abolished turning tendencies across all velocities. For individual blocks, we recovered effects whose general direction had been described before²¹: T4 block flies always rotated in the direction of OFF edges and T5 block flies consistently followed motion of ON edges (**Fig. 4b**). Notably, these block effects were most pronounced at different velocities. For T4 block flies, the curve peaked at 160° s^{-1} . For T5 block flies, the maximum was found at 80° s^{-1} . This roughly confirmed the edge tuning curves from tangential cell recordings (**Fig. 3f**) under the assumption that each individual block was reasonably complete, leaving only one pathway intact. From this, we generated linear predictions for wild-type behavior. *Post hoc* tuning curves were calculated by either subtracting edge tuning curves measured as average voltage or summing the behavioral curves of T4 block and T5 block flies (**Fig. 4d**). Both models successfully predicted response signs and approximate zero crossing of control flies, corroborating the notion that tangential cells combine T4 and T5 signals in an approximately linear regime and then control turning behavior directly.

Despite their comparable performance during naturalistic velocity estimation, the ON and OFF pathways represented by T4 and T5 are tuned to different velocity regimes at both the electrophysiological and behavioral level. We next explored whether this tuning asymmetry is critical for their estimation fidelity.

Optimized detectors are ON-OFF asymmetric

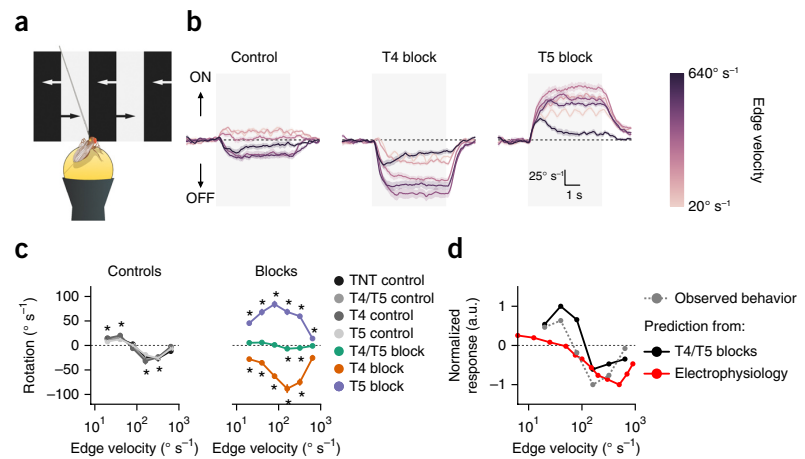
The *Drosophila* motion detection system is well described by a two-quadrant ON-OFF detector: the combination of two motion detectors, one processing only ON signals akin to the physiological T4 channel and one processing only OFF signals akin to the physiological

Figure 4 Asymmetry between ON and OFF channels persists at the behavioral level.

(a) Schematic drawing of balanced motion stimulus with ON and OFF edges simultaneously moving into opposite directions at various velocities. (b) Rotational responses for TNT control flies as well as T4 and T5 block flies. Trace color indicates velocity of edges. Positive responses are syndirectional with ON edge motion; negative responses follow OFF edge motion. Gray-shaded area denotes epoch during which edges were moving. T4 and T5 block flies are consistently biased away from the disrupted polarity. For control flies, the dominant polarity changes with velocity.

(c) Quantification of turning responses averaged over stimulation period (3 to 7 s; $N = 12$ for TNT control, $N = 12$ for T4/T5 control, $N = 12$ for T4 control, $N = 13$ for T5 control, $N = 12$ for T4/T5 block, $N = 15$ for T4 block, $N = 14$ for T5 block). For controls, asterisks indicate responses that are significantly different from zero ($*P < 0.05$).

For block genotypes, asterisks indicate significant differences from both corresponding Gal4 and UAS controls (Bonferroni-corrected t tests, $*P < 0.05$). (d) Comparison of observed control tuning curves (gray) with tuning curves linearly predicted from either the sum of behavioral T4 block and T5 block tuning curves (black) or the difference between electrophysiologically determined ON and OFF tuning curves (red; Fig. 3). Vertical bars and shaded areas surrounding traces signify bootstrapped 68% confidence intervals around the mean. Exact test statistics are reported in **Supplementary Table 5**.



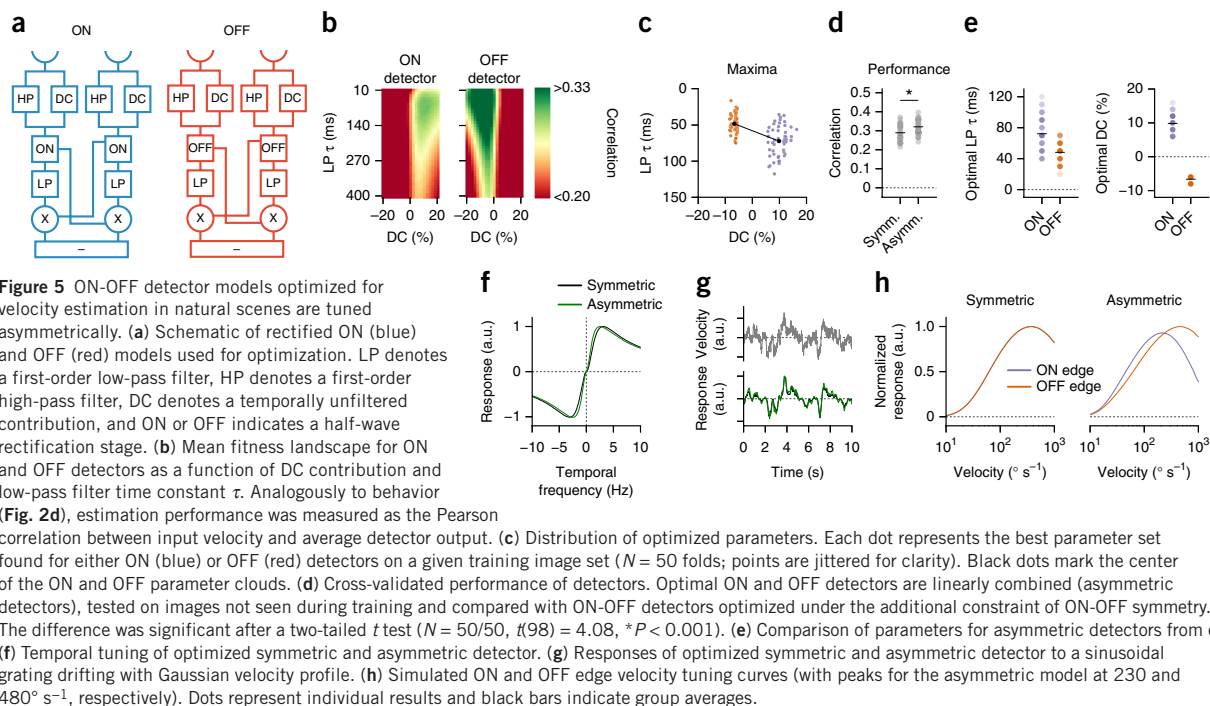
T5 channel¹⁰. Each subunit then computes motion according to the well-established Hassenstein-Reichardt correlation model based on the multiplication of differentially filtered, spatially separated signals¹¹. Counter-intuitively, such models are capable of explaining complex phenomena such as the reverse-phi effect observed for motion accompanied by contrast reversals^{10,19,36}. Critical for this is the inclusion of a weighted tonic signal (DC component) in addition to the high-pass signal modeling processing in lamina monopolar cells. Parameters for the model are generally chosen such that the ON and OFF subunits of the detector remain symmetric^{10,19}. Our results concerning edge velocity tuning, however, speak in favor of asymmetric tuning. Moreover, work on natural scenes has repeatedly shown that realistic environments are strongly asymmetric with regard to ON and OFF^{2,12,13}. What does an ON-OFF detector look like that is tuned to naturalistic environments?

Various estimation objectives may be prioritized, depending on the given task^{29,37}. For this study, we operationalized detector fitness analogously to previous studies¹² and equivalently to our own behavioral experiments as the linear correlation between the velocity of a rigidly translating natural image and time-averaged detector output. Given that Hassenstein-Reichardt detectors directly explain many aspects of fly optomotor behavior^{1,9}, and considering that flies achieve extremely high correlation values in the corresponding experimental setting (Fig. 2), this seemed to be a sensible target for the model. We optimized by exhaustively scanning the parameter space spanned by low-pass filter time constant and DC component of simplified ON and OFF detectors (Fig. 5a). This was done in a cross-validated manner. We chose a small set of parameters for optimization in which ON-OFF asymmetries had been observed previously. Our own results on edge tuning (Fig. 3e,f) indicated that there were large temporal tuning differences between ON and OFF pathways. Physiological characterization of medulla interneurons Mi1 and Tm3 for T4 as well as Tm1 and Tm2 for T5 has revealed distinct differences with regard to the strength of DC signals present at the input of motion detectors²⁴. Thus, we looked for combinations of low-pass filter time constants and DC weightings that would maximize velocity estimation performance of isolated ON and OFF detectors for a large

set of natural scenes from the van Hateren image database⁶. Velocities were drawn from a Gaussian distribution whose width was based on turning speed distributions determined in our closed-loop experiments. Optimized parameters were modulated in physiologically plausible ranges; all other settings were chosen based on previous modeling work¹⁰ and not tuned for any particular result.

The resulting fitness landscape as a function of low-pass time constant and DC component was smooth and strongly asymmetric with respect to ON and OFF (Fig. 5b). Indeed, when we extracted the parameter sets that maximized fitness for independent ON and OFF detectors, we found that optimal settings were ON-OFF asymmetric with respect to both parameters (Fig. 5c). Specifically, the best time constants for ON detectors were larger than those achieving maximum correlation for OFF detectors. The best DC weights had higher values for ON detectors than for OFF detectors and opposite signs (Fig. 5c).

To ascertain whether parameter asymmetry improved velocity estimation over that achieved by symmetric models, we compared equally weighted combinations of independently optimized ON and OFF detectors to optimized detectors that were constrained to be symmetric. The cross-validated performance improvement was small but significant ($t(98) = 4.08$, $P < 0.001$), suggesting that detector asymmetry is an advantageous strategy (Fig. 5d). The differences between ON and OFF parameters of optimal asymmetric models were substantial (Fig. 5e). We therefore looked for functional disparities between the average optimized models. Simulated temporal frequency tuning curves for sinusoidal gratings were highly similar, with slightly shifted response optima (Fig. 5f). The asymmetric and the symmetric model also produced comparable output for a dynamically moving grating (Fig. 5g). When we simulated edge velocity tuning curves as we had measured experimentally (Figs. 3 and 4), the symmetric model exhibited identical tuning for ON and OFF edges, as was expected from identical temporal parameters. Our asymmetric model, however, correctly replicated the shift between optima for ON and OFF edges with the detector being tuned to higher OFF than ON edge velocities (Fig. 5h). In addition, the asymmetric model predicted a difference in overall strength between ON and



OFF edge responses (**Fig. 3f**) even though subunits were summed at equal gain. The modeled edge optima occurred at higher velocities than those we had determined experimentally. As optimized parameters for the detectors depended on the s.d. of the distribution from which test velocities were drawn, their absolute scale was

somewhat arbitrary; conditional on behavioral state, turning speed distributions may differ substantially. The direction of the asymmetry, however, was consistent with experimental findings.

We then determined natural image features necessary for asymmetries to appear in tuned ON-OFF detectors. To this end, we repeated the optimization procedure for image sets in which we had manipulated specific statistical properties. First, for the unaltered set, the best asymmetric ON and OFF detectors showed large differences for both low-pass time constant, as well as absolute DC level (**Fig. 6a**). Second, we randomized the phase structure of every image, thereby removing all higher level features such as textures or edges, as well as making scenes largely ON-OFF symmetric¹³, while retaining the typical power spectrum of natural scenes. Here, the asymmetry of time constants disappeared (**Fig. 6b**). Third, we artificially reinstated the natural luminance distribution in phase-randomized images (**Fig. 6c**). This manipulation rescued the time constant asymmetry, suggesting that a skewed luminance distribution is the critical constraint forcing filter

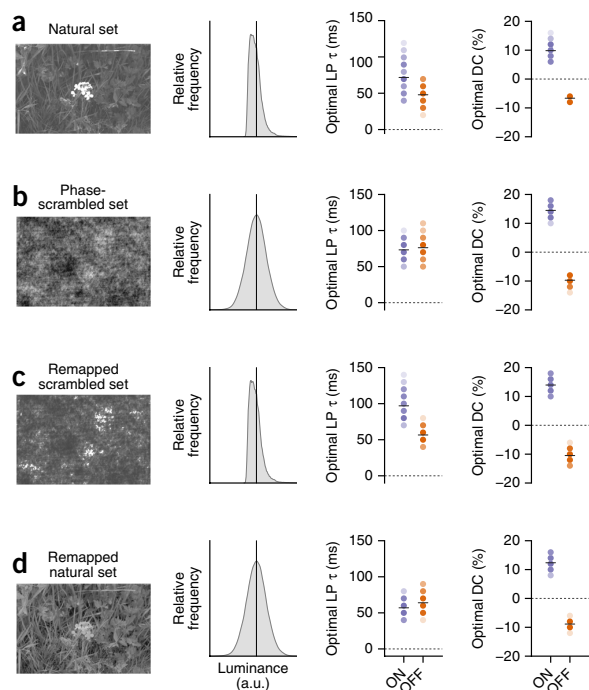
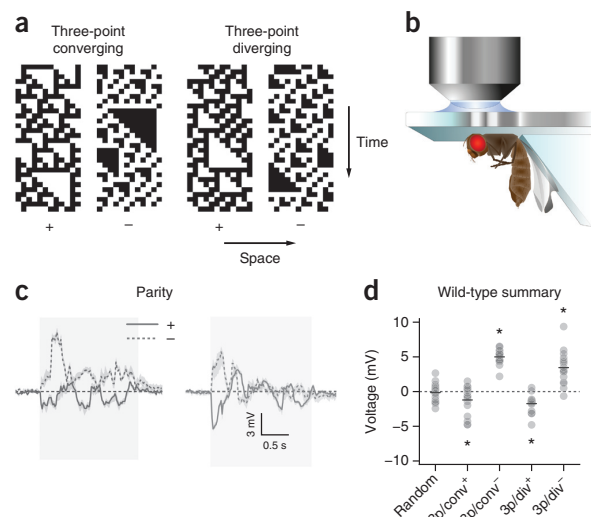
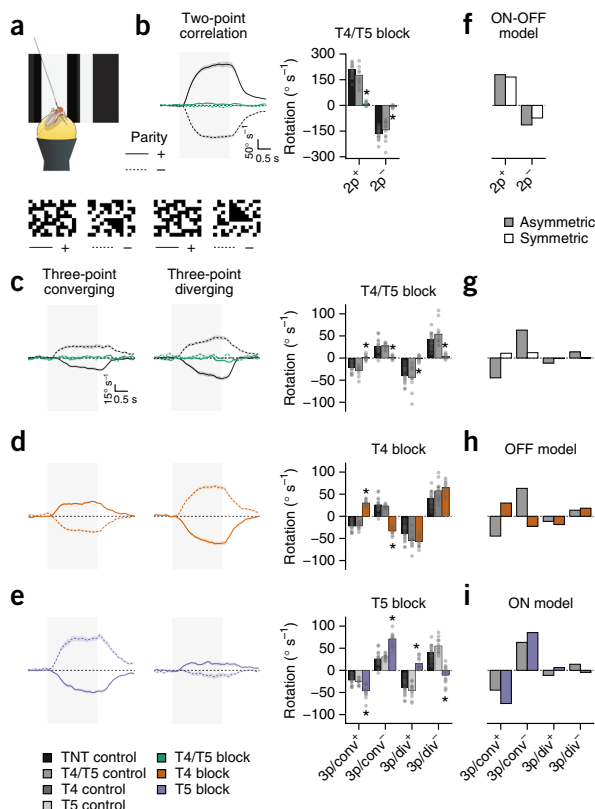


Figure 7 LPTCs are sensitive to higher order correlation stimuli.

(a) Space-time plots of glider stimuli used to probe LPTC sensitivity to triple correlations. (b) Schematic drawing of *in vivo* electrophysiology preparation and setup. (c) Average responses to full-field three-point glider stimulation of pooled vertical and horizontal system cells ($n = 16$ cells from $N = 12$ flies). Gray shaded area shows duration of stimulus presentation. Shaded areas surrounding traces signify bootstrapped 68% confidence intervals around the mean. (d) Quantification of integrated responses (averaged over the first second of stimulus presentation); “3p/conv” or “3p/div” indicate three-point converging or diverging glider orientation, respectively, and superscript the stimulus parity. All recordings were done in wild-type Canton S flies. Depicted responses are the difference between glider presentation in preferred and null direction. Dots represent individual observations and black bars show group averages. Asterisks indicate significant differences from zero after two-tailed *t* tests ($*P < 0.05$); exact test statistics are reported in **Supplementary Table 6**.

properties to diverge between ON and OFF channels. Finally, replacing the skewed luminance distribution of natural images with a symmetric one again abolished the temporal tuning differences (**Fig. 6d**). Notably, the DC asymmetry did not depend on higher order statistics of the stimulus. This particular tuning difference may be advantageous for ON-OFF detectors regardless of image statistics.

Taken together, our optimization findings demonstrate that, in realistic environments, the ON and OFF channels of motion detectors that were optimal under our criterion were tuned asymmetrically. The specific parameters that best estimated motion in natural scenes reproduced tuning properties of the biological fly motion detector we determined experimentally. At no point did we use our previous experimental findings as a constraint during optimization; the procedure arrived at this specific asymmetry independently.



Higher-order motion sensitivity derives from ON-OFF asymmetry

Theoretical considerations indicate that spatiotemporal correlations of orders higher than two become informative indicators of visual motion in environments that are ON-OFF asymmetric¹⁴. Hassenstein-Reichardt detectors exclusively capture two-point correlations. Experimental work, however, confirmed that *Drosophila* responds to triple correlations¹². This suggests that such correlations are either computed explicitly by secondary circuits or implicitly extracted by detectors that treat ON and OFF motion differentially. We assessed whether an asymmetric detector can account for *Drosophila*'s sensitivity to higher order motion.

First, we tested whether tangential cells respond to higher order motion cues given that these neurons receive their primary direction-selective input from T4 and T5 (ref. 30). We made use of previously characterized three-point glider stimuli^{12,15} (**Fig. 7a**), which enforce the mean sign of correlations across three spatiotemporal points. They have four possible forms: converging or diverging, depending on their spatiotemporal orientation, and either positive or negative parity. Notably, they are guaranteed to contain on average zero

Figure 8 Behavioral sensitivity to higher order correlations depends on T4 and T5 and is predicted by an asymmetric ON-OFF model.

(a) Illustration of behavioral experiment. (b) Two-point glider responses. Left, average response traces for two-point glider stimuli. Here, as in all following panels, the gray shaded area indicates stimulus presentation. Right, rotational responses for two-point gliders representing phi and reverse-phi motion are abolished in T4/T5 block flies. (c) Control flies respond to three-point gliders in a specific pattern. Blocking T4 and T5 in conjunction eliminates these responses completely. (d, e) Silencing T4 or T5 modulates responses by reversing rotation for converging or diverging gliders, respectively. (f) Asymmetric and symmetric models account for two-point glider responses. (g) Only the asymmetric model correctly predicts three-point glider responses of control flies. (h, i) Simulating individual T4 and T5 blocks in the asymmetric ON-OFF model by setting the gain for either ON (red) or OFF (blue) channel to zero replicates the behavioral effects. Shaded areas surrounding traces signify bootstrapped 68% confidence intervals around the mean. Dots represent individual flies and bars show group averages. Asterisks indicate significant differences of block flies from both Gal4 and UAS controls after Bonferroni-corrected two-tailed *t* tests ($N = 18$ for TNT control, $N = 12$ for T4/T5 control, $N = 12$ for T4 control, $N = 12$ for T5 control, $N = 14$ for T4/T5 block, $N = 13$ for T4 block, $N = 17$ for T5 block; $*P < 0.05$). Exact test statistics are reported in **Supplementary Table 7**.

directed two-point correlations, allowing the isolated characterization of responses to higher order motion. When we recorded from tangential cells of both the horizontal and vertical system (Fig. 7b), they responded to single instantiations of three-point gliders with complex dynamics (Fig. 7c). Their time-averaged voltage signals replicated the response pattern observed for behaving flies¹² (Fig. 7d). Given that fly locomotion is thought to reflect integrated tangential cell responses²⁶, the combination of T4 and T5 thus appeared to be sufficient for higher order motion sensitivity.

We then examined the necessity of T4 and T5 for three-point glider responses. Tethered walking flies were presented with a complete set of two-point and three-point gliders (Fig. 8a). Next, we silenced T4 and T5 in isolation as well as simultaneously. For control flies, turning responses to two-point correlations were as expected for standard phi and reverse-phi stimuli: flies turned strongly in the direction of positive correlations (positive glider parity) and reversed this tendency for negative correlations (negative glider parity; Fig. 8b). Blocking T4 and T5 in conjunction completely abolished sensitivity to all two-point gliders. This is, to the best of our knowledge, the first demonstration that reverse-phi motion, defined by spatiotemporal anti-correlations, depends on the combined activity of ON and OFF motion detectors^{10,19,36}. We then replicated the previously reported behavioral response pattern for three-point gliders¹². Flies in which both T4 and T5 were silenced failed to respond to any of the higher order motion stimuli, indicating that T4 and T5 are also necessary for motion detection beyond two-point correlations (Fig. 8c). Blocking T4 or T5 in isolation had no effect on two-point responses (Supplementary Fig. 6a–c). We were, however, surprised to find that isolated T4 or T5 blocks resulted in particular three-point glider phenotypes. Silencing the ON pathway specifically reversed the flies' turning tendency for converging gliders while slightly boosting diverging glider responses (Fig. 8d). For OFF block flies, the opposite pattern emerged (Fig. 8e).

Finally, we probed our symmetric and asymmetric detector models for higher order motion sensitivity. Both produced comparable two-point glider responses (Fig. 8f). For three-point gliders, both detectors generated nonzero output, but only the asymmetric model qualitatively matched the pattern we observed in our electrophysiological experiments as well as in walking flies (Fig. 8g). Notably, when evaluating detector responses to individual glider instantiations, we found complex and strongly fluctuating responses that resembled tangential cell responses (Supplementary Fig. 6d,g). Responses became smooth and regular only after integration of many repetitions (Fig. 7 and Supplementary Fig. 6e,f,h,i). We then simulated T4 or T5 silencing by setting ON or OFF gain to zero. These models reliably predicted the specific response reversals (Fig. 8h,i) observed in behavior (Fig. 8d,e). We therefore posit that T4 and T5 are capable of extracting triple correlations on their own. ON and OFF edges have been found to contain a particular combination of triple correlations¹². The reverse also held: three-point gliders elicited strong signals of opposite sign in pure ON or OFF detectors (Fig. 8d,e,h,i). Only if the pathways were perfectly symmetric did these responses cancel out. If they were asymmetric, as in our optimized detector or the *Drosophila* visual system, then residual responses remained. Our optimized models correctly predicted the sign and relative magnitude of these effects, suggesting that the asymmetries we found *in silico* track the asymmetries of the biological system.

DISCUSSION

We studied the roles of ON and OFF motion pathways for velocity estimation in natural scenes. *Drosophila* stabilized their walking trajectories in a closed-loop virtual environment whose statistics

resembled those of natural scenes. Genetically silencing cells T4 and T5 rendered flies unable to perform this path correction. In an open-loop setting, flies reliably tracked whole-field motion of naturalistic images. Interrupting the activity of ON or OFF pathways did not affect this capability, suggesting that the two channels subserve redundant functions in information-rich natural scenes. In physiological and behavioral experiments, we found that ON and OFF motion estimators exhibit diverging temporal tuning. When we optimized the estimation performance of an ON-OFF motion detector, we obtained asymmetric models whose temporal tuning properties resembled those found for the biological system. This suggests that *Drosophila* motion detectors are tailored to an ON-OFF asymmetric visual world, with each channel covering the most informative temporal range. In a final set of experiments and without specific tuning of the model, we found that *Drosophila's* sensitivity to certain types of higher order motion has a straightforward explanation in this framework of differentially tuned pathways.

One could interpret the shifted tuning ranges of T4 and T5 as a solution for maximizing information transfer by avoiding coding redundancy. However, for the asymmetric detector, pathways were optimized independently, forcing both to adequately encode the input velocity distribution. We therefore favor the interpretation that features reliably indicating scene velocity operate on time scales that differ between ON and OFF signals. The skewed luminance distribution of real images (Fig. 6a) offers an intuition for this notion: ON signals are dominated by infrequent and large positive deflections, whereas OFF signals are generally smaller and more regular. As neither RC filters nor lamina cells act as perfect differentiators, these differences plausibly persist at later levels of motion detection, where they may be exploited by appropriately tuned mechanisms¹³. Notably, detector performance was generally better for OFF detectors than for ON detectors (Fig. 5b), possibly reflecting the sparseness of informative ON signals.

During conditioning of detector parameters on natural images, we also optimized the weight of the tonic DC signal. We found nonzero optima for both pathways, as postulated in previous studies on reverse-phi responses¹⁰. Electrophysiologically, ON pathway interneurons Mi1 and Tm3 did indeed show static responses to absolute brightness levels with the amplitude ratio between high-pass and DC signal qualitatively matching our findings²⁴. In contrast to our prediction, OFF intermediaries Tm1 and Tm2 did not exhibit inverted tonic signals. However, other cells presynaptic to T5 still await characterization¹⁷. How DC signals can be reconciled with our demonstration that T4 and T5 responses are fully polarity specific remains unclear. In particular, theoretical considerations on the basis of the response properties of Mi1 and Tm3 predict sensitivity to OFF edges for T4 (ref. 24). This is not borne out by our experiments (Fig. 3).

Theoretical studies have proposed that responding to higher order correlations allows motion detectors to exploit natural ON-OFF asymmetries^{12,14}. The asymmetry between ON and OFF pathways reported here does indeed confer sensitivity to triple correlations. Only under the assumption that ON and OFF steps are processed equally do spurious two-point correlations vanish. However, whether *Drosophila's* higher order motion responses are an epiphenomenon of detector asymmetries or whether detector asymmetry represents a way of accessing higher order correlations is up for debate. Moreover, it remains to be seen whether the findings at hand generalize to other forms of higher order motion perceived by *Drosophila*³⁸.

Our previous characterization of cell types T4 and T5 revealed only minor differences in temporal frequency tuning for gratings²¹. It is currently not well understood how physiological tuning curves for edges and gratings relate to each other. Given the drastically different

kinetics of the two stimuli, large ON-OFF differences for one may lead to only small ON-OFF differences for the other. In addition, we suggest that edges provide a better approximation of visual kinetics in the real world than artificial gratings that are periodic as well as constant in mean luminance, contrast and geometry. Moreover, measurements from tangential cells in behaving flies have indicated grating response optima that are shifted toward higher frequencies compared with quiescence^{26,39,40}. How this state dependency translates to the tuning for edge velocity is unclear. Indeed, our linear prediction of opposing edge responses from physiological edge tuning underestimates the true crossing point between ON and OFF dominance (Fig. 4d). A shift toward higher preferred velocities, as observed for grating optima, could account for this discrepancy. Notably, our behavioral data demonstrate that basic characteristics of temporal ON-OFF asymmetries are preserved in active flies.

The ON-OFF asymmetry we describe represents one of many examples for the adaptation of sensory systems to the environment in which they evolved^{5,6,13,41}. Contrast asymmetries between ON and OFF are a widespread feature shared by most visual niches. It therefore seems probable that the sensory asymmetries found in *Drosophila* are conserved across species. ON-OFF divergence has previously been described for several computations in vertebrate visual systems^{42–44}. It will be interesting to examine the effects on optimal tuning exerted by features of the mammalian retina, such as contrast normalization⁴⁵. Finally, motion energy models have been successfully used to explain the psychophysics of motion perception in higher organisms⁴⁶. Given that Hassenstein-Reichardt detectors and motion energy models are generally mathematically equivalent⁴⁷, our optimization results could also emerge for an appropriately rectified ON-OFF motion energy detector.

T4 and T5 are critically involved in behaviors other than the optomotor response. Recently, studies have implicated motion detectors in object fixation²⁷, depth perception⁴⁸ or looming responses⁴⁹. Given the variety of tasks and resulting visual statistics, optimal tuning needs to be examined under various constraints. Finally, we believe this ecological perspective on biological motion detection could have a decisive role in the continued mapping of the fly visual system. The abundance of information-bearing features in natural visual scenes may necessitate complex filter banks and multi-cell processing stages^{17,20,23,50}. Real-world demands will then be critical constraints when assigning function to cells in the *Drosophila* optic lobe.

METHODS

Methods and any associated references are available in the [online version of the paper](#).

Note: Any Supplementary Information and Source Data files are available in the online version of the paper.

ACKNOWLEDGMENTS

A. Nern and G.M. Rubin (Janelia Research Campus) generated and kindly provided the splitGal4 line targeting T4 and T5. We are grateful for fly work and behavioral experiments performed by R. Kutlesa, C. Theile and W. Essbauer. We thank A. Arenz and A. Mauss for carefully reading the manuscript, T. Schilling for fly illustrations, and all of the members of the Borst laboratory for extensive discussions. The Bernstein Center for Computational Neuroscience Munich supplied computing resources for our simulations. A.L., G.A., M.M., E.S., A. Bahl and A. Borst are members of the Graduate School for Systemic Neurosciences, Munich.

AUTHOR CONTRIBUTIONS

A.L., G.A. and A. Borst designed the study. A.L. performed behavioral experiments, associated data analysis and all modeling work. G.A., M.M. and E.S. performed electrophysiological experiments. G.A. performed calcium imaging. A.L. and

G.A. analyzed physiological data. A. Bahl designed the behavioral apparatuses and performed behavioral experiments. A.L. wrote the manuscript with help from all of the authors.

COMPETING FINANCIAL INTERESTS

The authors declare no competing financial interests.

Reprints and permissions information is available online at <http://www.nature.com/reprints/index.html>.

- Borst, A. Fly visual course control: behavior, algorithms and circuits. *Nat. Rev. Neurosci.* **15**, 590–599 (2014).
- Ruderman, D.L. & Bialek, W. Statistics of natural images: Scaling in the woods. *Phys. Rev. Lett.* **73**, 814–817 (1994).
- Simoncelli, E.P. & Olshausen, B.A. Natural image statistics and neural representation. *Annu. Rev. Neurosci.* **24**, 1193–1216 (2001).
- Field, D.J. Relations between the statistics of natural images and the response properties of cortical cells. *J. Opt. Soc. Am. A* **4**, 2379–2394 (1987).
- Laughlin, S. A simple coding procedure enhances a neuron's information capacity. *Z. Naturforsch. C* **36**, 910–912 (1981).
- van Hateren, J.H. & van der Schaaf, A. Independent component filters of natural images compared with simple cells in primary visual cortex. *Proc. Biol. Sci.* **265**, 359–366 (1998).
- Yu, Y., Schmid, A.M. & Victor, J.D. Visual processing of informative multipoint correlations arises primarily in V2. *eLife* **4**, e06604 (2015).
- Gjorgjieva, J., Sompolinsky, H. & Meister, M. Benefits of pathway splitting in sensory coding. *J. Neurosci.* **34**, 12127–12144 (2014).
- Borst, A. & Helmstaedter, M. Common circuit design in fly and mammalian motion vision. *Nat. Neurosci.* **18**, 1067–1076 (2015).
- Eichner, H., Joesch, M., Schnell, B., Reiff, D.F. & Borst, A. Internal structure of the fly elementary motion detector. *Neuron* **70**, 1155–1164 (2011).
- Hassenstein, B. & Reichardt, W. Systemtheoretische Analyse der Zeit-, Reihenfolgen- und Vorzeichenbewertung bei der Bewegungsperzeption des Rüsselkäfers *Chlorophanus*. *Z. Naturforsch. B* **11**, 513–524 (1956).
- Clark, D.A. *et al.* Flies and humans share a motion estimation strategy that exploits natural scene statistics. *Nat. Neurosci.* **17**, 296–303 (2014).
- Ratliff, C.P., Borghuis, B.G., Kao, Y.-H., Sterling, P. & Balasubramanian, V. Retina is structured to process an excess of darkness in natural scenes. *Proc. Natl. Acad. Sci. USA* **107**, 17368–17373 (2010).
- Fitzgerald, J.E., Katsov, A.Y., Clandinin, T.R. & Schnitzer, M.J. Symmetries in stimulus statistics shape the form of visual motion estimators. *Proc. Natl. Acad. Sci. USA* **108**, 12909–12914 (2011).
- Hu, Q. & Victor, J.D. A set of high-order spatiotemporal stimuli that elicit motion and reverse-phi percepts. *J. Vis.* **10**, 9.1–9.16 (2010).
- Takemura, S.-Y. *et al.* A visual motion detection circuit suggested by *Drosophila* connectomes. *Nature* **500**, 175–181 (2013).
- Shinomiya, K. *et al.* Candidate neural substrates for off-edge motion detection in *Drosophila*. *Curr. Biol.* **24**, 1062–1070 (2014).
- Joesch, M., Schnell, B., Raghu, S.V., Reiff, D.F. & Borst, A. ON and OFF pathways in *Drosophila* motion vision. *Nature* **468**, 300–304 (2010).
- Clark, D.A., Bursztyn, L., Horowitz, M.A., Schnitzer, M.J. & Clandinin, T.R. Defining the computational structure of the motion detector in *Drosophila*. *Neuron* **70**, 1165–1177 (2011).
- Silies, M. *et al.* Modular use of peripheral input channels tunes motion-detecting circuitry. *Neuron* **79**, 111–127 (2013).
- Maisak, M.S. *et al.* A directional tuning map of *Drosophila* elementary motion detectors. *Nature* **500**, 212–216 (2013).
- Meier, M. *et al.* Neural circuit components of the *Drosophila* OFF motion vision pathway. *Curr. Biol.* **24**, 385–392 (2014).
- Ammer, G., Leonhardt, A., Bahl, A., Dickson, B.J. & Borst, A. Functional specialization of neural input elements to the *Drosophila* ON motion detector. *Curr. Biol.* **25**, 2247–2253 (2015).
- Behnia, R., Clark, D.A., Carter, A.G., Clandinin, T.R. & Desplan, C. Processing properties of ON and OFF pathways for *Drosophila* motion detection. *Nature* **512**, 427–430 (2014).
- Haikala, V., Joesch, M., Borst, A. & Mauss, A.S. Optogenetic control of fly optomotor responses. *J. Neurosci.* **33**, 13927–13934 (2013).
- Schnell, B., Weir, P.T., Roth, E., Fairhall, A.L. & Dickinson, M.H. Cellular mechanisms for integral feedback in visually guided behavior. *Proc. Natl. Acad. Sci. USA* **111**, 5700–5705 (2014).
- Bahl, A., Ammer, G., Schilling, T. & Borst, A. Object tracking in motion-blind flies. *Nat. Neurosci.* **16**, 730–738 (2013).
- Joesch, M., Plett, J., Borst, A. & Reiff, D.F. Response properties of motion-sensitive visual interneurons in the lobula plate of *Drosophila melanogaster*. *Curr. Biol.* **18**, 368–374 (2008).
- Warzecha, A.-K. & Egelhaaf, M. Intrinsic properties of biological motion detectors prevent the optomotor control system from getting unstable. *Phil. Trans. R. Soc. Lond. B* **351**, 1579–1591 (1996).
- Schnell, B., Raghu, S.V., Nern, A. & Borst, A. Columnar cells necessary for motion responses of wide-field visual interneurons in *Drosophila*. *J. Comp. Physiol. A Neuroethol. Sens. Neural Behav. Physiol.* **198**, 389–395 (2012).

ARTICLES

31. Brand, A.H. & Perrimon, N. Targeted gene expression as a means of altering cell fates and generating dominant phenotypes. *Development* **118**, 401–415 (1993).
32. Sweeney, S.T., Broadie, K., Keane, J., Niemann, H. & O’Kane, C.J. Targeted expression of tetanus toxin light chain in *Drosophila* specifically eliminates synaptic transmission and causes behavioral defects. *Neuron* **14**, 341–351 (1995).
33. Straw, A.D., Rainsford, T. & O’Carroll, D.C. Contrast sensitivity of insect motion detectors to natural images. *J. Vis.* **8**, 32.1–32.9 (2008).
34. Chen, T.-W. *et al.* Ultrasensitive fluorescent proteins for imaging neuronal activity. *Nature* **499**, 295–300 (2013).
35. Mauss, A.S. *et al.* Neural circuit to integrate opposing motions in the visual field. *Cell* **162**, 351–362 (2015).
36. Tuthill, J.C., Chiappe, M.E. & Reiser, M.B. Neural correlates of illusory motion perception in *Drosophila*. *Proc. Natl. Acad. Sci. USA* **108**, 9685–9690 (2011).
37. Dror, R.O., O’Carroll, D.C. & Laughlin, S.B. Accuracy of velocity estimation by Reichardt correlators. *J. Opt. Soc. Am. A Opt. Image Sci. Vis.* **18**, 241–252 (2001).
38. Theobald, J.C., Duistermars, B.J., Ringach, D.L. & Frye, M.A. Flies see second-order motion. *Curr. Biol.* **18**, R464–R465 (2008).
39. Jung, S.N., Borst, A. & Haag, J. Flight activity alters velocity tuning of fly motion-sensitive neurons. *J. Neurosci.* **31**, 9231–9237 (2011).
40. Chiappe, M.E., Seelig, J.D., Reiser, M.B. & Jayaraman, V. Walking modulates speed sensitivity in *Drosophila* motion vision. *Curr. Biol.* **20**, 1470–1475 (2010).
41. Dyakova, O., Lee, Y.-J., Longden, K.D., Kiselev, V.G. & Nordström, K. A higher order visual neuron tuned to the spatial amplitude spectra of natural scenes. *Nat. Commun.* **6**, 8522 (2015).
42. Komban, S.J. *et al.* Neuronal and perceptual differences in the temporal processing of darks and lights. *Neuron* **82**, 224–234 (2014).
43. Chichilnisky, E.J. & Kalmar, R.S. Functional asymmetries in ON and OFF ganglion cells of primate retina. *J. Neurosci.* **22**, 2737–2747 (2002).
44. Pandarinath, C., Victor, J.D. & Nirenberg, S. Symmetry breakdown in the ON and OFF pathways of the retina at night: functional implications. *J. Neurosci.* **30**, 10006–10014 (2010).
45. Carandini, M. & Heeger, D.J. Normalization as a canonical neural computation. *Nat. Rev. Neurosci.* **13**, 51–62 (2012).
46. Adelson, E.H. & Bergen, J.R. Spatiotemporal energy models for the perception of motion. *J. Opt. Soc. Am. A* **2**, 284–299 (1985).
47. van Santen, J.P. & Sperling, G. Elaborated Reichardt detectors. *J. Opt. Soc. Am. A* **2**, 300–321 (1985).
48. Schwegmann, A., Lindemann, J.P. & Egelhaaf, M. Depth information in natural environments derived from optic flow by insect motion detection system: a model analysis. *Front. Comput. Neurosci.* **8**, 83 (2014).
49. Schilling, T. & Borst, A. Local motion detectors are required for the computation of expansion flow-fields. *Biol. Open* **4**, 1105–1108 (2015).
50. Burge, J. & Geisler, W.S. Optimal speed estimation in natural image movies predicts human performance. *Nat. Commun.* **6**, 7900 (2015).



ONLINE METHODS

Fly strains and genetics. We raised *Drosophila melanogaster* on cornmeal-agar medium under standard conditions (60% humidity, 18 °C for behavioral and 25 °C for physiology experiments, 12-h light/12-h dark schedule) for the full duration of their developmental cycle. Female flies were used in all experiments. For physiological experiments, we selected flies 5–20 h post-eclosion. Flies in behavioral experiments were 1–3 d old. Behavioral experiments targeting T4 or T5 used the following driver lines, as described previously²¹: T4-Gal4 (VT37588) and T5-Gal4 (R42H07). When targeting T4 and T5 simultaneously, we employed a new, highly specific driver line: T4/T5-splitGal4 (R59E08-AD; R42F06-DBD), kindly provided to us by A. Nern and G.M. Rubin at Janelia Research Campus. For visualization of expression patterns (Supplementary Fig. 1), we crossed driver lines to UAS-mCD8GFP reporter flies. For experiments, Gal4 flies were then crossed to either wild type Canton S flies or UAS-TNT-E flies resulting in Gal4 control or block flies, respectively. Crossing UAS-TNT-E flies to Canton S flies generated UAS control flies. For calcium imaging, we combined two different Gal4 lines (VT25965 and VT37588) that in conjunction expressed at comparable levels in T4 and T5. These were crossed to UAS-GCaMP6³⁴ flies. Genotypes derived from these crossings and their aliases as used throughout the text are listed in the supplementary material (Supplementary Table 1).

Immunohistochemistry. Antibody stainings (Supplementary Fig. 1) were performed as described previously⁵¹. We used the following antibodies and dilutions. Primary antibodies: rabbit anti-GFP (Torri Pines, TP401, 1:2,000), mouse anti-nc82 (DSHB, AB_2314866, 1:25); secondary antibodies: goat anti-rabbit 488 (Invitrogen, A-11008, 1:500), goat anti-mouse 633 (Invitrogen, A-21053, 1:500). Imaging was performed on a SP5 confocal microscope (Leica) at a resolution of $1,024 \times 1,024$. Images were processed in ImageJ 1.46f (US National Institutes of Health). Single z-slices are shown for horizontal views.

Behavioral experiments. We performed behavioral experiments as described previously^{21,23,27}. Briefly, tethered flies were placed on an air-suspended polyurethane ball in a virtual environment consisting of three computer screens covering a substantial part of the animal's visual field (approximately 270° in azimuth and 120° in elevation). Experiments were run on six set-ups in parallel; two of them displayed visual stimuli at 120 Hz and the remaining four at 144 Hz with all screens calibrated to display at comparable contrast and brightness. We never observed any differences in behavior between refresh rates. All stimuli were rendered in real-time using the graphics engine Panda3D, allowing visual feedback based on flies' instantaneous walking behavior. Due to high pixel density on all computer screens, stimulus pixel size was well below the resolution limit of *Drosophila*. The immediate surround of the ball was temperature-controlled by means of a closed-loop thermoregulation system. Each experiment used the same temperature protocol: Temperature was kept at 25 °C for the first 5 min and then linearly raised to 34 °C within 10 min.

All behavioral experiments ran for 60–90 min and comprised 50–60 repeated trials, except for open-loop velocity estimation experiments (Fig. 2) that lasted 280 trials. In each trial, we randomized stimulus presentation order. Movement of the ball was tracked at 4 kHz and down-sampled to 20 Hz for offline analysis. For each fly, we manually selected a continuous range of 100–200 (Fig. 2) or 25 trials (other experiments) based on the following criteria: First, the temperature was at a constant 34 °C. Second, the average forward walking speed of the fly was above 0.3 cm s^{-1} , indicating healthy locomotion and visual responsiveness. Third, the average turning tendency of the fly was stable and close to 0° s^{-1} . These criteria excluded approximately 20% of all flies we measured. During analysis, we averaged traces across trials, resulting in a single walking trace per fly per experimental condition. Where applicable (Figs. 1, 4 and 8, and Supplementary Fig. 5), we then subtracted responses to mirror-symmetric stimulus presentations to minimize the impact of small rotational biases in turning behavior. Traces were filtered using a first-order low-pass filter ($\tau = 100 \text{ ms}$). In open-loop experiments (Fig. 2), we generated a regression model for each fly that mapped rotation of the environment to the turning response of the fly (averaged over 1 s after stimulus onset) using least-squares fitting. Response gain was then defined as the slope of this model. The intercepts clustered around 0° s^{-1} , indicating trajectories that were on average straight. For additional analysis (Supplementary Fig. 3), we constructed Bayesian decoders that minimize the squared error of their estimates. This was done on a fly-by-fly basis. We first split the data set consisting of pairs of image

velocity and turning response as for the correlation analysis (Fig. 2) into training and test sets at a ratio of 3:1, approximated the posterior distribution through application of Bayes' rule to the joint probability generated from appropriate histograms, and estimated image velocity as the expected value of the posterior for a given response. Finally, we assessed decoding performance of resulting mapping functions by calculating the root-mean-square error after application to the test set. The behavioral data analysis pipeline was implemented in Python 2.7 using pandas 15.1, NumPy 1.6, SciPy 0.15, matplotlib 1.3 and Numba 0.18.

Electrophysiology. Electrophysiological *in vivo* patch-clamp recordings from lobula plate tangential cells closely followed previously described protocols^{21,22,28}. Recordings were low-pass filtered with a cut-off frequency of 3 kHz and digitized at 10 kHz. Data acquisition was based on Matlab R2011A (MathWorks). We identified cell types based on their response profile when stimulated with moving gratings. In addition, cells were dye-filled and anatomically verified whenever possible.

We visually stimulated flies using a custom-built LED arena spanning approximately 180° in azimuth and 90° in elevation of the fly's visual field with a spatial resolution of 1.5° per individual LED. The LED refresh rate was in the kHz range; stimulus images were then updated with up to 600 Hz. Maximum luminance was 80 cd m^{-2} . During offline data analysis, recorded traces were down-sampled to 2 kHz and averaged across 2–5 trials per cell. We randomized the order of stimulus presentation within trials. Cells that did not respond reliably to grating stimulation were excluded from further analysis. Before we extracted response maxima and minima for edge responses (Fig. 3), electrophysiological traces were filtered with a second-order Savitzky-Golay kernel that was 40 samples wide. The electrophysiological data analysis pipeline was implemented in Python 2.7 using pandas 15.1, NumPy 1.6, matplotlib 1.3 and Numba 0.18.

Calcium imaging. We employed a custom-built two-photon laser scanning microscope as described previously^{21,22}. We prepared flies analogously to electrophysiology experiments. Images were recorded at a resolution of 256×128 pixels and a frame rate of 3.74 Hz. Raw images were then converted into relative fluorescence change ($\Delta F/F$) series by using the mean of three frames before stimulation onset as a baseline. For summary images, the resulting images were averaged across time; for time-resolved traces, we defined relevant regions of interest and collapsed signals within the defined borders by averaging across pixels. We used the LED arena described above for visual stimulation. Data acquisition and analysis were performed in Matlab R2011a (MathWorks) using ScanImage 3.8.

Image sets. Two image sets were used throughout the study. First, for all behavioral experiments involving natural images, we generated a small library of 60 panoramic images spanning approximately 360° in azimuth using a consumer-grade camera (iPhone 5s; Apple). The resolution of each image was $10,800 \times 2,460$ pixels. Images were taken in various natural environments covering different visual statistics: woods (30%), open rural spaces (30%), urban landscapes (20%), and laboratories (20%). We used raw images without processing or calibration and converted them to gray scale by averaging across color channels. Critical image statistics such as RMS contrast (that is, the s.d. of pixel values), luminance distribution, and power spectrum were comparable to other scientific image libraries. Second, for all *in silico* experiments, we made use of calibrated images from the van Hateren natural image database⁶. No image category was excluded and we performed no further sorting, yielding 4,167 images at a resolution of $1,536 \times 1,024$ pixels. One pixel corresponded to one arc minute of visual angle. We normalized the set through subtraction of and division by the mean pixel value for each image^{12,45}. Kernel density estimates (Figs. 2 and 6) were generated using a routine in the SciPy library. Gaussian kernels were used, and we determined bandwidth via Silverman's rule.

We scaled the contrast of our in-house image set by subtracting the image's mean luminance, applying the specified multiplicative factor, and then adding the initial mean luminance (Figs. 1 and 2). Phase-scrambling of the van Hateren image set was achieved by performing a Fourier transform, replacing the phase spectrum with that of a Gaussian random image of equal mean luminance, and finally recovering the phase-randomized image via the inverse Fourier transform (Fig. 6b). The luminance-remapped scrambled set was generated by replacing each pixel value of a phase-randomized image with the value corresponding to

the same luminance-ordered rank in the original image (Fig. 6c). Analogously, we generated the luminance-remapped natural set by drawing pixel values from the corresponding phase-scrambled image (Fig. 6d).

Visual stimuli. On every trial of the closed-loop course stabilization experiment (Fig. 1), a random image was chosen from our in-house image library and projected onto a virtual cylinder surrounding the fly. In order to cover the visual field without significant distortion, the panorama was mirrored across the fly's elevation axis. Each trial lasted 5 s. The rotational component of the walking trajectory was used as a feedback signal for the azimuthal orientation of the virtual cylinder, effectively giving flies control over their angular orientation relative to the environment. Feedback gain was set to unity. Between 1.5 s and 3.5 s, we additionally rotated the virtual environment at a constant 80° s^{-1} in clockwise or counter-clockwise direction. Contrast was scaled in accordance with the procedure described above to 12.5%, 25%, 50% and 100% of the original RMS value.

For open-loop velocity estimation experiments (Fig. 2), images were chosen and projected as above while feedback gain was set to zero. On each trial, a random velocity was drawn from a Gaussian distribution centered at 0° s^{-1} with a s.d. of 50° s^{-1} . Trials lasted 3.5 s. Between 1.5 s and 2 s, the virtual environment rotated with the constant velocity drawn earlier. The border where the image on the cylinder wrapped around was placed such that it remained in the back of the fly on most trials. Here, we added the 6% contrast condition.

We used single bright and dark edges for characterizing the physiological response properties of ON and OFF channels (Fig. 3). During electrophysiology experiments, we presented edges moving at 12 constant velocities across two orders of magnitude (6.25, 12.5, 25, 50, 75, 100, 150, 200, 300, 500, 700 and 900° s^{-1}). When recording from vertical system or horizontal system cells, edges traveled along the vertical or horizontal axis, respectively, and in the preferred direction of the cell. Edges used during calcium imaging always moved at 25° s^{-1} and either downwards or from front to back (no differences between the two directions were observed). Physiology stimuli (Fig. 3) had a Michelson contrast of 100%, starting from either a dark (ON) or bright (OFF) background. For additional experiments (Supplementary Fig. 4), edges started from an equal background luminance of 10.7 cd m^{-2} . As the stimulation device only allowed discrete steps, ON edges then had a contrast of 76% and OFF edges a contrast of 100%.

The behavioral balanced motion stimulus resembled previous iterations^{19,21,23}. Briefly, we presented flies with a stationary square wave grating that had an initial spatial wavelength of 45° and Michelson contrast of 50%. Each individual trial lasted 9 s. Between 2 s and 7 s, bright and dark edges moved in opposite directions at the same velocity. In contradistinction to previous experiments, we reset the stimulus to the initial state after edges had traversed 20° of visual angle, allowing us to keep stimulus duration fixed regardless of edge velocity. After each reset, we applied a random phase shift in order to minimize the effect of initial grating position relative to the fly. This was done for six velocities (20, 40, 80, 160, 320 and 640° s^{-1}) in clockwise and counter-clockwise direction. Pulse experiments (Supplementary Fig. 5) were performed analogously, with edge movement being limited to the indicated duration (500 ms, 250 ms or 100 ms).

Glider experiments (Figs. 7 and 8) were performed as described previously¹². Briefly, the visual field was divided into vertical stripes that had an azimuthal extent of 6° (behavior) or 4.5° (electrophysiology). Each bar could either be dark or bright; Michelson contrast for these experiments was 50% (behavior) or 100% (electrophysiology). Initial bars were seeded with a random binary pattern. Depending on the glider, bars were then updated according to the corresponding deterministic rule. The glider update frequency was either 24 Hz (behavior) or 10 Hz (electrophysiology). For electrophysiological experiments, we used a single pre-generated glider sequence. Here, preferred direction was defined as the update direction that would depolarize cells for two-point gliders.

Modeling. The ON-OFF detector used in this study (Figs. 5, 6 and 8) was derived from a previously published two-quadrant model¹⁰. Briefly, we modeled photoreceptor signals as time series with a resolution of 10 ms (for optimization experiments) or 1 ms (for other experiments) per step. Lamina processing was then approximated as the linear sum of a high-pass-filtered signal (first-order RC filter with $\tau = 250 \text{ ms}$) and an unfiltered tonic component (DC) with variable weight. This was followed by a half-wave rectification step. For the pure ON detector, signals were rectified with the threshold set to exactly zero. For the pure OFF detector, the signal was inverted and then rectified with the threshold set to exactly

zero. Further processing was identical for both: The signal was first-order low-pass filtered with variable time constant τ and then multiplied with an unfiltered signal from the other spatial location. This was done twice in a mirror-symmetrical fashion, followed by subtraction, yielding a fully opponent direction-selective signal. For the full ON-OFF detector, an ON detector and an OFF detector were summed with equal weight. Unlike previous versions¹⁰, our simplified detector did not make use of shifted rectification thresholds or unequally weighted detector halves. Outside of natural image experiments, stimuli were rendered at a spatial resolution of 0.1° . We modeled the spatial acceptance profile of photoreceptors as Gaussians with a half-width at maximum of 5° . The symmetric detectors (Figs. 5 and 8) had, by definition, zero DC component and identical filter time constants for the ON and the OFF channel as determined by the optimization procedure. The asymmetric detector had DC components and time constants that were allowed to differ between ON and OFF during optimization.

The detector characterization (Fig. 5) depicts results from a combination of 20 detectors separated by 6.5° . The spatial wavelength of all gratings was 20° with velocity being defined by temporal frequency. Simulations for grating and edge tunings ran for 10 s each; output was averaged across detectors and time. For the velocity profile (Fig. 5g), we used a time series drawn from a Gaussian distribution with s.d. = 20° s^{-1} that was first-order low-pass filtered with $\tau = 500 \text{ ms}$. Units were discarded for display purposes. Modeled edge stimuli lasted for 15 s, with movement starting after 2 s. The starting condition was fixed at 1.0 and followed by a jump to 1.2 for ON edges or 0.8 for OFF edges. Detector output was averaged for the duration of edge motion, which depended on velocity. We simulated 50 velocities on a logarithmic scale from 10° s^{-1} to $1,000^\circ \text{ s}^{-1}$. Glider stimuli (Fig. 8) were rendered as idealized signals mapping 21 virtual stripes to the 21 virtual photoreceptors of an array of 20 detectors, without any spatial overlap. The array was seeded with a random combination of binary dark and bright values (arbitrarily defined as 1.0 and 3.0, respectively) and then updated according to previously described rules¹² at a frequency of 5 Hz. Glider simulations ran for 5 s each and were averaged across 500 instantiations and time (Fig. 8f–i). We approximated compressive characteristics of the visuo-motor transformation by multiplying two-point and three-point responses with slightly different gain values ($2,500^\circ \text{ s}^{-1}$ and $3,500^\circ \text{ s}^{-1}$, respectively) when translating detector output into turning tendency. All simulations were implemented in Python 2.7 using NumPy 1.6 and Numba 0.18.

Detector optimization. Optimization of detector models was based on an exhaustive cross-validated search on a two-dimensional parameter grid. We generated 50 random training-to-test splits from the 4,167 images of the van Hateren data set with a training-to-test ratio of 4:1. All images received a luminance bias of 3.0 and were clipped at zero in order to ensure that only positive signals arrived at detector inputs while keeping mean values constant. The optimization procedure was then performed independently for each training fold.

We scanned a parameter space comprising 40×21 combinations of low-pass time constants (from 10 to 400 ms in 10-ms steps) and DC contribution (from -20% to $+20\%$ in 2% steps). For each parameter set, three detectors with the corresponding parameter settings were simulated: a pure ON detector, a pure OFF detector, and a symmetric ON-OFF detector where ON and OFF channels used the same parameters. Fitness of a given detector was determined as follows, based on previous studies¹² and analogously to behavioral experiments (Fig. 2): on each iteration, we drew a random image from the training set and a random velocity from a Gaussian distribution centered at zero with s.d. = 25° s^{-1} . We then generated two time series corresponding to a simulated pair of photoreceptors separated by 6.5° traveling across the horizontal middle row of the image at the constant velocity drawn before and for a duration of 1,000 ms. The signals were fed into each of the three detectors. Detector output was averaged across time. We repeated this procedure 50,000 times per parameter set. Detector fitness was then defined as the Pearson correlation between input velocity and average detector output. During testing, we assembled two detectors per test set. The optimal symmetric detector was the best-performing detector constrained to use equal ON and OFF settings and zero DC. The optimal asymmetric detector was the linear combination of the best performing ON detector and the best performing OFF detector. The performance of both was then evaluated on the corresponding test set; here, detector evaluations were repeated 100,000 times. This was done for the natural, phase-scrambled and luminance-remapped image sets.

We implemented the optimization procedure in Python 2.7 using NumPy 1.6, SciPy 0.15, Numba 0.18, and IPython 3.0. Parallel operations were distributed across 128 CPUs on a Beowulf cluster consisting of eight physical machines.

Code availability. Python and Matlab code used throughout analysis, modeling, and optimization is available upon request to the authors.

Statistics. All statistical tests were two-tailed Student's *t* tests at a significance level of 0.05, assuming unequal variance unless stated otherwise. Where necessary, conservative Bonferroni correction was applied in order to correct for multiple hypothesis testing. Normality of data was confirmed visually and not formally tested. We did not predetermine sample sizes using statistical tests, but numbers

are in line with established work^{12,20,21,23,27}. Our confidence intervals were computed according to a bootstrapping procedure based on 1,000 re-samplings of the data set. We did not differentiate levels of significance; only single asterisks are used regardless of *P* value. Statistical procedures were used as implemented in SciPy 0.15. All experiments and data analysis were performed without blinding to conditions or genotypes.

A **Supplementary Methods Checklist** is available.

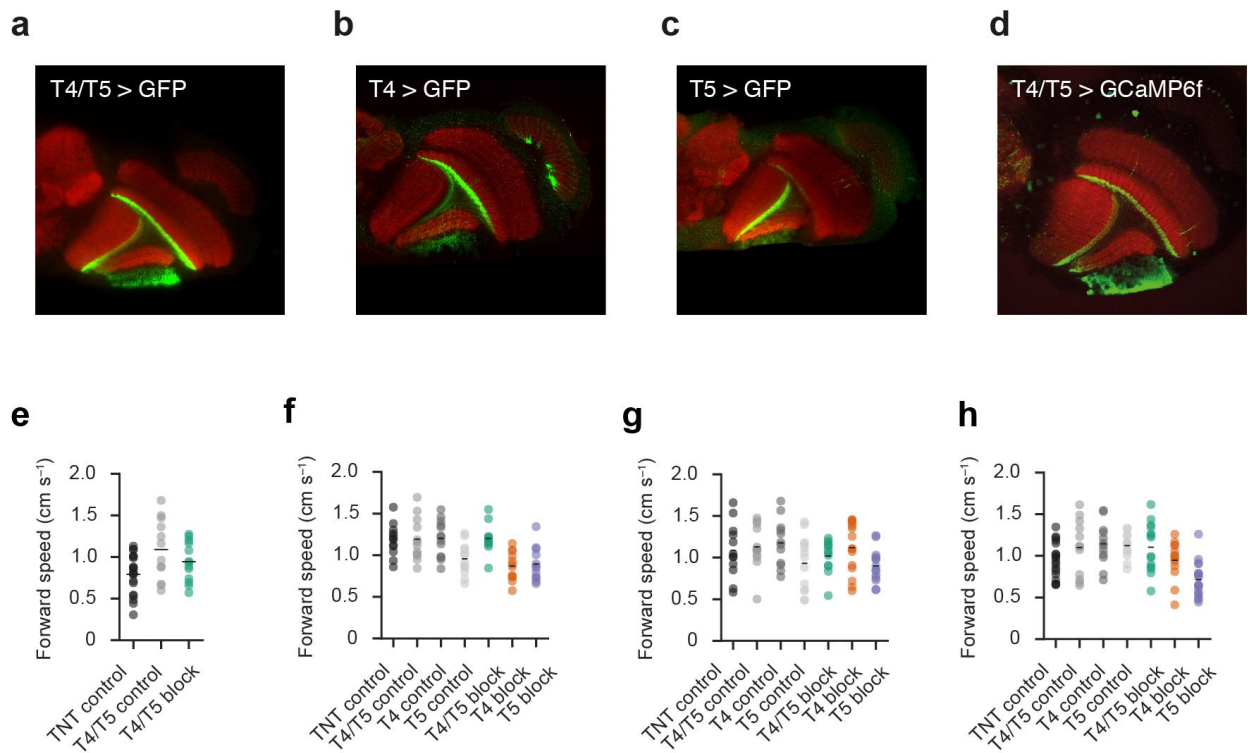
51. Yu, J.Y., Kanai, M.I., Demir, E., Jefferis, G.S.X.E. & Dickson, B.J. Cellular organization of the neural circuit that drives *Drosophila* courtship behavior. *Curr. Biol.* **20**, 1602–1614 (2010).



Erratum: Asymmetry of *Drosophila* ON and OFF motion detectors enhances real-world velocity estimation

Aljoscha Leonhardt, Georg Ammer, Matthias Meier, Etienne Serbe, Armin Bahl & Alexander Borst
Nat. Neurosci.; doi:10.1038/nn.4262; corrected online 7 March 2016

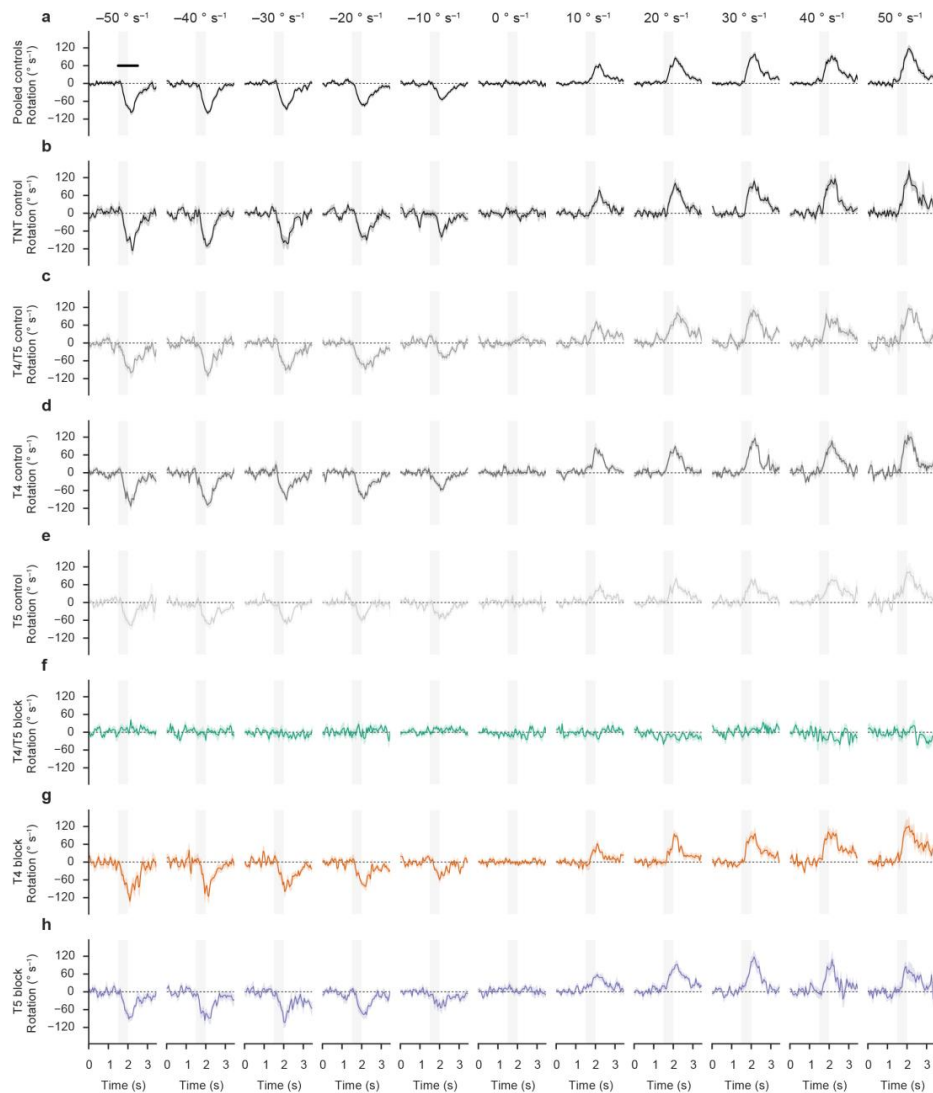
In the version of this article initially published online, the second and third authors of ref. 40, J.D. Seelig and M.B. Reiser, were replaced by the second author of ref. 39, A. Borst. The error has been corrected for the print, PDF and HTML versions of this article.



Supplementary Figure 1

Auxiliary data for Gal4 lines used throughout the study.

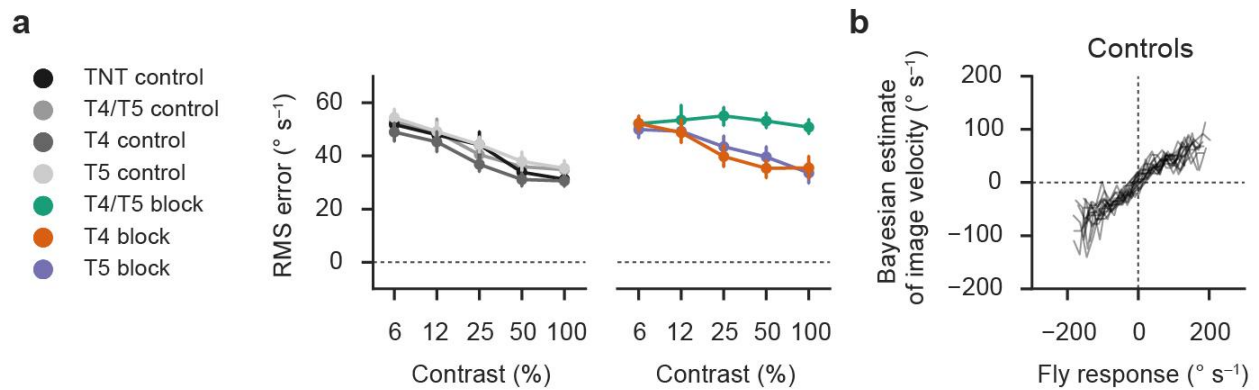
(a-d) UAS-mCD8GFP or UAS-GCaMP6f were driven by Gal4 driver lines used throughout the text and visualized using confocal images of the optic lobe. (a) GFP expression of splitGal4 line labeling T4 and T5. (b) GFP expression of Gal4 line labeling T4. (c) GFP expression of Gal4 line labeling T5. (d) GCaMP6f expression of combined Gal4 line labeling T4 and T5. See Online Methods for Gal4 line names and details of the immunohistochemistry procedures. (e-h) Locomotor integrity for each behavioral experiment was quantified as the mean forward velocity across conditions, with values close to control level indicating a general ability to respond to visual stimuli. (e) Walking speeds for closed-loop experiments (Fig. 1). (f) Walking speeds for open-loop experiments (Fig. 2). (g) Walking speeds for opposing edge experiments (Fig. 4). (h) Walking speeds for glider experiments (Fig. 8). Dots represent individual flies. Black bars mark the group mean for each genotype.



Supplementary Figure 2

Walking traces for open-loop velocity estimation experiment.

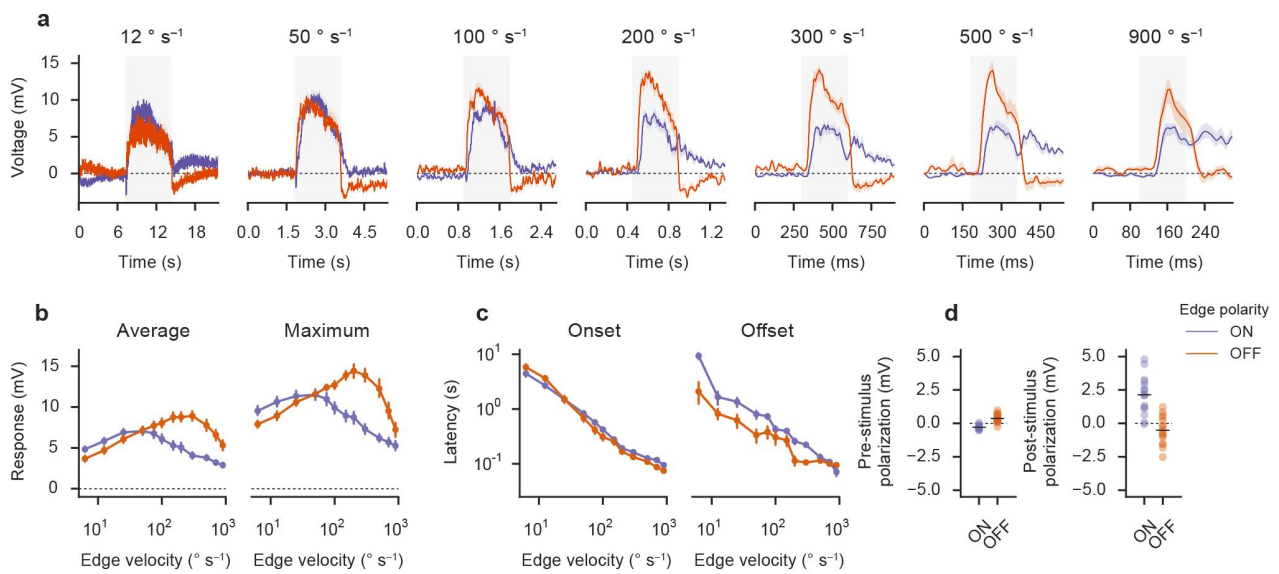
Binned response traces for all genotypes used throughout the stochastic open loop velocity estimation experiment (**Fig. 2**). In order to generate velocity-specific traces, stimulus velocities were sorted into bins spanning 5° s^{-1} centered about the value indicated above each column. The corresponding traces were then averaged for each fly. Shaded areas indicate the bootstrapped 68% confidence interval across flies (N as in main figure; **Fig. 2**). Notably, traces were not low-pass filtered and the sampling base for each fly decreases with distance from zero velocity due to the stimulus distribution. The black line in the top leftmost panel indicates the period over which we averaged in order to generate responses for main experiment (**Fig. 2**). See Online Methods for details. (a) Responses for pooled controls as in main experiment (**Fig. 2b**). (b-h) Responses for individual genotypes.



Supplementary Figure 3

Bayesian analysis of open-loop behavioral data.

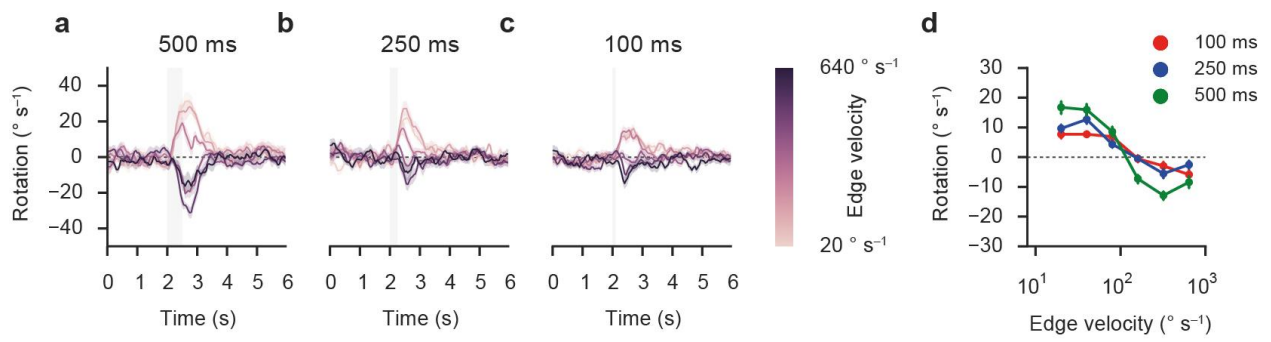
Using open-loop behavioral data (**Fig. 2**), we generated Bayesian decoders according to the procedure outlined in the Online Methods. For details about quantification and subject numbers, refer to main experiment (**Fig. 2**). **(a)** Mapping error across image contrast values, quantified as the root-mean-square error after application to the test data set. With higher contrasts, the quality of the estimate improves; this resembles results based on linear correlation. For T4/T5 block flies, the error stays flat. T4 or T5 block cannot be distinguished from wild-type behavior. **(b)** Visualization of resulting mapping functions, transforming fly responses into Bayesian estimates of input image velocity. Each line corresponds to a single fly. No significance tests were performed.



Supplementary Figure 4

Physiological edge velocity tuning for fixed starting luminance.

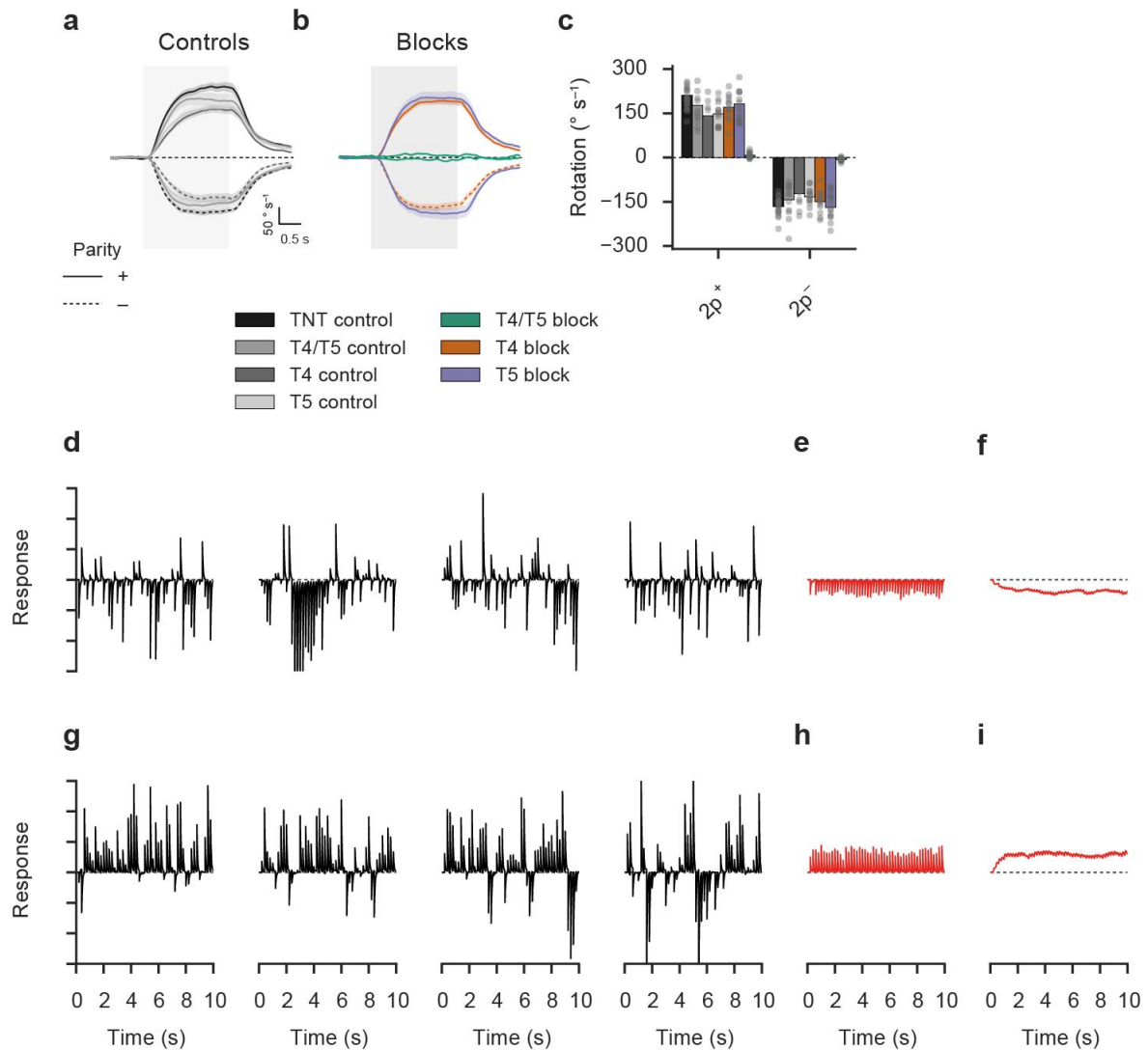
Lobula plate tangential cell responses to ON and OFF edges for equalized initial mean luminance ($N=16$ by pooling 12 vertical system/4 horizontal system cells). See legend of main experiment (**Fig. 3**) as well as Online Methods for details. **(a)** Response traces for edges moving at various velocities. Note that the timescale depends on edge velocity. **(b)** Quantification of velocity tuning. **(c)** Quantification of response dynamics (with latency being defined as the time to maximal response during stimulation for onset or time to minimal response after stimulation for offset). **(d)** Quantification of polarization before and after stimulus presentation. No significance tests were performed.



Supplementary Figure 5

Opposing edge responses for varying stimulus durations.

Presentation and quantification are analogous to main experiment (**Fig. 4**; see Online Methods and associated legend for details). Depicted flies were T4/T5 control flies. (**a-c**) Turning responses for edge pulses of 500 ms ($N=12$), 250 ms ($N=12$), and 100 ms ($N=14$) duration, respectively. (**d**) Quantification of turning responses.



Supplementary Figure 6

Extended data for higher-order motion experiments and simulations.

(a-c) T4 block flies and T5 block flies show 2-point glider responses at control level. (a) Control responses for 2-point gliders of positive or negative parity. (b) Block fly responses. (c) Summary of average turning tendency. Shaded area indicates stimulation period (see Online Methods and legend of main experiment for details; Fig. 8). (d-i) Time- and instantiation-resolved output of the asymmetric detector for converging 3-point gliders. Black traces are arbitrarily scaled detector responses for five random starting conditions of the pattern. (d) Single traces for positive parity. (e) Average time-resolved output for positive parity across 100 instantiations of the stimulus. (f) Low-pass filtered trace from e (first order with time constant of 500 ms followed by multiplicative scaling with a factor of four, approximating the behavioral response). (g) Single traces for negative parity. (h) Average time-resolved output for negative parity across 100 instantiations of the stimulus. (i) Low-pass filtered and scaled trace from h (procedure as in f).

Supplementary Table 1

Alias	Genotype	Experiments
T4/T5 block	w ⁺ /w ⁻ ; UAS-TNT-E/Gal4-R59E08-AD; +/Gal4-R42F06	Figs. 1, 2, 4, 8, S1, S2, S3, S6
T4/T5 imaging	w ⁻ ; UAS-GCaMP6f; Gal4-VT25965/Gal4-VT37588	Fig. 3, S1
T4 block	w ⁺ /w ⁻ ; UAS-TNT-E/+; +/Gal4-VT37588	Figs. 2, 4, 8, S1, S2, S3, S6
T5 block	w ⁺ /w ⁻ ; UAS-TNT-E/+; +/Gal4-R42H07	Figs. 2, 4, 8, S1, S2, S3, S6
TNT control	w ⁺ /w ⁻ ; UAS-TNT-E/+; +/+	Figs. 1, 2, 4, 8, S1, S2, S3, S6
T4/T5 control	w ⁺ /w ⁻ ; +/Gal4-R59E08-AD; +/Gal4-R42F06	Figs. 1, 2, 4, 8, S1, S2, S3, S5, S6
T4 control	w ⁺ /w ⁻ ; +/+; +/Gal4-VT37588	Figs. 2, 4, 8, S1, S2, S3, S6
T5 control	w ⁺ /w ⁻ ; +/+; +/Gal4-R42H07	Figs. 2, 4, 8, S1, S2, S3, S6
Canton S	w ⁺ ; +/+; +/+	Figs. 3, 7, S4

Supplementary Table 2

12.5% contrast			25% contrast		
Genotype		T4/T5 block (n=13)	Genotype		T4/T5 block (n=13)
UAS control	n	19	UAS control	n	19
	t	9.27		t	12.2
	p	2.83e-10		p	3.89e-13
Gal4 control	n	12	Gal4 control	n	12
	t	11.2		t	16.4
	p	1.35e-9		p	3.75e-14

50% contrast			100% contrast		
Genotype		T4/T5 block (n=13)	Genotype		T4/T5 block (n=13)
UAS control	n	19	UAS control	n	19
	t	14.4		t	12.9
	p	4.55e-13		p	3.56e-12
Gal4 control	n	12	Gal4 control	n	12
	t	13.7		t	13.9
	p	1.47e-12		p	3.36e-12

Extended statistics for Fig. 1. For each contrast condition, we determined significance by comparing the block group to both control groups (UAS control and Gal4 control) using a two-tailed Student's *t* test. Blocks were declared significantly different if and only if both control groups were significantly different at a level of 0.05. For multiple comparisons, Bonferroni correction was applied. Red fields indicate significant differences after Bonferroni correction. The number indicated by n is the number of individual flies.

Supplementary Table 3

Correlation coefficient (Fig. 2d)

c = 6.25%

Genotype		T4/T5 block (n=11)	T4 block (n=12)	T5 block (n=12)
UAS control	n	12	12	12
	t	-3.98	0.673	-0.862
	p	7.06e-4	0.508	0.398
Gal4 control	n	12	13	12
	t	-6.20	-1.95	-0.923
	p	3.89e-6	0.0631	0.368

c = 12.5%

Genotype		T4/T5 block (n=11)	T4 block (n=12)	T5 block (n=12)
UAS control	n	12	12	12
	t	-9.15	0.968	-1.49
	p	4.05e-8	0.344	0.150
Gal4 control	n	12	13	12
	t	-14.7	-2.38	-1.57
	p	2.86e-12	0.0277	0.130

c = 25%

Genotype		T4/T5 block (n=11)	T4 block (n=12)	T5 block (n=12)
UAS control	n	12	12	12
	t	-13.2	0.108	-0.545
	p	2.50e-11	0.915	0.591
Gal4 control	n	12	13	12
	t	-19.1	-2.53	0.0875
	p	7.56e-14	0.0198	0.931

c = 50%

Genotype		T4/T5 block (n=11)	T4 block (n=12)	T5 block (n=12)
UAS control	n	12	12	12
	t	-31.5	-0.499	-2.02
	p	1.42e-17	0.624	0.0608
Gal4 control	n	12	13	12
	t	-28.2	-1.49	-0.832
	p	4.00e-18	0.156	0.415

c = 100%

Genotype		T4/T5 block (n=11)	T4 block (n=12)	T5 block (n=12)
UAS control	n	12	12	12
	t	-24.0	-1.89	-2.25
	p	4.04e-13	0.0803	0.0362
Gal4 control	n	12	13	12
	t	-22.3	-2.17	-0.458
	p	6.25e-14	0.0495	0.652

Gain (Fig. 2e)

Genotype		T4/T5 block (n=11)	T4 block (n=12)	T5 block (n=12)
UAS control	n	12	12	12
	t	-4.13	0.175	-1.34
	p	5.41e-4	0.863	0.193
Gal4 control	n	12	13	12
	t	-5.99	-1.81	-0.987
	p	1.15e-5	0.0853	0.336

Genotype		T4/T5 block (n=11)	T4 block (n=12)	T5 block (n=12)
UAS control	n	12	12	12
	t	-8.66	0.0732	-1.58
	p	5.01e-7	0.942	0.129
Gal4 control	n	12	13	12
	t	-10.5	-1.55	-0.614
	p	9.04e-8	0.136	0.546

Genotype		T4/T5 block (n=11)	T4 block (n=12)	T5 block (n=12)
UAS control	n	12	12	12
	t	-11.3	-0.161	-0.828
	p	4.18e-8	0.874	0.417
Gal4 control	n	12	13	12
	t	-14.4	-1.82	0.969
	p	2.00e-9	0.0810	0.344

Genotype		T4/T5 block (n=11)	T4 block (n=12)	T5 block (n=12)
UAS control	n	12	12	12
	t	-19.3	-1.38	-2.35
	p	1.53e-10	0.185	0.0300
Gal4 control	n	12	13	12
	t	-17.3	-0.927	0.328
	p	7.31e-10	0.364	0.747

Genotype		T4/T5 block (n=11)	T4 block (n=12)	T5 block (n=12)
UAS control	n	12	12	12
	t	-16.0	-1.68	-2.00
	p	1.42e-9	0.110	0.0596
Gal4 control	n	12	13	12
	t	-19.2	-1.23	0.404
	p	4.77e-11	0.235	0.692

Extended statistics for Fig. 2. Test details were as in Supplementary Table 2. c denotes contrast. Red fields indicate significant differences after Bonferroni correction. The number indicated by n is the number of individual flies.

Supplementary Table 4

Feature		Mean (n=70)	Maximum (n=70)	Onset latency (n=70)	Offset latency (n=70)	Pre-stimulus polarization (n=70)	Post-stimulus polarization (n=70)
ON vs. OFF	t	-7.30	-5.50	5.18	5.63	-17.2	11.1
	p	3.76e-10	6.13e-7	2.13e-6	3.63e-7	1.12e-26	6.10e-17

Extended statistics for Fig. 3. We compared response features between ON and OFF edge presentation. Responses were always averaged across velocities and then tested using two-tailed Student's *t* tests at a significance level of 0.05. Red fields indicate significant differences. The number indicated by n is the number of individual cells pooled from vertical and horizontal system cells.

Supplementary Table 5

Difference from zero

$v = 20^\circ/s$

Genotype	TNT control (n=12)	T4/T5 control (n=13)	T4 control (n=12)	T5 control (n=13)
versus 0				
t	6.36	6.64	5.57	4.90
p	5.34e-5	2.39e-5	1.67e-4	3.65e-4

$v = 40^\circ/s$

Genotype	TNT control (n=12)	T4/T5 control (n=13)	T4 control (n=12)	T5 control (n=13)
versus 0				
t	4.77	5.88	5.33	6.36
p	5.77e-4	7.51e-5	2.40e-4	3.60e-5

$v = 80^\circ/s$

Genotype	TNT control (n=12)	T4/T5 control (n=13)	T4 control (n=12)	T5 control (n=13)
versus 0				
t	0.703	-0.765	-1.44	0.249
p	0.497	0.459	0.178	0.808

$v = 160^\circ/s$

Genotype	TNT control (n=12)	T4/T5 control (n=13)	T4 control (n=12)	T5 control (n=13)
versus 0				
t	-4.57	-8.74	-5.78	-7.81
p	8.02e-4	1.50e-6	1.23e-4	4.78e-6

$v = 320^\circ/s$

Genotype	TNT control (n=12)	T4/T5 control (n=13)	T4 control (n=12)	T5 control (n=13)
versus 0				
t	-5.67	-7.97	-5.44	-11.1
p	1.45e-4	3.93e-6	2.04e-4	1.14e-7

$v = 640^\circ/s$

Genotype	TNT control (n=12)	T4/T5 control (n=13)	T4 control (n=12)	T5 control (n=13)
versus 0				
t	-2.50	-1.54	-1.15	-2.64
p	0.0297	0.149	0.274	0.0216

Difference from control

Genotype	T4/T5 block (n=12)	T4 block (n=15)	T5 block (n=14)
UAS control			
n	12	12	12
t	-2.66	-14.9	6.80
p	0.0143	5.04e-13	1.32e-6
Gal4 control			
n	13	12	13
t	-2.08	-13.5	8.60
p	0.0502	2.15e-11	1.27e-7

Genotype	T4/T5 block (n=12)	T4 block (n=15)	T5 block (n=14)
UAS control			
n	12	12	12
t	-2.20	-13.1	8.85
p	0.0399	4.12e-12	2.80e-8
Gal4 control			
n	13	12	13
t	-2.90	-12.4	9.65
p	8.33e-3	1.26e-10	3.65e-8

Genotype	T4/T5 block (n=12)	T4 block (n=15)	T5 block (n=14)
UAS control			
n	12	12	12
t	-0.324	-11.8	11.3
p	0.749	1.07e-11	4.30e-10
Gal4 control			
n	13	12	13
t	0.921	-9.70	12.7
p	0.367	6.14e-10	1.86e-9

Genotype	T4/T5 block (n=12)	T4 block (n=15)	T5 block (n=14)
UAS control			
n	12	12	12
t	3.18	-6.82	12.3
p	7.32e-3	4.96e-7	7.74e-12
Gal4 control			
n	13	12	13
t	6.02	-5.98	15.0
p	1.29e-5	3.56e-6	9.84e-12

Genotype	T4/T5 block (n=12)	T4 block (n=15)	T5 block (n=14)
UAS control			
n	12	12	12
t	3.99	-6.06	14.2
p	9.22e-4	2.95e-6	1.16e-12
Gal4 control			
n	13	12	13
t	4.66	-6.45	19.0
p	1.10e-4	1.24e-6	7.84e-15

Genotype	T4/T5 block (n=12)	T4 block (n=15)	T5 block (n=14)
UAS control			
n	12	12	12
t	2.25	-2.21	4.54
p	0.0439	0.0368	1.89e-4
Gal4 control			
n	13	12	13
t	1.18	-4.80	5.05
p	0.256	1.06e-4	3.73e-5

Extended statistics for Fig. 4. For each velocity condition, we determined significance by comparing control groups to zero or block groups to both corresponding control groups (UAS control and Gal4 control) using a two-tailed Student's t test. Blocks were declared significantly different if and only if both control groups were significantly different at a significance level of 0.05. v denotes velocity. For multiple comparisons, Bonferroni correction was applied. Red fields indicate significant differences after Bonferroni correction. The number indicated by n is the number of individual flies.

Supplementary Table 6

Stimulus		Random (n=16)	3p/conv/+ (n=16)	3p/conv/- (n=16)	3p/div/+ (n=16)	3p/div/- (n=16)
versus 0	t	-0.426	-2.33	18.4	-5.44	5.73
	p	0.676	0.0341	1.02e-11	6.89e-5	3.98e-5

Extended statistics for Fig. 7. We compared glider voltage responses to zero. Responses were tested using two-tailed Student's *t* tests at a significance level of 0.05. Red fields indicate significant differences. The number indicated by *n* is the number of individual cells pooled across cells from the horizontal and vertical systems.

Supplementary Table 7

Positive parity

Negative parity

2-point

Genotype		T4/T5 block (n=14)	T4 block (n=13)	T5 block (n=17)
UAS control	n	18	18	18
	t	-16.2	-2.41	-1.33
	p	2.17e-12	0.0228	0.194
Gal4 control	n	12	12	12
	t	-7.93	1.82	1.54
	p	5.91e-6	0.0814	0.136

Genotype		T4/T5 block (n=14)	T4 block (n=13)	T5 block (n=17)
UAS control	n	18	18	18
	t	21.3	1.29	-0.169
	p	1.43e-14	0.211	0.867
Gal4 control	n	12	12	12
	t	8.08	-1.79	-1.91
	p	5.28e-6	0.0869	0.0679

3-point/conv.

Genotype		T4/T5 block (n=14)	T4 block (n=13)	T5 block (n=17)
UAS control	n	18	18	18
	t	7.82	16.7	-5.85
	p	2.73e-8	4.72e-16	1.85e-6
Gal4 control	n	12	12	12
	t	8.57	19.3	-5.49
	p	2.56e-7	2.39e-15	1.11e-5

Genotype		T4/T5 block (n=14)	T4 block (n=13)	T5 block (n=17)
UAS control	n	18	18	18
	t	-6.44	-14.0	6.83
	p	3.12e-6	1.30e-13	2.01e-7
Gal4 control	n	12	12	12
	t	-12.4	-23.7	7.00
	p	4.45e-10	1.88e-15	1.00e-6

3-point/div.

Genotype		T4/T5 block (n=14)	T4 block (n=13)	T5 block (n=17)
UAS control	n	18	18	18
	t	8.58	-3.34	10.8
	p	2.83e-8	2.32e-3	8.68e-12
Gal4 control	n	12	12	12
	t	5.36	-0.354	11.4
	p	1.85e-4	0.727	7.10e-10

Genotype		T4/T5 block (n=14)	T4 block (n=13)	T5 block (n=17)
UAS control	n	18	18	18
	t	-9.25	4.52	-8.51
	p	8.57e-9	1.01e-4	1.36e-9
Gal4 control	n	12	12	12
	t	-6.82	0.991	-9.76
	p	2.12e-5	0.335	3.33e-10

Extended statistics for Fig. 8. Test details were as in Supplementary Table 2. Red fields indicate significant differences after Bonferroni correction. The number indicated by n is the number of individual flies.

3

DISCUSSION

Investigation of fly motion vision provides a compelling example for the methods and goals of systems neuroscience. To extract optic flow from reflected light, the nervous system needs to perform non-trivial but clearly circumscribed computations. Flies accomplish the task using a small number of neurons and within few synapses, suggesting that the project of delivering a circuit-level description of direction selectivity is indeed tractable. Algorithmic models provide the computational context in which we can embed circuit schemes derived from experimental work. Additionally, motion is a critically relevant stimulus for animals in virtually all ecological niches. Optic flow provides information about our own movement, depth in a visual scene, as well as the movement of conspecifics, prey, and predators. The fact that motion represents such a fundamental cue allows us to put our models of the circuit in the functional context of defined goals.

In the course of this cumulative thesis, my collaborators and I have made substantial progress toward neurally plausible models of motion detection in the fruit fly *D. melanogaster*. First, we were able to identify cell groups T4 and T5 as the direction-selective output elements of the ON and OFF motion pathways in the fly optic lobe (Maisak et al., 2013). They form a retinotopic map that delivers locally motion-sensitive signals to the wide-field tangential cells of the lobula plate. Two major functional divisions emerged, one separating contrast polarities and the other concerning directions in visual space. T4 responds only to ON motion defined by brightness increases and T5 only to corresponding OFF motion defined by brightness decreases. Four sub-types of each are selective for only one of the four cardinal directions. When T4 or T5 were silenced, downstream responses both in tangential cells and walking flies were affected in a polarity-specific fashion. In conjunction with the finding that combined silencing of T4 and T5 abolishes all wide-field motion responses, this indicated that the two cell arrays are the dominant source of motion information in the fly brain.

Second, we investigated medulla elements feeding into the T4 pathway (Ammer et al., 2015). Dense reconstruction had suggested a circuit layout in which Mi1 and Tm3 represent the two arms of a Reichardt-type motion detector. Contrary to predictions from this model, only silencing of Mi1 abolished motion responses in tangential cells. Inactivation of Tm3 only had an effect on the specific stimulus regime of fast velocities. Behavioral work confirmed the findings. This ruled out the Mi1-Tm3 model and indicated further neural complexity that was recently confirmed through further high-resolution reconstruction efforts (Takemura et al., 2017). Third, we explored this type of architectural complexity in the context of the T5 pathway where we studied the response properties and functional roles of input elements Tm1, Tm2, Tm4, and Tm9 using imaging and genetic silencing (Serbe et al., 2016). These cells provide a broad spectrum of temporal and spatial

filters to T5 which are well suited to the computation of motion under a Reichardt-type model. Critically, none of them are themselves direction selective. When inactivated, physiological and behavioral phenotypes showed that all play a role in OFF motion detection.

Fourth and finally, having established some of the neural basis of motion detection, we related the emerging two-pathway architecture to its functional context (Leonhardt et al., 2016). In both behavior and physiology, we discovered substantial asymmetries in temporal tuning between the ON and the OFF channel. Simulation work suggested that these asymmetries constitute an adaptation to the particular demands of natural scene statistics. Moreover, they appear to be a critical determinant in the fruit fly's responses to higher-order motion.

3.1 A NEURAL MODEL FOR MOTION DETECTION

Key impetus for the projects I pursued during my doctoral studies was the goal of mapping algorithmic elements onto concrete neural implementation. The Reichardt detector and its elaborations have been exceedingly successful at accounting for input-output relationships. Even detailed aspects of optomotor response and neural properties of tangential cells are well predicted by a simple combination of linear filtering and elementary mathematical operations (Borst and Egelhaaf, 1989; Borst and Haag, 2002). It was an open question whether this simplicity would be reflected by neural circuitry. In this section, I discuss correspondences particularly in light of more recent developments.

3.1.1 Input lines

Standard models of local direction-selective units are based on two spatially separated arms that filter visual signals asymmetrically. Work on T4 and T5 inputs, including ours, has hinted at surprising complexity in the presynaptic structure of fly elementary motion detectors. No obvious one-to-one correspondence between algorithm and circuit has emerged. So how should we map neural elements in the medulla onto algorithmic inputs?

ON pathway

Based on connectivity and a limited spatial offset between projection fields that correlated with the preferred direction of the targeted cell, Takemura et al. (2013) had proposed a two-arm model in which Mi1 and Tm3 relay visual input to the dendrites of T4. There, motion is then computed through a correlation-type mechanism. Electrophysiological recordings from cell bodies of these two cells constrained the model further as the estimated time constant of a filter fit to Mi1 responses was somewhat larger than that of Tm3 (Behnia et al., 2014). Neither Mi1 nor Tm3 were already selective for direction. Together, these findings predicted that input signals are combined on T4 dendrites in a non-linearly opponent fashion as in the model proposed by Barlow and Levick (1965). The correspondence between circuit

and a subunit of the Reichardt model would then have been almost one-to-one: starting from photoreceptors, the L1-Mi1 and L1-Tm3 pathways carry a slow and a fast signal, respectively, to the non-linearity implemented by T4.

Several factors detracted from the plausibility of this model. First, the reported difference between filter peaks was approximately 18 ms and thus exceedingly small compared to standard values used for modelling of tangential cell responses (Behnia et al., 2014). The steady-state frequency optimum of a simple low-pass Reichardt detector is given by $(2\pi\tau)^{-1}$ which would require $\tau \approx 150$ ms for the typical post-subtraction peak at 1 Hz. While a direct transfer between time constant and delay shift is not trivial, particularly when the measured filter function is of higher order, the gap remains large. A quantitative model proposed by Behnia et al. (2014) was only able to replicate a well-defined optimum at 1 Hz due to the high-pass characteristic of the measured filters and, importantly, due to the subtraction of oppositely tuned units. Compared to the magnitude of input signals, output at the subtraction stage was minuscule. Any circuit based on small differences between large signals, however, suffers from a lack of noise robustness. Moreover, the dendrites of T4 already appear to be highly direction selective but there is now substantial evidence that the subtraction stage is implemented downstream of T4 (see Mauss et al., 2015, and the sections below).

Second, the reported separation between centers of mass of Mi1 and Tm3 projection fields was on the order of 1° in visual space, corresponding to only 20% of inter-ommatidial distance. While this separation is sufficient to generate direction selectivity, it again negatively impacts the signal-to-noise characteristics of the resulting circuit. Third, the circuit model clearly predicts that silencing of one input line should abolish direction selectivity fully. This was not borne out by our findings. Only inactivation of Mi1 affected downstream ON motion responses across the full range of tested stimuli. Note, however, that Strother et al. (2017) found a more completely abolished grating response when imaging T4 in Tm3-silenced flies. Nonetheless, the available evidence pointed toward a more complex circuit layout.

Further studies have recently filled in some of the gaps in our understanding of medulla circuitry feeding into T4 (Figure 8a). The reconstruction effort that had suggested the two-arm Mi1-Tm3 model was subject to methodological constraints that led to an incomplete connectivity matrix (Takemura et al., 2013). In particular, not all processes impinging on T4 dendrites were followed to their originating columns. Subsequent work used focused ion beam scanning electron microscopy (FIB-SEM) to image and reconstruct a full cartridge along with its six adjacent columns at an improved voxel size of approximately 10 nm (Takemura et al., 2017). In the resulting circuit diagram, Mi1 and Tm3 were confirmed as major inputs to T4 that jointly represent $\approx 50\%$ of synapses. The spatial shift between projection fields could not be replicated. Several additional numerically relevant inputs were identified, chief among them Mi4 and Mi9 (complemented by C3, CT1, TmY15, as well as other T4 cells). Dendritic trees of T4 have an elongated structure that covers multiple columns of the medulla and whose orientation correlates with the lobula plate layer to which the sub-type projects. Intriguingly, while Mi1 as well as Tm3 projections tend to target the central area of the dendrite, both Mi4 and Mi9 form synapses in a spatial pattern that depends

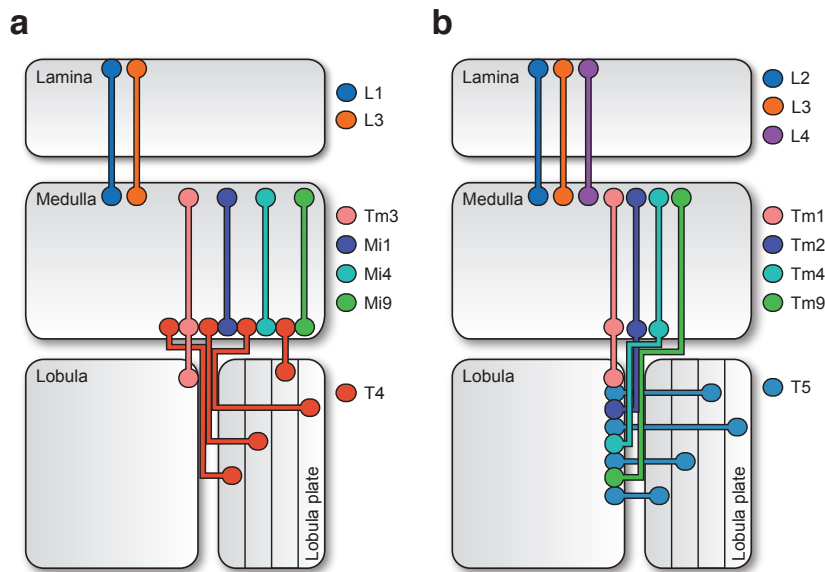


Figure 8: Neural architecture of motion pathways based on updated electron microscopy reconstructions. **a** Schematic of the ON pathway. **b** Schematic of the OFF pathway. Illustration by M. Meier and modified with permission.

on the preferred direction of the T₄ cell. For upward-sensitive T_{4c} cells, for instance, Mi₄ connects primarily on the dorsal end while Mi₉ does so ventrally. This yields a mean offset between center and flanking cell of at least one column. The layout and in particular the separation of projection fields between Mi₁/Tm₃ and Mi₄ or Mi₉ lend themselves well to Reichardt-type motion computations.

Calcium imaging from these additional medulla cells has critically added to the purely structural view of the T₄ circuit (Strother et al., 2014; Arenz et al., 2017; Strother et al., 2017). As in the OFF pathway, neither of the four inputs is direction selective by itself which confirms that T₄ dendrites are the locus where motion is first extracted (Strother et al., 2017). Arenz et al. (2017) used white-noise stimuli to map spatiotemporal receptive fields and found two transient units which were well-approximated by band-pass filters (Mi₁ and Tm₃) as well as two tonic units resembling low-pass filters (Mi₄ and Mi₉). Measurement of step responses yielded comparable results (Strother et al., 2017). An interesting complication arises from the response sign of Mi₉. While all other cells increase their calcium levels in response to ON stimulation, Mi₉ is activated by OFF stimulation instead. In terms of connectivity, this finds a convenient explanation in the fact that Mi₉ lies downstream of OFF-implicated lamina monopolar cell L₃. It is conceivable that the synapse connecting Mi₉ and T₄ effectively reverses the response sign, thereby providing an ON-like signal to T₄. Taken together, the filter bank offers a much larger range of temporal properties than what Behnia et al. (2014) had put forward, with time constant differences reaching hundreds of milliseconds. A broad spectrum of course then greatly simplifies the construction of highly direction-selective units.

Given that signals from Mi1 and Tm3 target overlapping parts of the central T4 dendrite and largely come from the same central cartridge, it is a distinct possibility that they interact to form a single functional input arm. There are at least three lines of evidence additionally supporting this notion. First, the FIB-SEM connectome indicates that Mi1 is itself presynaptic to Tm3. In fact, Mi1 is the numerically strongest Tm3 input surpassed only by L1. Second, [Strother et al. \(2017\)](#) performed optogenetic activation experiments using UAS-CsChrimson to test functional connectivity between candidate medulla cells and T4 ([Klapoetke et al., 2014](#)). Intriguingly, while the isolated activation of Mi1 or Tm3 only had negligible effects on calcium activity of T4 cells, joint excitation of the cell pair resulted in significant signals that were non-linearly amplified over the simple sum of individual responses. Third, our blocking experiments could show that Tm3 plays a critical role in ON motion detection when edge velocities were at the higher end of tested velocities. One could imagine that Tm3 serves to shape and possibly sharpen signals emanating from the central portion of the visual field, in concert with primary projections from Mi1. Silencing of this channel may then only result in clear phenotypes when input dynamics are fast. Overall, the observed complexity highlights that the mapping from circuit to algorithm does not have to be one from single neurons to individual filters and input lines. Individual algorithmic components could well be implemented by a group of neurally segregated units.

OFF pathway

Our work on OFF pathway elements paints a similar picture as the one that has now emerged for its ON counterpart (Figure 8b). Tm1, Tm2, Tm4, and Tm9 jointly account for a vast majority of the input synapses onto T5 ([Shinomiya et al., 2014](#)). None of them are direction selective, which confines the critical computation to the dendrites of T5. As with Mi1, Tm3, Mi4, and Mi9, they have varying filter properties ranging from the slow and tonic (Tm9) to the fast and phasic (Tm2 and Tm4) with Tm1 showing intermediate kinetics. A Reichardt detector using, for instance, Tm9 and Tm2 as delayed and direct line, respectively, exhibits high direction selectivity and a frequency optimum in the physiologically plausible range. Conversely, some combinations like Tm2 and Tm4 provided little directional signal, making them unlikely candidates for inputs to the motion detector.

Interestingly, while agreeing on delay direction, we observed a much larger difference between the temporal response dynamics of Tm1 and Tm2 than what [Behnia et al. \(2014\)](#) had reported previously. Possible reasons include calcium kinetics that exaggerate voltage timing differences or asymmetries between measurements in cell bodies and terminals. Note that for Tm2, step calcium responses are indeed slightly faster than the corresponding voltage deflections (see Figure 2b in [Behnia et al. \(2014\)](#) and Figure 3b in [Serbe et al. \(2016\)](#) for comparison).

In our measurements, spatial receptive fields of all T5 inputs were small, isotropic, and retinotopic, with separation and half-width approximately corresponding to what was expected from the facet layout. Additionally, all exhibited lateral inhibition; responses to large stimuli were suppressed.

This was later corroborated by filter estimates derived from white-noise responses (Arenz et al., 2017). In contrast, Fisher et al. (2015a) employed reverse-correlation and determined receptive fields for Tm9 whose extent was in excess of 60° in both elevation and azimuth. The reason for this drastic discrepancy remains unclear. Our work used a different GAL4 line to target Tm9. However, temporal tuning measurements as well as phenotypes in Tm9-silenced flies were in agreement across studies, casting doubt on this explanation. An interesting feature we found when establishing the size tuning of Tm9 using flickering bars of various sizes was an increase in response strength when the bars became large enough to resemble full-field flicker. Through some global pooling mechanism, Tm9 cells appear to have access to information from remote parts of visual space. This observation may be a first step toward reconciling the measurements if one assumes that the measurements by Fisher et al. (2015a) were performed in a way that would affect the global properties of the stimulus. For instance, if the recorded terminals have receptive fields close to the borders of the retinotopic map, asymmetric lateral signals may lead to a broadening of the input field of Tm9. From an algorithmic point of view, however, it remains unclear how true wide-field input would critically contribute to direction selectivity in T5.

The strength of the behavioral phenotypes we found using physiological and behavioral measurements correlated distinctly with the number of synaptic contacts between the respective cell and T5 dendrites. Critically, all four blocks had an impact on downstream motion responses. This lack of redundancy does not indicate a simple division of labor between the potential input arms of the OFF motion detector. In contrast to our work on the ON pathway, temporal tuning curves did not reveal velocity-dependent functional specialization; the reduction in OFF response strength was generally conserved across stimulus frequencies. The strongest effects resulted from blocking Tm2 and Tm9 either individually or in combination. A simple conclusion from this would be to propose Tm2 as the fast and Tm9 as the slow arm of an elementary motion detector. However, this does little to explain the contribution of Tm1 or Tm4 whose silencing, particularly in combination, also produced substantial phenotypes.

Biophysical origin of delays

In principle, three delay implementations are conceivable. First, temporal filtering could be intrinsic to the input lines; in this case, the signals arriving at the synapses to T4 and T5 already exhibit appropriate phase shifts. Second, temporal delays could be accomplished by the synaptic apparatus connecting input cell and T4 or T5. Third, filtering could occur along the dendritic tree of T cells. Little is known about the biophysical properties of these dendrites, so I focus on the first two options and discuss them in turn.

So far, I have tacitly assumed that the temporal filtering of signals reaching T4 is purely intrinsic to the input cells. Given the substantial temporal variety observed at the level of medulla output lines, this is a reasonable assumption. For instance, our modelling indicates that the non-linear interaction of high-pass filtered signals in Tm2 terminals and low-pass filtered signals in Tm9 terminals would result in highly direction-selective output.

However, it is currently not fully understood how medulla cells generate and tune these filtering properties.

First, filter properties may simply be inherited from upstream lamina cells. This accounts for a significant fraction of the observed variability. In the OFF pathway, high-pass units Tm₁, Tm₂, and Tm₄ all receive input from the transiently responding L₂ (Fischbach and Dittrich, 1989; Rivera-Alba et al., 2011; Takemura et al., 2017), with L₄ additionally connecting to Tm₂. Tonic Tm₉ cells, on the other hand, are primarily postsynaptic to L₃ for which slow kinetics have been demonstrated (Silies et al., 2013). Within the ON pathway, transient L₁ projects to band-pass cells Mi₁ and Tm₃ while the tonic Mi₉ lies downstream of L₃. Mi₄ is targeted by L₅ for which photoreceptor input originates from reciprocal connections with L₁ (but note that little is known about the intrinsic tuning of L₅). Under this scheme, the medulla filter bank is generated by summing lamina output kinetics in various configurations. This provides numerous degrees of freedom. Lamina cells then represent building blocks from which more varied filters can be derived, which attributes interesting functional significance to the multiplexed structure of the fly optic lobe. However, while basic characteristics appear to be derived from upstream processing, further differentiation can be observed. Tm₁ and Tm₄, for instance, exhibit differing kinetics despite their shared main input L₂.

Second, cell-intrinsic mechanisms in medulla pathways could further refine temporal tuning. Moreover, even if temporal tuning is inherited from upstream inputs, this begs the question of how lamina cells generate timing differences in the first place. Passive, purely electrotonic properties of the membrane in neural "cables" produce effects like signal attenuation along appropriately constructed neurites. This results in delays and low-pass filtering of voltage signals that depend on the geometry of processes (Koch, 2004). Active conductances along the path may additionally shape signals through, say, non-linear amplification or slow kinetics that introduce temporal offsets. Moreover, synapses represent junction points at which elaborate signal modifications can be implemented through transmission machinery. High-pass filtering, for instance, resembles adaptation. If a synapse removes the long-term mean of the signal through rapid habituation, only sensitivity to fast changes remains. By modulating the kinetics of this adaptation process, different high- or band-pass characteristics are achieved. Adaptive mechanisms have previously been employed to explain phasic output in lamina monopolar cells (Laughlin and Hardie, 1978). Alternatively, high-pass characteristics also emerge when taking the difference of asymmetrically low-pass filtered signals. This offers yet another biophysically simple mechanism for rendering output transiently sensitive.

As mentioned above, not all temporal filtering has to be present in the output of medulla inputs. Indeed, the synaptic apparatus connecting them to T₄ or T₅ may plausibly contribute to the required differential filtering. For instance, there is now evidence from RNA profiling of isolated T₄ and T₅ cells that these cells express both ionotropic and metabotropic variants of acetylcholine receptors (Shinomiya et al., 2014; Pankova and Borst, 2016). If cholinergic input from one spatial location triggers a slow, muscarinic version and the other a fast, nicotonic version, resulting timing differences may

be sufficient to permit the disambiguation of motion direction. More complete neurotransmitter profiles of medulla cells are now available: [Shinomiya et al. \(2014\)](#) propose that all four T5 inputs are cholinergic while findings by [Pankova and Borst \(2017\)](#) as well as [Takemura et al. \(2017\)](#) suggest that Mi1 and Tm3 are cholinergic, Mi4 GABAergic, and Mi9 glutamatergic. This variety offers substantial leeway for synaptic implementations of temporal filtering. Additionally, it is entirely possible that a combination of cell-intrinsic and synaptic mechanisms gives rise to the temporal input profile. Note, however, that the measured cell-intrinsic delays of certain medulla cell combinations are by themselves sufficient to generate strong direction selectivity ([Arenz et al., 2017](#)).

3.1.2 Nature of the non-linearity

The comprehensive mapping of medulla input cells along with the finding that T cell neurites targeting the lobula plate are already selective for direction had revealed T4 and T5 as the locus of the non-linear interaction underlying motion detection. However, the details of this computation remained elusive.

Detailing the neural implementation of a multiplication-like operation has the potential to clarify functional segregation of presynaptic elements. After all, input cells clearly outnumber input lines of the Reichardt detector in both pathways. With the exception of velocity-dependence for Tm3, none of the silencing experiments had pinpointed particular functional division among the complex input structure of T4 and T5. The neural non-linearity could shed light on the function of medulla cells.

Dual mechanisms

Subunits of the Reichardt detector and Barlow-Levick schemes share the basic principle of differentially delaying spatially adjacent signals and then comparing them in order to establish temporal order. Where they differ is the choice of non-linearity that implements comparison. For the Reichardt detector, this is correlation as realized by mathematical multiplication. Large output signals occur when two inputs are in phase after one of them is delayed. For Barlow-Levick detectors, the essential operation is an AND-NOT gate. Only inputs with appropriate phase relationships pass; signals resulting from null motion are vetoed. The two layouts make clear predictions about the placement of the delay as well as the input-output signature of the operation that combines inputs. One of them is fundamentally facilitating; the other one is fundamentally suppressive.

Several studies have now made progress toward a neural understanding of the operations implemented by fly motion-sensitive neurons. First, [Fisher et al. \(2015b\)](#) used apparent motion to discriminate excitatory and inhibitory interactions on dendrites of genetically singled-out T4 and T5 cells. When stimulated with spatially neighboring, temporally separated flashes along the cells' preferred direction, T4 dendrites showed direction-selective calcium increases that exceeded the linear prediction calculated from the sum of responses to isolated flashes. The same facilitating response was observed

for T5¹. This indicated that the non-linear interaction on both T4 and T5 dendrites is based on the amplification of coincident signals, in line with what the Reichardt model had predicted.

Second, [Leong et al. \(2016\)](#) used system identification methods to fit T5 white-noise responses. Given the inherent non-linearity of direction-selective responses, they built a cascade that consisted of chained linear (L) receptive fields and point non-linearities (N), forming a LNLN feedforward model that also modelled calcium binding dynamics. Such a phenomenological model contrasts with mechanistic accounts like the Reichardt detector. As expected and in line with the internal structure of motion energy models, response variance was best explained by a spatiotemporally slanted receptive field combined with polynomial non-linearities of orders 3 and above. Within the linear spatiotemporal filter, two spatially separated sub-fields could be identified: one with positive sign, one with negative sign. The authors interpreted this as a dual mechanism for generating OFF-specific direction selectivity that recruits both facilitation and suppression. Note, however, that their method does not allow for conclusive disambiguation of, say, ON facilitation and OFF suppression.

Third and finally, [Haag et al. \(2016\)](#) probed the dendritic non-linearity through a combination of precisely targeted apparent motion and layer-specific read-out of T4 activity. The former was accomplished by telescopic stimulation of isolated neuro-cartridges; the second by expressing the calcium indicator under the control of a T4c-exclusive driver line. Single T4 cells had elongated receptive fields that spanned multiple columns. When apparent motion consisting of ON illumination steps was focused on the center, both non-linear amplification of preferred direction sequences as well as non-linear suppression of null direction sequences could be observed. This demonstrated explicitly that both mechanisms underlie direction selectivity on T4 dendrites. Critically, at the dorsal and ventral end of the receptive field only suppression and facilitation, respectively, occurred. This indicated a clear functional division among input elements at opposite ends of the dendritic tree.

In concert, these studies argue in favor of a synthesis of Reichardt and Barlow-Levick models. The biological algorithm draws from at least three visual inputs to implement both an excitatory and an inhibitory non-linearity. [Haag et al. \(2016\)](#) put forward a simple extension of the standard correlation scheme in which the output of a multiplicative Reichardt sub-unit is divided by a third spatially displaced input, effectively creating a serial circuit consisting of two equally tuned half-detectors (Figure 9). In this model, the central arm is a fast line and the flanking inputs contain appropriate delays. The model mimics T4 responses to apparent motion closely and produces plausible frequency tuning curves.

Importantly, it resolves a puzzling observation regarding the T4 and T5 measurements that were part of our initial functional characterization. Sub-units of Reichardt detectors show little direction selectivity by themselves; they generally respond vigorously to motion in both preferred and null direction. Only after subtraction do responses become unambiguously sensi-

¹ Interestingly, [Fisher et al. \(2015b\)](#) also reported a non-linear suppression of responses to apparent motion along the null direction but discarded this as motion-unselective adaptation.

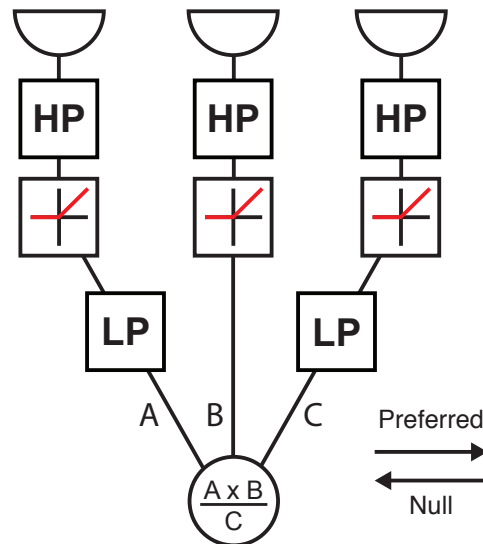


Figure 9: Simplified schematic of signal flow in the three-arm detector for T4 motion responses as proposed by Haag et al. (2016). Input stages resemble the previous two-quadrant iteration, with high-pass filtering being followed by half-wave rectification. Input B mediates a fast central signal. Inputs A and C supply delayed facilitating and suppressing signals, respectively. Note that for reasons of simplicity, the DC contribution is omitted in this illustration.

tive to one or the other. Our initial assumption was that T4 and T5 are ON- and OFF-specific half-detectors as in the two-quadrant model suggested by Eichner et al. (2011). However, both neurons exhibited remarkable selectivity for direction when stimulated with gratings or edges. That is, responses of T4 and T5 sub-types were sharply tuned to one direction in visual space and suffered from little off-target activation. The three-arm detector provides a consistent explanation for this property: if enhancement of preferred stimuli and suppression of non-preferred stimuli act in concert, crisp tuning follows even at the level of half-detectors. This architecture ensures high signal-to-noise ratio already at the local stage that precedes subtractive or spatial integration. Given the data by Leong et al. (2016) and follow-up work using telescopic stimulation (Jürgen Haag, personal communication), it is probable that motion extraction in T5 relies on a comparable dual non-linearity.

The elaboration of the correlation detector also contextualizes the input complexity that our work on T4 and T5 inputs has suggested. A motion detector of this type requires at least three arms, which reduces the number of seemingly extraneous input cells to just one. Moreover, given their relative spatial displacement, T4 inputs Mi1/Tm3, Mi4, and Mi9 now map neatly onto central and peripheral lines of this novel architecture. Taking this as well as temporal filter properties into account, Arenz et al. (2017) could show through simulations that a detector in which Mi9 acts as a delayed facilitating input, Mi1 as a fast central input, and Mi4 as a delayed inhibitory input exhibits high direction selectivity. Finally, T4 inputs release a wide spectrum of neurotransmitters including glutamate, acetylcholine, and GABA

(Pankova and Borst, 2017; Takemura et al., 2017). This offers opportunity for postsynaptic receptors to realize various non-linear interactions.

Due to a lack of dense reconstructions that trace processes back to the medulla, our understanding of how Tm1, Tm2, Tm4, and Tm9 synapses cluster on T5 dendrites is fundamentally limited (Shinomiya et al., 2014). This hinders the mapping between cells and input lines of a three-arm detector. Quantitative work based on their filter properties finds that the best performing three-arm detectors have Tm2 as the fast central arm, Tm9 as the slow inhibitory arm, and either Tm1 or Tm4 as the facilitating arm (Arenz et al., 2017). It is noteworthy that the OFF pathway appears to lack a second true low-pass filter next to Tm9. This poses a challenge when constructing parallel correlation detectors. Curiously, all T5 inputs appear to be cholinergic (Shinomiya et al., 2014). However, methodological concerns cast doubt on the finding. While it is possible that acetylcholine receptor diversity is sufficient to realize differential non-linearities, further RNA profiling efforts could revise this picture in the future.

Biophysical implementation

The exact nature of both facilitating and suppressing non-linearity currently awaits detailed investigation. A standard Reichardt detector uses full multiplication to correlate incoming signals. Motion-energy models rely on output of the form $(a + b)^2$ which of course implicitly contains the product of inputs $2ab$. One study analyzed the spectral properties of tangential cell responses to local grating motion, assumed to only stimulate individual motion detector units, and concluded that the comparison is indeed almost perfectly multiplicative with little contribution from higher-order non-linearities (Egelhaaf et al., 1989).

From a biophysical point of view, it is unlikely that individual neurons compute sign-correct multiplication. This would require excessively complex synaptic machinery. Even at the algorithmic level, however, the problem can be transformed to become more tractable without losing essential properties of multiplication. The *Drosophila* visual system, for instance, reduces implementation complexity by only considering two quadrants of the full operation, namely the multiplication of equally signed ON-ON or OFF-OFF inputs (Eichner et al., 2011). Each non-linearity then operates on appropriately half-wave rectified positive signals and produces exclusively positive output. Similar tricks have successfully been applied to the design of analog electric circuits (Mead, 1989). In the context of looming sensitivity in giant locust neurons, Gabbiani et al. (2002) proposed a straightforward decomposition of the product ab into the exponentiation of summed log-transformed inputs, $\exp(\log a + \log b)$. Both logarithmic response curves and exponentiation through active conductances are of course common response features of real neurons (Koch, 2004). Null direction inhibition, on the other hand, could plausibly be achieved through linear summation of appropriately signed inputs followed by application of a threshold.

We can additionally imagine various molecular ways in which excitatory or inhibitory coincidence detection could be implemented. To be sensitive to temporal order, two sets of channels need to be linked in a causally asym-

metric manner. Consider a piece of membrane in which the delayed input targets a metabotropic, G-protein coupled receptor and the direct input an ionotropic receptor. If the cascade downstream of the metabotropic receptor renders the ligand-gated ion channel more sensitive, then preferred direction stimuli result in non-linearly amplified cation flux through the second channel. This ultimately depolarizes the cell. Out-of-sequence stimulation still produces potentials but at substantially smaller magnitude. Alternatively, the G-protein cascade is replaced by a ligand-gated calcium channel; within the cell, these ions then modulate the sensitivity of the secondary input. Vetoing of signals for the suppressive arm could rely on ligand-gated anion channels that realize a type of divisive or shunting inhibition. For a tractable electric model of how this may be achieved, see for instance [Torre and Poggio \(1978\)](#).

In the case of motion detection, many different types of non-linear interactions result in similar outcomes. Note, however, that the exact properties of facilitation and suppression are not necessarily mere implementation details. [Fitzgerald and Clark \(2015\)](#), for instance, demonstrate that elaborations of the non-linear step of correlator models yield improvements in velocity estimation performance for natural scenes. Our work on response asymmetries represents a specific example in the fruit fly visual system. Here, the reduced implementation of multiplication in separate ON and OFF channels provides additional degrees of freedom for precise tuning to realistic statistics.

3.1.3 Integration of signals

Following non-linear interaction, Reichardt-type models of both tangential cell and optomotor responses contain multiple stages of integration. First, oppositely tuned half-detectors are subtracted from each other. Second, a large number of adequately weighted local detectors is summed to produce a global estimate of optic flow. Subtraction in particular greatly enhances the direction selectivity of resulting output, but note that combined facilitation and suppression on T₄/T₅ dendrites already improves signal quality in the half-detector ([Borst and Egelhaaf, 1990](#); [Haag et al., 2016](#)). While generally depicted in this order, linearity ensures that the exact sequence does not matter.

Integration of local information on the finely tuned dendrites of tangential cells is well understood due to extensive work in larger flies (see [Borst et al., 2010](#)). Our characterization of T₄ and T₅ added another stage to this circuit layout. Up to the lobula plate where tangential cells pool the output of hundreds of input neurons of both types, motion information remains segregated into polarity-specific ON and OFF channels. Only then do these processing streams merge. Models generally assume that this summation is approximately linear; see for instance the two-quadrant detector outlined above. Yet, it is entirely conceivable that a more complex combination of polarity-selective signals occurs. For typical flow fields generated by ego-motion, ON and OFF motion are strongly correlated. Consider moving your head toward the left in front of a spatially confined dark object. In the ref-

erence frame of the retina, this object moves toward the right. Direction signalled by its leading dark edge is precisely correlated with trailing bright edge motion, simply due to rigidity of the scene. Integration mechanisms could take advantage of such correlations when globally combining ON- and OFF-derived flow. Whether this speculation has any grounding in physiological reality and how this could be exploited, however, remains to be seen.

Subsequent work has clarified the neural substrate of subtractive motion opponency. In a first study, [Mauss et al. \(2014\)](#) used whole-cell patch clamp to monitor the potential of tangential cells while optogenetically activating the full array of T4 and T5 cells. They observed a biphasic response that consisted of fast depolarization followed by delayed and prolonged hyperpolarization. Through pharmacological intervention, the excitatory potential could be identified as cholinergically mediated while chloride conductances appeared to underlie inhibitory potentials. In sum, these findings strongly suggested that T4 and T5 neurons from one layer provide excitatory input to LPTCs while corresponding units from the oppositely tuned layer produce null direction hyperpolarization via some inhibitory interneuron. This fit well with the finding that T4 and T5 are cholinergic ([Raghu and Borst, 2011](#); [Shinomiya et al., 2014](#); [Pankova and Borst, 2016](#)) and excluded the hypothesis that unidentified secondary units provide null direction signals computed *de novo*.

These intermediaries have since been identified as glutamatergic lobula plate-intrinsic (LPi) neurons ([Mauss et al., 2015](#)). They exhibit appropriate connectivity from oppositely tuned layers, produce inhibitory potentials in tangential cells upon optogenetic activation, respond to motion in a predictably tuned fashion, and are critically necessary for null direction-driven LPTC hyperpolarization. Using a variety of visual stimuli, it was possible to show that their action confers drastically enhanced flow field selectivity to downstream sensors (see [Krapp and Hengstenberg, 1996](#)). Even if the hyperpolarization of LPTCs does not control behavioral output, this could represent a key justification for opponent wiring at this level.

An interesting observation from studies on tangential cell responses was the asymmetry between preferred and null direction tuning, with the latter generally being weaker than the former ([Egelhaaf et al., 1989](#); [Joesch et al., 2008](#)). Various models including the two-quadrant detector have incorporated incomplete motion opponency to explain, for instance, residual flicker responses ([Eichner et al., 2011](#)). Physiologically, this may be due to the activation threshold of LPi neurons. Its functional significance remains unclear.

3.1.4 Emergence of polarity selectivity

Our initial calcium imaging experiments on lobula plate terminals of T4 and T5 had indicated that when stimulated with edges, both are strongly selective for polarity. OFF edge responses in T4, for instance, were drastically smaller than corresponding ON edge responses, but some residual cross-polarity activity was observed. It was not clear whether this was due to insufficiently specific GAL4 lines or if it did indeed reflect imperfect sep-

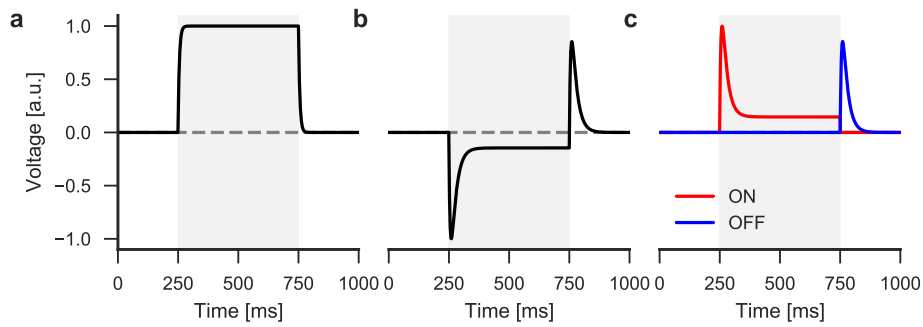


Figure 10: Schematic of early visual processing in the fly (see Laughlin and Hardie, 1978; Eichner et al., 2011). **a** Photoreceptor response to step illumination during time indicated by shaded area (modelled as a low-pass filter with $\tau = 5$ ms). Following the brightness increase, cells depolarize quickly. **b** Lamina monopolar cell responses (modelled as inverted sum of high-pass filtered photoreceptor signal and 10% of unfiltered input; $\tau = 20$ ms). L1 and L2 hyperpolarize transiently in response to positive luminance changes, maintain residual polarization throughout illumination period, and depolarize transiently following negative luminance changes. **c** Responses of polarity-specific ON or OFF downstream cells (modelled as appropriately inverted, halfwave-rectified lamina signals).

aration of ON and OFF. We were later able to show that when imaged in medulla or lobula where T4 and T5 do not intermingle, cross-polarity responses are indeed zero. This poses an interesting question. The visual system operates on photoreceptor input that encodes both brightness increases and decreases. The final product of the motion detection system is strongly half-wave rectified. Where does this selectivity arise, and how is it achieved?

Neural level

Some evidence has pointed toward the lamina. While fly photoreceptors are known to depolarize tonically in response to step illumination (Figure 10a), sharp-electrode recordings from monopolar cells in large flies reveal a high-pass filtered signal that phasically hyperpolarizes for ON and phasically depolarizes for OFF (Figure 10b). This is accompanied by persistent hyperpolarization throughout the illumination period (Laughlin and Hardie, 1978). The calcium level of L1 and L2 axon terminals in *Drosophila* is transiently responsive to both negative and positive changes in luminance, but there are indications of amplitude asymmetries in L2 that favor OFF stimuli as would be expected for inputs to the pathway terminating in T5 (Reiff et al., 2010; Clark et al., 2011). High-pass filtering followed by transmission of only positive or negative signals is a simple recipe for ON-OFF splitting. For instance, if presynaptic calcium channels in lamina projection neurons only open upon depolarization and remain closed for hyperpolarization, then transmitter release to downstream cells is restricted to one polarity (Figure 10c). Yet, more sustained lamina cells like L3 have been implicated as input elements to both ON and OFF motion computation, suggesting that signal rectification is not complete at the earliest level of pathway separation (Silies et al., 2013; Takemura et al., 2017).

Moreover, medulla cell recordings paint a somewhat fuzzy picture. In line with expectations and with only one exception (Mi9), response signs of signals are transformed by intermediate synapses such that ON pathway cells are activated by brightening stimuli and OFF pathway cells by darkening stimuli. Behnia et al. (2014) estimated rectification by fitting a linear-nonlinear cascade model to white-noise voltage responses of Mi1, Tm3, Tm1, and Tm2. Critically, none exhibited strong polarity-specificity. This was reflected by subsequent simulations. When putting empirical filters of, for instance, Mi1 and Tm3 into a Reichardt detector model, only mild selectivity for edge polarity was observed. This contrasts with our findings in T4 and T5 and suggests additional mechanisms. For instance, the non-linear step in T4 and T5 could be implemented in a way that enhances half-wave rectification. Moreover, Yang et al. (2016) compared membrane potential and calcium concentration under visual stimulation using genetically encoded indicators for both. They observed that calcium activity of motion-related medulla cells was more selective for ON or OFF than electrical activity, implicating the transformation between the two in the implementation of half-wave rectification.

Our measurements of OFF pathway input cells yielded three cells whose calcium activity was insensitive to ON edge stimulation. Tm9, however, encoded low-pass filtered brightness changes in both directions through increases and decreases of calcium levels. This demonstrates that information about both polarities remains available at the level of medulla terminals, which is further emphasized by the subsequent finding that one ON pathway cell increases its calcium levels for OFF stimuli (Arenz et al., 2017; Strother et al., 2017). Moreover, the degree of rectification appears to depend on the particular stimulation regime tested, with continuously varying stimuli like white-noise generally producing smaller asymmetries between ON and OFF response magnitudes than step inputs (Reiff et al., 2010; Clark et al., 2011; Behnia et al., 2014; Arenz et al., 2017). We quantified selectivity for polarity by stimulating with locally step-like edges. It would thus be worthwhile to additionally explore separation using other stimulus dynamics.

Algorithmic level

The question of rectification also affects quantitative descriptions of motion detection circuits. The two-quadrant model as proposed by Eichner et al. (2011) implemented pathway separation through high-pass filtering (or pseudo-differentiation) of positive brightness signals, adjustment of the response sign for ON or OFF subunits, and subsequent half-wave rectification to remove information about the other direction of change (see Figure 6d). This layout modeled response properties of L1 and L2 and corresponding silencing experiments effectively (Laughlin and Hardie, 1978; Joesch et al., 2010, 2013) but requires modifications in light of the updated circuit scheme. Given the filtering properties and strong blocking phenotype of Tm9, for instance, it is likely that a pure low-pass filter feeds into the T5 non-linearity. L3 is thought to supply tonic signals to both pathways (Silies et al., 2013; Takemura et al., 2017). Overall, the input structure appears to be much less clearly delineated than anticipated. To maintain polarity selectivity af-

ter the non-linearity while incorporating knowledge about the multi-input structure, additional rectification steps seem to be required.

Reverse-phi is yet another factor in need of reconciliation with the strong polarity selectivity we observed. Robust responses to spatiotemporal correlations of ON and OFF can be observed in tangential cells (Egelhaaf and Borst, 1992; Eichner et al., 2011) and optomotor behavior (Tuthill et al., 2011; Clark et al., 2011). In the two-quadrant detector, this is resolved by allowing for a small and positive tonic luminance component to feed into both sub-units (see also Kern and Egelhaaf, 2000). Interactions at the border of apparent motion steps, for instance, then result in negative responses for mixed-polarity combinations. Additionally, DC can account for retained sensitivity for apparent motion that is separated by extreme durations of more than 10 s, which exceed estimated neural time constants by orders of magnitude (Eichner et al., 2011). My optimization experiments using natural images revealed that limited DC enhances velocity estimation performance. Interestingly, this improvement was largely independent of scene statistics. It is possible that DC sensitivity adds to the robustness of output for noisy stimuli; minor ON-OFF interactions could mediate a noise cancellation mechanism that attenuates the impact of non-linearly amplified fluctuations. Neural evidence for retained DC sensitivity even in the responses of transient lines like Mi1 or Tm3 exists (Behnia et al., 2014). Additionally, our measurements in the OFF pathway as well as subsequent work clearly demonstrate the presence of tonic inputs to both T4 and T5, such as Mi4 or Tm9.

The DC model of reverse-phi responses appears to be in conflict with our observation that for edge stimulation, no cross-polarity responses occur for either T4 or T5. Given the minor weight of tonic sensitivity, it is possible that residual responses for the opposite edge polarity are too small to trigger calcium channels. Using voltage indicators to study sub-threshold events in T4 or T5 under mixed stimulation could provide critical evidence. In any case, the problem of how to integrate polarity selectivity and reverse-phi output awaits further investigation.

3.1.5 Sources of asymmetry

Both edge velocity tuning measured in tangential cells and optomotor responses elicited by a balanced edge stimulus confirmed that *Drosophila* motion pathways differ in temporal tuning. Optimal OFF edge velocities are larger than peak ON edge velocities. We could show that this was not due to electrophysiological consequences of differential adaptation state. The neural basis of these asymmetries is currently not clear. Behnia et al. (2014) showed similar delays for the two cell pairs they tested. However, it is now evident that T4 and T5 each derive motion-critical inputs from at least four input cells. Depending on how the non-linearity combines these inputs, a broad range of velocity optima is possible. Indeed, when Arenz et al. (2017) calculated temporal tuning for three-arm detectors based on all possible input combinations, they found that most T5 models had slightly higher peak frequencies than corresponding T4 models. Due to uncertainty about the exact division of labor among the numerous T4 and T5 inputs as well as the

biophysical implementation of the non-linearity, however, we can currently not yet pinpoint the exact mechanisms that give rise to a particular velocity tuning.

Measurements in T₄ and T₅ have so far not revealed the asymmetries that are clearly observed in downstream tangential cells. Our own data indicate a temporal frequency optimum of ≈ 1 Hz for both channels. Differences in stimulus statistics may contribute to these discrepancies. The transformation of inputs up to motion-selective stages is unlikely to be purely linear, so temporal characteristics could well be different for step-like edges when compared to dynamic noise or patterns like sine-wave gratings. Under this model, asymmetries would only emerge for particular stimulus conditions. Yet, [Arenz et al. \(2017\)](#) determined edge velocity tuning curves for T₄ and T₅ and again found little evidence for asymmetries. It is possible that small tuning differences are amplified through summation subsequent to initial motion computation. For instance, T₄ and T₅ responses peak for very slow edge velocities below 10° s^{-1} ; only spatiotemporal integration shifts them into the range of 100° s^{-1} to 300° s^{-1} which is observed at later stages.

3.1.6 Further elaborations

Recent inquiries into the neural circuitry of fly motion vision, including the studies that comprise this thesis, have made significant headway toward a neurally plausible model of how direction selectivity arises. Nonetheless, critical question marks remain. First, our algorithmic models are pure feedforward systems. There is substantial evidence in favor of multiplexed feedback from downstream stages modulating the activity of lamina and medulla ([Fischbach and Dittrich, 1989](#); [Takemura et al., 2017](#)). For instance, silencing lamina feedback neuron Lawf2 specifically alters the lower range of temporal frequency tuning in flight optomotor responses ([Tuthill et al., 2014](#)). It is possible that such projections are primarily useful for state-dependent modulation of response properties, but blocking feedback neurons C₂ and C₃ has been shown to affect the visual detection of gap width in exploring flies ([Triphan et al., 2016](#)). Feedback may conceivably underlie aspects of computation, so future investigations will have to incorporate these projections into their models of the circuit.

Lateral connections are currently equally under-explored. Our OFF pathway characterization of input neurons shows that most units are size-tuned, suggesting lateral inhibition. Indeed, spatial filters estimated from white-noise responses generally consist of an excitatory center and a subtractive surround ([Arenz et al., 2017](#)). For the L₂ pathway, some of this processing may already originate in the lamina ([Freifeld et al., 2013](#)). It is unclear whether lateral effects are purely subtractive or whether non-linear normalization also occurs. An interesting data point comes from Tm₉ which shows size-tuning as well as substantial full-field flicker responses. It is possible that non-linear, potentially divisive lateral inhibition is responsible for this effect ([Carandini and Heeger, 2012](#)). Anatomical mapping of the medulla offers several candidate cells whose ramifications span multiple columns ([Fischbach and Dittrich, 1989](#)). Elaborate signal normalization could help to

explain the peculiar contrast tuning exhibited by tangential cell and optomotor responses when flies are stimulated with natural images. Here, artificially imposed global changes in scene contrast, but not natural contrast variation, strongly modulates the amplitude of responses (see our work as well as [Straw et al., 2008](#)). This could be due to mechanisms that adjust the neural operating range locally but not globally.

3.2 COMPARATIVE VIEWS

3.2.1 Parallels to other visual systems

Motion detection represents a fundamental computation that underlies a multitude of behaviors in many species. Remarkably, work on the optomotor response in beetles and an investigation of direction selectivity in the rabbit retina both resulted in similar correlation-based algorithmic models: the Reichardt and Barlow-Levick detectors, respectively ([Hassenstein and Reichardt, 1956](#); [Barlow and Levick, 1965](#)). It stands to reason that not only phenomenology but also mechanism is conserved across animals. In the following section, I briefly discuss similarities between invertebrate and vertebrate motion vision at the level of neural implementation.

Genetic accessibility has made fruit fly and mouse key targets for tackling early mechanisms of motion vision (for thorough reviews, see [Borst and Helmstaedter, 2015](#); [Euler et al., 2014](#)). The mammalian retina is a layered, retinotopically organized structure that consists of photoreceptor layer, outer nuclear layer, outer plexiform (synaptic) layer, inner nuclear layer, inner plexiform layer, and ganglion cell layer. Light is transduced by two types of photoreceptors, cones and rods, which primarily but not exclusively specialize in day- and nighttime vision, respectively. Interestingly, the structure of the retina is anatomically inverted with respect to processing direction: incoming light passes all layers before it reaches the innermost receptors. Unlike the fly photoreceptor, rods and cones hyperpolarize in response to brightness increases. This means that in the absence of light, they constantly release glutamate (giving rise to the term "dark current"). The crucial downstream cell types are horizontal, bipolar, amacrine, and ganglion cells. Bipolar cells are the main relay between photoreceptors, which they contact in the outer plexiform layer, and ganglion cells, which they contact in the inner plexiform layer. Through the optic nerve, ganglion cell axons project to various downstream areas including the lateral geniculate nucleus of the thalamus from which visual signals reach cortex.

At the level of bipolar cells, a crucial parallel between invertebrate and vertebrate systems arises. As in lamina and medulla of the fly optic lobe, signals become separated into ON and OFF channels. OFF bipolar cell dendrites express glutamate-gated ion channels that depolarize the cell for brightness decreases. For ON bipolar cells, a metabotropic glutamate receptor reverses the sign of responses and thus depolarizes the cell for brightness increases. Bipolar cell projections in the inner plexiform layer are then stratified according to the transmitted contrast polarity. Bipolar cells implement substantial multiplexing of signals across at least 13 identified sub-types. This resem-

bles the large number of retinotopic medulla channels in the fly visual system. Almost each of these bipolar cell types densely tiles the retina, forming a grid that determines the system's spatial resolution. Ganglion cells generally pool from multiple bipolar cells, rendering the grid somewhat coarser, and can be subdivided into a large number of types based on anatomy and function. Recent high-throughput classification attempts, for instance, have identified more than 35 functionally distinct classes (Baden et al., 2016).

Within the outer plexiform layer, inhibitory horizontal cells mediate lateral interactions at the level of the photoreceptor-bipolar synapse. Similarly, inhibitory amacrine cells within the inner plexiform layer provide lateral connectivity among ganglion cells. These cells can roughly be divided into small-field, glycine-releasing and wide-field, GABA-releasing units.

At least three retinal ganglion cell types spike in a direction-selective fashion: four sub-types of polarity-unselective ON-OFF cells, each sensitive to a single cardinal direction; three sub-types of ON cells, which divide visual space into three equally spaced directions; and invariably upward-selective OFF JAM-B cells. So-called starburst amacrine cells are critically required for motion extraction in the ON-OFF type and have been found to be direction-selective themselves, with the preferred direction running from soma to tip of their circular dendritic tree. Interestingly, this radial arrangement means that starburst cells compute motion along many more directions than T4 or T5 which sample only four cardinal directions through their four appropriately aligned sub-types.

Starburst cells are now thought to be the stage where a delay-and-compare strategy is implemented, hinting at a further parallel to T4 and T5 cells in the fly visual system. Bipolar cell projections to the inner plexiform layer show a broad range of response kinetics, with slower characteristics dominating at the fringe and faster responses being prevalent toward the center of both ON and OFF layer (Baden et al., 2013). This bears a striking resemblance to the spectrum of temporal filters we measured for OFF input cells as well as more recent work on the full set of ON input cells (Arenz et al., 2017; Strother et al., 2017). Assuming that faster bipolar cells synapse with starburst cells near their dendritic tips while slower inputs connect close to the soma, an appropriate non-linearity could render these branches direction-selective. Indeed, reconstruction efforts have uncovered spatially precise connectivity that matches this scheme (Kim et al., 2014) which implies that a Reichardt-type facilitation scheme underlies direction selectivity in starburst cells. This layout lines up well with the elongated, multi-columnar structure of T4 dendrites as well as the spatial specificity of synapses made with asymmetrically filtered input lines (Takemura et al., 2017).

In visual cortex, direction selectivity is found in regions as early as V1 and propagated downstream to integration areas where increasingly abstract representations and global estimates of optic flow are computed (for a review of motion-critical primate area MT, see Born and Bradley, 2005). This processing stream could be construed as paralleling the pooling that occurs in the fly lobula plate. However, flow field sensitivities of fly tangential cells appear tightly coupled to particular visuomotor reflexes, casting doubt on the notion of abstraction. There is no clear consensus to what degree motion is computed *de novo* in the cortex, but evidence points toward a complex mix-

ture of newly generated and retina-inherited motion responses (Cruz-Martin et al., 2014).

3.2.2 ON and OFF processing

The separation of changes in sensory magnitude into increases and decreases is a leitmotif of my thesis. Throughout the four collected studies, we investigated both how and why this split occurs in the context of fly motion vision. Employing simulations and experiments, we were able to demonstrate that ON and OFF channels in *Drosophila* are differentially tuned and that these asymmetries may reflect tuning to natural stimulus statistics. Of course, the division of ON and OFF represents a ubiquitous principle that spans modalities and species. Examples include thermosensation in fruit flies (Gallio et al., 2011), olfactory processing in *C. elegans* (Chalasani et al., 2007), auditory processing in the rat (Scholl et al., 2010), and electrosensation in fish (Clarke et al., 2015). Moreover, separation of ON and OFF has been demonstrated in visual systems ranging from flies (Joesch et al., 2010) over mice (Euler et al., 2014), cats (Wässle, 2004), and primates (Field and Chichilnisky, 2007) to humans (Hashimoto et al., 2013). The sheer universality makes it likely that polarity-specific sensory computation confers general advantages that go beyond the requirements of isolated tasks.

First, I have discussed above that the biophysical implementation of a non-linearity that can compute ON-ON and OFF-OFF motion in one step would require exquisitely complicated physiological machinery. After all, this operation demands that very different inputs (for instance, correlated positive or negative changes in membrane potential) result in identical output. If incoming signals are restricted to one direction of possible change per pathway, the task reduces to a much more tractable problem. The fundamental issue of correlating signals is of course not restricted to motion vision. Barn owls, for instance, localize potential prey based on minute phase differences between acoustic signals impinging on their ears. This mechanism bears striking resemblance to how Reichardt-type models extract motion. There is strong evidence that coincidence detection of differentially delayed signals supports this ability in the owl (Jeffress, 1948; Carr and Konishi, 1988). Separate processing of ON and OFF may simplify computations of this type in other modalities.

Second, given the implementation cost incurred by a dual-pathway architecture, one may wonder why it is insufficient to just extract motion for one of the two polarities. As mentioned above, in most environments optic flow as generated by ego-motion around various body axes results in substantial ON as well as OFF motion. Visually confined objects, for instance, are usually represented by contrast changes of both polarities at their leading and trailing edges. Tangential cells would therefore be able to extract reasonably reliable flow fields from just T₄ or T₅ activity. However, the two motion pathways feed into multiple behaviorally relevant downstream circuits whose demands could well differ. A survival-critical example is the visually mediated escape response. Approaching objects or landmarks—in contradistinction to objects rotating around an observer—produce looming

optic flow that is defined by only one edge polarity. Only if ON and OFF motion are both extracted does the fly retain the ability to evade predators under all illumination conditions. In line with this, experiments have shown that T₄/T₅ block flies lose their ability to steer away from expanding stimuli (Schilling and Borst, 2015). Generally speaking, animals cannot afford to neglect approximately 50 % of all available sensory input.

Third, the natural statistics of any sensory modality can exhibit asymmetries between contrast polarities. Separate processing then gives the brain an opportunity to tailor response properties to the particular demands of positive and negative stimuli. My work on fruit fly motion vision offers one such example where differential temporal tuning appears to confer an adaptive advantage when estimating the velocity of a rigidly translating natural image. The causally relevant skewness of luminance in the real world also affects other visual tasks, so it is a distinct possibility that ON/OFF asymmetries in other organisms' visual systems serve a similar function. Chichilnisky and Kalmar (2002), for instance, observed timing differences, asymmetric levels of rectification, and varying receptive field sizes between ON and OFF retinal ganglion cells in the primate retina. In contradistinction to our observations, they found OFF cells to slightly lag their ON counterparts. A plethora of studies has now accumulated substantial evidence for functional asymmetries between ON and OFF in vertebrate systems (Copenhagen et al., 1983; Zemon et al., 1988; Zaghoul et al., 2003; Gollisch and Meister, 2008; Yeh et al., 2009; Pandarinath et al., 2010; Jin et al., 2011; Burkhardt, 2011). Physiologically, a difference in temporal kinetics between ON and OFF responses originates immediately at the level of photoreceptor synapses. As outlined above, OFF bipolar cells receive input via fast ionotropic receptors while ON units rely on slower metabotropic receptors. Remarkably, there is evidence that these asymmetries persist up to the level of visual cortex and even perceptual decisions, so a functional role seems probable (Komban et al., 2014). Most of these studies used flash stimuli and did not specifically focus on motion processing in retina or cortex. It will be interesting to see whether the specific asymmetries we report transfer to other species. In general, the task-centric perspective could shed light on why functional differences propagate to higher processing stages.

Fourth and finally, considerations from information theory provide a principled reason for why dual-channel processing is preferential. In order to code changes in both directions of interest using a single output, sensory cells have to maintain intermediate activity levels even in the absence of salient stimuli. Gjorgjieva et al. (2014) studied information transmission in either single polarity systems consisting of two ON units or mixed ON-OFF configurations. Interestingly, both exhibited identical maximum information rates when their peak firing rate was constrained. However, the ON-OFF system required substantially fewer spikes for the same task. The observed gain in efficiency was even larger when the stimulus distribution contained rare but large sensory events. A key advantage of separate ON and OFF processing may therefore be metabolic efficiency, a goal that ultimately constrains all sensory systems.

3.3 BEHAVIORAL INVESTIGATION OF NEURAL CIRCUITS

One of my core contributions to the papers of this cumulative thesis was experimental work on genetically manipulated walking flies. Behavioral assays enjoy a long tradition in the research of neural systems, going back to cyberneticists following von Uexküll, Wiener, and many others. Teasing apart the internal rules that govern an organism's behavior through observations of behavioral input-output relationships offers a principled way of studying information-processing apparatuses. However, it is also subject to certain limitations, particularly when investigating intermediate neural representations. The genetic methods outlined in the introduction and used throughout the main part have greatly improved this aspect of behavioral experiments. In the following section, I discuss various pitfalls and advantages of the behavioral approach as applied to sensory neuroscience.

3.3.1 Visuomotor transformation

Of chief interest throughout my doctoral work was the algorithmic and neural structure of the elementary motion detector in *Drosophila*. Behind the approach taken lay the assumption that optomotor responses of walking or flying flies represent a faithful read-out of activity in circuits close to the sensory periphery. To a certain extent, this supposition holds. As seen in the exposition, motion-driven locomotion recapitulates many response features of LPTCs or T4 and T5 activity, like tuning to temporal frequency or dependency on contrast. However, it is essential to note that the output of local motion detectors goes through a complex and lengthy cascade of additional processing steps.

There is now significant evidence for the causal link between tangential cell responses and subsequent motor output. Early lesion studies and experiments on mutants with abnormal lobula plate elements could show that resulting optomotor deficits were severe and specific (Heisenberg et al., 1978; Geiger and Nässel, 1981; Hausen and Wehrhahn, 1983). Naturally, these manipulations were too coarse to establish precise links between particular LPTCs and behavioral capability. Recently, genetic experiments on GAL4-targeted tangential cells have advanced the state of the art. As for sufficiency, Haikala et al. (2013) demonstrated that optogenetic activation of HS cells elicits yaw movements of head and body in tethered flying *Drosophila*. The response sign depended on the stimulation side in a predictable manner. With regard to necessity, Kim et al. (2017) used UAS-Kir2.1 to disrupt signalling in HS and VS cells and found yaw-induced head motion to be completely abolished. Interestingly, they only observed a partial reduction of motion-dependent wing beat differences. This hints at additional complexity and may implicate additional sets of LPTCs in the control of flight maneuvers.

While lobula plate output appears critically required for the optomotor response, LPTCs are not true pre-motor neurons; signals are further filtered, gated, and gathered by downstream stages. A substantial part of our knowledge concerning the connections between optic lobe and motor circuits con-

trolling walking or flying comes from studies on larger flies (Strausfeld and Bassemir, 1985; Strausfeld and Gronenberg, 1990; Haag et al., 2007; Wertz et al., 2008). It is now clear that many features of downstream projections are indeed conserved in the fruit fly (for instance, see Suver et al., 2016). In addition to projections to head motor systems, axons of lobula plate neurons ramify in the so-called posterior slope of the central brain. From here, neurons target the thoracic ganglion and ventral nerve cord. These parts of the nervous system house the motor control centers that guide whole-body steering efforts. Note that lobula plate projections form but a small part of the estimated 1100 descending neurons in the fruit fly (Hsu and Bhandawat, 2016).

There is ample evidence that post-LPTC machinery implements non-trivial processing as part of the visuomotor transformation. For *Calliphora vicina*, Wertz et al. (2009) could show that descending neurons of the ocellar and vertical system (DNOVS) render the coding of optic flow associated with particular body rotations more robust when compared to their upstream inputs, VS cells. Non-linear gating through other sensory modalities like wind as well as behavioral state was revealed by experiments on visual properties of ventral cervical nerve motor neurons (Haag et al., 2010). In the fruit fly, work by Suver et al. (2016) suggests that a set of DNOVS-like descending neurons computes specific linear combinations of VS and HS inputs and is directly associated with stereotyped motor programs. Yet another example for a presumably motion-driven descending unit is the giant fiber neuron that triggers rapid evasive take-offs in response to looming (von Reyn et al., 2014). Finally, the mapping between sensorimotor and flight muscle commands indicates remarkable multiplexing into large, phasically active actuators that mediate rapid turns and small, tonically active actuators that mediate continuous small-scale turning (Lindsay et al., 2017).

For models of elementary motion detection derived from behavioral assays, this poses a challenge. Visuomotor processing may well affect our conclusions about peripheral sensory mechanisms. However, past success justifies the approach: despite the apparent complexity, simplistic approximations of the transform have enabled the development of influential models like the Reichardt detector (Hassenstein and Reichardt, 1956). These models have proven intriguingly adept at explaining even primary stages of computation. Critically, early sensory networks represent bottlenecks. Many fundamental tuning properties are thus necessarily inherited by the ensuing cascade that gives rise to motor commands. Particularly in combination with genetic approaches, we can use the optomotor response as a powerful read-out of detector activity and draw conclusions about mechanisms of direction selectivity. Behavioral experiments in this thesis have generally replicated tangential cell phenotypes; the velocity-specific impairment following blockage of Tm3 is a noteworthy example.

3.3.2 State dependencies

Flies are dynamic animals that navigate a dynamic world. For reasons of both efficiency and effectiveness, sensory systems ought to adjust their prop-

erties to current behavioral demands. This implies that the visual system of the fly is not a static feedforward processor. State-dependencies severely complicate the investigation of visual mechanisms, especially when using behavioral tools for circuit mapping. Expectations about visual statistics affect fly behavior on several timescales. Our work on adaptation through tuning asymmetries presumably operates on the slowest, evolutionary ones. In the following, I discuss shorter-term modulation.

Slow adjustment

Behavioral modes critically influence expected visual statistics. The average velocity of rotational optic flow, for instance, greatly differs between rest, walking, and flight. To maximize the impact of the optomotor system and avoid saturation, motion circuits should adjust their operating range depending on the current state of the animal. A fundamental observation with regard to such modulations is the almost tenfold difference between frequency optima determined in LPTCs of immobile flies and walking or flying animals (Joesch et al., 2008; Duistermars et al., 2007).

Several studies have tracked state-dependent visual properties in the fly optic lobe. Chiappe et al. (2010) used calcium imaging to measure frequency tuning curves in HS cells of fruit flies walking on a treadmill set-up. During walking, LPTC responses increased substantially and particularly at high frequencies. In a closely related study, Maimon et al. (2010) recorded from VS cells during tethered flight. Locomotor activity boosted response gain and lowered passive membrane resistance. LPTCs in large flies are subject to similar modulations of temporal response curves, especially at large stimulus frequencies expected during flight (Jung et al., 2011). Intriguingly, the latter study was able to mimic the active behavioral state via ectopic application of an octopamine agonist, chlordimeform (CDM). The neuromodulator octopamine appears to be the crucial mediator of state throughout the fly nervous system. Suver et al. (2012) could alter temporal tuning in the fruit fly by genetically silencing or activating octopaminergic projection neurons.

Intriguingly, the effects of state modulation are measurable even at early stages of visual processing (Arenz et al., 2017). After CDM was applied, both T₄ and T₅ shifted their sensitivity toward higher stimulus frequencies and temporal filter properties of all tested medulla inputs sped up. This is not entirely surprising: in a correlation-based model, velocity tuning is not affected by response filtering subsequent to the non-linearity that gives rise to direction selectivity. Nonetheless, it is an impressive demonstration for the malleability and flexibility of sensory circuits in the fly.

More generally, the finding that even peripheral processing is affected by behavioral variables casts doubt on the notion that sensory and motor processing is separable at a neural level. LPTCs are often described as matched filters for optic flow that feed into motor circuits (Krapp and Hengstenberg, 1996). However, there are strong indications that HS cells additionally encode an estimate of walking speed (Fujiwara et al., 2017). Given these data, it appears that even the optic lobe is better described as a visuomotor area than a purely visual one. This design principle is sensible when considering the minuscule size of the fly brain. If the number of neurons is limited, early spe-

cialization and optimizing for behavioral relevance are advantageous. Note that research on mice has uncovered motor signals in primary visual cortex (Keller et al., 2012; Saleem et al., 2013), so significantly larger brains appear to follow comparable design principles.

Fast adjustment

Drosophila flight is separated into at least two locomotor motifs: straight, continuous flight and rapid saccades. For most of the flight duration, flies maintain straight heading. These segments are interrupted by extremely fast adjustments of trajectory; within milliseconds, flies turn at an approximately right angle and easily reach speeds of thousands of degrees per second (Mronz and Lehmann, 2008; Straw et al., 2011; Muijres et al., 2014). Interestingly, body saccades appear to be both spontaneous and triggered by visual input (Tammero and Dickinson, 2002; Mronz and Lehmann, 2008; Censi et al., 2013). Saccade-like high-velocity turning is observed even in tethered flight (Götz, 1968). Of course, the presence of the optomotor system then poses a problem. If the fly turns to the right voluntarily, the resulting optic flow would evoke a reflex that directly counteracts the saccade and keeps the animal on a straight course.

Several potential solutions for this challenge have been devised. First, the frequency optimum of the optomotor response may weaken its effect on saccadic turns. If a rotation is sufficiently fast, resulting optic flow exceeds the sensitive range of the motion detector and no response is generated. However, natural scenes have significant power in the range of large spatial wavelengths, so even at high turning velocities residual reflexive locomotion could hamper the fly's ability to reorient. Second, an influential model for how stabilizing feedback loops can be reconciled with voluntary perturbation is the notion of efference copies, which goes back to von Helmholtz (1867) and was refined by von Holst and Mittelstaedt (1950). The optomotor reflex represents a simple control loop that mitigates deviations from a set point. By taking into account the sensory feedback that is expected from a motor command when computing these deviations, internally generated turns can be passed through. Indeed, Kim et al. (2015) described motor-related potentials in LPTCs whose sign and timing were such that they would cancel visual signals generated through saccade-like voluntary turns. There are now indications that these potentials do not represent a blanket shutdown of all LTPC activity for the duration of the saccade. Instead, they are precisely targeted to the lobula plate units for which any given flight maneuver would produce undesirable output (Kim et al., 2017). Other tangential cells retain their ability to suppress unwanted perturbations for the duration.

3.3.3 Motion detectors as feedback sensors

As mentioned above, optomotor responses implement a stabilizing system that prevents course deviations through visual feedback (Götz, 1965). In an important sense, motion-sensitive elements in the lobula plate thus act as the

sensors of a simple controller, signalling the error that downstream motor command centers attempt to reduce.

During my simulations as part of the investigation of asymmetries between ON and OFF, I used a tractable objective function to optimize the performance of the Reichardt-type model: correlation between the velocity of a rigidly translating visual scene and average detector output. At the surface level, this seems sensible; a reliable estimate of true rotational velocity allows for precisely controlled countermeasures. However, I did not analyze optimality in the context of a dynamical system like the optomotor feedback controller. [Warzecha and Egelhaaf \(1996\)](#), for instance, studied stabilization behavior of tethered flying flies in artificial visual environments and argued that non-proportional velocity tuning helps stabilizing the feedback loop by suppressing large oscillations. Constraints of this type only emerge in closed-loop settings. It would be of interest to optimize detector parameters in a feedback regime and compare results to the open-loop tuning I performed.

Feedback controllers are prevalent throughout many engineering disciplines. A particularly popular approach makes use of so-called PID controllers ([Astrom and Murray, 2008](#)). They base their corrective output on three parallel signals: one proportional to the current error; one that integrates the error and thus guarantees that the system approaches zero for constant deviations; and one that differentiates the error, which effectively implements a type of predictive counteraction. There is substantial evidence for proportional but little for differential control in the fly. [Schnell et al. \(2014\)](#) recently suggested that integration of motion-evoked calcium levels occurs in the terminals of HS cells. This clashes with our observation that walking flies do not fully counteract externally imposed offset from straight heading in closed-loop experiments. If the corrective signal was truly integrative, steady-state deviations should eventually go to zero. It seems conceivable that the observed effects are due to strong temporal low-pass filtering instead.

The relationship between LPTC response and magnitude of locomotor output appears to be strongly amplifying: even small depolarizations or "errors" can result in substantial turning vigor. This transfer function ensures that the feedback controller has appropriate gain even under adverse signal conditions. However, it may well mask silencing phenotypes if the block is not complete. Intermediate residual activity then affords virtually unchanged behavioral output. Yet, through appropriately designed stimuli, the robustness of the transformation can be put to use by exploiting it to amplify a phenotype of interest. Throughout the studies of this thesis, I employed balanced motion stimuli (modified from [Clark et al., 2011](#)) which consisted of continuously resetting ON and OFF edges that simultaneously drifted in opposite directions. Wild-type LPTC signals are then approximately zero because functional ON and OFF channels cancel each other. Only when the two pathways diverge do motion responses arise. Even small phenotypes are then amplified by the compressive transfer function. This way, we were able to detect ON/OFF asymmetries as well as phenotypes induced by silencing of T4 and T5 input cells. Indeed, the amplification effect may even confer increased sensitivity over direct LPTC measurements; a subtle velocity-specific effect was observed when blocking Tm2, which disproportionately affected

higher velocities compared to Tm1, Tm4, and Tm9. Moreover, comparing the magnitudes of tangential cell and behavioral block phenotypes for the OFF pathway allowed us to quantify the transformation in detail. This revealed a clearly non-linear relationship that hinted at logarithmic visuomotor transformation.

3.3.4 Post-hoc approaches

All experimental assays I applied to the problem of motion detection were fundamentally interventionist in nature. By varying visual input in concert with targeted genetic manipulations, we were able to characterize response properties and build models of the circuit. Laboratory experiments always run the risk of distilling artificial behavioral motifs or pushing neural circuitry into synthetic regimes that do not reflect ethological function (Krakauer et al., 2017). As mentioned in the introduction, the choice of causal intervention often determines what we can get out of a non-linear system. We only ever see particular projections, and these projections may or may not reflect the system's true nature.

Recently, post-hoc perspectives have again gained traction (Gomez-Marin et al., 2014). Instead of manipulating organisms, one could track natural behavior in great detail and infer patterns or even mechanisms after the fact. This ethological approach is greatly simplified by state of the art methods for observing, recording, and analyzing complex behavioral sequences. Advances in machine learning have been particularly important in this development as they allow the rigorous extraction of patterns in high-dimensional representations (for instance, see Kabra et al., 2013). Branson et al. (2009) analyzed *Drosophila* behavior in a high-throughput screen by applying statistical methods to time-resolved walking traces. Interestingly, it was possible to identify the genotypes of flies after the fact purely based on these observations. It would be worthwhile to apply these methods to motion-guided visual behavior as it could simplify the search for neural candidates. Yet, for clearly defined behavioral motifs like the motion-guided responses under study here, the interventionist method takes clear precedence.

3.4 OUTLOOK

In the course of my work on fly motion vision, I could contribute toward a neural understanding of optomotor behavior and investigated how neural circuitry is shaped by its natural context. The emerging neural layout exhibits intriguing complexity, with a larger than expected number of cells determining the responses of elementary motion detectors. Fly motion vision thus represents a compelling example for the multifaceted interplay between neural processing systems and their environment.

From here on, several lines of inquiry suggest themselves. First, the exact functional division among T4 and T5 input cells remains unclear and many hypotheses are based on mere compatibility. The combination of high-precision read-outs like telescopic stimulation and genetic silencing of in-

dividual input neurons may yield further insight into the mechanisms that produce preferred direction enhancement and null direction suppression. Molecular and physiological investigation of the functional properties of synapses that connect input arms to T₄ or T₅ dendrites will be equally critical in this endeavor. Recent innovations in the design of genetically encoded voltage indicators could further illuminate the sub-threshold processes that ultimately generate direction selectivity. Finally, optogenetic activation has shed some light on non-linear interactions among T₄ inputs (Strother et al., 2017). Artificial induction of realistic motion responses using patterned optogenetic illumination would be a significant step toward mechanistic understanding, putting a physiological spin on the idea that we do not understand a system until we can build it ourselves.

Second, at the behavioral level, a broadening of the range of stimuli used to probe the optomotor response is required. During our characterization of Mi₁ and Tm₃ as well as Tm₁, Tm₂, Tm₄, and Tm₉, we only scanned a single parameter: pattern velocity. In the OFF pathway, this was of course motivated by the differential temporal tuning we had observed in calcium responses. However, it is possible that functional separation runs along other lines such as luminance or contrast. This may be particularly relevant for the question of why there are more than three input cells per pathway; a potential modulatory function of the fourth arm could be restricted to specific stimulus regimes.

Third, we focused on velocity estimation when optimizing detector parameters in the context of temporal asymmetries between ON and OFF. The activity of elementary motion detectors is likely to underlie a multitude of tasks in addition to the optomotor response, like looming-triggered escape or even depth perception (Schilling and Borst, 2015; Schwegmann et al., 2014). Exploring the constraints imposed by these behavioral programs could help to unravel the intricacies of the *Drosophila* optic lobe. It is testament to the complexity of seemingly tractable fly brains that despite all progress, we have not run out of fundamental questions to ask.

BIBLIOGRAPHY

Adelson, E. H. and J. R. Bergen

1985. Spatiotemporal energy models for the perception of motion. *Journal of the Optical Society of America. A, Optics and image science*, 2(2):284–299.

Adelson, E. H. and J. A. Movshon

1982. Phenomenal coherence of moving visual patterns. *Nature*, 300(5892):523–525.

Adrian, E. D.

1928. *The Basis of Sensation*. WW Norton & Co.

Ammer, G., A. Leonhardt, A. Bahl, B. J. Dickson, and A. Borst

2015. Functional Specialization of Neural Input Elements to the *Drosophila* ON Motion Detector. *Current Biology*, 25(17):2247–2253.

Anstis, S. M.

1970. Phi movement as a subtraction process. *Vision Research*, 10(12):1411–1430.

Anstis, S. M. and B. J. Rogers

1975. Illusory reversal of visual depth and movement during changes of contrast. *Vision Research*, 15:957–961.

Aptekar, J. W. and M. A. Frye

2013. Higher-order figure discrimination in fly and human vision. *Current Biology*, 23(16):694–700.

Arenz, A., M. S. Drews, F. G. Richter, G. Ammer, and A. Borst

2017. The Temporal Tuning of the *Drosophila* Motion Detectors Is Determined by the Dynamics of Their Input Elements. *Current Biology*, 27(7):929–944.

Arnold, G.

1974. Rheotropism in fishes. *Biological Reviews*, 49(4):515–576.

Astrom, K. J. and R. M. Murray

2008. *Feedback Systems: An Introduction for Scientists and Engineers*. Princeton, NJ, USA: Princeton University Press.

Atick, J. J. and A. N. Redlich

1992. What Does the Retina Know about Natural Scenes? *Neural Computation*, 4(2):196–210.

Attneave, F.

1954. Some informational aspects of visual perception. *Psychological Review*, 61(3):183–193.

- Baden, T., P. Berens, M. Bethge, and T. Euler
2013. Spikes in mammalian bipolar cells support temporal layering of the inner retina. *Current Biology*, 23(1):48–52.
- Baden, T., P. Berens, K. Franke, M. Roman Roson, M. Bethge, and T. Euler
2016. The functional diversity of retinal ganglion cells in the mouse. *Nature*, 529(7586):345–350.
- Bahl, A., G. Ammer, T. Schilling, and A. Borst
2013. Object tracking in motion-blind flies. *Nature Neuroscience*, 16(6):730–738.
- Bahl, A., E. Serbe, M. Meier, G. Ammer, and A. Borst
2015. Neural Mechanisms for *Drosophila* Contrast Vision. *Neuron*, 88(6):1240–1252.
- Baines, R. A., J. P. Uhler, A. Thompson, S. T. Sweeney, and M. Bate
2001. Altered electrical properties in *Drosophila* neurons developing without synaptic transmission. *Journal of Neuroscience*, 21(5):1523–1531.
- Barlow, H.
1961. Possible principles underlying the transformation of sensory messages. In *Sensory Communication*, W. A. Rosenblith, ed. Cambridge: MIT Press.
- Barlow, H. and W. R. Levick
1965. The mechanism of directionally selective units in rabbit's retina. *Journal of Physiology*, 178(3):477.
- Barnett, P. D., K. Nordström, and D. C. O'Carroll
2007. Retinotopic organization of small-field-target-detecting neurons in the insect visual system. *Current Biology*, 17(7):569–578.
- Bath, D. E., J. R. Stowers, D. Hormann, A. Poehlmann, B. J. Dickson, and A. D. Straw
2014. FlyMAD: rapid thermogenetic control of neuronal activity in freely walking *Drosophila*. *Nature Methods*, 11(7):756–762.
- Bausenwein, B., A. P. Dittrich, and K. F. Fischbach
1992. The optic lobe of *Drosophila melanogaster*. II. Sorting of retinotopic pathways in the medulla. *Cell and Tissue Research*, 267(1):17–28.
- Bausenwein, B. and K. F. Fischbach
1992. Activity labeling patterns in the medulla of *Drosophila melanogaster* caused by motion stimuli. *Cell and Tissue Research*, 270(1):25–35.
- Behnia, R., D. A. Clark, A. G. Carter, T. R. Clandinin, and C. Desplan
2014. Processing properties of ON and OFF pathways for *Drosophila* motion detection. *Nature*, 512(7515):427–430.
- Bell, A. and T. Sejnowski
1997. The "independent components" of natural scenes are edge filters. *Vision Research*, 37(23):3327–3338.

- Benzer, S.
1967. Behavioral mutants of *Drosophila* isolated by countercurrent distribution. *Proceedings of the National Academy of Sciences of the United States of America*, 58(3):1112–1119.
- Bialek, W., F. Rieke, R. R. de Ruyter van Steveninck, and D. Warland
1991. Reading a neural code. *Science*, 252(5014):1854–1857.
- Bishop, C. M.
2006. *Pattern Recognition and Machine Learning (Information Science and Statistics)*. Secaucus, NJ, USA: Springer-Verlag New York, Inc.
- Bishop, L. G. and D. G. Keehn
1967. Neural correlates of the optomotor response in the fly. *Kybernetik*, 3(6):288–295.
- Blondeau, J. and M. Heisenberg
1982. The three-dimensional optomotor torque system of *Drosophila melanogaster*. *Journal of Comparative Physiology. A, Neuroethology, Sensory, Neural, and Behavioral Physiology*, 145(3):321–329.
- Bloomquist, B. T., R. D. Shortridge, S. Schneuwly, M. Perdew, C. Montell, H. Steller, G. Rubin, and W. L. Pak
1988. Isolation of a putative phospholipase C gene of *Drosophila*, *norpA*, and its role in phototransduction. *Cell*, 54(5):723–733.
- Bohm, R. A., W. P. Welch, L. K. Goodnight, L. W. Cox, L. G. Henry, T. C. Gunter, H. Bao, and B. Zhang
2010. A genetic mosaic approach for neural circuit mapping in *Drosophila*. *Proceedings of the National Academy of Sciences of the United States of America*, 107(37):16378–16383.
- Born, R. T. and D. C. Bradley
2005. Structure and function of visual area MT. *Annual Review of Neuroscience*, 28:157–189.
- Borst, A.
1986. Time course of the houseflies' landing response. *Biological Cybernetics*, 54(6):379–383.
- Borst, A.
2007. Correlation versus gradient type motion detectors: the pros and cons. *Philosophical Transactions of the Royal Society B: Biological Sciences*, 362(1479):369–374.
- Borst, A.
2009. *Drosophila's* view on insect vision. *Current Biology*, 19(1):36–47.
- Borst, A.
2014. Fly visual course control: behaviour, algorithms and circuits. *Nature Reviews Neuroscience*, 15(9):590–599.

- Borst, A. and S. Bahde
1986. What kind of movement detector is triggering the landing response of the housefly? *Biological Cybernetics*, 55(1):59–69.
- Borst, A. and M. Egelhaaf
1989. Principles of visual motion detection. *Trends in Neurosciences*, 12(8):297–306.
- Borst, A. and M. Egelhaaf
1990. Direction selectivity of blowfly motion-sensitive neurons is computed in a two-stage process. *Proceedings of the National Academy of Sciences of the United States of America*, 87(23):9363–9367.
- Borst, A. and T. Euler
2011. Seeing things in motion: models, circuits, and mechanisms. *Neuron*, 71(6):974–994.
- Borst, A., V. L. Flanagan, and H. Sompolinsky
2005. Adaptation without parameter change: Dynamic gain control in motion detection. *Proceedings of the National Academy of Sciences of the United States of America*, 102(17):6172–6176.
- Borst, A. and J. Haag
2002. Neural networks in the cockpit of the fly. *Journal of Comparative Physiology. A, Neuroethology, Sensory, Neural, and Behavioral Physiology*, 188(6):419–437.
- Borst, A., J. Haag, and D. F. Reiff
2010. Fly motion vision. *Annual Review of Neuroscience*, 33:49–70.
- Borst, A. and M. Helmstaedter
2015. Common circuit design in fly and mammalian motion vision. *Nature Neuroscience*, 18(8):1067–1076.
- Borst, A., C. Reisenman, and J. Haag
2003. Adaptation of response transients in fly motion vision. II: Model studies. *Vision Research*, 43(11):1309–1322.
- Borst, A. and F. E. Theunissen
1999. Information theory and neural coding. *Nature Neuroscience*, 2(11):947–957.
- Borst, A. and F. Weber
2011. Neural action fields for optic flow based navigation: a simulation study of the fly lobula plate network. *PLoS ONE*, 6(1):e16303.
- Boyden, E. S., F. Zhang, E. Bamberg, G. Nagel, and K. Deisseroth
2005. Millisecond-timescale, genetically targeted optical control of neural activity. *Nature Neuroscience*, 8(9):1263–1268.
- Brady, N. and D. J. Field
2000. Local contrast in natural images: normalisation and coding efficiency. *Perception*, 29(9):1041–1055.

- Braitenberg, V.
1967. Patterns of projection in the visual system of the fly. I. Retina-lamina projections. *Experimental Brain Research*, 3(3):271–298.
- Braitenberg, V. and C. T. Ferretti
1966. Landing reaction of *Musca domestica* induced by visual stimuli. *Naturwissenschaften*, 53(6):155.
- Brand, A. H. and N. Perrimon
1993. Targeted gene expression as a means of altering cell fates and generating dominant phenotypes. *Development*, 118(2):401–415.
- Branson, K., A. A. Robie, J. Bender, P. Perona, and M. H. Dickinson
2009. High-throughput ethomics in large groups of *Drosophila*. *Nature Methods*, 6(6):451–457.
- Brenner, N., W. Bialek, and R. R. de Ruyter van Steveninck
2000. Adaptive rescaling maximizes information transmission. *Neuron*, 26(3):695–702.
- Briggman, K. L., M. Helmstaedter, and W. Denk
2011. Wiring specificity in the direction-selectivity circuit of the retina. *Nature*, 471(7337):183–188.
- Buchner, E.
1976. Elementary movement detectors in an insect visual system. *Biological Cybernetics*, 24(2):85–101.
- Buchner, E., S. Buchner, and I. Bülthoff
1984. Deoxyglucose mapping of nervous activity induced in *Drosophila* brain by visual movement. *Journal of Comparative Physiology. A, Neuroethology, Sensory, Neural, and Behavioral Physiology*, 155(4):471–483.
- Bülthoff, H., K. G. Götz, and M. Herre
1982. Recurrent inversion of visual orientation in the walking fly, *Drosophila melanogaster*. *Journal of Comparative Physiology. A, Neuroethology, Sensory, Neural, and Behavioral Physiology*, 148(4):471–481.
- Burkhardt, D. A.
2011. Contrast processing by ON and OFF bipolar cells. *Visual Neuroscience*, 28(1):69–75.
- Büttner, U. and O. Kremmyda
2007. Smooth pursuit eye movements and optokinetic nystagmus. *Developments in Ophthalmology*, 40:76–89.
- Cadieu, C. F., H. Hong, D. L. K. Yamins, N. Pinto, D. Ardila, E. A. Solomon, N. J. Majaj, and J. J. DiCarlo
2014. Deep neural networks rival the representation of primate IT cortex for core visual object recognition. *PLoS Computational Biology*, 10(12):e1003963.

- Carandini, M. and D. J. Heeger
2012. Normalization as a canonical neural computation. *Nature Reviews Neuroscience*, 13(1):51–62.
- Card, G. and M. H. Dickinson
2008. Visually mediated motor planning in the escape response of *Drosophila*. *Current Biology*, 18(17):1300–1307.
- Carpenter, F. W.
1905. The reactions of the pomace fly (*Drosophila ampelophila* Loew) to light, gravity, and mechanical stimulation. *The American Naturalist*, 39(459):157–171.
- Carr, C. E. and M. Konishi
1988. Axonal delay lines for time measurement in the owl's brainstem. *Proceedings of the National Academy of Sciences of the United States of America*, 85(21):8311–8315.
- Censi, A., A. D. Straw, R. W. Sayaman, R. M. Murray, and M. Dickinson
2013. Discriminating External and Internal Causes for Heading Changes in Freely Flying *Drosophila*. *PLoS Computational Biology*, 9(2):e1002891–14.
- Chalasani, S. H., N. Chronis, M. Tsunozaki, J. M. Gray, D. Ramot, M. B. Goodman, and C. I. Bargmann
2007. Dissecting a circuit for olfactory behaviour in *Caenorhabditis elegans*. *Nature*, 450(7166):63–70.
- Chalfie, M., Y. Tu, G. Euskirchen, W. W. Ward, and D. C. Prasher
1994. Green fluorescent protein as a marker for gene expression. *Science*, 263(5148):802–805.
- Chen, T.-W., T. J. Wardill, Y. Sun, S. R. Pulver, S. L. Renninger, A. Baohan, E. R. Schreiter, R. A. Kerr, M. B. Orger, V. Jayaraman, L. L. Looger, K. Svoboda, and D. S. Kim
2013. Ultrasensitive fluorescent proteins for imaging neuronal activity. *Nature*, 499(7458):295–300.
- Chiappe, M. E., J. D. Seelig, M. B. Reiser, and V. Jayaraman
2010. Walking modulates speed sensitivity in *Drosophila* motion vision. *Current Biology*, 20(16):1470–1475.
- Chichilnisky, E. J. and R. S. Kalmar
2002. Functional asymmetries in ON and OFF ganglion cells of primate retina. *Journal of Neuroscience*, 22(7):2737–2747.
- Chubb, C. and G. Sperling
1989. Two motion perception mechanisms revealed through distance-driven reversal of apparent motion. *Proceedings of the National Academy of Sciences of the United States of America*, 86(8):2985–2989.
- Clark, D. A., L. Bursztyn, M. A. Horowitz, M. J. Schnitzer, and T. R. Clanin
2011. Defining the computational structure of the motion detector in *Drosophila*. *Neuron*, 70(6):1165–1177.

- Clark, D. A., J. E. Fitzgerald, J. M. Ales, D. M. Gohl, M. A. Silies, A. M. Norcia, and T. R. Clandinin
2014. Flies and humans share a motion estimation strategy that exploits natural scene statistics. *Nature Neuroscience*, 17(2):296–303.
- Clarke, S. E., A. Longtin, and L. Maler
2015. Contrast coding in the electrosensory system: parallels with visual computation. *Nature Reviews Neuroscience*, 16(12):733–744.
- Cooper, E. A. and A. M. Norcia
2015. Predicting cortical dark/bright asymmetries from natural image statistics and early visual transforms. *PLoS Computational Biology*, 11(5):e1004268.
- Copenhagen, D. R., J. F. Ashmore, and J. K. Schnapf
1983. Kinetics of synaptic transmission from photoreceptors to horizontal and bipolar cells in turtle retina. *Vision Research*, 23(4):363–369.
- Cover, T. M. and J. A. Thomas
2006. *Elements of Information Theory (Wiley Series in Telecommunications and Signal Processing)*. Wiley-Interscience.
- Cruz-Martin, A., R. N. El-Danaf, F. Osakada, B. Sriram, O. S. Dhande, P. L. Nguyen, E. M. Callaway, A. Ghosh, and A. D. Huberman
2014. A dedicated circuit links direction-selective retinal ganglion cells to the primary visual cortex. *Nature*, 507(7492):358–361.
- Dan, Y., J. J. Atick, and R. C. Reid
1996. Efficient coding of natural scenes in the lateral geniculate nucleus: experimental test of a computational theory. *Journal of Neuroscience*, 16(10):3351–3362.
- Darwin, C.
1859. *On the Origin of Species*. New York: D. Appleton and Co.
- Dayan, P. and L. F. Abbott
2001. *Theoretical Neuroscience*. Cambridge, MA: MIT Press.
- de Ruyter van Steveninck, R. R., G. D. Lewen, S. P. Strong, R. Koberle, and W. Bialek
1997. Reproducibility and variability in neural spike trains. *Science*, 275(5307):1805–1808.
- de Vries, S. E. and T. R. Clandinin
2012. Loom-sensitive neurons link computation to action in the *Drosophila* visual system. *Current Biology*, 22(5):353–362.
- Deisseroth, K.
2011. Optogenetics. *Nature Methods*, 8(1):26–29.
- Denk, W. and H. Horstmann
2004. Serial block-face scanning electron microscopy to reconstruct three-dimensional tissue nanostructure. *PLoS Biology*, 2(11):e329.

- Denk, W., J. H. Strickler, and W. W. Webb
1990. Two-photon laser scanning fluorescence microscopy. *Science*, 248(4951):73–76.
- DeVoe, R. D.
1980. Movement sensitivities of cells in the fly's medulla. *Journal of Comparative Physiology. A, Neuroethology, Sensory, Neural, and Behavioral Physiology*, 138(2):93–119.
- Dickinson, M. H.
2014. Death Valley, *Drosophila*, and the Devonian toolkit. *Annual Review of Entomology*, 59:51–72.
- Dong, W. and J. Atick
1995. Statistics of natural time-varying images. *Network Computation in Neural Systems*, 6(3):345–358.
- Douglass, J. K. and N. J. Strausfeld
1995. Visual motion detection circuits in flies: peripheral motion computation by identified small-field retinotopic neurons. *Journal of Neuroscience*, 15(8):5596–5611.
- Douglass, J. K. and N. J. Strausfeld
1996. Visual motion-detection circuits in flies: parallel direction- and non-direction-sensitive pathways between the medulla and lobula plate. *Journal of Neuroscience*, 16(15):4551–4562.
- Doya, K., S. Ishii, A. Pouget, and R. P. N. Rao
2007. *Bayesian brain: Probabilistic approaches to neural coding*. Cambridge, MA: MIT Press.
- Dror, R. O., D. C. O'Carroll, and S. B. Laughlin
2000. The Role of Natural Image Statistics in Biological Motion Estimation. In *Biologically Motivated Computer Vision*, Pp. 492–501. Berlin, Heidelberg: Springer.
- Dror, R. O., D. C. O'Carroll, and S. B. Laughlin
2001. Accuracy of velocity estimation by Reichardt correlators. *Journal of the Optical Society of America. A, Optics, image science, and vision*, 18(2):241–252.
- Duistermars, B. J., D. M. Chow, M. Condro, and M. A. Frye
2007. The spatial, temporal and contrast properties of expansion and rotation flight optomotor responses in *Drosophila*. *Journal of Experimental Biology*, 210(18):3218–3227.
- Dyakova, O., Y.-J. Lee, K. D. Longden, V. G. Kiselev, and K. Nordström
2015. A higher order visual neuron tuned to the spatial amplitude spectra of natural scenes. *Nature Communications*, 6:8522.
- Eckert, H.
1980. Functional properties of the H1-neurone in the third optic ganglion of the blowfly, *Phaenicia*. *Journal of Comparative Physiology. A, Neuroethology, Sensory, Neural, and Behavioral Physiology*, 135(1):29–39.

- Egelhaaf, M.
1985. On the neuronal basis of figure-ground discrimination by relative motion in the visual system of the fly. *Biological Cybernetics*, 52(2):123–140.
- Egelhaaf, M. and A. Borst
1989. Transient and steady-state response properties of movement detectors. *Journal of the Optical Society of America. A, Optics and image science*, 6(1):116–127.
- Egelhaaf, M. and A. Borst
1992. Are there separate ON and OFF channels in fly motion vision? *Visual Neuroscience*, 8(2):151–164.
- Egelhaaf, M., A. Borst, and W. Reichardt
1989. Computational structure of a biological motion-detection system as revealed by local detector analysis in the fly's nervous system. *Journal of the Optical Society of America. A, Optics and image science*, 6(7):1070–1087.
- Eichner, H., M. Joesch, B. Schnell, D. F. Reiff, and A. Borst
2011. Internal structure of the fly elementary motion detector. *Neuron*, 70(6):1155–1164.
- Euler, T., S. Haverkamp, T. Schubert, and T. Baden
2014. Retinal bipolar cells: elementary building blocks of vision. *Nature Reviews Neuroscience*, 15(8):507–519.
- Exner, S.
1894. *Entwurf zu einer physiologischen Erklärung der psychischen Erscheinungen*. F. Deuticke.
- Fairhall, A. L., G. D. Lewen, W. Bialek, and R. R. de Ruyter van Steveninck
2001. Efficiency and ambiguity in an adaptive neural code. *Nature*, 412(6849):787–792.
- Feinberg, E. H., M. K. Vanhoven, A. Bendesky, G. Wang, R. D. Fetter, K. Shen, and C. I. Bargmann
2008. GFP Reconstitution Across Synaptic Partners (GRASP) defines cell contacts and synapses in living nervous systems. *Neuron*, 57(3):353–363.
- Felleman, D. J. and D. C. Van Essen
1991. Distributed hierarchical processing in the primate cerebral cortex. *Cerebral Cortex*, 1(1):1–47.
- Fennema, C. L. and W. B. Thompson
1979. Velocity determination in scenes containing several moving objects. *Computer Graphics and Image Processing*, 9(4):301–315.
- Fermi, G. and W. Reichardt
1963. Optomotorische Reaktionen der Fliege *Musca Domestica*. *Kybernetik*, 2(1):15–28.
- Field, D. J.
1987. Relations between the statistics of natural images and the response properties of cortical cells. *Journal of the Optical Society of America. A, Optics and image science*, 4(12):2379–2394.

- Field, G. D. and E. J. Chichilnisky
2007. Information processing in the primate retina: circuitry and coding. *Annual Review of Neuroscience*, 30:1–30.
- Fischbach, K. and M. Heisenberg
1981. Structural brain mutant of *Drosophila melanogaster* with reduced cell number in the medulla cortex and with normal optomotor yaw response. *Proceedings of the National Academy of Sciences of the United States of America*, 78(2):1105–1109.
- Fischbach, K.-F. and A. Dittrich
1989. The optic lobe of *Drosophila melanogaster*. I. A Golgi analysis of wild-type structure. *Cell and Tissue Research*, 258(3):441–475.
- Fisher, Y. E., J. C. Leong, K. Sporar, M. D. Ketkar, D. M. Gohl, T. R. Clandinin, and M. Silies
2015a. A Class of Visual Neurons with Wide-Field Properties Is Required for Local Motion Detection. *Current Biology*, 25(24):3178–3189.
- Fisher, Y. E., M. Silies, and T. R. Clandinin
2015b. Orientation Selectivity Sharpens Motion Detection in *Drosophila*. *Neuron*, 88(2):390–402.
- Fitzgerald, J. E. and D. A. Clark
2015. Nonlinear circuits for naturalistic visual motion estimation. *eLife*, 4:e09123.
- Flight, M. H.
2013. Visual system: Mapping motion detection. *Nature Reviews Neuroscience*, 14(10):669.
- Franceschini, N., K. Kirschfeld, and B. Minke
1981. Fluorescence of photoreceptor cells observed in vivo. *Science*, 213(4513):1264–1267.
- Franceschini, N., A. Riehle, and A. Le Nestour
1989. Directionally selective motion detection by insect neurons. In *Facets of vision*, Pp. 360–390. Berlin Heidelberg: Springer.
- Freifeld, L., D. A. Clark, M. J. Schnitzer, M. A. Horowitz, and T. R. Clandinin
2013. GABAergic lateral interactions tune the early stages of visual processing in *Drosophila*. *Neuron*, 78(6):1075–1089.
- Fujiwara, T., T. L. Cruz, J. P. Bohnslav, and M. E. Chiappe
2017. A faithful internal representation of walking movements in the *Drosophila* visual system. *Nature Neuroscience*, 20(1):72–81.
- Fukushima, K.
1980. Neocognitron: a self organizing neural network model for a mechanism of pattern recognition unaffected by shift in position. *Biological Cybernetics*, 36(4):193–202.

- Gabbiani, F., H. G. Krapp, C. Koch, and G. Laurent
2002. Multiplicative computation in a visual neuron sensitive to looming. *Nature*, 420(6913):320–324.
- Gallio, M., T. A. Ofstad, L. J. Macpherson, J. W. Wang, and C. S. Zuker
2011. The coding of temperature in the *Drosophila* brain. *Cell*, 144(4):614–624.
- Gao, S., S.-y. Takemura, C.-Y. Ting, S. Huang, Z. Lu, H. Luan, J. Rister, A. S. Thum, M. Yang, S.-T. Hong, J. W. Wang, W. F. Odenwald, B. H. White, I. A. Meinertzhagen, and C.-H. Lee
2008. The neural substrate of spectral preference in *Drosophila*. *Neuron*, 60(2):328–342.
- Geiger, G. and D. R. Nässel
1981. Visual orientation behaviour of flies after selective laser beam ablation of interneurons. *Nature*, 293(5831):398–399.
- Geisler, W. S.
2008. Visual perception and the statistical properties of natural scenes. *Annual Review of Psychology*, 59:167–192.
- Gengs, C., H.-T. Leung, D. R. Skingsley, M. I. Iovchev, Z. Yin, E. P. Semenov, M. G. Burg, R. C. Hardie, and W. L. Pak
2002. The target of *Drosophila* photoreceptor synaptic transmission is a histamine-gated chloride channel encoded by *ort* (*hclA*). *Journal of Biological Chemistry*, 277(44):42113–42120.
- Gilbert, C.
2013. Brain connectivity: revealing the fly visual motion circuit. *Current Biology*, 23(18):R851–853.
- Gjorgjieva, J., H. Sompolinsky, and M. Meister
2014. Benefits of pathway splitting in sensory coding. *Journal of Neuroscience*, 34(36):12127–12144.
- Golic, K. G. and S. Lindquist
1989. The FLP recombinase of yeast catalyzes site-specific recombination in the *Drosophila* genome. *Cell*, 59(3):499–509.
- Gollisch, T. and M. Meister
2008. Rapid neural coding in the retina with relative spike latencies. *Science*, 319(5866):1108–1111.
- Gomez-Marin, A., J. J. Paton, A. R. Kampff, R. M. Costa, and Z. F. Mainen
2014. Big behavioral data: psychology, ethology and the foundations of neuroscience. *Nature Neuroscience*, 17(11):1455–1462.
- Goodfellow, I., Y. Bengio, and A. Courville
2016. *Deep Learning*. Cambridge, MA: MIT Press.
- Goodman, L. J.
1960. The landing responses of insects. I. The landing response of the fly, *Lucilia sericata*, and other Calliphoridae. *Journal of Experimental Biology*, 37(4):854–878.

- Göppert-Mayer, M.
1931. Über Elementarakte mit zwei Quantensprüngen. *Annalen der Physik*, 401(3):273–294.
- Götz, K. G.
1964. Optomotorische Untersuchung des visuellen Systems einiger Augenmutanten der Fruchtfliege *Drosophila*. *Kybernetik*, 2(2):77–92.
- Götz, K. G.
1965. Die optischen Übertragungseigenschaften der Komplexaugen von *Drosophila*. *Biological Cybernetics*, 2(5):215–221.
- Götz, K. G.
1968. Flight control in *Drosophila* by visual perception of motion. *Kybernetik*, 4(6):199–208.
- Götz, K. G.
1970. Fractionation of *Drosophila* populations according to optomotor traits. *Journal of Experimental Biology*, 52(2):419–436.
- Götz, K. G.
1975. The optomotor equilibrium of the *Drosophila* navigation system. *Journal of Comparative Physiology. A, Neuroethology, Sensory, Neural, and Behavioral Physiology*, 99(3):187–210.
- Götz, K. G.
1987. Course-control, metabolism and wing interference during ultralong tethered flight in *Drosophila melanogaster*. *Journal of Experimental Biology*, 128(1):35–46.
- Götz, K. G. and H. Wenking
1973. Visual control of locomotion in the walking fruit fly *Drosophila*. *Journal of Comparative Physiology. A, Neuroethology, Sensory, Neural, and Behavioral Physiology*, 85(3):235–266.
- Gradinaru, V., K. R. Thompson, and K. Deisseroth
2008. eNpHR: a *Natronomonas* halorhodopsin enhanced for optogenetic applications. *Brain Cell Biology*, 36(1-4):129–139.
- Haag, J., A. Arenz, E. Serbe, F. Gabbiani, and A. Borst
2016. Complementary mechanisms create direction selectivity in the fly. *eLife*, 5:e2247.
- Haag, J. and A. Borst
1998. Active membrane properties and signal encoding in graded potential neurons. *Journal of Neuroscience*, 18(19):7972–7986.
- Haag, J. and A. Borst
2004. Neural mechanism underlying complex receptive field properties of motion-sensitive interneurons. *Nature Neuroscience*, 7(6):628–634.
- Haag, J., W. Denk, and A. Borst
2004. Fly motion vision is based on Reichardt detectors regardless of the signal-to-noise ratio. *Proceedings of the National Academy of Sciences of the United States of America*, 101(46):16333–16338.

- Haag, J., A. Wertz, and A. Borst
2007. Integration of lobula plate output signals by DNOVS₁, an identified premotor descending neuron. *Journal of Neuroscience*, 27(8):1992–2000.
- Haag, J., A. Wertz, and A. Borst
2010. Central gating of fly optomotor response. *Proceedings of the National Academy of Sciences of the United States of America*, 107(46):20104–20109.
- Hadjiconomou, D., S. Rotkopf, C. Alexandre, D. M. Bell, B. J. Dickson, and I. Salecker
2011. Flybow: genetic multicolor cell labeling for neural circuit analysis in *Drosophila melanogaster*. *Nature Methods*, 8(3):260–266.
- Haikala, V., M. Joesch, A. Borst, and A. S. Mauss
2013. Optogenetic control of fly optomotor responses. *Journal of Neuroscience*, 33(34):13927–13934.
- Hampel, S., P. Chung, C. E. McKellar, D. Hall, L. L. Looger, and J. H. Simpson
2011. *Drosophila* Brainbow: a recombinase-based fluorescence labeling technique to subdivide neural expression patterns. *Nature Methods*, 8(3):253–259.
- Hardie, R. C.
1989. A histamine-activated chloride channel involved in neurotransmission at a photoreceptor synapse. *Nature*, 339(6227):704–706.
- Hardie, R. C. and K. Franze
2012. Photomechanical responses in *Drosophila* photoreceptors. *Science*, 338(6104):260–263.
- Hardie, R. C. and M. Juusola
2015. Phototransduction in *Drosophila*. *Current Opinion in Neurobiology*, 34:37–45.
- Hardie, R. C. and P. Raghu
2001. Visual transduction in *Drosophila*. *Nature*, 413(6852):186–193.
- Harris, R. A., D. C. O’Carroll, and S. B. Laughlin
1999. Adaptation and the temporal delay filter of fly motion detectors. *Vision Research*, 39(16):2603–2613.
- Harz, H. and P. Hegemann
1991. Rhodopsin-regulated calcium currents in *Chlamydomonas*. *Nature*, 351:489–491.
- Hashimoto, T., S. Katai, Y. Saito, F. Kobayashi, and T. Goto
2013. ON and OFF channels in human retinal ganglion cells. *Journal of Physiology*, 591(1):327–337.
- Hassenstein, B.
1951. Ommatidienraster und afferente Bewegungsintegration. *Journal of Comparative Physiology. A, Neuroethology, Sensory, Neural, and Behavioral Physiology*, 33(4):301–326.

- Hassenstein, B.
1991. Der Biologe Bernhard Hassenstein. *Freiburger Universitätsblätter*, 114:85–112.
- Hassenstein, B. and W. Reichardt
1956. Systemtheoretische Analyse der Zeit-, Reihenfolgen- und Vorzeichenbewertung bei der Bewegungsperzeption des Rüsselkäfers *Chlorophanus*. *Zeitschrift für Naturforschung B*, 11(9-10):513–524.
- Hausen, K.
1976. Functional characterization and anatomical identification of motion sensitive neurons in the lobula plate of the blowfly *Calliphora erythrocephala*. *Zeitschrift für Naturforschung C*, 31(9-10):629–634.
- Hausen, K.
1982a. Motion sensitive interneurons in the optomotor system of the fly: I. The horizontal cells: Structure and signals. *Biological Cybernetics*, 45(2):143–156.
- Hausen, K.
1982b. Motion sensitive interneurons in the optomotor system of the fly: II. The horizontal cells: Receptive field organization and response characteristics. *Biological Cybernetics*, 46:67–79.
- Hausen, K. and C. Wehrhahn
1983. Microsurgical Lesion of Horizontal Cells Changes Optomotor Yaw Responses in the Blowfly *Calliphora erythrocephala*. *Proceedings of the Royal Society B: Biological Sciences*, 219(1215):211–216.
- Hecht, S. and G. Wald
1934. The visual acuity and intensity discrimination of *Drosophila*. *The Journal of General Physiology*, 17(4):517–547.
- Heim, R., A. B. Cubitt, and R. Y. Tsien
1995. Improved green fluorescence. *Nature*, 373(6516):663–664.
- Heisenberg, M. and E. Buchner
1977. The role of retinula cell types in visual behavior of *Drosophila melanogaster*. *Journal of Comparative Physiology. A, Neuroethology, Sensory, Neural, and Behavioral Physiology*, 117(2):127–162.
- Heisenberg, M. and K. G. Götz
1975. The use of mutations for the partial degradation of vision in *Drosophila melanogaster*. *Journal of Comparative Physiology. A, Neuroethology, Sensory, Neural, and Behavioral Physiology*, 98(3):217–241.
- Heisenberg, M. and R. Wolf
1984. *Vision in Drosophila: Genetics of Microbehavior*, Experimental Brain Research Supplementum. Berlin Heidelberg: Springer.
- Heisenberg, M., R. Wonneberger, and R. Wolf
1978. optomotor-blind^{H31} — a *Drosophila* Mutant of the Lobula Plate Giant Neurons. *Journal of Comparative Physiology. A, Neuroethology, Sensory, Neural, and Behavioral Physiology*, 124(4):287–296.

- Helmchen, F. and W. Denk
2005. Deep tissue two-photon microscopy. *Nature Methods*, 2(12):932–940.
- Helmstaedter, M., K. L. Briggman, S. C. Turaga, V. Jain, H. S. Seung, and W. Denk
2013. Connectomic reconstruction of the inner plexiform layer in the mouse retina. *Nature*, 500(7461):168–174.
- Hendel, T., M. Mank, B. Schnell, O. Griesbeck, A. Borst, and D. F. Reiff
2008. Fluorescence changes of genetic calcium indicators and OGB-1 correlated with neural activity and calcium in vivo and in vitro. *Journal of Neuroscience*, 28(29):7399–7411.
- Hengstenberg, R.
1982. Common visual response properties of giant vertical cells in the lobula plate of the blowfly *Calliphora*. *Journal of Comparative Physiology. A, Neuroethology, Sensory, Neural, and Behavioral Physiology*, 149(2):179–193.
- Hengstenberg, R.
1988. Mechanosensory control of compensatory head roll during flight in the blowfly *Calliphora erythrocephala* Meig. *Journal of Comparative Physiology. A, Neuroethology, Sensory, Neural, and Behavioral Physiology*, 163(2):151–165.
- Hermundstad, A. M., J. J. Briguglio, M. M. Conte, J. D. Victor, V. Balasubramanian, and G. Tkačik
2014. Variance predicts salience in central sensory processing. *eLife*, 3:e03722.
- Hildreth, E. C. and C. Koch
1987. The analysis of visual motion: from computational theory to neuronal mechanisms. *Annual Review of Neuroscience*, 10:477–533.
- Horn, E. and R. Wehner
1975. The mechanism of visual pattern fixation in the walking fly, *Drosophila melanogaster*. *Journal of Comparative Physiology. A, Neuroethology, Sensory, Neural, and Behavioral Physiology*, 101(1):39–56.
- Hsu, C. T. and V. Bhandawat
2016. Organization of descending neurons in *Drosophila melanogaster*. *Scientific Reports*, 6:20259.
- Hu, Q. and J. D. Victor
2010. A set of high-order spatiotemporal stimuli that elicit motion and reverse-phi percepts. *Journal of Vision*, 10(3):1–16.
- Huang, J., A. B. Lee, and D. Mumford
2000. Statistics of range images. In *2000 Conference on Computer Vision and Pattern Recognition (CVPR 2000), 13-15 June 2000, Hilton Head, SC, USA*, Pp. 1324–1331.
- Hyvärinen, A., J. Hurri, and P. O. Hoyer
2009. *Natural Image Statistics*, volume 39 of *A Probabilistic Approach to Early Computational Vision*. London: Springer Science & Business Media.

- Ito, K., K. Shinomiya, M. Ito, J. D. Armstrong, G. Boyan, V. Hartenstein, S. Harzsch, M. Heisenberg, U. Homberg, A. Jenett, H. Keshishian, L. L. Restifo, W. Rossler, J. H. Simpson, N. J. Strausfeld, R. Strauss, and L. B. Vosshall
2014. A systematic nomenclature for the insect brain. *Neuron*, 81(4):755–765.
- Jain, V., H. S. Seung, and S. C. Turaga
2010. Machines that learn to segment images: a crucial technology for connectomics. *Current Opinion in Neurobiology*, 20(5):653–666.
- Jeffress, L. A.
1948. A place theory of sound localization. *Journal of Comparative and Physiological Psychology*, 41(1):35–39.
- Jenett, A., G. M. Rubin, T. T. Ngo, D. Shepherd, C. Murphy, H. Dionne, B. D. Pfeiffer, A. Cavallaro, D. Hall, J. Jeter, N. Iyer, D. Fetter, J. H. Hausenfluck, H. Peng, E. T. Trautman, R. R. Svirskas, E. W. Myers, Z. R. Iwinski, Y. Aso, G. M. DePasquale, A. Enos, P. Hulamm, S. C. Lam, H. H. Li, T. R. Lavery, F. Long, L. Qu, S. D. Murphy, K. Rokicki, T. Safford, K. Shaw, J. H. Simpson, A. Sowell, S. Tae, Y. Yu, and C. T. Zugates
2012. A GAL4-driver line resource for *Drosophila* neurobiology. *Cell Reports*, 2(4):991–1001.
- Jin, J., Y. Wang, R. Lashgari, H. A. Swadlow, and J. M. Alonso
2011. Faster thalamocortical processing for dark than light visual targets. *Journal of Neuroscience*, 31(48):17471–17479.
- Joesch, M., J. Plett, A. Borst, and D. F. Reiff
2008. Response properties of motion-sensitive visual interneurons in the lobula plate of *Drosophila melanogaster*. *Current Biology*, 18(5):368–374.
- Joesch, M., B. Schnell, S. V. Raghu, D. F. Reiff, and A. Borst
2010. ON and OFF pathways in *Drosophila* motion vision. *Nature*, 468(7321):300–304.
- Joesch, M., F. Weber, H. Eichner, and A. Borst
2013. Functional specialization of parallel motion detection circuits in the fly. *Journal of Neuroscience*, 33(3):902–905.
- Johnston, A. and C. Clifford
1995. A unified account of three apparent motion illusions. *Vision Research*, 35(8):1109–1123.
- Jung, S. N., A. Borst, and J. Haag
2011. Flight activity alters velocity tuning of fly motion-sensitive neurons. *Journal of Neuroscience*, 31(25):9231–9237.
- Kabra, M., A. A. Robie, M. Rivera-Alba, S. Branson, and K. Branson
2013. JAABA: interactive machine learning for automatic annotation of animal behavior. *Nature Methods*, 10(1):64–67.

- Kalmus, H.
1943. The optomotor responses of some eye mutants of *Drosophila*. *Journal of Genetics*, 45(2):206–213.
- Katsov, A. Y. and T. R. Clandinin
2008. Motion processing streams in *Drosophila* are behaviorally specialized. *Neuron*, 59(2):322–335.
- Keller, G. B., T. Bonhoeffer, and M. Hübener
2012. Sensorimotor mismatch signals in primary visual cortex of the behaving mouse. *Neuron*, 74(5):809–815.
- Kern, R. and M. Egelhaaf
2000. Optomotor course control in flies with largely asymmetric visual input. *Journal of Comparative Physiology. A, Neuroethology, Sensory, Neural, and Behavioral Physiology*, 186(1):45–55.
- Kim, A. J., L. M. Fenk, C. Lyu, and G. Maimon
2017. Quantitative Predictions Orchestrate Visual Signaling in *Drosophila*. *Cell*, 168(1-2):280–294.
- Kim, A. J., J. K. Fitzgerald, and G. Maimon
2015. Cellular evidence for efference copy in *Drosophila* visuomotor processing. *Nature Neuroscience*, 18(9):1247–1255.
- Kim, J. S., M. J. Greene, A. Zlateski, K. Lee, M. Richardson, S. C. Turaga, M. Purcaro, M. Balkam, A. Robinson, B. F. Behabadi, M. Campos, W. Denk, and H. S. Seung
2014. Space-time wiring specificity supports direction selectivity in the retina. *Nature*, 509(7500):331–336.
- Kirschfeld, K.
1967. Die Projektion der optischen Umwelt auf das Raster der Rhabdomere im Komplexauge von *Musca*. *Experimental Brain Research*, 3(3):248–270.
- Kitamoto, T.
2001. Conditional modification of behavior in *Drosophila* by targeted expression of a temperature-sensitive *shibire* allele in defined neurons. *Journal of Neurobiology*, 47(2):81–92.
- Klapoetke, N. C., Y. Murata, S. S. Kim, S. R. Pulver, A. Birdsey-Benson, Y. K. Cho, T. K. Morimoto, A. S. Chuong, E. J. Carpenter, Z. Tian, J. Wang, Y. Xie, Z. Yan, Y. Zhang, B. Y. Chow, B. Surek, M. Melkonian, V. Jayaraman, M. Constantine-Paton, G. K. Wong, and E. S. Boyden
2014. Independent optical excitation of distinct neural populations. *Nature Methods*, 11(3):338–346.
- Knoll, M. and E. Ruska
1932. Das Elektronenmikroskop. *Zeitschrift für Physik. A, Hadrons and Nuclei*, 78(5):318–339.
- Knowles, E.
2005. *The Oxford Dictionary of Phrase and Fable*. New York, NY, USA: Oxford University Press.

- Knöpfel, T.
2012. Genetically encoded optical indicators for the analysis of neuronal circuits. *Nature Reviews Neuroscience*, 13(10):687–700.
- Koch, C.
2004. *Biophysics of Computation: Information Processing in Single Neurons (Computational Neuroscience Series)*. New York, NY, USA: Oxford University Press.
- Koenderink, J. J.
1986. Optic flow. *Vision Research*, 26(1):161–179.
- Komban, S. J., J. Kremkow, J. Jin, Y. Wang, R. Lashgari, X. Li, Q. Zaidi, and J.-M. Alonso
2014. Neuronal and perceptual differences in the temporal processing of darks and lights. *Neuron*, 82(1):224–234.
- Krakauer, J. W., A. A. Ghazanfar, A. Gomez-Marin, M. A. MacIver, and D. Poeppel
2017. Neuroscience Needs Behavior: Correcting a Reductionist Bias. *Neuron*, 93(3):480–490.
- Krapp, H. G., B. Hengstenberg, and R. Hengstenberg
1998. Dendritic structure and receptive-field organization of optic flow processing interneurons in the fly. *Journal of Neurophysiology*, 79(4):1902–1917.
- Krapp, H. G. and R. Hengstenberg
1996. Estimation of self-motion by optic flow processing in single visual interneurons. *Nature*, 384(6608):463–466.
- Krekelberg, B. and T. D. Albright
2005. Motion mechanisms in macaque MT. *Journal of Neurophysiology*, 93(5):2908–2921.
- Kvon, E. Z., T. Kazmar, G. Stampfel, J. O. Yanez-Cuna, M. Pagani, K. Scherhuber, B. J. Dickson, and A. Stark
2014. Genome-scale functional characterization of *Drosophila* developmental enhancers in vivo. *Nature*, 512(7512):91–95.
- Lai, S. L. and T. Lee
2006. Genetic mosaic with dual binary transcriptional systems in *Drosophila*. *Nature Neuroscience*, 9(5):703–709.
- Land, M. F.
1997. Visual acuity in insects. *Annual Review of Entomology*, 42:147–177.
- Land, M. F. and T. S. Collett
1974. Chasing behaviour of houseflies (*Fannia canicularis*). *Journal of Comparative Physiology. A, Neuroethology, Sensory, Neural, and Behavioral Physiology*, 89(4):331–357.

- Laughlin, S. B.
1981. A simple coding procedure enhances a neuron's information capacity. *Zeitschrift für Naturforschung. Section C: Biosciences*, 36(9-10):910–912.
- Laughlin, S. B.
1996. Matched filtering by a photoreceptor membrane. *Vision Research*, 36(11):1529–1541.
- Laughlin, S. B. and R. C. Hardie
1978. Common strategies for light adaptation in the peripheral visual systems of fly and dragonfly. *Journal of Comparative Physiology. A, Neuroethology, Sensory, Neural, and Behavioral Physiology*, 128(4):319–340.
- Laughlin, S. B. and D. Osorio
1989. Mechanisms for neural signal enhancement in the blowfly compound eye. *Journal of Experimental Biology*, 144(1):113–146.
- LeCun, Y., Y. Bengio, and G. Hinton
2015. Deep learning. *Nature*, 521(7553):436–444.
- LeCun, Y., B. Boser, J. S. Denker, D. Henderson, R. E. Howard, W. Hubbard, and L. D. Jackel
1989. Backpropagation applied to handwritten zip code recognition. *Neural Computation*, 1(4):541–551.
- Lee, T. and L. Luo
1999. Mosaic analysis with a repressible cell marker for studies of gene function in neuronal morphogenesis. *Neuron*, 22(3):451–461.
- Lei, S. and A. Borst
2006. Propagation of photon noise and information transfer in visual motion detection. *Journal of Computational Neuroscience*, 20(2):167–178.
- Leong, J. C. S., J. J. Esch, B. Poole, S. Ganguli, and T. R. Clandinin
2016. Direction Selectivity in *Drosophila* Emerges from Preferred-Direction Enhancement and Null-Direction Suppression. *Journal of Neuroscience*, 36(31):8078–8092.
- Leonhardt, A., G. Ammer, M. Meier, E. Serbe, A. Bahl, and A. Borst
2016. Asymmetry of *Drosophila* ON and OFF motion detectors enhances real-world velocity estimation. *Nature Neuroscience*, 19(5):706–715.
- Lewen, G. D., W. Bialek, and R. R. de Ruyter van Steveninck
2001. Neural coding of naturalistic motion stimuli. *Network*, 12(3):317–329.
- Lima, S. Q. and G. Miesenböck
2005. Remote control of behavior through genetically targeted photostimulation of neurons. *Cell*, 121(1):141–152.
- Limb, J. and J. Murphy
1975. Estimating the velocity of moving images in television signals. *Computer Graphics and Image Processing*, 4(4):311–327.

- Lindsay, T., A. Suster, and M. Dickinson
2017. The Function and Organization of the Motor System Controlling Flight Maneuvers in Flies. *Current Biology*, 27(3):345–358.
- Looger, L. L. and O. Griesbeck
2012. Genetically encoded neural activity indicators. *Current Opinion in Neurobiology*, 22(1):18–23.
- Lu, Z. L. and G. Sperling
2001. Three-systems theory of human visual motion perception: review and update. *Journal of the Optical Society of America. A, Optics, image science, and vision*, 18(9):2331–2370.
- Luan, H., N. C. Peabody, C. R. Vinson, and B. H. White
2006. Refined spatial manipulation of neuronal function by combinatorial restriction of transgene expression. *Neuron*, 52(3):425–436.
- Maimon, G., A. D. Straw, and M. Dickinson
2008. A Simple Vision-Based Algorithm for Decision Making in Flying *Drosophila*. *Current Biology*, 18(6):464–470.
- Maimon, G., A. D. Straw, and M. Dickinson
2010. Active flight increases the gain of visual motion processing in *Drosophila*. *Nature Neuroscience*, 13(3):393–399.
- Maisak, M. S., J. Haag, G. Ammer, E. Serbe, M. Meier, A. Leonhardt, T. Schilling, A. Bahl, G. M. Rubin, A. Nern, B. J. Dickson, D. F. Reiff, E. Hopp, and A. Borst
2013. A directional tuning map of *Drosophila* elementary motion detectors. *Nature*, 500(7461):212–216.
- Mank, M., A. F. Santos, S. Drenth, T. D. Mrsic-Flogel, S. B. Hofer, V. Stein, T. Hendel, D. F. Reiff, C. Levelt, A. Borst, T. Bonhoeffer, M. Hübener, and O. Griesbeck
2008. A genetically encoded calcium indicator for chronic in vivo two-photon imaging. *Nature Methods*, 5(9):805–811.
- Markram, H., E. Muller, S. Ramaswamy, M. W. Reimann, M. Abdellah, C. A. Sanchez, A. Ailamaki, L. Alonso-Nanclares, N. Antille, S. Arsever, et al.
2015. Reconstruction and simulation of neocortical microcircuitry. *Cell*, 163(2):456–492.
- Marr, D. and S. Ullman
1981. Directional selectivity and its use in early visual processing. *Proceedings of the Royal Society B: Biological Sciences*, 211(1183):151–180.
- Marvin, J. S., B. G. Borghuis, L. Tian, J. Cichon, M. T. Harnett, J. Akerboom, A. Gordus, S. L. Renninger, T. W. Chen, C. I. Bargmann, M. B. Orger, E. R. Schreiter, J. B. Demb, W. B. Gan, S. A. Hires, and L. L. Looger
2013. An optimized fluorescent probe for visualizing glutamate neurotransmission. *Nature Methods*, 10(2):162–170.

- Masland, R. H.
2013. Neuroscience: Accurate maps of visual circuitry. *Nature*, 500(7461):154–155.
- Mauss, A. S., M. Meier, E. Serbe, and A. Borst
2014. Optogenetic and pharmacologic dissection of feedforward inhibition in *Drosophila* motion vision. *Journal of Neuroscience*, 34(6):2254–2263.
- Mauss, A. S., K. Pankova, A. Arenz, A. Nern, G. M. Rubin, and A. Borst
2015. Neural Circuit to Integrate Opposing Motions in the Visual Field. *Cell*, 162(2):351–362.
- McGuire, S. E., P. T. Le, A. J. Osborn, K. Matsumoto, and R. L. Davis
2003. Spatiotemporal rescue of memory dysfunction in *Drosophila*. *Science*, 302(5651):1765–1768.
- Mead, C.
1989. *Analog VLSI and Neural Systems*. Boston, MA, USA: Addison-Wesley Longman Publishing Co., Inc.
- Meier, M., E. Serbe, M. S. Maisak, J. Haag, B. J. Dickson, and A. Borst
2014. Neural circuit components of the *Drosophila* OFF motion vision pathway. *Current Biology*, 24(4):385–392.
- Meinertzhagen, I. A. and S. O’Neil
1991. Synaptic organization of columnar elements in the lamina of the wild type in *Drosophila melanogaster*. *Journal of Comparative Neurology*, 305(2):232–263.
- Menne, D. and H.-C. Spatz
1977. Colour vision in *Drosophila melanogaster*. *Journal of Comparative Physiology*, 114(3):301–312.
- Mimura, K.
1972. Neural mechanisms, subserving directional selectivity of movement in the optic lobe of the fly. *Journal of Comparative Physiology. A, Neuroethology, Sensory, Neural, and Behavioral Physiology*, 80(4):409–437.
- Minsky, M.
1988. Memoir on inventing the confocal scanning microscope. *Scanning*, 10(4):128–138.
- Morante, J. and C. Desplan
2004. Building a projection map for photoreceptor neurons in the *Drosophila* optic lobes. *Seminars in Cell and Developmental Biology*, 15(1):137–143.
- Morgan, T. H.
1910. Sex limited inheritance in *Drosophila*. *Science*, 32(812):120–122.
- Mronz, M. and F.-O. Lehmann
2008. The free-flight response of *Drosophila* to motion of the visual environment. *Journal of Experimental Biology*, 211(13):2026–2045.

- Mu, L., K. Ito, J. P. Bacon, and N. J. Strausfeld
2012. Optic glomeruli and their inputs in *Drosophila* share an organizational ground pattern with the antennal lobes. *Journal of Neuroscience*, 32(18):6061–6071.
- Muijres, F. T., M. J. Elzinga, J. M. Melis, and M. H. Dickinson
2014. Flies evade looming targets by executing rapid visually directed banked turns. *Science*, 344(6180):172–177.
- Murthy, M., I. Fiete, and G. Laurent
2008. Testing odor response stereotypy in the *Drosophila* mushroom body. *Neuron*, 59(6):1009–1023.
- Nagel, G., M. Brauner, J. F. Liewald, N. Adeishvili, E. Bamberg, and A. Gottschalk
2005. Light activation of channelrhodopsin-2 in excitable cells of *Caenorhabditis elegans* triggers rapid behavioral responses. *Current Biology*, 15(24):2279–2284.
- Nagel, G., T. Szellas, W. Huhn, S. Kateriya, N. Adeishvili, P. Berthold, D. Ollig, P. Hegemann, and E. Bamberg
2003. Channelrhodopsin-2, a directly light-gated cation-selective membrane channel. *Proceedings of the National Academy of Sciences of the United States of America*, 100(24):13940–13945.
- Nakai, J., M. Ohkura, and K. Imoto
2001. A high signal-to-noise Ca(2+) probe composed of a single green fluorescent protein. *Nature Biotechnology*, 19(2):137–141.
- Nern, A., B. D. Pfeiffer, and G. M. Rubin
2015. Optimized tools for multicolor stochastic labeling reveal diverse stereotyped cell arrangements in the fly visual system. *Proceedings of the National Academy of Sciences of the United States of America*, 112(22):E2967–2976.
- Nitabach, M. N., Y. Wu, V. Sheeba, W. C. Lemon, J. Strumbos, P. K. Zelensky, B. H. White, and T. C. Holmes
2006. Electrical hyperexcitation of lateral ventral pacemaker neurons desynchronizes downstream circadian oscillators in the fly circadian circuit and induces multiple behavioral periods. *Journal of Neuroscience*, 26(2):479–489.
- O’Carroll, D. C., P. D. Barnett, and K. Nordström
2011. Local and global responses of insect motion detectors to the spatial structure of natural scenes. *Journal of Vision*, 11(14):20–20.
- Ofstad, T. A., C. S. Zuker, and M. B. Reiser
2011. Visual place learning in *Drosophila melanogaster*. *Nature*, 474(7350):204–207.
- Olshausen, B. A. and D. J. Field
1996. Emergence of simple-cell receptive field properties by learning a sparse code for natural images. *Nature*, 381(6583):607–609.

- Orger, M. B., M. C. Smear, S. M. Anstis, and H. Baier
2000. Perception of Fourier and non-Fourier motion by larval zebrafish. *Nature Neuroscience*, 3(11):1128–1133.
- O'Tousa, J. E., W. Baehr, R. L. Martin, J. Hirsh, W. L. Pak, and M. L. Applebury
1985. The *Drosophila ninaE* gene encodes an opsin. *Cell*, 40(4):839–850.
- Otsuna, H. and K. Ito
2006. Systematic analysis of the visual projection neurons of *Drosophila melanogaster*. I. Lobula-specific pathways. *Journal of Comparative Neurology*, 497(6):928–958.
- Pak, W. L., J. Grossfield, and K. S. Arnold
1970. Mutants of the visual pathway of *Drosophila melanogaster*. *Nature*, 227(5257):518–520.
- Pandarinath, C., J. D. Victor, and S. Nirenberg
2010. Symmetry breakdown in the ON and OFF pathways of the retina at night: functional implications. *Journal of Neuroscience*, 30(30):10006–10014.
- Pankova, K. and A. Borst
2016. RNA-Seq Transcriptome Analysis of Direction-Selective T4/T5 Neurons in *Drosophila*. *PLoS ONE*, 11(9):e0163986.
- Pankova, K. and A. Borst
2017. Transgenic line for the identification of cholinergic release sites in *Drosophila melanogaster*. *Journal of Experimental Biology*, 220(8):1405–1410.
- Parisky, K. M., J. Agosto, S. R. Pulver, Y. Shang, E. Kuklin, J. J. Hodge, K. Kang, K. Kang, X. Liu, P. A. Garrity, M. Rosbash, and L. C. Griffith
2008. PDF cells are a GABA-responsive wake-promoting component of the *Drosophila* sleep circuit. *Neuron*, 60(4):672–682.
- Pecka, M., Y. Han, E. Sader, and T. D. Mrsic-Flogel
2014. Experience-dependent specialization of receptive field surround for selective coding of natural scenes. *Neuron*, 84(2):457–469.
- Pfeiffer, B. D., A. Jenett, A. S. Hammonds, T.-T. B. Ngo, S. Misra, C. Murphy, A. Scully, J. W. Carlson, K. H. Wan, T. R. Laverty, et al.
2008. Tools for neuroanatomy and neurogenetics in *Drosophila*. *Proceedings of the National Academy of Sciences of the United States of America*, 105(28):9715–9720.
- Pfeiffer, B. D., T. T. Ngo, K. L. Hibbard, C. Murphy, A. Jenett, J. W. Truman, and G. M. Rubin
2010. Refinement of tools for targeted gene expression in *Drosophila*. *Genetics*, 186(2):735–755.
- Pfeiffer, B. D., J. W. Truman, and G. M. Rubin
2012. Using translational enhancers to increase transgene expression in *Drosophila*. *Proceedings of the National Academy of Sciences of the United States of America*, 109(17):6626–6631.

- Pick, B.
1974. Visual flicker induces orientation behaviour in the fly *Musca*. *Zeitschrift für Naturforschung C*, 29(5-6):310–312.
- Poggio, T. and W. Reichardt
1973. A theory of the pattern induced flight orientation of the fly *Musca domestica*. *Biological Cybernetics*, 12(4):185–203.
- Portugues, R. and F. Engert
2009. The neural basis of visual behaviors in the larval zebrafish. *Current Opinion in Neurobiology*, 19(6):644–647.
- Potter, C. J., B. Tasic, E. V. Russler, L. Liang, and L. Luo
2010. The Q system: a repressible binary system for transgene expression, lineage tracing, and mosaic analysis. *Cell*, 141(3):536–548.
- Potters, M. and W. Bialek
1994. Statistical mechanics and visual signal processing. *Journal de Physique I*, 4(11):1755–1775.
- Raghu, S. V. and A. Borst
2011. Candidate glutamatergic neurons in the visual system of *Drosophila*. *PLoS ONE*, 6(5):e19472.
- Ramón y Cajal, S. and D. Sánchez
1915. *Contribución al conocimiento de los centros nerviosos de los insectos*.
- Ratliff, C. P., B. G. Borghuis, Y.-H. Kao, P. Sterling, and V. Balasubramanian
2010. Retina is structured to process an excess of darkness in natural scenes. *Proceedings of the National Academy of Sciences of the United States of America*, 107(40):17368–17373.
- Reichardt, W.
1961. Autocorrelation, a principle for evaluation of sensory information by the central nervous system. In *Sensory Communication*, W. A. Rosenblith, ed. Cambridge: MIT Press.
- Reichardt, W.
1973. Musterinduzierte Flugorientierung. *Naturwissenschaften*, 60(3):122–138.
- Reichardt, W.
1987. Evaluation of optical motion information by movement detectors. *Journal of Comparative Physiology. A, Neuroethology, Sensory, Neural, and Behavioral Physiology*, 161(4):533–547.
- Reichardt, W. and H. Wenking
1969. Optical detection and fixation of objects by fixed flying flies. *Naturwissenschaften*, 56(8):424–425.
- Reiff, D. F., J. Plett, M. Mank, O. Griesbeck, and A. Borst
2010. Visualizing retinotopic half-wave rectified input to the motion detection circuitry of *Drosophila*. *Nature Neuroscience*, 13(8):973–978.

- Rieke, F., D. A. Bodnar, and W. Bialek
1995. Naturalistic stimuli increase the rate and efficiency of information transmission by primary auditory afferents. *Proceedings of the Royal Society B: Biological Sciences*, 262(1365):259–265.
- Rister, J., D. Pauls, B. Schnell, C.-Y. Ting, C.-H. Lee, I. Sinakevitch, J. Morante, N. J. Strausfeld, K. Ito, and M. Heisenberg
2007. Dissection of the peripheral motion channel in the visual system of *Drosophila melanogaster*. *Neuron*, 56(1):155–170.
- Rivera-Alba, M., S. N. Vitaladevuni, Y. Mischenko, Z. Lu, S. Takemura, L. J. Scheffer, I. A. Meinertzhagen, D. B. Chklovskii, and G. G. de Polavieja
2011. Wiring economy and volume exclusion determine neuronal placement in the *Drosophila* brain. *Current Biology*, 21(23):2000–2005.
- Rosenzweig, M., K. M. Brennan, T. D. Tayler, P. O. Phelps, A. Patapoutian, and P. A. Garrity
2005. The *Drosophila* ortholog of vertebrate TRPA1 regulates thermotaxis. *Genes & Development*, 19(4):419–424.
- Roth, S. and M. J. Black
2005. On the spatial statistics of optical flow. In *International Conf. on Computer Vision*, Pp. 42–49.
- Roth, S. and M. J. Black
2007. On the Spatial Statistics of Optical Flow. *International Journal of Computer Vision*, 74(1):33–50.
- Rubin, G. M. and A. C. Spradling
1982. Genetic transformation of *Drosophila* with transposable element vectors. *Science*, 218(4570):348–353.
- Ruderman, D. and W. Bialek
1994. Statistics of natural images: Scaling in the woods. *Physical Review Letters*, 73(6):814–817.
- Ruderman, D. L., T. W. Cronin, and C.-C. Chiao
1998. Statistics of cone responses to natural images: Implications for visual coding. *Journal of the Optical Society of America A*, 15:2036–2045.
- Sakmann, B. and E. Neher
1984. Patch clamp techniques for studying ionic channels in excitable membranes. *Annual Review of Physiology*, 46:455–472.
- Saleem, A. B., A. Ayaz, K. J. Jeffery, K. D. Harris, and M. Carandini
2013. Integration of visual motion and locomotion in mouse visual cortex. *Nature Neuroscience*, 16(12):1864–1869.
- Schilling, T. and A. Borst
2015. Local motion detectors are required for the computation of expansion flow-fields. *Biology Open*, 4(9):1105–1108.

- Schnaitmann, C., C. Garbers, T. Wachtler, and H. Tanimoto
2013. Color discrimination with broadband photoreceptors. *Current Biology*, 23(23):2375–2382.
- Schnell, B., M. Joesch, F. Forstner, S. V. Raghu, H. Otsuna, K. Ito, A. Borst, and D. F. Reiff
2010. Processing of horizontal optic flow in three visual interneurons of the *Drosophila* brain. *Journal of Neurophysiology*, 103(3):1646–1657.
- Schnell, B., S. V. Raghu, A. Nern, and A. Borst
2012. Columnar cells necessary for motion responses of wide-field visual interneurons in *Drosophila*. *Journal of Comparative Physiology. A, Neuroethology, Sensory, Neural, and Behavioral Physiology*, 198(5):389–395.
- Schnell, B., P. T. Weir, E. Roth, A. L. Fairhall, and M. Dickinson
2014. Cellular mechanisms for integral feedback in visually guided behavior. *Proceedings of the National Academy of Sciences of the United States of America*, 111(15):5700–5705.
- Scholl, B., X. Gao, and M. Wehr
2010. Nonoverlapping sets of synapses drive on responses and off responses in auditory cortex. *Neuron*, 65(3):412–421.
- Schwegmann, A., J. P. Lindemann, and M. Egelhaaf
2014. Depth information in natural environments derived from optic flow by insect motion detection system: a model analysis. *Frontiers in Computational Neuroscience*, 8:83.
- Scott, E. K., T. Raabe, and L. Luo
2002. Structure of the vertical and horizontal system neurons of the lobula plate in *Drosophila*. *Journal of Comparative Neurology*, 454(4):470–481.
- Seelig, J. D., M. E. Chiappe, G. K. Lott, A. Dutta, J. E. Osborne, M. B. Reiser, and V. Jayaraman
2010. Two-photon calcium imaging from head-fixed *Drosophila* during optomotor walking behavior. *Nature Methods*, 7(7):535–540.
- Seelig, J. D. and V. Jayaraman
2013. Feature detection and orientation tuning in the *Drosophila* central complex. *Nature*, 503(7475):262–266.
- Seiger, M. B.
1966. The effects of chromosome substitution on male body weight of *Drosophila melanogaster*. *Genetics*, 53(2):237–248.
- Serbe, E., M. Meier, A. Leonhardt, and A. Borst
2016. Comprehensive Characterization of the Major Presynaptic Elements to the *Drosophila* OFF Motion Detector. *Neuron*, 89(4):829–841.
- Shannon, C. E.
1948. A mathematical theory of communication. *Bell System Technical Journal*, 27.

- Shinomiya, K., T. Karuppudurai, T.-Y. Lin, Z. Lu, C.-H. Lee, and I. A. Meinertzhagen
2014. Candidate neural substrates for off-edge motion detection in *Drosophila*. *Current Biology*, 24(10):1062–1070.
- Shinomiya, K., S. Y. Takemura, P. K. Rivlin, S. M. Plaza, L. K. Scheffer, and I. A. Meinertzhagen
2015. A common evolutionary origin for the ON- and OFF-edge motion detection pathways of the *Drosophila* visual system. *Frontiers in Neural Circuits*, 9:33.
- Silies, M., D. M. Gohl, Y. E. Fisher, L. Freifeld, D. A. Clark, and T. R. Clandinin
2013. Modular use of peripheral input channels tunes motion-detecting circuitry. *Neuron*, 79(1):111–127.
- Simoncelli, E. P.
2003. Vision and the statistics of the visual environment. *Current Opinion in Neurobiology*, 13(2):144–149.
- Simoncelli, E. P. and B. A. Olshausen
2001. Natural image statistics and neural representation. *Annual Review of Neuroscience*, 24(1):1193–1216.
- Srinivasan, M.
1990. Generalized gradient schemes for the measurement of two-dimensional image motion. *Biological Cybernetics*, 63(6):421–431.
- Srinivasan, M. V., S. B. Laughlin, and A. Dubs
1982. Predictive coding: a fresh view of inhibition in the retina. *Proceedings of the Royal Society B: Biological Sciences*, 216(1205):427–459.
- Sterling, P. and S. Laughlin
2015. *Principles of Neural Design*. Cambridge, MA: MIT Press.
- Strausfeld, N. J., ed.
1976. *Atlas of an Insect Brain*. Berlin Heidelberg: Springer.
- Strausfeld, N. J. and U. Bassemir
1985. Lobula plate and ocellar interneurons converge onto a cluster of descending neurons leading to neck and leg motor neuropil in *Calliphora erythrocephala*. *Cell and Tissue Research*, 240(3):617–640.
- Strausfeld, N. J. and W. Gronenberg
1990. Descending neurons supplying the neck and flight motor of Diptera: organization and neuroanatomical relationships with visual pathways. *Journal of Comparative Neurology*, 302(4):954–972.
- Strauss, R., S. Schuster, and K. G. Götz
1997. Processing of artificial visual feedback in the walking fruit fly *Drosophila melanogaster*. *Journal of Experimental Biology*, 200(9):1281–1296.

- Straw, A. D., K. Branson, T. R. Neumann, and M. Dickinson
2011. Multi-camera real-time three-dimensional tracking of multiple flying animals. *Journal of the Royal Society Interface*, 8(56):395–409.
- Straw, A. D., T. Rainsford, and D. C. O'Carroll
2008. Contrast sensitivity of insect motion detectors to natural images. *Journal of Vision*, 8(3):32.1–9.
- Strother, J. A., A. Nern, and M. B. Reiser
2014. Direct observation of ON and OFF pathways in the *Drosophila* visual system. *Current Biology*, 24(9):976–983.
- Strother, J. A., S. T. Wu, A. M. Wong, A. Nern, E. M. Rogers, J. Q. Le, G. M. Rubin, and M. B. Reiser
2017. The Emergence of Directional Selectivity in the Visual Motion Pathway of *Drosophila*. *Neuron*, 94(1):168–182.
- Struhl, G. and K. Basler
1993. Organizing activity of wingless protein in *Drosophila*. *Cell*, 72(4):527–540.
- Suver, M. P., A. Huda, N. Iwasaki, S. Safarik, and M. H. Dickinson
2016. An Array of Descending Visual Interneurons Encoding Self-Motion in *Drosophila*. *Journal of Neuroscience*, 36(46):11768–11780.
- Suver, M. P., A. Mamiya, and M. Dickinson
2012. Octopamine Neurons Mediate Flight-Induced Modulation of Visual Processing in *Drosophila*. *Current Biology*, 22(24):2294–2302.
- Sweeney, S. T., K. Broadie, J. Keane, H. Niemann, and C. J. O'Kane
1995. Targeted expression of tetanus toxin light chain in *Drosophila* specifically eliminates synaptic transmission and causes behavioral defects. *Neuron*, 14(2):341–351.
- Takemura, S.
2015. Connectome of the fly visual circuitry. *Microscopy*, 64(1):37–44.
- Takemura, S., A. Bharioke, Z. Lu, A. Nern, S. N. Vitaladevuni, P. K. Rivlin, W. T. Katz, D. J. Olbris, S. M. Plaza, P. Winston, T. Zhao, J. A. Horne, R. D. Fetter, S. Takemura, K. Blazek, L.-A. Chang, O. Ogundeyi, M. A. Saunders, V. Shapiro, C. Sigmund, G. M. Rubin, L. J. Scheffer, I. A. Meinertzhagen, and D. B. Chklovskii
2013. A visual motion detection circuit suggested by *Drosophila* connectomics. *Nature*, 500(7461):175–181.
- Takemura, S., T. Karuppudurai, C.-Y. Ting, Z. Lu, C.-H. Lee, and I. A. Meinertzhagen
2011. Cholinergic circuits integrate neighboring visual signals in a *Drosophila* motion detection pathway. *Current Biology*, 21(24):2077–2084.
- Takemura, S., Z. Lu, and I. A. Meinertzhagen
2008. Synaptic circuits of the *Drosophila* optic lobe: the input terminals to the medulla. *Journal of Comparative Neurology*, 509(5):493–513.

- Takemura, S., A. Nern, D. B. Chklovskii, L. K. Scheffer, G. M. Rubin, and I. A. Meinertzhagen
2017. The comprehensive connectome of a neural substrate for 'ON' motion detection in *Drosophila*. *eLife*, 6.
- Tammero, L. F. and M. H. Dickinson
2002. Collision-avoidance and landing responses are mediated by separate pathways in the fruit fly, *Drosophila melanogaster*. *Journal of Experimental Biology*, 205(18):2785–2798.
- Theobald, J. C., B. J. Duistermars, D. L. Ringach, and M. A. Frye
2008. Flies see second-order motion. *Current Biology*, 18(11):464–5.
- Theobald, J. C., D. L. Ringach, and M. A. Frye
2010. Dynamics of optomotor responses in *Drosophila* to perturbations in optic flow. *Journal of Experimental Biology*, 213(8):1366–1375.
- Tkačik, G., P. Garrigan, C. Ratliff, G. Milčinski, J. M. Klein, L. H. Seyfarth, P. Sterling, D. H. Brainard, and V. Balasubramanian
2011. Natural images from the birthplace of the human eye. *PLoS ONE*, 6(6):e20409.
- Tkačik, G., J. S. Prentice, J. D. Victor, and V. Balasubramanian
2010. Local statistics in natural scenes predict the saliency of synthetic textures. *Proceedings of the National Academy of Sciences of the United States of America*, 107(42):18149–18154.
- Torre, V. and T. Poggio
1978. A synaptic mechanism possibly underlying directional selectivity to motion. *Proceedings of the Royal Society B: Biological Sciences*, 202(1148):409–416.
- Triphan, T., A. Nern, S. F. Roberts, W. Korff, D. Q. Naiman, and R. Strauss
2016. A screen for constituents of motor control and decision making in *Drosophila* reveals visual distance-estimation neurons. *Scientific Reports*, 6:27000.
- Trujillo-Cenóz, O. and J. Melamed
1966. Compound eye of dipterans: anatomical basis for integration—an electron microscope study. *Journal of Ultrastructure Research*, 16(3-4):395–398.
- Tuthill, J. C. and B. G. Borghuis
2016. Four to Foxtrot: How Visual Motion Is Computed in the Fly Brain. *Neuron*, 89(4):677–680.
- Tuthill, J. C., M. E. Chiappe, and M. B. Reiser
2011. Neural correlates of illusory motion perception in *Drosophila*. *Proceedings of the National Academy of Sciences of the United States of America*, 108(23):9685–9690.
- Tuthill, J. C., A. Nern, S. L. Holtz, G. M. Rubin, and M. B. Reiser
2013. Contributions of the 12 neuron classes in the fly lamina to motion vision. *Neuron*, 79(1):128–140.

- Tuthill, J. C., A. Nern, G. M. Rubin, and M. B. Reiser
2014. Wide-Field Feedback Neurons Dynamically Tune Early Visual Processing. *Neuron*, 82(4):887–895.
- van Hateren, J. H.
1992. A theory of maximizing sensory information. *Biological Cybernetics*, 68(1):23–29.
- van Hateren, J. H.
1993. Spatiotemporal contrast sensitivity of early vision. *Vision Research*, 33(2):257–267.
- van Hateren, J. H.
1997. Processing of natural time series of intensities by the visual system of the blowfly. *Vision Research*, 37(23):3407–3416.
- van Hateren, J. H. and A. van der Schaaf
1998. Independent component filters of natural images compared with simple cells in primary visual cortex. *Proceedings of the Royal Society B: Biological Sciences*, 265(1394):359–366.
- van Santen, J. P. and G. Sperling
1984. Temporal covariance model of human motion perception. *Journal of the Optical Society of America. A, Optics and image science*, 1(5):451–473.
- van Santen, J. P. and G. Sperling
1985. Elaborated Reichardt detectors. *Journal of the Optical Society of America. A, Optics and image science*, 2(2):300–321.
- Venken, K. J. T., J. H. Simpson, and H. J. Bellen
2011. Genetic manipulation of genes and cells in the nervous system of the fruit fly. *Neuron*, 72(2):202–230.
- von Helmholtz, H.
1867. *Handbuch der physiologischen Optik*, volume 3. Leipzig: L. Voss.
- von Holst, E. and H. Mittelstaedt
1950. Das Reafferenzprinzip: Wechselwirkungen zwischen Zentralnervensystem und Peripherie. *Naturwissenschaften*, 37:464–476.
- von Reyn, C. R., P. Breads, M. Y. Peek, G. Z. Zheng, W. R. Williamson, A. L. Yee, A. Leonardo, and G. M. Card
2014. A spike-timing mechanism for action selection. *Nature Neuroscience*, 17(7):962–970.
- Wachtler, T., T. W. Lee, and T. J. Sejnowski
2001. Chromatic structure of natural scenes. *Journal of the Optical Society of America. A, Optics, image science, and vision*, 18(1):65–77.
- Wardill, T. J., O. List, X. Li, S. Dongre, M. McCulloch, C. Y. Ting, C. J. O’Kane, S. Tang, C. H. Lee, R. C. Hardie, and M. Juusola
2012. Multiple spectral inputs improve motion discrimination in the *Drosophila* visual system. *Science*, 336(6083):925–931.

- Warland, D. K., P. Reinagel, and M. Meister
1997. Decoding visual information from a population of retinal ganglion cells. *Journal of Neurophysiology*, 78(5):2336–2350.
- Warzecha, A.-K. and M. Egelhaaf
1996. Intrinsic Properties of Biological Motion Detectors Prevent the Optomotor Control System from Getting Unstable. *Philosophical Transactions of the Royal Society B: Biological Sciences*, 351(1347):1579–1591.
- Warzecha, A.-K. and M. Egelhaaf
1998. On the performance of biological movement detectors and ideal velocity sensors in the context of optomotor course stabilization. *Visual Neuroscience*, 15(1):113–122.
- Wässle, H.
2004. Parallel processing in the mammalian retina. *Nature Reviews Neuroscience*, 5(10):747–757.
- Watson, A. B. and A. J. Ahumada
1985. Model of human visual-motion sensing. *Journal of the Optical Society of America. A, Optics and image science*, 2(2):322–341.
- Weber, F., C. K. Machens, and A. Borst
2010. Spatiotemporal response properties of optic-flow processing neurons. *Neuron*, 67(4):629–642.
- Weber, F., C. K. Machens, and A. Borst
2012. Disentangling the functional consequences of the connectivity between optic-flow processing neurons. *Nature Neuroscience*, 15(3):441–8.
- Weir, P. T. and M. H. Dickinson
2012. Flying *Drosophila* orient to sky polarization. *Current Biology*, 22(1):21–27.
- Wernet, M. F., M. M. Velez, D. A. Clark, F. Baumann-Klausener, J. R. Brown, M. Klovstad, T. Labhart, and T. R. Clandinin
2012. Genetic dissection reveals two separate retinal substrates for polarization vision in *Drosophila*. *Current Biology*, 22(1):12–20.
- Wertheimer, M.
1912. Experimentelle Studien über das Sehen von Bewegung. *Zeitschrift für Psychologie*, 61:161–265.
- Wertz, A., A. Borst, and J. Haag
2008. Nonlinear integration of binocular optic flow by DNOVS2, a descending neuron of the fly. *Journal of Neuroscience*, 28(12):3131–3140.
- Wertz, A., B. Gaub, J. Plett, J. Haag, and A. Borst
2009. Robust coding of ego-motion in descending neurons of the fly. *Journal of Neuroscience*, 29(47):14993–15000.
- Wessel, R., C. Koch, and F. Gabbiani
1996. Coding of time-varying electric field amplitude modulations in a wave-type electric fish. *Journal of Neurophysiology*, 75(6):2280–2293.

- Wilson, R. I., G. C. Turner, and G. Laurent
2004. Transformation of olfactory representations in the *Drosophila* antennal lobe. *Science*, 303(5656):366–370.
- Wolf, R. and M. Heisenberg
1986. Visual orientation in motion-blind flies is an operant behaviour. *Nature*, 323(6084):154–156.
- Wolf, R., A. Voss, S. Hein, M. Heisenberg, and G. Sullivan
1992. Can a fly ride a bicycle? [and discussion]. *Philosophical Transactions of the Royal Society B: Biological Sciences*, 337(1281):261–269.
- Yamaguchi, S., R. Wolf, C. Desplan, and M. Heisenberg
2008. Motion vision is independent of color in *Drosophila*. *Proceedings of the National Academy of Sciences of the United States of America*, 105(12):4910–4915.
- Yamins, D. L. K. and J. J. DiCarlo
2016. Using goal-driven deep learning models to understand sensory cortex. *Nature Neuroscience*, 19(3):356–365.
- Yamins, D. L. K., H. Hong, C. F. Cadieu, E. A. Solomon, D. Seibert, and J. J. DiCarlo
2014. Performance-optimized hierarchical models predict neural responses in higher visual cortex. *Proceedings of the National Academy of Sciences of the United States of America*, 111(23):8619–8624.
- Yang, H. H., F. St-Pierre, X. Sun, X. Ding, M. Z. Lin, and T. R. Clandinin
2016. Subcellular Imaging of Voltage and Calcium Signals Reveals Neural Processing In Vivo. *Cell*, 166(1):245–257.
- Yeh, C. I., D. Xing, and R. M. Shapley
2009. "Black" responses dominate macaque primary visual cortex V1. *Journal of Neuroscience*, 29(38):11753–11760.
- Yonehara, K. and B. Roska
2013. Motion detection: neuronal circuit meets theory. *Cell*, 154(6):1188–1189.
- Zaghloul, K. A., K. Boahen, and J. B. Demb
2003. Different circuits for ON and OFF retinal ganglion cells cause different contrast sensitivities. *Journal of Neuroscience*, 23(7):2645–2654.
- Zemon, V., J. Gordon, and J. Welch
1988. Asymmetries in ON and OFF visual pathways of humans revealed using contrast-evoked cortical potentials. *Visual Neuroscience*, 1(1):145–150.
- Zhou, L., A. Schnitzler, J. Agapite, L. M. Schwartz, H. Steller, and J. R. Nambu
1997. Cooperative functions of the reaper and head involution defective genes in the programmed cell death of *Drosophila* central nervous system midline cells. *Proceedings of the National Academy of Sciences of the United States of America*, 94(10):5131–5136.

ACKNOWLEDGEMENTS

First and foremost, I thank Axel Borst for being an inspiration, a role model, and a guide throughout these formative years. He taught me a unique way of thinking about both neural circuits and science in general (as well as filter theory which I suspect precedes them all). Through his approach, Axel fosters an atmosphere of curiosity, creativity, and intellectual camaraderie that I can only hope to carry forward. Not a day goes by without considering myself lucky to be part of his team.

Many have accompanied me on this scientific journey. In no particular order, I thank Armin Bahl for teaching me how to tackle a problem; Hubert Eichner for spotting non-answers from a distance; Georg Ammer for knowing everything I didn't; Michael Drews for a demonstration of how to immerse yourself in science; Florian Richter, Anna Schützenberger, and Sandra Fendl for spirited discussions and general loveliness; Isabella Kauer for steering me back toward music; Alexander Arenz for an unquenchable enthusiasm in all things science; Alex Mauss for being on top of things; Jürgen Haag for having been on top of things since before I was born; Franz Weber for an introduction to theoretical patch clamp; Stefan Prech for technical ideas and skill at turning them into useful tools; Ruben Portugues and Stefan Glasauer for their advice as part of a belated thesis committee; Romina Kutlesa and Christian Theile for their support with experiments; everyone in our group for making it a little bubble of joy both scientific and not; everyone at the Max-Planck-Institute for turning these grey walls into a place worth missing; and most importantly Matthias Meier and Etienne Serbe for things too numerous to write down.

Alex, Alexander, and Matthias kindly read and greatly improved this thesis. I remain indebted to the administrative team of the Graduate School for Systemic Neurosciences.

For supporting me throughout these years, I am grateful to all friends not named so far and of course my family. Finally, I thank Emilia Geiger for everything; without her, these pages would be empty.

CURRICULUM VITAE

EDUCATION

- 2012–present: PhD student at Graduate School for Systemic Neurosciences (LMU Munich)/Max-Planck-Institute for Neurobiology, Germany; supervised by Alexander Borst
- 2011–2012: Preparatory year in Neuroscience at Graduate School for Systemic Neurosciences (LMU Munich), Germany
- 2008–2011: BA in Natural Sciences at University of Cambridge, UK
- 2007: Abitur at Gymnasium Gars, Germany

CONFERENCES & MEETINGS

- 2017: Poster presentation at Cosyne (Salt Lake City, US)
- 2016: Poster presentation at FENS Meeting (Copenhagen, Denmark)
- 2015: Poster presentation at Janelia Insect Vision Conference (Ashburn, US)
- 2015: Talk for Max-Planck-Center Symposium at Hebrew University (Jerusalem, Israel)
- 2014: Poster presentation at FENS Meeting (Milan, Italy)

TEACHING

- Teaching assistant for *Methods in Animal Physiology* in 2014, 2016, and 2017 (LMU Munich)
- Teaching assistant for *Advanced Scientific Programming* in 2014 (LMU Munich)

PERSONAL INFORMATION

- Birthday: 30th November 1988
- Nationality: German
- Languages: German (native), English (fluent)
- Programming languages: Python, MATLAB, LaTeX (expert); Java, C, Scala (experienced)

PUBLICATIONS

- **Leonhardt A**, Ammer G, Meier M, Serbe E, Bahl A, Borst A (2016). Asymmetry of *Drosophila* ON and OFF motion detectors enhances real-world velocity estimation. *Nature Neuroscience* 19(5):706-15.
- Serbe E, Meier M, **Leonhardt A**, Borst A (2016). Comprehensive Characterization of the Major Presynaptic Elements to the *Drosophila* OFF Motion Detector. *Neuron* 89(4):829-41.
- Ammer G, **Leonhardt A**, Bahl A, Dickson BJ, Borst A (2015). Functional Specialization of Neural Input Elements to the *Drosophila* ON Motion Detector. *Current Biology* 25(17):2247-53.
- Sobolev A, Stoewer A, **Leonhardt A**, Rautenberg PL, Kellner CJ, Garbers C, Wachtler T (2014). Integrated platform and API for electrophysiological data. *Frontiers in Neuroinformatics* 8:32.
- Maisak MS, Haag J, Ammer G, Serbe E, Meier M, **Leonhardt A**, Schilling T, Bahl A, Rubin GM, Nern A, Dickson BJ, Reiff DF, Hopp E, Borst A (2013). A directional tuning map of *Drosophila* elementary motion detectors. *Nature* 500(7461):212-6.

AFFIDAVIT

Hiermit versichere ich an Eides statt, dass ich die vorliegende Dissertation **Circuits and algorithms underlying *Drosophila* motion vision in natural environments** selbstständig angefertigt habe, mich außer der angegebenen keiner weiteren Hilfsmittel bedient und alle Erkenntnisse, die aus dem Schrifttum ganz oder annähernd übernommen sind, als solche kenntlich gemacht und nach ihrer Herkunft unter Bezeichnung der Fundstelle einzeln nachgewiesen habe.

I hereby confirm that the dissertation **Circuits and algorithms underlying *Drosophila* motion vision in natural environments** is the result of my own work and that I have only used sources or materials listed and specified in the dissertation.

.....
München, den
Munich, Date

.....
Unterschrift
Signature

CONTRIBUTIONS

- Maisak MS, Haag J, Ammer G, Serbe E, Meier M, **Leonhardt A**, Schilling T, Bahl A, Rubin GM, Nern A, Dickson BJ, Reiff DF, Hopp E, Borst A (2013). A directional tuning map of *Drosophila* elementary motion detectors. *Nature* 500(7461):212-6.
 - M.S.M. and J.H. jointly performed and, together with A.Bo., evaluated all calcium imaging experiments. G.A., E.S. M.M. recorded from tangential cells. **A.L.**, T.S. and A.Ba. performed the behavioral experiments. G.R., B.D. and A.N. generated the driver lines and characterized their expression pattern. D.F.R. performed preliminary imaging experiments. E.H. helped with programming and developed the PMT shielding for the two-photon microscope. A.Bo. designed the study and wrote the manuscript with the help of all authors. M.S.M. and J.H. contributed equally to this article.
- Ammer G, **Leonhardt A**, Bahl A, Dickson BJ, Borst A (2015). Functional Specialization of Neural Input Elements to the *Drosophila* ON Motion Detector. *Current Biology* 25(17):2247-53.
 - G.A. and A. Borst designed the study. G.A. performed electrophysiological experiments and anatomical characterization of expression patterns, analyzed the data, and wrote the manuscript with the help of A. Borst, **A.L.**, and A. Bahl. **A.L.** and A. Bahl performed behavioral experiments and analyzed data. B.J.D. generated SplitGal4 fly lines and hosted G.A. for characterization of Gal4 lines. A. Borst performed computational modeling.
- Serbe E, Meier M, **Leonhardt A**, Borst A (2016). Comprehensive Characterization of the Major Presynaptic Elements to the *Drosophila* OFF Motion Detector. *Neuron* 89(4):829-41.
 - E.S. and M.M. jointly performed and evaluated all calcium imaging and electrophysiology experiments. **A.L.** performed and evaluated the behavioral experiments. **A.L.** and A.B. performed computer simulations. A.B., E.S., and M.M. designed the study. E.S. and M.M. wrote the manuscript with the help of the other authors. E.S. and M.M. contributed equally to this article.
- **Leonhardt A**, Ammer G, Meier M, Serbe E, Bahl A, Borst A (2016). Asymmetry of *Drosophila* ON and OFF motion detectors enhances real-world velocity estimation. *Nature Neuroscience* 19(5):706-15.
 - **A.L.**, G.A. and A. Borst designed the study. **A.L.** performed behavioral experiments, associated data analysis and all modeling work. G.A., M.M. and E.S. performed electrophysiological experiments. G.A. performed calcium imaging. **A.L.** and G.A. analyzed physiological data. A. Bahl designed the behavioral apparatuses and per-

formed behavioral experiments. A.L. wrote the manuscript with help from all of the authors. A.L. and G.A. contributed equally to this article.

.....
Aljoscha Leonhardt

.....
Georg Ammer
Co-author

.....
Prof. Dr. Alexander Borst
Supervisor